BNL-NCS-32614
DOE/NDC-30/U
NEANDC(US)-216/U
INDC(USA)-91/L
Informal Report
Limited Distribution

REPORTS TO THE DOE NUCLEAR DATA COMMITTEE

Compiled by
NATIONAL NUCLEAR DATA CENTER
for the
U.S. Department of Energy
Nuclear Data Committee

May 1983

BROOKHAVEN NATIONAL LABORATORY
ASSOCIATED UNIVERSITIES, INC.
UPTON, LONG ISLAND, NEW YORK 11973

National
Nuclear
Data
Center

BNL-NCS-32614
DOE/NDC-30/U

REPORTS TO THE DOE NUCLEAR DATA COMMITTEE

May 1983

Compiled by
NATIONAL NUCLEAR DATA CENTER
for the
U.S. Department of Energy
Nuclear Data Committee

NATIONAL NUCLEAR DATA CENTER

BROOKHAVEN NATIONAL LABORATORY
ASSOCIATED UNIVERSITIES, INC.

UNDER CONTRACT NO. DE-AC02-76CH00016 WITH THE

UNITED STATES DEPARTMENT OF ENERGY

Printed in the United States of America
Available from
National Technical Information Service
U.S. Department of Commerce
5285 Port Royal Road
Springfield, VA 22161

NTIS price codes:
Printed Copy: A10; Microfiche Copy: A01

PREFACE

The reports in this document were submitted to the Department of Energy, Nuclear Data Committee (DOE-NDC) in April, 1983. The reporting laboratories are those with a substantial program for the measurement of neutron and nuclear cross sections of relevance to the U.S. applied nuclear energy program.

The authors of the Status Report contributions are responsible for collecting and editing individual contributions from their laboratory and are not necessarily the sole authors of the contributions. The scientists responsible for the work described in each individual contributions are listed at the beginning of the contribution.

The material contained in these reports is to be regarded as comprised of informal statements of recent developments and preliminary data. Persons wishing to make use of these data should contact the individual experimenter for further details. The data which appear in this document should be quoted only by permission of the contributor and should be referenced as private communication, and not by this document number. Appropriate subjects are listed as follows:

1. Microscopic neutron cross sections relevant to the nuclear energy program, including shielding. Inverse reactions where pertinent are included.

2. Charged-particle cross sections, where they are relevant to (1.) above, and where relevant to developing and testing nuclear models.

3. Gamma ray production, radioactive decay, and theoretical developments in nuclear structure which are applicable to nuclear energy programs.

4. Proton and alpha-particle cross sections, at energies of up to 1 GeV, which are of interest to the space program.

These reports cannot be regarded as a complete summary of the nuclear research efforts in the U.S. A number of laboratories whose research is less programmatically oriented do not submit reports; neither do the submitted reports reflect all the work related to nuclear data in progress at the submitting laboratory.

This compilation has been produced almost completely from master copies prepared by the individual contributors listed in the Table of Contents, and reports are reproduced without change from these master copies.

The CINDA-type index which follows the Table of Contents was prepared by Norman E. Holden of the National Nuclear Data Center, Brookhaven National Laboratory, Upton, Long Island, New York.

TABLE OF CONTENTS

TABLE OF CONTENTS (cont.)

NEUTRON DATA REFERENCES

Element	Quantity	Energy (eV) Min	Max	Type	Documentation Ref	Page	Date	Lab	Comments
Li	$\sigma_{n,\alpha}$	8.0+6	1.5+7	Expt	DOE-NDC-30	172	Apr83	AI	Kneff+ NDG.
^{6}Li	σ_{tot}	2.5-2	4.0+6	Eval	DOE-NDC-30	153	Apr83	OHO	Knox+NDG.R-MATRIX ANALY.
^{6}Li	$\sigma_{el}(\theta)$	2.5-2	4.0+6	Eval	DOE-NDC-30	153	Apr83	OHO	Knox+NDG.R-MATRIX ANALY.
^{6}Li	$\sigma_{el}(\theta)$	7.0+6	1.5+7	Exth	DOE-NDC-30	176	Apr83	TNL	Byrd+SPHERICAL OM CALC CFD EXPT
^{6}Li	σ_{pol}	2.5-2	4.0+6	Eval	DOE-NDC-30	153	Apr83	OHO	Knox+NDG.R-MATRIX ANALY.
^{6}Li	$\sigma_{dif.inl}$	7.0+6	1.5+7	Exth	DOE-NDC-30	176	Apr83	TNL	Byrd+SPHERICAL OM CALC CFD EXPT
^{6}Li	$\sigma_{n,t}$	8.0+6	1.5+7	Expt	DOE-NDC-30	172	Apr83	AI	Kneff+ NDG.
^{6}Li	$\sigma_{n,t}$	2.5-2	4.0+6	Eval	DOE-NDC-30	153	Apr83	OHO	Knox+NDG.R-MATRIX ANALY.
^{6}Li	$\sigma_{n,t}$	2.0+6	3.5+6	Expt	DOE-NDC-30	152	Apr83	OHO	Knox+ NDG. DIFF.CS
^{7}Li	$\sigma_{el}(\theta)$	7.0+6	1.5+7	Exth	DOE-NDC-30	176	Apr83	TNL	Byrd+SPHERICAL OM CALC CFD EXPT
^{7}Li	$\sigma_{dif.inl}$	7.0+6	1.5+7	Exth	DOE-NDC-30	176	Apr83	TNL	Byrd+SPHERICAL OM CALC CFD EXPT
^{7}Li	$\sigma_{n,\alpha}$	8.0+6	1.5+7	Expt	DOE-NDC-30	172	Apr83	AI	Kneff+ NDG.
^{9}Be	$\sigma_{el}(\theta)$	1.5+7		Expt	DOE-NDC-30	88	Apr83	LRL	Dietrich+GRPH.EN=14.6MEV,OM CFD XPT
^{9}Be	$\sigma_{el}(\theta)$	7.0+6	1.5+7	Exth	DOE-NDC-30	176	Apr83	TNL	Byrd+SPHERICAL OM CALC CFD EXPT
^{9}Be	$\sigma_{dif.inl}$	7.0+6	1.5+7	Exth	DOE-NDC-30	176	Apr83	TNL	Byrd+SPHERICAL OM CALC CFD EXPT
^{9}Be	$\sigma_{n,\alpha}$	8.0+6	1.5+7	Expt	DOE-NDC-30	172	Apr83	AI	Kneff+ TBD.
B	$\sigma_{n,\alpha}$	8.0+6	1.5+7	Expt	DOE-NDC-30	172	Apr83	AI	Kneff+ NDG.
^{10}B	$\sigma_{el}(\theta)$	7.0+6	1.5+7	Exth	DOE-NDC-30	176	Apr83	TNL	Byrd+SPHERICAL OM CALC CFD EXPT
^{10}B	$\sigma_{dif.inl}$	7.0+6	1.5+7	Exth	DOE-NDC-30	176	Apr83	TNL	Byrd+SPHERICAL OM CALC CFD EXPT
^{10}B	$\sigma_{n,\alpha}$	8.0+6	1.5+7	Expt	DOE-NDC-30	172	Apr83	AI	Kneff+ NDG.
^{11}B	$\sigma_{el}(\theta)$	4.8+6	7.6+6	Expt	DOE-NDC-30	147	Apr83	OHO	Koehler+ NP A394,221 (83)
^{11}B	$\sigma_{el}(\theta)$	7.0+6	1.5+7	Exth	DOE-NDC-30	176	Apr83	TNL	Byrd+SPHERICAL OM CALC CFD EXPT
^{11}B	$\sigma_{dif.inl}$	4.8+6	7.6+6	Expt	DOE-NDC-30	147	Apr83	OHO	Koehler+ NP A394,221 (83)
^{11}B	$\sigma_{dif.inl}$	7.0+6	1.5+7	Exth	DOE-NDC-30	176	Apr83	TNL	Byrd+SPHERICAL OM CALC CFD EXPT
^{11}B	$\sigma_{n,\alpha}$	8.0+6	1.5+7	Expt	DOE-NDC-30	172	Apr83	AI	Kneff+ NDG.
^{12}C	Evaluation	NDG		Eval	DOE-NDC-30	145	Apr83	ORL	Fu. NDG
^{12}C	σ_{tot}	1.9+6	2.0+7	Expt	DOE-NDC-30	4	Apr83	ANL	Poenitz+NDG.NO 8 PCT ERR WITH ENDF
^{12}C	$\sigma_{el}(\theta)$	1.5+7		Expt	DOE-NDC-30	88	Apr83	LRL	Dietrich+GRPH.EN=14.6MEV,OM CFD XPT
^{12}C	$\sigma_{el}(\theta)$	2.6+7	3.0+7	Expt	DOE-NDC-30	79	Apr83	LRL	Hansen+PRELIMINARY.NDG
^{12}C	$\sigma_{el}(\theta)$	2.1+7	2.6+7	Expt	DOE-NDC-30	147	Apr83	OHO	Meigooni+NDG.BAPS 27,544(82)
^{12}C	$\sigma_{el}(\theta)$	2.0+7	4.0+7	Eval	DOE-NDC-30	154	Apr83	OHO	Meigooni+OPT.MDL.+CC CALC.
^{12}C	$\sigma_{el}(\theta)$	7.0+6	1.5+7	Exth	DOE-NDC-30	176	Apr83	TNL	Byrd+SPHERICAL OM CALC CFD EXPT
^{12}C	$\sigma_{el}(\theta)$	1.0+7		Expt	DOE-NDC-30	180	Apr83	TNL	Anderson+GRPH.LOW ANGLE

NEUTRON DATA REFERENCES

Element	Quantity	Energy (eV) Min	Max	Type	Documentation Ref	Page	Date	Lab	Comments
^{12}C	$\sigma_{dif.inl}$	2.1+7	2.6+7	Expt	DOE-NDC-30	147	Apr83	OHO	Meigooni+NDG.BAPS 27,544(82)
^{12}C	$\sigma_{dif.inl}$	2.0+7	4.0+7	Eval	DOE-NDC-30	154	Apr83	OHO	Meigooni+OPT.MDL.+CC CALC.
^{12}C	$\sigma_{dif.inl}$	2.2+7	2.4+7	Expt	DOE-NDC-30	148	Apr83	OHO	Petler+NDG.2ES CFD OTHR
^{12}C	$\sigma_{dif.inl}$	7.0+6	1.5+7	Exth	DOE-NDC-30	176	Apr83	TNL	Byrd+SPHERICAL OM CALC CFD EXPT
^{12}C	$\sigma_{n,n'\gamma}$	4.8+6	1.0+8	Expt	DOE-NDC-30	94	Apr83	LAS	Wender+GRPH.EXC.FCN. 4.4MEV GAMMA PR
^{12}C	$\sigma_{n,p}$	2.7+7	6.1+7	Expt	DOE-NDC-30	39	Apr83	DAV	Subramanian+GRPHS DOUBL.DSIG VS CALC
^{12}C	$\sigma_{n,d}$	2.7+7	6.1+7	Expt	DOE-NDC-30	39	Apr83	DAV	Subramanian+GRPHS DOUBL.DSIG VS CALC
^{12}C	$\sigma_{n,t}$	2.7+7	6.1+7	Expt	DOE-NDC-30	39	Apr83	DAV	Subramanian+GRPHS DOUBL.DSIG VS CALC
^{12}C	$\sigma_{n,}{}^{3}He$	2.7+7	6.1+7	Expt	DOE-NDC-30	39	Apr83	DAV	Subramanian+GRPHS DOUBL.DSIG VS CALC
^{12}C	$\sigma_{n,\alpha}$	8.0+6	1.5+7	Expt	DOE-NDC-30	172	Apr83	AI	Kneff+ NDG.
^{12}C	$\sigma_{n,\alpha}$	2.7+7	6.1+7	Expt	DOE-NDC-30	39	Apr83	DAV	Subramanian+GRPHS DOUBL.DSIG VS CALC
^{12}C	$\sigma_{n,\alpha}$	1.4+7		Expt	DOE-NDC-30	78	Apr83	LRL	Haight+CS,ANGDIST FOR KERMA CALC
^{13}C	$\sigma_{el}(\theta)$	4.5+6	1.1+7	Expt	DOE-NDC-30	148	Apr83	OHO	Resler+ NDG
^{13}C	$\sigma_{el}(\theta)$	7.0+6	1.5+7	Exth	DOE-NDC-30	176	Apr83	TNL	Byrd+SPHERICAL OM CALC CFD EXPT
^{13}C	$\sigma_{dif.inl}$	4.5+6	1.1+7	Expt	DOE-NDC-30	148	Apr83	OHO	Resler+ NDG
^{13}C	$\sigma_{dif.inl}$	7.0+6	1.5+7	Exth	DOE-NDC-30	176	Apr83	TNL	Byrd+SPHERICAL OM CALC CFD EXPT
^{14}N	$\sigma_{n,\alpha}$	8.0+6	1.5+7	Expt	DOE-NDC-30	172	Apr83	AI	Kneff+ TBD.
^{16}O	$\sigma_{el}(\theta)$	9.2+6	1.5+7	Expt	DOE-NDC-30	175	Apr83	TNL	Byrd+ NSE 82,393 (82)
^{16}O	$\sigma_{el}(\theta)$	7.0+6	1.5+7	Exth	DOE-NDC-30	176	Apr83	TNL	Byrd+SPHERICAL OM CALC CFD EXPT
^{16}O	$\sigma_{dif.inl}$	7.0+6	1.5+7	Exth	DOE-NDC-30	176	Apr83	TNL	Byrd+SPHERICAL OM CALC CFD EXPT
^{18}O	$\sigma_{el}(\theta)$	5.5+6	7.3+6	Expt	DOE-NDC-30	148	Apr83	OHO	Koehler+ NDG.
^{18}O	$\sigma_{dif.inl}$	5.5+6	7.3+6	Expt	DOE-NDC-30	148	Apr83	OHO	Koehler+ NDG.
^{19}F	$\sigma_{n,\alpha}$	8.0+6	1.5+7	Expt	DOE-NDC-30	172	Apr83	AI	Kneff+ NDG.
^{26}Mg	$\sigma_{el}(\theta)$	2.4+7		Expt	DOE-NDC-30	149	Apr83	OHO	Tailor+ NDG.TBP NP/A
^{26}Mg	$\sigma_{dif.inl}$	2.4+7		Expt	DOE-NDC-30	149	Apr83	OHO	Tailor+ NDG.TBP NP/A
^{27}Al	$\sigma_{el}(\theta)$	1.5+7		Expt	DOE-NDC-30	88	Apr83	LRL	Dietrich+GRPH.EN=14.6MEV,OM CFD XPT
^{27}Al	$\sigma_{n,\alpha}$	8.0+6	1.5+7	Expt	DOE-NDC-30	172	Apr83	AI	Kneff+ NDG.
^{28}Si	$\sigma_{el}(\theta)$	8.0+6	1.4+7	Expt	DOE-NDC-30	177	Apr83	TNL	Byrd+ NDG.
^{28}Si	σ_{pol}	1.0+7	1.4+7	Expt	DOE-NDC-30	177	Apr83	TNL	Byrd+ 2ES.NDG
^{28}Si	$\sigma_{dif.inl}$	8.0+6	1.4+7	Expt	DOE-NDC-30	177	Apr83	TNL	Byrd+ NDG.
^{32}S	$\sigma_{el}(\theta)$	8.0+6	1.4+7	Expt	DOE-NDC-30	177	Apr83	TNL	Byrd+ NDG.
^{32}S	σ_{pol}	1.0+7	1.4+7	Expt	DOE-NDC-30	177	Apr83	TNL	Byrd+ 2ES.NDG
^{32}S	$\sigma_{dif.inl}$	8.0+6	1.4+7	Expt	DOE-NDC-30	177	Apr83	TNL	Byrd+ NDG.

NEUTRON DATA REFERENCES

Element	Quantity	Energy (eV) Min	Max	Type	Documentation Ref	Page	Date	Lab	Comments
Ca	Evaluation	NDG		Eval	DOE-NDC-30	145	Apr83	ORL	Fu. NDG
^{40}Ca	Evaluation	2.0+7	4.0+7	Eval	DOE-NDC-30	145	Apr83	ORL	Hetrick+ NDG
^{40}Ca	$\sigma_{el}(\theta)$	1.2+7		Exth	DOE-NDC-30	177	Apr83	TNL	Byrd+NDG.CC CALC.TBP NP/A
^{40}Ca	$\sigma_{dif.inl}$	1.2+7		Exth	DOE-NDC-30	177	Apr83	TNL	Byrd+NDG.CC CALC.TBP NP/A
^{40}Ca	σ_{nem}	6.5+7		Expt	DOE-NDC-30	34	Apr83	DAV	Ford+ GRPH NEUT. SPECTRUM
^{45}Sc	σ_{tot}	1.9+6	2.0+7	Expt	DOE-NDC-30	4	Apr83	ANL	Poenitz+NDG.
^{45}Sc	$\sigma_{el}(\theta)$		4.0+6	Expt	DOE-NDC-30	8	Apr83	ANL	Smith+ TB ANALYZED
^{45}Sc	$\sigma_{dif.inl}$		4.0+6	Expt	DOE-NDC-30	8	Apr83	ANL	Smith+ TB ANALYZED
Ti	$\sigma_{n,\alpha}$	8.0+6	1.5+7	Expt	DOE-NDC-30	172	Apr83	AI	Kneff+ NDG.
^{47}Ti	$\sigma_{n,p}$	1.2+6	9.0+6	Expt	DOE-NDC-30	8	Apr83	ANL	Smith+ NDG
^{51}V	$\sigma_{dif.inl}$	2.6+7		Expt	DOE-NDC-30	149	Apr83	OHO	Alarcon+ NDG.PRELIMINARY
^{55}Mn	$\sigma_{n,\alpha}$	8.0+6	1.5+7	Expt	DOE-NDC-30	172	Apr83	AI	Kneff+ TBD.
Fe	Evaluation	NDG		Eval	DOE-NDC-30	145	Apr83	ORL	Fu. NDG
Fe	$\sigma_{el}(\theta)$	2.6+7	3.0+7	Expt	DOE-NDC-30	79	Apr83	LRL	Hansen+PRELIMINARY.NDG
^{54}Fe	σ_{tot}	5.0+5	4.0+6	Expt	DOE-NDC-30	5	Apr83	ANL	Guenther+NDG
^{54}Fe	σ_{tot}	7.0+6	2.6+7	Exth	DOE-NDC-30	88	Apr83	LRL	Dietrich+OPT.MDL.CALC CFD EXPT
^{54}Fe	$\sigma_{el}(\theta)$	1.2+6	4.0+6	Expt	DOE-NDC-30	5	Apr83	ANL	Guenther+ GRPH
^{54}Fe	$\sigma_{el}(\theta)$	7.0+6	2.6+7	Exth	DOE-NDC-30	88	Apr83	LRL	Dietrich+OPT.MDL.CALC CFD EXPT
^{54}Fe	$\sigma_{el}(\theta)$	2.0+7	2.6+7	Expt	DOE-NDC-30	150	Apr83	OHO	Mellema+NDG. CFD CALC
^{54}Fe	$\sigma_{el}(\theta)$	8.0+6	1.4+7	Expt	DOE-NDC-30	177	Apr83	TNL	Byrd+NDG. TBP NP/A
^{54}Fe	$\sigma_{dif.inl}$	1.2+6	4.0+6	Expt	DOE-NDC-30	5	Apr83	ANL	Guenther+NDG
^{54}Fe	$\sigma_{dif.inl}$	2.0+7	2.6+7	Expt	DOE-NDC-30	150	Apr83	OHO	Mellema+NDG. CFD CALC
^{54}Fe	$\sigma_{dif.inl}$	8.0+6	1.4+7	Expt	DOE-NDC-30	177	Apr83	TNL	Byrd+NDG. TBP NP/A
^{54}Fe	$\sigma_{n,n'\gamma}$	1.2+6	4.0+6	Expt	DOE-NDC-30	5	Apr83	ANL	Guenther+GRPHS.LVL GAMMA RAY PROD.
^{56}Fe	σ_{tot}	7.0+6	2.6+7	Exth	DOE-NDC-30	88	Apr83	LRL	Dietrich+OPT.MDL.CALC CFD EXPT
^{56}Fe	$\sigma_{el}(\theta)$	7.0+6	2.6+7	Exth	DOE-NDC-30	88	Apr83	LRL	Dietrich+GRPH EN=14.6MEV OM CFD EXPT
^{56}Fe	$\sigma_{el}(\theta)$	2.6+7		Expt	DOE-NDC-30	150	Apr83	OHO	Mellema+NDG. CFD CALC
^{56}Fe	$\sigma_{el}(\theta)$	8.0+6	1.4+7	Expt	DOE-NDC-30	177	Apr83	TNL	Byrd+NDG. TBP NP/A
^{56}Fe	$\sigma_{dif.inl}$	2.6+7		Expt	DOE-NDC-30	150	Apr83	OHO	Mellema+NDG. CFD CALC
^{56}Fe	$\sigma_{dif.inl}$	8.0+6	1.4+7	Expt	DOE-NDC-30	177	Apr83	TNL	Byrd+NDG. TBP NP/A
^{56}Fe	$\sigma_{n,n'\gamma}$	3.6+6	4.5+6	Expt	DOE-NDC-30	66	Apr83	KTY	O Brien+GAMMA RAY EXCIT FCNS MEAS.
^{57}Fe	$\sigma_{n,\gamma}$	1.6+5	2.1+7	Expt	DOE-NDC-30	138	Apr83	ORL	Bell+NDG.DETECTED GAMMA RAYS
^{57}Fe	$\sigma_{n,n'\gamma}$	1.6+5	2.1+7	Expt	DOE-NDC-30	138	Apr83	ORL	Bell+NDG.DETECTED GAMMA RAYS

NEUTRON DATA REFERENCES

Element	Quantity	Energy (eV) Min	Max	Type	Documentation Ref	Page	Date	Lab	Comments
^{57}Fe	$\sigma_{n,2n}$	1.6+5	2.1+7	Expt	DOE-NDC-30	138	Apr83	ORL	Bell+CS(15 MEV) GT 1 BARN
^{57}Fe	$\sigma_{n,p}$	1.6+5	2.1+7	Expt	DOE-NDC-30	138	Apr83	ORL	Bell+ CS(9 MEV) GT 0.2 BARNS
^{57}Fe	$\sigma_{n,\alpha}$	1.6+5	2.1+7	Expt	DOE-NDC-30	138	Apr83	ORL	Bell+NDG.DETECTED GAMMA RAYS
^{59}Co	$\sigma_{el}(\theta)$	1.0+6	4.0+6	Expt	DOE-NDC-30	7	Apr83	ANL	Smith+ TB ANALYZED
^{59}Co	$\sigma_{el}(\theta)$	1.5+7		Expt	DOE-NDC-30	88	Apr83	LRL	Dietrich+GRPH.EN=14.6MEV,OM CFD XPT
^{59}Co	$\sigma_{dif.inl}$	1.0+6	4.0+6	Expt	DOE-NDC-30	7	Apr83	ANL	Smith+ TB ANALYZED
Ni	σ_{tot}	2.0+3	2.0+7	Expt	DOE-NDC-30	134	Apr83	ORL	Larson+ABST.ORNL-TM-8203
^{58}Ni	$\sigma_{el}(\theta)$	1.0+7	1.4+7	Exth	DOE-NDC-30	178	Apr83	TNL	Byrd+NDG. CC CALC.
^{58}Ni	$\sigma_{dif.inl}$	1.0+7	1.4+7	Exth	DOE-NDC-30	178	Apr83	TNL	Byrd+NDG. CC CALC.
^{58}Ni	$\sigma_{n,p}$	5.0+6	5.5+7	Theo	DOE-NDC-30	36	Apr83	DAV	Castaneda+GRPHS CALC VS EXPTL SPECTR
^{58}Ni	$\sigma_{n,p}$	9.5+6	1.1+7	Expt	DOE-NDC-30	152	Apr83	OHO	Graham+NDG.CFD H-F CALC
^{58}Ni	$\sigma_{n,d}$	8.0+6	1.1+7	Expt	DOE-NDC-30	152	Apr83	OHO	Graham+NDG.NOT DET.BELOW 11 MEV
^{58}Ni	$\sigma_{n,\alpha}$	9.5+6	1.1+7	Expt	DOE-NDC-30	152	Apr83	OHO	Graham+NDG.CFD H-F CALC
^{60}Ni	σ_{tot}	+0	1.8+5	Expt	DOE-NDC-30	134	Apr83	ORL	Perey+ PR/C TBP
^{60}Ni	$\sigma_{el}(\theta)$	1.0+7	1.4+7	Exth	DOE-NDC-30	178	Apr83	TNL	Byrd+NDG. CC CALC.
^{60}Ni	$\sigma_{dif.inl}$	1.0+7	1.4+7	Exth	DOE-NDC-30	178	Apr83	TNL	Byrd+NDG. CC CALC.
^{60}Ni	$\sigma_{n,\gamma}$	2.5+3	5.0+6	Expt	DOE-NDC-30	134	Apr83	ORL	Perey+ PR/C TBP
^{60}Ni	$\sigma_{n,p}$	5.0+6	5.5+7	Theo	DOE-NDC-30	36	Apr83	DAV	Castaneda+GRPHS CALC VS EXPTL SPECTR
^{60}Ni	$\sigma_{n,p}$	1.1+7		Expt	DOE-NDC-30	152	Apr83	OHO	Graham+NDG.CFD H-F CALC
^{60}Ni	$\sigma_{n,d}$	8.0+6	1.1+7	Expt	DOE-NDC-30	152	Apr83	OHO	Graham+NDG.NOT DET.BELOW 11 MEV
^{60}Ni	$\sigma_{n,\alpha}$	1.1+7		Expt	DOE-NDC-30	152	Apr83	OHO	Graham+NDG.CFD H-F CALC
^{60}Ni	Res.Params.	NDG		Expt	DOE-NDC-30	134	Apr83	ORL	Perey+ PR/C TBP
^{60}Ni	$\langle\Gamma\rangle/D$	1.0+3	4.5+5	Expt	DOE-NDC-30	134	Apr83	ORL	Perey+ PR/C TBP
^{62}Ni	$\sigma_{n,p}$	5.0+6	5.5+7	Theo	DOE-NDC-30	36	Apr83	DAV	Castaneda+GRPHS CALC VS EXPTL SPECTR
^{64}Ni	$\sigma_{n,p}$	5.0+6	5.5+7	Theo	DOE-NDC-30	36	Apr83	DAV	Castaneda+GRPHS CALC VS EXPTL SPECTR
Cu	Evaluation	NDG		Eval	DOE-NDC-30	145	Apr83	ORL	Fu. NDG
Cu	σ_{tot}	1.2+6	4.5+6	Expt	DOE-NDC-30	5	Apr83	ANL	Guenther+NDG
Cu	σ_{tot}	NDG		Expt	DOE-NDC-30	4	Apr83	ANL	Poenitz+NDG.
Cu	$\sigma_{el}(\theta)$	1.5+6	4.0+6	Expt	DOE-NDC-30	5	Apr83	ANL	Guenther+NDG
Cu	$\sigma_{dif.inl}$	1.5+6	4.0+6	Expt	DOE-NDC-30	5	Apr83	ANL	Guenther+NDG
Cu	$\sigma_{n,n'\gamma}$	1.5+6	4.0+6	Expt	DOE-NDC-30	5	Apr83	ANL	Guenther+ TB ANALYZED
Cu	$\sigma_{n,n'\gamma}$	7.0+5	1.1+7	Expt	DOE-NDC-30	137	Apr83	ORL	Slaughter+NDG.CS 22 GAMMA RAYS
^{63}Cu	$\sigma_{el}(\theta)$	8.0+6	1.4+7	Expt	DOE-NDC-30	177	Apr83	TNL	Byrd+NDG. TBP NP/A

NEUTRON DATA REFERENCES

Element	Quantity	Energy (eV) Min	Max	Type	Documentation Ref	Page	Date	Lab	Comments
^{63}Cu	$\sigma_{dif.inl}$	8.0+6	1.4+7	Expt	DOE-NDC-30	177	Apr83	TNL	Byrd+NDG. TBP NP/A
^{65}Cu	$\sigma_{el}(\theta)$	8.0+6	1.4+7	Expt	DOE-NDC-30	177	Apr83	TNL	Byrd+NDG. TBP NP/A
^{65}Cu	$\sigma_{dif.inl}$	8.0+6	1.4+7	Expt	DOE-NDC-30	177	Apr83	TNL	Byrd+NDG. TBP NP/A
Zn	σ_{tot}	1.9+6	2.0+7	Expt	DOE-NDC-30	4	Apr83	ANL	Poenitz+NDG.
^{76}Se	$\sigma_{el}(\theta)$	8.0+6	1.0+7	Expt	DOE-NDC-30	151	Apr83	OHO	Kurup+ NDG.
^{76}Se	$\sigma_{dif.inl}$	8.0+6	1.0+7	Expt	DOE-NDC-30	151	Apr83	OHO	Kurup+ NDG.
^{80}Se	$\sigma_{el}(\theta)$	8.0+6	1.0+7	Expt	DOE-NDC-30	151	Apr83	OHO	Kurup+ NDG.
^{80}Se	$\sigma_{dif.inl}$	8.0+6	1.0+7	Expt	DOE-NDC-30	151	Apr83	OHO	Kurup+ NDG.
^{86}Sr	$\sigma_{n,\gamma}$	1.0+3	2.0+5	Expt	DOE-NDC-30	80	Apr83	LRL	Mathews+S-PROCESS MONITOR.NDG
^{87}Sr	$\sigma_{n,\gamma}$	1.0+3	2.0+5	Expt	DOE-NDC-30	80	Apr83	LRL	Mathews+S-PROCESS MONITOR.NDG
^{88}Sr	$\sigma_{n,\gamma}$	1.0+3	2.0+5	Expt	DOE-NDC-30	80	Apr83	LRL	Mathews+TBD
^{89}Y	σ_{tot}	1.9+6	2.0+7	Expt	DOE-NDC-30	4	Apr83	ANL	Poenitz+NDG.
^{89}Y	$\sigma_{el}(\theta)$	8.0+6	1.4+7	Expt	DOE-NDC-30	178	Apr83	TNL	Byrd+ NDG.
^{89}Y	$\sigma_{n,\gamma}$	5.0+5	4.0+6	Expt	DOE-NDC-30	4	Apr83	ANL	Poenitz.NDG.REL AU
^{89}Y	$\sigma_{n,\alpha}$	8.0+6	1.5+7	Expt	DOE-NDC-30	172	Apr83	AI	Kneff+ NDG.
Zr	σ_{tot}	1.9+6	2.0+7	Expt	DOE-NDC-30	4	Apr83	ANL	Poenitz+NDG.
Zr	$\sigma_{dif.inl}$	2.6+7		Expt	DOE-NDC-30	149	Apr83	OHO	Alarcon+ NDG.PRELIMINARY
Zr	$\sigma_{n,\gamma}$	5.0+5	4.0+6	Expt	DOE-NDC-30	4	Apr83	ANL	Poenitz.NDG.REL AU
^{93}Nb	σ_{tot}	1.9+6	2.0+7	Expt	DOE-NDC-30	4	Apr83	ANL	Poenitz+NDG.
^{93}Nb	$\sigma_{el}(\theta)$	1.5+7		Expt	DOE-NDC-30	79	Apr83	LRL	Hansen+EN=14.6MEV.NDG
^{93}Nb	$\sigma_{el}(\theta)$	8.0+6	1.4+7	Expt	DOE-NDC-30	178	Apr83	TNL	Byrd+ GRPH CFD EXPT
^{93}Nb	$\sigma_{dif.inl}$	1.5+7		Expt	DOE-NDC-30	79	Apr83	LRL	Hansen+EN=14.6MEV.NDG
Mo	σ_{tot}	1.9+6	2.0+7	Expt	DOE-NDC-30	4	Apr83	ANL	Poenitz+NDG.
Mo	$\sigma_{el}(\theta)$	1.5+6	4.0+6	Theo	DOE-NDC-30	5	Apr83	ANL	Smith+REGIONAL OPT.MDL.CFD MEAS
Mo	$\sigma_{n,\gamma}$	5.0+5	4.0+6	Expt	DOE-NDC-30	4	Apr83	ANL	Poenitz.NDG.REL AU
^{103}Rh	σ_{tot}	1.9+6	2.0+7	Expt	DOE-NDC-30	4	Apr83	ANL	Poenitz+NDG.
^{103}Rh	$\sigma_{el}(\theta)$	1.5+6	4.0+6	Expt	DOE-NDC-30	5	Apr83	ANL	Smith+REGIONAL OPT.MDL.CFD MEAS
Pd	σ_{tot}	1.9+6	2.0+7	Expt	DOE-NDC-30	4	Apr83	ANL	Poenitz+NDG.
Pd	$\sigma_{el}(\theta)$	1.5+6	4.0+6	Theo	DOE-NDC-30	5	Apr83	ANL	Smith+REGIONAL OPT.MDL.CFD MEAS
Ag	σ_{tot}	1.9+6	2.0+7	Expt	DOE-NDC-30	4	Apr83	ANL	Poenitz+NDG.
Ag	$\sigma_{el}(\theta)$	1.5+6	4.0+6	Expt	DOE-NDC-30	5	Apr83	ANL	Smith+REGIONAL OPT.MDL.CFD MEAS
Ag	$\sigma_{n,\gamma}$	5.0+5	4.0+6	Expt	DOE-NDC-30	4	Apr83	ANL	Poenitz.NDG.REL AU
Ag	$\sigma_{n,\alpha}$	8.0+6	1.5+7	Expt	DOE-NDC-30	172	Apr83	AI	Kneff+ TBD.

NEUTRON DATA REFERENCES

Element	Quantity	Energy (eV) Min	Max	Type	Documentation Ref	Page	Date	Lab	Comments
Cd	$\sigma_{el}(\theta)$	1.5+6	4.0+6	Expt	DOE-NDC-30	5	Apr83	ANL	Smith+REGIONAL OPT.MDL.CFD MEAS
Cd	$\sigma_{n,\gamma}$	5.0+5	4.0+6	Expt	DOE-NDC-30	4	Apr83	ANL	Poenitz.NDG.REL AU
^{120}Cd	$\sigma_{n,\gamma}$	Maxw		Theo	DOE-NDC-30	90	Apr83	LRL	Mathews+GRPH DIR CAPT VS STAT.MDL
^{121}Cd	$\sigma_{n,\gamma}$	Maxw		Theo	DOE-NDC-30	90	Apr83	LRL	Mathews+GRPH DIR CAPT VS STAT.MDL
^{122}Cd	$\sigma_{n,\gamma}$	Maxw		Theo	DOE-NDC-30	90	Apr83	LRL	Mathews+GRPH DIR CAPT VS STAT.MDL
^{123}Cd	$\sigma_{n,\gamma}$	Maxw		Theo	DOE-NDC-30	90	Apr83	LRL	Mathews+GRPH DIR CAPT VS STAT.MDL
^{124}Cd	$\sigma_{n,\gamma}$	Maxw		Theo	DOE-NDC-30	90	Apr83	LRL	Mathews+GRPH DIR CAPT VS STAT.MDL
^{125}Cd	$\sigma_{n,\gamma}$	Maxw		Theo	DOE-NDC-30	90	Apr83	LRL	Mathews+GRPH DIR CAPT VS STAT.MDL
^{126}Cd	$\sigma_{n,\gamma}$	Maxw		Theo	DOE-NDC-30	90	Apr83	LRL	Mathews+GRPH DIR CAPT VS STAT.MDL
^{127}Cd	$\sigma_{n,\gamma}$	Maxw		Theo	DOE-NDC-30	90	Apr83	LRL	Mathews+GRPH DIR CAPT VS STAT.MDL
^{128}Cd	$\sigma_{n,\gamma}$	Maxw		Theo	DOE-NDC-30	90	Apr83	LRL	Mathews+GRPH DIR CAPT VS STAT.MDL
^{129}Cd	$\sigma_{n,\gamma}$	Maxw		Theo	DOE-NDC-30	90	Apr83	LRL	Mathews+GRPH DIR CAPT VS STAT.MDL
^{130}Cd	$\sigma_{n,\gamma}$	Maxw		Theo	DOE-NDC-30	90	Apr83	LRL	Mathews+GRPH DIR CAPT VS STAT.MDL
^{131}Cd	$\sigma_{n,\gamma}$	Maxw		Theo	DOE-NDC-30	90	Apr83	LRL	Mathews+GRPH DIR CAPT VS STAT.MDL
^{132}Cd	$\sigma_{n,\gamma}$	Maxw		Theo	DOE-NDC-30	90	Apr83	LRL	Mathews+GRPH DIR CAPT VS STAT.MDL
^{133}Cd	$\sigma_{n,\gamma}$	Maxw		Theo	DOE-NDC-30	90	Apr83	LRL	Mathews+GRPH DIR CAPT VS STAT.MDL
^{134}Cd	$\sigma_{n,\gamma}$	Maxw		Theo	DOE-NDC-30	90	Apr83	LRL	Mathews+GRPH DIR CAPT VS STAT.MDL
^{135}Cd	$\sigma_{n,\gamma}$	Maxw		Theo	DOE-NDC-30	90	Apr83	LRL	Mathews+GRPH DIR CAPT VS STAT.MDL
^{136}Cd	$\sigma_{n,\gamma}$	Maxw		Theo	DOE-NDC-30	90	Apr83	LRL	Mathews+GRPH DIR CAPT VS STAT.MDL
^{137}Cd	$\sigma_{n,\gamma}$	Maxw		Theo	DOE-NDC-30	90	Apr83	LRL	Mathews+GRPH DIR CAPT VS STAT.MDL
^{138}Cd	$\sigma_{n,\gamma}$	Maxw		Theo	DOE-NDC-30	90	Apr83	LRL	Mathews+GRPH DIR CAPT VS STAT.MDL
^{139}Cd	$\sigma_{n,\gamma}$	Maxw		Theo	DOE-NDC-30	90	Apr83	LRL	Mathews+GRPH DIR CAPT VS STAT.MDL
^{140}Cd	$\sigma_{n,\gamma}$	Maxw		Theo	DOE-NDC-30	90	Apr83	LRL	Mathews+GRPH DIR CAPT VS STAT.MDL
In	σ_{tot}	1.9+6	2.0+7	Expt	DOE-NDC-30	4	Apr83	ANL	Poenitz+NDG.
In	$\sigma_{el}(\theta)$	1.5+6	4.0+6	Expt	DOE-NDC-30	5	Apr83	ANL	Smith+REGIONAL OPT.MDL.CFD MEAS
In	$\sigma_{n,\gamma}$	5.0+5	4.0+6	Expt	DOE-NDC-30	4	Apr83	ANL	Poenitz.NDG.REL AU
^{115}In	$\sigma_{el}(\theta)$	1.5+7		Expt	DOE-NDC-30	79	Apr83	LRL	Hansen+EN=14.6MEV.NDG
^{115}In	$\sigma_{dif.inl}$	1.5+7		Expt	DOE-NDC-30	79	Apr83	LRL	Hansen+EN=14.6MEV.NDG
Sn	σ_{tot}	1.9+6	2.0+7	Expt	DOE-NDC-30	4	Apr83	ANL	Poenitz+NDG.
^{116}Sn	σ_{tot}	3.0+5	5.0+6	Expt	DOE-NDC-30	67	Apr83	KTY	Harper+ PR/C 26,1432 (82)
^{116}Sn	$\sigma_{el}(\theta)$	1.0+6	4.0+6	Expt	DOE-NDC-30	67	Apr83	KTY	Harper+3 ENS.TBP
^{116}Sn	$\sigma_{el}(\theta)$	1.0+7		Exth	DOE-NDC-30	177	Apr83	TNL	Byrd+NDG.CC CALC.TBP NP/A
^{116}Sn	$\sigma_{el}(\theta)$	1.0+7	1.4+7	Expt	DOE-NDC-30	178	Apr83	TNL	Byrd+ NDG.

NEUTRON DATA REFERENCES

Element	Quantity	Energy (eV) Min	Max	Type	Documentation Ref	Page	Date	Lab	Comments
^{116}Sn	$\sigma_{dif.inl}$	1.0+6	4.0+6	Expt	DOE-NDC-30	67	Apr83	KTY	Harper+3 ENS.TBP
^{116}Sn	$\sigma_{dif.inl}$	1.0+7		Exth	DOE-NDC-30	177	Apr83	TNL	Byrd+NDG.CC CALC.TBP NP/A
^{116}Sn	$\sigma_{n,n'\gamma}$	1.9+6	3.6+6	Expt	DOE-NDC-30	65	Apr83	KTY	Sa+GAMMA RAY EXCIT.FCNS MEAS.
^{118}Sn	σ_{tot}	3.0+5	5.0+6	Expt	DOE-NDC-30	67	Apr83	KTY	Harper+ PR/C 26,1432 (82)
^{118}Sn	$\sigma_{el}(\theta)$	1.0+6	4.0+6	Expt	DOE-NDC-30	67	Apr83	KTY	Harper+3 ENS.TBP
^{118}Sn	$\sigma_{dif.inl}$	1.0+6	4.0+6	Expt	DOE-NDC-30	67	Apr83	KTY	Harper+3 ENS.TBP
^{120}Sn	σ_{tot}	3.0+5	5.0+6	Expt	DOE-NDC-30	67	Apr83	KTY	Harper+ PR/C 26,1432 (82)
^{120}Sn	$\sigma_{el}(\theta)$	1.0+6	4.0+6	Expt	DOE-NDC-30	67	Apr83	KTY	Harper+3 ENS.TBP
^{120}Sn	$\sigma_{el}(\theta)$	1.0+7		Exth	DOE-NDC-30	177	Apr83	TNL	Byrd+NDG.CC CALC.TBP NP/A
^{120}Sn	$\sigma_{el}(\theta)$	1.0+7	1.7+7	Expt	DOE-NDC-30	178	Apr83	TNL	Byrd+ GRPH CFD CC CALC
^{120}Sn	$\sigma_{dif.inl}$	1.0+6	4.0+6	Expt	DOE-NDC-30	67	Apr83	KTY	Harper+3 ENS.TBP
^{120}Sn	$\sigma_{dif.inl}$	1.0+7		Exth	DOE-NDC-30	177	Apr83	TNL	Byrd+NDG.CC CALC.TBP NP/A
^{120}Sn	$\sigma_{n,n'\gamma}$	NDG		Expt	DOE-NDC-30	65	Apr83	KTY	Sa+ TBD
^{122}Sn	σ_{tot}	3.0+5	5.0+6	Expt	DOE-NDC-30	67	Apr83	KTY	Harper+ PR/C 26,1432 (82)
^{122}Sn	$\sigma_{el}(\theta)$	1.0+6	4.0+6	Expt	DOE-NDC-30	67	Apr83	KTY	Harper+3 ENS.TBP
^{122}Sn	$\sigma_{dif.inl}$	1.0+6	4.0+6	Expt	DOE-NDC-30	67	Apr83	KTY	Harper+3 ENS.TBP
^{124}Sn	σ_{tot}	3.0+5	5.0+6	Expt	DOE-NDC-30	67	Apr83	KTY	Harper+ PR/C 26,1432 (82)
^{124}Sn	$\sigma_{el}(\theta)$	1.0+6	4.0+6	Expt	DOE-NDC-30	67	Apr83	KTY	Harper+3 ENS.TBP
^{124}Sn	$\sigma_{dif.inl}$	1.0+6	4.0+6	Expt	DOE-NDC-30	67	Apr83	KTY	Harper+3 ENS.TBP
^{124}Sn	$\sigma_{n,n'\gamma}$	2.3+6	3.7+6	Expt	DOE-NDC-30	65	Apr83	KTY	Sa+51 GAMMA RAY PROD CS MEAS
Sb	σ_{tot}	1.9+6	2.0+7	Expt	DOE-NDC-30	4	Apr83	ANL	Poenitz+NDG.
Sb	$\sigma_{n,\gamma}$	5.0+5	4.0+6	Expt	DOE-NDC-30	4	Apr83	ANL	Poenitz.NDG.REL AU
^{139}La	σ_{tot}	2.5+6	6.0+7	Expt	DOE-NDC-30	81	Apr83	LRL	Phillips+ OPT.MDL. CHECK
^{139}La	$\sigma_{n,\gamma}$	5.0+5	4.0+6	Expt	DOE-NDC-30	4	Apr83	ANL	Poenitz.NDG.REL AU
^{140}Ce	σ_{tot}	2.5+6	6.0+7	Expt	DOE-NDC-30	81	Apr83	LRL	Phillips+ OPT.MDL. CHECK
^{140}Ce	$\sigma_{el}(\theta)$	1.5+7		Expt	DOE-NDC-30	79	Apr83	LRL	Hansen+EN=14.6MEV.NDG
^{140}Ce	$\sigma_{dif.inl}$	1.5+7		Expt	DOE-NDC-30	79	Apr83	LRL	Hansen+EN=14.6MEV.NDG
^{142}Ce	σ_{tot}	2.5+6	6.0+7	Expt	DOE-NDC-30	81	Apr83	LRL	Phillips+ OPT.MDL. CHECK
^{141}Pr	σ_{tot}	2.5+6	6.0+7	Expt	DOE-NDC-30	81	Apr83	LRL	Phillips+ OPT.MDL. CHECK
Nd	σ_{tot}	1.9+6	2.0+7	Expt	DOE-NDC-30	4	Apr83	ANL	Poenitz+NDG.
^{142}Nd	$\sigma_{n,\gamma}$	1.0+3	2.5+5	Expt	DOE-NDC-30	81	Apr83	KFK	Mathews+CS(30KEV)=62+-6 MB
^{143}Nd	$\sigma_{n,\gamma}$	1.0+3	2.5+5	Expt	DOE-NDC-30	81	Apr83	KFK	Mathews+CS(30KEV)=298+-28 MB
^{144}Nd	$\sigma_{n,\gamma}$	1.0+3	2.5+5	Expt	DOE-NDC-30	81	Apr83	KFK	Mathews+CS(30KEV)=154+-8 MB

NEUTRON DATA REFERENCES

Element	Quantity	Energy (eV) Min	Max	Type	Documentation Ref	Page	Date	Lab	Comments
Eu	$\sigma_{n,\gamma}$	5.0+5	4.0+6	Expt	DOE-NDC-30	4	Apr83	ANL	Poenitz.NDG.REL AU
Gd	$\sigma_{n,\gamma}$	5.0+5	4.0+6	Expt	DOE-NDC-30	4	Apr83	ANL	Poenitz.NDG.REL AU
^{159}Tb	$\sigma_{n,\gamma}$	5.0+5	4.0+6	Expt	DOE-NDC-30	4	Apr83	ANL	Poenitz.NDG.REL AU
Dy	$\sigma_{n,\gamma}$	5.0+5	4.0+6	Expt	DOE-NDC-30	4	Apr83	ANL	Poenitz.NDG.REL AU
Er	$\sigma_{n,\gamma}$	5.0+5	4.0+6	Expt	DOE-NDC-30	4	Apr83	ANL	Poenitz.NDG.REL AU
^{169}Tm	σ_{tot}	NDG		Theo	DOE-NDC-30	100	Apr83	LAS	Young+NDG.
^{169}Tm	$\sigma_{el}(\theta)$	5.7+5		Theo	DOE-NDC-30	100	Apr83	LAS	Young+GRPH.CALC ANGDIST CFD EXPT
^{169}Tm	$\sigma_{dif.inl}$	5.7+5		Theo	DOE-NDC-30	100	Apr83	LAS	Young+GRPH.CALC ANGDIST CFD EXPT
^{169}Tm	$\sigma_{n,\gamma}$	NDG		Theo	DOE-NDC-30	100	Apr83	LAS	Young+NDG.
^{169}Tm	$\sigma_{n,2n}$	NDG		Theo	DOE-NDC-30	100	Apr83	LAS	Young+NDG.
^{169}Tm	$\sigma_{n,xn}$	NDG		Theo	DOE-NDC-30	100	Apr83	LAS	Young+NDG.
Yb	$\sigma_{n,\gamma}$	5.0+5	4.0+6	Expt	DOE-NDC-30	4	Apr83	ANL	Poenitz.NDG.REL AU
Hf	σ_{tot}	1.9+6	2.0+7	Expt	DOE-NDC-30	4	Apr83	ANL	Poenitz+NDG.
Hf	$\sigma_{n,\gamma}$	5.0+5	4.0+6	Expt	DOE-NDC-30	4	Apr83	ANL	Poenitz.NDG.REL AU
^{181}Ta	σ_{tot}	1.9+6	2.0+7	Expt	DOE-NDC-30	4	Apr83	ANL	Poenitz+NDG.
^{181}Ta	$\sigma_{el}(\theta)$	1.5+7		Expt	DOE-NDC-30	88	Apr83	LRL	Dietrich+GRPH.EN=14.6MEV,OM CFD XPT
^{181}Ta	$\sigma_{n,\alpha}$	8.0+6	1.5+7	Expt	DOE-NDC-30	172	Apr83	AI	Kneff+ NDG.
W	$\sigma_{n,\gamma}$	5.0+5	4.0+6	Expt	DOE-NDC-30	4	Apr83	ANL	Poenitz.NDG.REL AU
W	$\sigma_{n,\alpha}$	8.0+6	1.5+7	Expt	DOE-NDC-30	172	Apr83	AI	Kneff+ TBD.
^{182}W	$\sigma_{dif.inl}$	Fast		Expt	DOE-NDC-30	8	Apr83	ANL	Guenther+ ANALYSIS TBD
^{182}W	$\sigma_{n,n'\gamma}$	Fast		Expt	DOE-NDC-30	8	Apr83	ANL	Guenther+ ANALYSIS TBD
^{184}W	$\sigma_{dif.inl}$	Fast		Expt	DOE-NDC-30	8	Apr83	ANL	Guenther+ ANALYSIS TBD
^{184}W	$\sigma_{n,n'\gamma}$	Fast		Expt	DOE-NDC-30	8	Apr83	ANL	Guenther+ ANALYSIS TBD
^{186}W	$\sigma_{dif.inl}$	Fast		Expt	DOE-NDC-30	8	Apr83	ANL	Guenther+ ANALYSIS TBD
^{186}W	$\sigma_{n,n'\gamma}$	Fast		Expt	DOE-NDC-30	8	Apr83	ANL	Guenther+ ANALYSIS TBD
Re	$\sigma_{n,\gamma}$	5.0+5	4.0+6	Expt	DOE-NDC-30	4	Apr83	ANL	Poenitz.NDG.REL AU
^{187}Os	$\sigma_{el}(\theta)$	6.1+4		Expt	DOE-NDC-30	66	Apr83	KTY	Hershberger+ANISOTROPIES MEAS.
^{187}Os	$\sigma_{dif.inl}$	NDG		Expt	DOE-NDC-30	66	Apr83	KTY	Hershberger+CS(9.75 KEV LVL) MEAS
^{187}Os	$\sigma_{dif.inl}$	3.4+4		Expt	DOE-NDC-30	137	Apr83	ORL	Macklin+CS(9.75 KEV LVL)=1.5+-0.2 B
^{188}Os	$\sigma_{el}(\theta)$	6.1+4		Expt	DOE-NDC-30	66	Apr83	KTY	Hershberger+ANISOTROPIES MEAS.
^{190}Os	$\sigma_{el}(\theta)$	2.5+6	4.0+6	Expt	DOE-NDC-30	67	Apr83	KTY	Cao+CS MEAS.ANALY TBD
^{190}Os	$\sigma_{dif.inl}$	2.5+6	4.0+6	Expt	DOE-NDC-30	67	Apr83	KTY	Cao+CS MEAS.ANALY TBD
^{192}Os	$\sigma_{el}(\theta)$	2.5+6		Expt	DOE-NDC-30	67	Apr83	KTY	Cao+CS MEAS.ANALY TBD

NEUTRON DATA REFERENCES

Element	Quantity	Energy (eV) Min	Max	Type	Documentation Ref	Page	Date	Lab	Comments
^{192}Os	$\sigma_{dif.inl}$	2.5+6		Expt	DOE-NDC-30	67	Apr83	KTY	Cao+CS MEAS.ANALY TBD
Pt	σ_{tot}	1.9+6	2.0+7	Expt	DOE-NDC-30	4	Apr83	ANL	Poenitz+NDG.
Pt	$\sigma_{n,\gamma}$	5.0+5	4.0+6	Expt	DOE-NDC-30	4	Apr83	ANL	Poenitz.NDG.REL AU
^{197}Au	σ_{tot}	1.9+6	2.0+7	Expt	DOE-NDC-30	4	Apr83	ANL	Poenitz+NDG.
^{197}Au	$\sigma_{el}(\theta)$	1.5+7		Expt	DOE-NDC-30	79	Apr83	LRL	Hansen+EN=14.6MEV.NDG
^{197}Au	$\sigma_{dif.inl}$	1.5+7		Expt	DOE-NDC-30	79	Apr83	LRL	Hansen+EN=14.6MEV.NDG
Pb	Evaluation	NDG		Eval	DOE-NDC-30	145	Apr83	ORL	Fu. NDG
Pb	$\sigma_{el}(\theta)$	1.0+7		Expt	DOE-NDC-30	180	Apr83	TNL	Anderson+GRPHS.LOW ANGLE
^{206}Pb	$\sigma_{el}(\theta)$	7.0+6		Expt	DOE-NDC-30	68	Apr83	KTY	Hanly+ NDG.
^{206}Pb	$\sigma_{dif.inl}$	7.0+6		Expt	DOE-NDC-30	68	Apr83	KTY	Hanly+ NDG.
^{208}Pb	σ_{tot}	7.0+6	2.6+7	Exth	DOE-NDC-30	88	Apr83	LRL	Dietrich+OPT.MDL.CALC CFD EXPT
^{208}Pb	$\sigma_{el}(\theta)$	7.0+6		Expt	DOE-NDC-30	68	Apr83	KTY	Hanly+ NDG.
^{208}Pb	$\sigma_{el}(\theta)$	7.0+6	2.6+7	Exth	DOE-NDC-30	88	Apr83	LRL	Dietrich+GRPH EN=14.6MEV OM CFD EXPT
^{208}Pb	$\sigma_{el}(\theta)$	7.2+6	2.4+7	Exth	DOE-NDC-30	155	Apr83	OHO	Dietrich+NDG.MEAS ANGDIST CFD CALC
^{208}Pb	$\sigma_{el}(\theta)$	4.0+6	6.0+6	Expt	DOE-NDC-30	151	Apr83	OHO	Annand+ NDG
^{208}Pb	$\sigma_{el}(\theta)$	1.0+7		Exth	DOE-NDC-30	177	Apr83	TNL	Byrd+NDG.CC CALC.TBP NP/A
^{208}Pb	$\sigma_{dif.inl}$	7.0+6		Expt	DOE-NDC-30	68	Apr83	KTY	Hanly+ NDG.
^{208}Pb	$\sigma_{dif.inl}$	4.0+6	6.0+6	Expt	DOE-NDC-30	151	Apr83	OHO	Annand+ NDG
^{208}Pb	$\sigma_{dif.inl}$	1.0+7		Exth	DOE-NDC-30	177	Apr83	TNL	Byrd+NDG.CC CALC.TBP NP/A
^{208}Pb	$\sigma_{n,n'\gamma}$	4.0+6	7.0+6	Expt	DOE-NDC-30	68	Apr83	KTY	Hanly+ NDG.
^{209}Bi	$\sigma_{el}(\theta)$	1.5+7		Expt	DOE-NDC-30	88	Apr83	LRL	Dietrich+GRPH.EN=14.6MEV,OM CFD XPT
^{209}Bi	$\sigma_{el}(\theta)$	4.0+6	6.0+6	Expt	DOE-NDC-30	151	Apr83	OHO	Annand+ NDG
^{209}Bi	$\sigma_{dif.inl}$	4.0+6	6.0+6	Expt	DOE-NDC-30	151	Apr83	OHO	Annand+ NDG
^{232}Th	σ_{tot}	1.8+6	2.2+7	Expt	DOE-NDC-30	1	Apr83	ANL	Poenitz+GRPH.CFD ENDF/B-V
^{232}Th	$\sigma_{el}(\theta)$	1.5+7		Expt	DOE-NDC-30	88	Apr83	LRL	Dietrich+GRPH.EN=14.6MEV,OM CFD XPT
^{232}Th	$\sigma_{el}(\theta)$	2.0+5	9.0+5	Expt	DOE-NDC-30	108	Apr83	LTI	Beghian+NDG.TBC
^{232}Th	$\sigma_{el}(\theta)$	9.0+5	2.4+6	Expt	DOE-NDC-30	108	Apr83	LTI	Beghian+GRPHS.
^{232}Th	σ_{inl}	1.0+6	4.0+6	Expt	DOE-NDC-30	3	Apr83	ANL	Smith+DERIVED CS CFD ENDF/B-V
^{232}Th	$\sigma_{dif.inl}$		1.0+6	Expt	DOE-NDC-30	1	Apr83	ANL	Smith+ TBC
^{232}Th	$\sigma_{dif.inl}$	2.0+5	9.0+5	Expt	DOE-NDC-30	108	Apr83	LTI	Beghian+NDG.TBC
^{232}Th	$\sigma_{dif.inl}$	8.0+5	3.5+6	Theo	DOE-NDC-30	112	Apr83	LTI	Sheldon+CALC CFD MEAS.NDG
^{232}Th	$\sigma_{dif.inl}$	9.0+5	2.4+6	Expt	DOE-NDC-30	108	Apr83	LTI	Beghian+GRPHS.
^{232}Th	$\sigma_{n,\gamma}$	2.3+4		Expt	DOE-NDC-30	122	Apr83	MHG	Wilderman+NDG XPT 10PCT GT EVAL.

NEUTRON DATA REFERENCES

Element	Quantity	Energy (eV) Min	Max	Type	Documentation Ref	Page	Date	Lab	Comments
^{232}Th	$\sigma_{n,\gamma}$	1.4+5	9.6+5	Expt	DOE-NDC-30	122	Apr83	MHG	Wilderman+MEAS 140,265,964 KEV.TBD
^{232}Th	$\sigma_{n,n'\gamma}$	9.0+5	2.4+6	Expt	DOE-NDC-30	108	Apr83	LTI	Beghian+GRPHS.
^{232}Th	$\sigma_{n,f}$	7.0+5	3.0+7	Expt	DOE-NDC-30	130	Apr83	LRL	Behrens+NSE 81,512 (82)
^{232}Th	$\sigma_{n,f}$	Fiss		Expt	DOE-NDC-30	124	Apr83	NBS	Grundl+TBL.252CF SPECTRUM
^{232}Th	$\sigma_{n,f}$	1.0+2	1.6+6	Expt	DOE-NDC-30	139	Apr83	ORL	Perez+ NDG. TBP NSE
^{232}Th	Frag Spectra	1.0+6	3.0+7	Expt	DOE-NDC-30	94	Apr83	LAS	Moore+FF ANG,E DIST.NDG
U	$\sigma_{el}(\theta)$	2.6+7	3.0+7	Expt	DOE-NDC-30	79	Apr83	LRL	Hansen+PRELIMINARY.NDG
^{233}U	σ_{tot}	1.8+6	2.2+7	Expt	DOE-NDC-30	1	Apr83	ANL	Poenitz+GRPH.CFD ENDF/B-V
^{233}U	σ_{inl}	1.0+6	4.0+6	Expt	DOE-NDC-30	3	Apr83	ANL	Smith+DERIVED CS CFD ENDF/B-V
^{233}U	$\sigma_{dif.inl}$		1.0+6	Expt	DOE-NDC-30	1	Apr83	ANL	Smith+ TBD
^{233}U	$\sigma_{n,f}$	1.5+7		Expt	DOE-NDC-30	118	Apr83	MHG	Mahdavi+EN=14.63MEV TBC
^{233}U	$\sigma_{n,f}$	Fiss		Expt	DOE-NDC-30	124	Apr83	NBS	Grundl+TBL.252CF SPECTRUM
^{233}U	Frag Spectra	1.5+7		Expt	DOE-NDC-30	120	Apr83	MHG	Mahdavi+EN=14.63 MEV TBC
^{235}U	σ_{tot}	1.8+6	2.2+7	Expt	DOE-NDC-30	1	Apr83	ANL	Poenitz+GRPH.CFD ENDF/B-V
^{235}U	σ_{inl}	1.0+6	4.0+6	Expt	DOE-NDC-30	3	Apr83	ANL	Smith+DERIVED CS CFD ENDF/B-V
^{235}U	$\sigma_{dif.inl}$		1.0+6	Expt	DOE-NDC-30	1	Apr83	ANL	Smith+ TBD
^{235}U	$\sigma_{n,f}$	1.0+5	9.4+6	Expt	DOE-NDC-30	9	Apr83	ANL	Meadows.GRPHS NP/235U CFD ENDF,EXPT
^{235}U	$\sigma_{n,f}$	7.0+5	3.0+7	Expt	DOE-NDC-30	130	Apr83	LRL	Behrens+NSE 81,512 (82)
^{235}U	$\sigma_{n,f}$	1.0+5	5.0+6	Theo	DOE-NDC-30	91	Apr83	LRL	White.NDG
^{235}U	$\sigma_{n,f}$	1.5+7		Expt	DOE-NDC-30	118	Apr83	MHG	Mahdavi+EN=14.63MEV GRPH CFD OTHR
^{235}U	$\sigma_{n,f}$	2.6+6		Expt	DOE-NDC-30	124	Apr83	NBS	Duvall+NDG.ASSOC.PART.TECHN.TBC
^{235}U	$\sigma_{n,f}$	Fiss		Expt	DOE-NDC-30	124	Apr83	NBS	Schroeder+NDG.252CF SOURCE.TBC
^{235}U	$\sigma_{n,f}$	2.0+6	6.0+6	Expt	DOE-NDC-30	123	Apr83	NBS	Dias+DUAL THIN SCINT.DET.NDG
^{235}U	$\sigma_{n,f}$	3.0+5	3.0+6	Expt	DOE-NDC-30	123	Apr83	NBS	Carlson+TOF BLACK DET.ANALY.TBD
^{235}U	$\sigma_{n,f}$	Fiss		Expt	DOE-NDC-30	124	Apr83	NBS	Grundl+TBL.252CF SPECTRUM
^{235}U	$\sigma_{n,f}$	5.0+3	2.0+7	Expt	DOE-NDC-30	141	Apr83	ORL	Weston+RATIO TO 239PU,240PU CFD ENDF
^{235}U	$\sigma_{n,f}$		1.0+5	Expt	DOE-NDC-30	95	Apr83	GEL	Moore+ NDG.
^{235}U	ν_d	Fast		Expt	DOE-NDC-30	113	Apr83	LTI	Couchell+LOW ENERGY SPECTRA STUDIED
^{235}U	ν_d	2.5-2		Expt	DOE-NDC-30	113	Apr83	LTI	Couchell+LOW ENERGY SPECTRA STUDIED
^{235}U	Frag Spectra	1.0+6	3.0+7	Expt	DOE-NDC-30	94	Apr83	LAS	Moore+FF ANG,E DIST.NDG
^{235}U	Frag Spectra	1.5+7		Expt	DOE-NDC-30	120	Apr83	MHG	Mahdavi+EN=14.63MEV.YLD(0)/(90DEGS)
^{238}U	σ_{tot}	4.4+4	2.0+7	Eval	DOE-NDC-30	13	Apr83	ANL	Smith+AGREES WITH ENDF/B-V
^{238}U	σ_{tot}	1.8+6	2.2+7	Expt	DOE-NDC-30	1	Apr83	ANL	Poenitz+GRPH.CFD ENDF/B-V

NEUTRON DATA REFERENCES

Element	Quantity	Energy (eV) Min	Max	Type	Documentation Ref	Page	Date	Lab	Comments
^{238}U	σ_{tot}	1.0+3	1.0+4	Expt	DOE-NDC-30	142	Apr83	ORL	Perez. TBD
^{238}U	$\sigma_{el}(\theta)$	1.5+7		Expt	DOE-NDC-30	88	Apr83	LRL	Dietrich+GRPH.EN=14.6MEV,OM CFD XPT
^{238}U	$\sigma_{el}(\theta)$	9.0+5	2.4+6	Expt	DOE-NDC-30	108	Apr83	LTI	Beghian+NDG
^{238}U	$\sigma_{el}(\theta)$	2.0+5	9.0+5	Expt	DOE-NDC-30	108	Apr83	LTI	Beghian+NDG.TBC
^{238}U	σ_{inl}	1.0+6	4.0+6	Expt	DOE-NDC-30	3	Apr83	ANL	Smith+DERIVED CS CFD ENDF/B-V
^{238}U	$\sigma_{dif.inl}$		1.0+6	Expt	DOE-NDC-30	1	Apr83	ANL	Smith+GRPH.MDL CALC TBD
^{238}U	$\sigma_{dif.inl}$	2.0+5	9.0+5	Expt	DOE-NDC-30	108	Apr83	LTI	Beghian+NDG.TBC
^{238}U	$\sigma_{dif.inl}$	8.0+5	3.5+6	Theo	DOE-NDC-30	112	Apr83	LTI	Sheldon+CALC CFD MEAS.NDG
^{238}U	$\sigma_{dif.inl}$	9.0+5	2.4+6	Expt	DOE-NDC-30	108	Apr83	LTI	Beghian+NDG
^{238}U	$\sigma_{n,\gamma}$	1.0+3	1.0+4	Expt	DOE-NDC-30	142	Apr83	ORL	Perez. TBD
^{238}U	$\sigma_{n,n'\gamma}$	9.0+5	2.4+6	Expt	DOE-NDC-30	108	Apr83	LTI	Beghian+NDG
^{238}U	$\sigma_{n,f}$	1.5+7		Expt	DOE-NDC-30	118	Apr83	MHG	Mahdavi+EN=14.63MEV TBC
^{238}U	$\sigma_{n,f}$	Fiss		Expt	DOE-NDC-30	124	Apr83	NBS	Grundl+TBL 252CF,235U,239PU SPECTRA
^{238}U	ν_d	Fast		Theo	DOE-NDC-30	106	Apr83	LAS	England+GRPHS CALC SPECTRA CFD ENDF
^{238}U	ν_d	NDG		Expt	DOE-NDC-30	113	Apr83	LTI	Couchell+NDG
^{238}U	Frag Spectra	1.9+6	9.0+6	Expt	DOE-NDC-30	9	Apr83	ANL	Meadows.ANG,E DIST REL 235U
^{238}U	Frag Spectra	1.0+6	3.0+7	Expt	DOE-NDC-30	94	Apr83	LAS	Moore+FF ANG,E DIST.NDG
^{238}U	Frag Spectra	1.5+7		Expt	DOE-NDC-30	120	Apr83	MHG	Mahdavi+EN=14.63 MEV TBC
^{236}Np	$\sigma_{n,f}$	2.5-2		Expt	DOE-NDC-30	82	Apr83	LRL	Lindner+TBL,REL U235 NF +CAPT/FISS
^{236}Np	Fiss.Yield	2.5-2		Expt	DOE-NDC-30	82	Apr83	LRL	Lindner+GRPH YLDS FROM GAMMA PEAKS
^{237}Np	σ_{tot}	NDG		Expt	DOE-NDC-30	95	Apr83	LAS	Moore+NDG.RES.SPINS ASSIGNED
^{237}Np	$\sigma_{n,f}$	1.0+5	9.4+6	Expt	DOE-NDC-30	9	Apr83	ANL	Meadows.GRPHS NP/235U CFD ENDF,EXPT
^{237}Np	$\sigma_{n,f}$	NDG		Expt	DOE-NDC-30	95	Apr83	LAS	Moore+NDG.RES.SPINS ASSIGNED
^{237}Np	$\sigma_{n,f}$	1.5+7		Expt	DOE-NDC-30	118	Apr83	MHG	Mahdavi+EN=14.63MEV TBC
^{237}Np	$\sigma_{n,f}$	Fiss		Expt	DOE-NDC-30	124	Apr83	NBS	Grundl+TBL 252CF,235U,239PU SPECTRA
^{237}Np	Frag Spectra	1.5+7		Expt	DOE-NDC-30	120	Apr83	MHG	Mahdavi+EN=14.63 MEV TBC
^{237}Np	Res.Params.	NDG		Expt	DOE-NDC-30	95	Apr83	LAS	Moore+NDG.RES.SPINS ASSIGNED
^{235}Pu	$\sigma_{n,f}$	+6	2.0+7	Exth	DOE-NDC-30	130	Apr83	NBS	Behrens.GRPH SYSTEMATIC STUDY
^{236}Pu	$\sigma_{n,f}$	+6	2.0+7	Exth	DOE-NDC-30	130	Apr83	NBS	Behrens.GRPH SYSTEMATIC STUDY
^{237}Pu	$\sigma_{n,f}$	+6	2.0+7	Exth	DOE-NDC-30	130	Apr83	NBS	Behrens.GRPH SYSTEMATIC STUDY
^{238}Pu	$\sigma_{n,f}$	+6	2.0+7	Exth	DOE-NDC-30	130	Apr83	NBS	Behrens.GRPH SYSTEMATIC STUDY
^{239}Pu	σ_{tot}	1.8+6	2.2+7	Expt	DOE-NDC-30	1	Apr83	ANL	Poenitz+GRPH.CFD ENDF/B-V
^{239}Pu	$\sigma_{el}(\theta)$	1.0+4	2.0+7	Theo	DOE-NDC-30	102	Apr83	LAS	Arthur.NDG

NEUTRON DATA REFERENCES

Element	Quantity	Energy (eV) Min	Max	Type	Documentation Ref	Page	Date	Lab	Comments
^{239}Pu	σ_{inl}	1.0+6	4.0+6	Expt	DOE-NDC-30	3	Apr83	ANL	Smith+DERIVED CS CFD ENDF/B-V
^{239}Pu	σ_{inl}	1.0+4	2.0+7	Theo	DOE-NDC-30	102	Apr83	LAS	Arthur.GRPH CFD ENDF/B-V
^{239}Pu	$\sigma_{dif.inl}$		1.0+6	Expt	DOE-NDC-30	1	Apr83	ANL	Smith+ TBD
^{239}Pu	$\sigma_{dif.inl}$	1.0+4	2.0+7	Theo	DOE-NDC-30	102	Apr83	LAS	Arthur.GRPH CFD EXPT
^{239}Pu	$\sigma_{n,f}$	1.0+4	2.0+7	Theo	DOE-NDC-30	102	Apr83	LAS	Arthur.NDG
^{239}Pu	$\sigma_{n,f}$	1.5+7		Expt	DOE-NDC-30	118	Apr83	MHG	Mahdavi+EN=14.63MEV GRPH CFD OTHR
^{239}Pu	$\sigma_{n,f}$	+6	2.0+7	Exth	DOE-NDC-30	130	Apr83	NBS	Behrens.GRPH SYSTEMATIC STUDY
^{239}Pu	$\sigma_{n,f}$	Fiss		Expt	DOE-NDC-30	124	Apr83	NBS	Grundl+TBL 252CF,235U SPECTRA
^{239}Pu	$\sigma_{n,f}$	5.0+3	2.0+7	Expt	DOE-NDC-30	141	Apr83	ORL	Weston+RATIO TO 235U,240PU CFD ENDF
^{239}Pu	ν_d	NDG		Expt	DOE-NDC-30	113	Apr83	LTI	Couchell+NDG
^{239}Pu	Fiss.Yield	1.7+5	7.9+6	Expt	DOE-NDC-30	11	Apr83	ANL	Gindler+GRPH CFD 14MEV VALUE
^{239}Pu	Frag Spectra	1.5+7		Expt	DOE-NDC-30	120	Apr83	MHG	Mahdavi+EN=14.63MEV.YLD(0)/(90DEGS)
^{240}Pu	σ_{tot}	1.8+6	2.2+7	Expt	DOE-NDC-30	1	Apr83	ANL	Poenitz+GRPH.CFD ENDF/B-V
^{240}Pu	σ_{inl}	1.0+6	4.0+6	Expt	DOE-NDC-30	3	Apr83	ANL	Smith+DERIVED CS CFD ENDF/B-V
^{240}Pu	$\sigma_{dif.inl}$		1.0+6	Expt	DOE-NDC-30	1	Apr83	ANL	Smith+ TBC
^{240}Pu	$\sigma_{dif.inl}$	8.0+5	3.5+6	Theo	DOE-NDC-30	112	Apr83	LTI	Sheldon+CALC CFD MEAS.NDG
^{240}Pu	$\sigma_{n,\gamma}$	Fast		Revw	DOE-NDC-30	141	Apr83	ORL	Weston.NDG.PROBLEMS DISCUSSED
^{240}Pu	$\sigma_{n,f}$	+6	2.0+7	Exth	DOE-NDC-30	130	Apr83	NBS	Behrens.GRPH SYSTEMATIC STUDY
^{240}Pu	$\sigma_{n,f}$	Fiss		Expt	DOE-NDC-30	124	Apr83	NBS	Grundl+TBL.252CF SPECTRUM
^{240}Pu	$\sigma_{n,f}$	5.0+3	2.0+7	Expt	DOE-NDC-30	141	Apr83	ORL	Weston+RATIO TO 235U,239PU CFD ENDF
^{241}Pu	$\sigma_{n,\gamma}$	Fast		Revw	DOE-NDC-30	141	Apr83	ORL	Weston.NDG.PROBLEMS DISCUSSED
^{241}Pu	$\sigma_{n,f}$	+6	2.0+7	Exth	DOE-NDC-30	130	Apr83	NBS	Behrens.GRPH SYSTEMATIC STUDY
^{241}Pu	$\sigma_{n,f}$	Fiss		Expt	DOE-NDC-30	124	Apr83	NBS	Grundl+TBL.252CF SPECTRUM
^{242}Pu	$\sigma_{dif.inl}$	8.0+5	3.5+6	Theo	DOE-NDC-30	112	Apr83	LTI	Sheldon+CALC CFD MEAS. NDG
^{242}Pu	$\sigma_{n,\gamma}$	Fast		Revw	DOE-NDC-30	141	Apr83	ORL	Weston.NDG.PROBLEMS DISCUSSED
^{242}Pu	$\sigma_{n,f}$	+6	2.0+7	Exth	DOE-NDC-30	130	Apr83	NBS	Behrens.GRPH SYSTEMATIC STUDY
^{243}Pu	$\sigma_{n,f}$	+6	2.0+7	Exth	DOE-NDC-30	130	Apr83	NBS	Behrens.GRPH SYSTEMATIC STUDY
^{244}Pu	$\sigma_{n,f}$	+6	2.0+7	Exth	DOE-NDC-30	130	Apr83	NBS	Behrens.GRPH SYSTEMATIC STUDY
^{245}Pu	$\sigma_{n,f}$	+6	2.0+7	Exth	DOE-NDC-30	130	Apr83	NBS	Behrens.GRPH SYSTEMATIC STUDY
^{246}Pu	$\sigma_{n,f}$	+6	2.0+7	Exth	DOE-NDC-30	130	Apr83	NBS	Behrens.GRPH SYSTEMATIC STUDY
^{241}Am	$\sigma_{n,\gamma}$	Fast		Revw	DOE-NDC-30	141	Apr83	ORL	Weston.NDG.PROBLEMS DISCUSSED
^{243}Am	$\sigma_{n,\gamma}$	NDG		Eval	DOE-NDC-30	41	Apr83	HED	Mann+H-F CALC.NDG
^{243}Cm	Fiss.Yield	2.5-2		Expt	DOE-NDC-30	138	Apr83	ORL	Breederland.NDG ABST ORNL-TM-8168

NEUTRON DATA REFERENCES

Element	Quantity	Energy (eV) Min	Max	Type	Documentation Ref	Page	Date	Lab	Comments
^{244}Cm	$\sigma_{n,f}$	1.0-1	8.0+4	Expt	DOE-NDC-30	155	Apr83	RPI	Block+GRPHS.CFD ENDF.REL 235U
^{245}Cm	$\sigma_{n,f}$	1.0+5	5.0+6	Theo	DOE-NDC-30	91	Apr83	LRL	White.NDG
^{246}Cm	$\sigma_{n,f}$	1.0-1	8.0+4	Expt	DOE-NDC-30	155	Apr83	RPI	Block+GRPHS.CFD ENDF.REL 235U
^{248}Cm	$\sigma_{n,f}$	1.0-1	8.0+4	Expt	DOE-NDC-30	155	Apr83	RPI	Block+GRPHS.CFD ENDF.REL 235U
^{252}Cf	ν_p	Spon		Theo	DOE-NDC-30	104	Apr83	LAS	Madland+PROMPT NU=3.783
^{252}Cf	Spect.fiss n	Spon		Expt	DOE-NDC-30	11	Apr83	ANL	Poenitz+AVG.EN.LOWER THAN CALC.
^{252}Cf	Spect.fiss n	Spon		Theo	DOE-NDC-30	104	Apr83	LAS	Madland+GRPH CFD XPT.EBAR=2.168MEV

ARGONNE NATIONAL LABORATORY

A. NEUTRON PHYSICS

1. Neutron Total Cross Sections of the Actinides from 1.8 to 20 MeV
(W. P. Poenitz and J. F. Whalen)

Previously reported measurements of the neutron total cross sections of the actinide nuclides ^{232}Th, ^{233}U, ^{235}U, ^{238}U, ^{239}Pu and ^{240}Pu[1] were extended to the higher-energy range. Measurements were possible up to ~ 22 MeV by utilizing the Li(d,n) reaction with a thick target as a neutron source. A Black Neutron detector with pulse-shape discrimination was used as a neutron detector. Background was determined with a shadowbar in place of one of the samples on the eight-position sample changer used in these measurements. The energy scale was determined from ^{12}C resonances.

The results from the new measurements are in very good agreement with our previous monoenergetic measurements in the overlap range from 1.8 to 4.5 MeV (see Fig. A-1). The present data were compared with ENDF/B-V over the entire energy range of the present measurement program. The values for the neutron total cross sections of ^{233}U and ^{238}U in ENDF/B-V were found to be in good agreement with the present results. ENDF/B-V data for ^{232}Th, ^{235}U, and ^{240}Pu are reasonable, though low for ^{232}Th between 100 and 500 keV, and above 8 MeV and low for ^{235}U between 100 and 500 keV. The ENDF/B-V data for ^{240}Pu are low between 60 and 700 keV, low between 2.5 and 6.5 MeV, and high above 8 MeV. The outstanding feature of ENDF/B-V for ^{240}Pu is an unphysical shape over the whole energy range. The poorest ENDF/B-V neutron total cross section is that for ^{239}Pu between 30 keV and 700 keV. The present measurements are very well described by an optical model.

[1] W. Poenitz et al., Nucl. Sci. and Eng. 78, 333 (1981).

2. Actinide-Scattering Cross Sections Below 1.0 MeV
(A. Smith and P. Guenther)

The importance of precise inelastic-scattering cross sections of the prominent actinides at several reference energies below 1.0 MeV, suitable for accurate normalization of model calculations, was recognized at the Paris Meeting on inelastic-neutron scattering (NEANDC-158"U") and it was recommended that such measurements be made. They are now in progress at ANL with targets of ^{232}Th, ^{233}U, ^{235}U, ^{238}U, ^{239}Pu and ^{240}Pu. Preliminary results to ± 3% accuracies are available for ^{232}Th, ^{238}U and ^{240}Pu, as illustrated by the ^{238}U results shown in Fig. A-2. The ^{238}U results preclude fluctuations in the inelastic-scattering cross section beyond ± 5% for several hundred keV about 500 keV, in contrast to the trends of some previously reported measurements. The ^{238}U angle-integrated inelastic-scattering

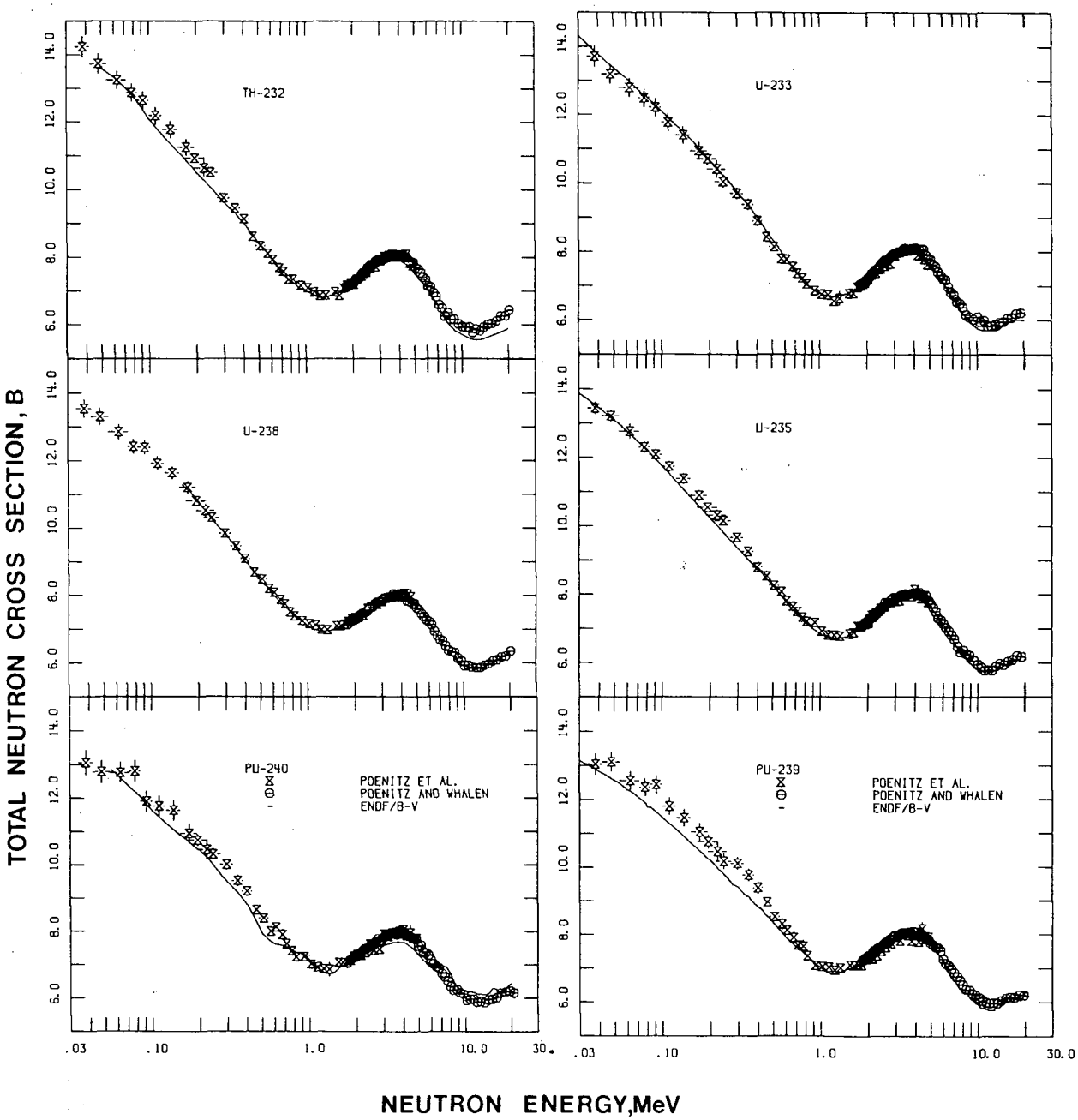

Fig. A-1. Measured (data symbols) and evaluated (curves) actinide neutron total cross sections.

cross sections are slightly lower than given in ENDF/B-V but the differences are smaller than the uncertainties associated with the evaluation alone. Extensive model interpretations of the experimental results are now in progress using a new version of the computer code ECIS including careful attention to compound-nucleus, capture and fission processes, as discussed below. In detail, the calculations tend to underpredict the inelastic-

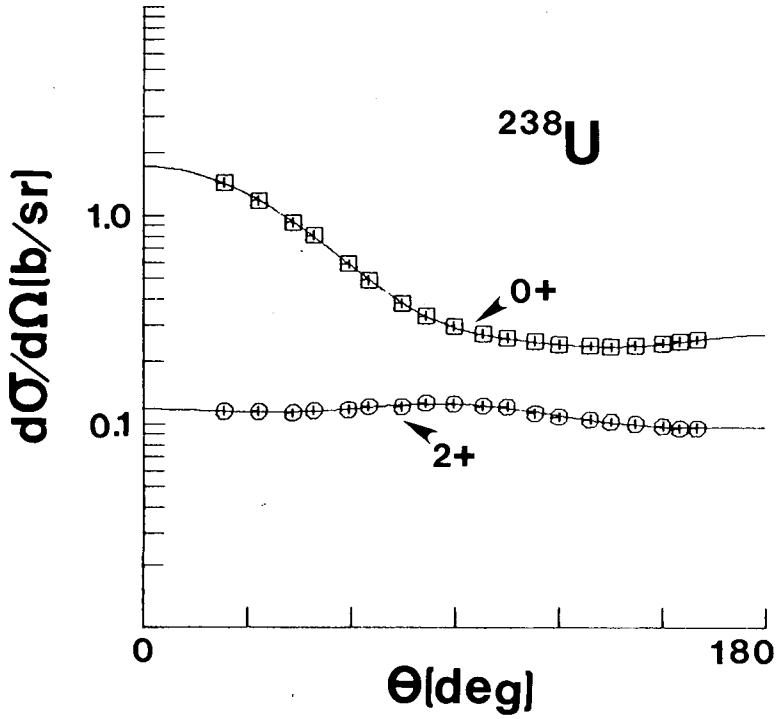

Fig. A-2. Cross Sections for the elastic (0+) and inelastic (2+, 44 keV) scattering of 598 keV neutrons from ^{238}U.

scattering cross-section magnitude in the manner that has been historically evident for many years although the difference is much smaller than usually reported.

3. Neutron Total Inelastic-Scattering Cross Sections of ^{232}Th, ^{233}U, ^{235}U, ^{238}U, ^{239}Pu and ^{240}Pu (A. B. Smith, P. T. Guenther and R. D. McKnight)

The measurements of neutron emission and total cross sections from 1-4 MeV and the derivation of the total inelastic-scattering cross section, outlined in the previous report, have been completed and the results reported at the Antwerp Conference. The additional results confirm the preliminary conclusions[1] that the experimentally deduced total inelastic-scattering cross sections of ^{232}Th and ^{238}U are consistent with ENDF/B-V to within the 5-8% experimental uncertainty. Similar consistencies are found for ^{233}U and ^{235}U to within the experimental uncertainties of 10-12%. However, the experimentally-based results for ^{240}Pu are 25-30% smaller than the evaluated inelastic cross sections of ENDF/B-V and 30-50% smaller for ^{239}Pu. These are two large discrepancies in important FBR core materials. A modified version of the ENDF/B-V ^{239}Pu file was prepared consistent with the above experimentally-based inelastic-scattering cross

sections. Other aspects of the ENDF/B-V file were kept constant (excepting only the elastic cross sections which were adjusted to obtain the necessary internal consistency) so that a direct assessment of the impact of changes in the inelastic-scattering cross sections could be made. The revised file is similar to that of Antsipov et al.[2] in the energy-averaged region. The impact of the changes in the inelastic-scattering cross sections was assessed using two extremes of critical enrichment; i) JEZEBEL (100%), and ii) ZPR-6/7 (very low enrichment FBR critical). In the case of JEZEBEL the changes in inelastic scattering had a large impact (e.g. +0.5% in eigenvalue and +3.7% in f28/f49). The effect was modest for the low-enrichment ZPR-6/7 assembly (e.g. +0.1% in eigenvalue and +0.6% in f28/f49). A realistic LMFBR core will lie between these two extremes and there will be an additional impact due to ^{240}Pu (which may be of 20-30% isotopic abundance) where similar large changes in the inelastic-scattering cross sections are indicated.

1 A. Smith and P. Guenther, ANL/NDM-63 (1982).
2 G. Antsipov et al., INDC(CCP)-116/CHJ (1981).

4. Fast-Neutron Capture Cross Sections
(W. P. Poenitz)

Neutron-radiative-capture cross sections of Y, Zr, Mo, Ag, Cd, In, Sb, La, Eu, Gd, Tb, Dy, Er, Yb, Hf, W, Re, and Pt were measured in the 0.5-4.0 MeV energy range. Data are sparse in this energy range and nuclear model calculations reported by various investigators differ by up to factors of ten at higher energies. A large-liquid-scintillator detector was used for detecting radiative capture events and a grey neutron detector was used as a neutron monitor. The reported cross sections are relative to the capture cross section of gold at 0.5 MeV.

The present data are lower for most elements where prior data exist, however, good agreement was obtained with very recent results reported by a group from Bruyeres-le-Chatel. The present data together with previously reported measurements for Nb, Rh, Pd, Nd, Sm, Ho, Ta, Au, and U span a wide range of medium and heavy mass nuclei and should be useful to improve the knowledge of capture in fission product nuclei (Mo, Ag, Eu, Rh, Pd, Nd, Sm) as well as helpful in developing improved systematics.

5. Total Cross Sections in the Light Fission-Product Mass Range
(W. Poenitz and J. F. Whalen)

The previously reported measurements of the neutron total cross sections of C, Y, Zr, Nb, Mo, Rh, Pd, Ag, In, Sn and Sb were extended to the energy range 1.9-20.0 MeV and new measurements were made for Sc, Zn, Hf, Nd, Ta, Au and Pt over the same energy range. In addition, Cu total cross sections were determined at lower energies using a variety of sample thicknesses. The latter data displayed strong selfshielding effects and were extrapolated to zero-sample thickness. The C results do not support the

recent findings, based upon shielding benchmark testing, that ENDF/B-V may be too large by 8% in the 8.4 MeV region.

6. The Optical Model of Few-MeV Neutron Interactions with Z=39 to 51 Targets (A. B. Smith and P. T. Guenther)

Neutron total and differential-elastic-scattering cross sections of Y, Zr, Nb, Mo, Rh, Pd, Ag, Cd, In, Sn and Sb have been measured to neutron energies of 4.0 MeV, as outlined in the past report. This comprehensive and internally consistent experimental data base was used to deduce a "regional" optical model. The applicable mass-energy domain (A=85-125, few-MeV) is a region of strong compound-nucleus effects that should reflect nuclear structure. The resulting "regional" model provides a very good description of the observables throughout the relevant mass-energy region, as illustrated in Fig. A-3. The model is suitable for interpolation between measured values and for extrapolation to unmeasurable light-mass fission products of applied interest. It is also a good starting point for the explicit parameterization of the observed neutron interaction with a specific target. The model parameters display; i) iso-scaler and iso-vector behavior of a conventional nature, ii) systematic mass dependences of the geometric factors, particularly where related to the absorption, and iii) a very strong shell dependence of the absorption with pronounce minima of the imaginary strength near N=50 and Z=50. These large regional trends strongly suggest that the conventional "global" optical-model representation is no more than qualitative in the light-fission-product region. A manuscript describing the details of the above "regional" model is in preparation.

7. Fast Neutron Total, Scattering, and Gamma-Ray-Production Cross Sections of ^{54}Fe and Elemental Copper (P. T. Guenther, D. L. Smith, A. B. Smith and J. F. Whalen)

Total and differential elastic- and inelastic-scattering cross sections were obtained using isotopically enriched ^{54}Fe iron samples. These measurements employed relatively broad resolutions of 50-150 keV with energy increments of 75 keV. The total cross sections range in incident neutron energies from 0.5 to 4.0 MeV and several transmission sample thicknesses were employed to account for the self-shielding effect. The scattering measurements were made using the incident neutron energy range of 1.2 to 4.0 MeV, employing 10 angles between 20 and 160 degrees. Inelastic cross sections were obtained for scattering from the levels at 1408, 2538, 2561, 2950 and 2959 keV. Complimentary measurements of the gamma-ray production cross sections were made corresponding to the gamma-ray energies of 1408, 1130, 1153, 412, 1551, 2959, 1758, 3166, and 757 keV. These gamma-ray results were found to be consistent with the neutron work within the experimental errors. The above data base was analyzed in terms of an spherical optical-statistical model and found to well described with an appropriate parameterization. Consideration was also given to direct-reaction vibrational coupling. While qualitatively in agreement with experiment, this more complex representation did not significantly improve upon the description

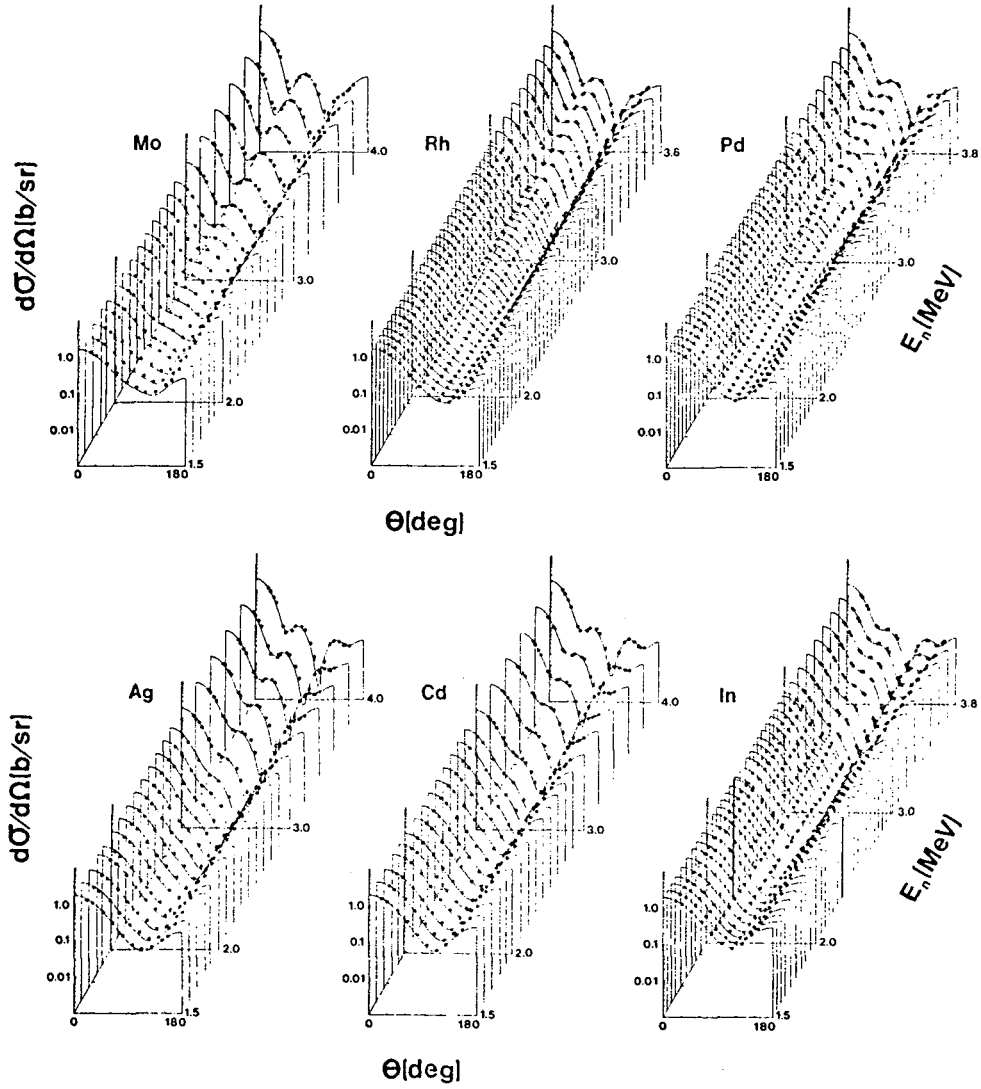

Fig. A-3. Comparison of measured (symbols) elastic-scattering results with those calculated using the "regional" model (curves).

of the experimental results in this energy range. In particular, the direct excitation of the first 2+ level at 1408 keV did contribute appreciably to the shape or magnitude of its cross section. Illustrative ^{54}Fe results are shown in Figs. A-4a and b.

A set of measurements, similar to the above, was made for elemental copper. The energy range for the total cross sections was 1.2 to 4.5 MeV, that for the scattering 1.5 to 4.0 MeV. All inelastic excitations up to 3 MeV have been accounted for either by 100-250 keV wide neutron groups or, in a few instances, by individual-level cross sections. These data have also been interpreted with a spherical optical-statistical model. All cross sections are reasonably well represented in this manner. The complimentary gamma-ray production measurements have been completed and are presently being analyzed.

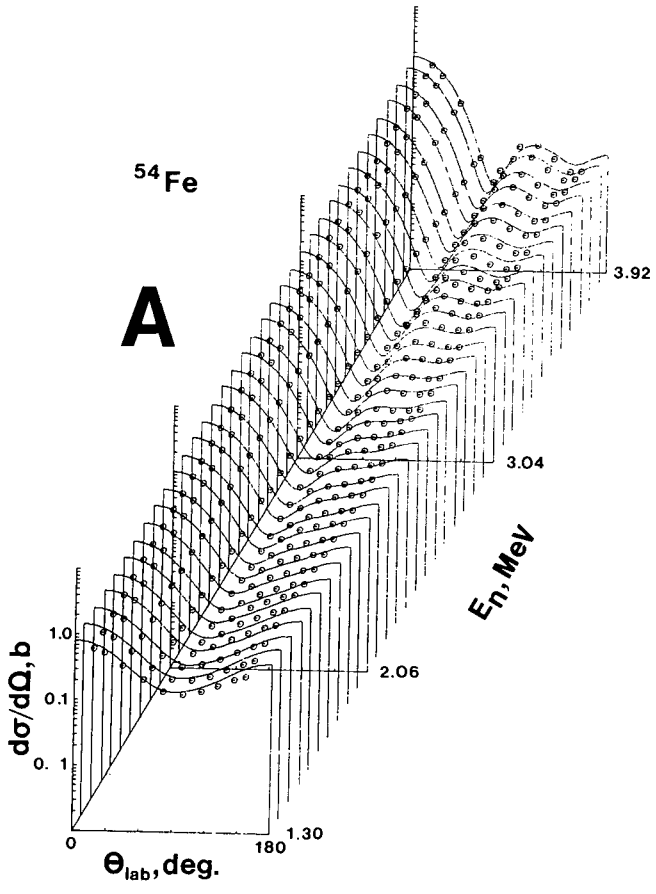

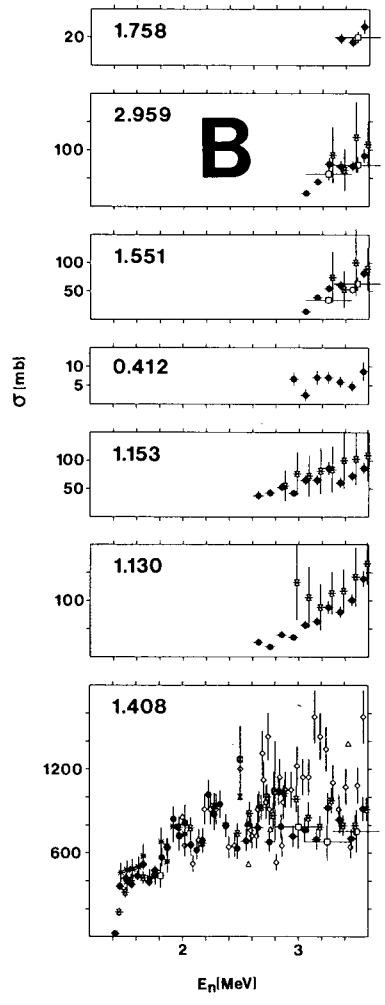

Fig. A-4a. Elastic Angular Distributions of Fast-Neutrons Scattered from ^{54}Fe. The symbols represent ± 100 keV averages of the basic data set. The curves represent spherical optical-model calculations.

Fig. A-4b. Gamma-Ray Production Cross Sections by Fast-Neutron Bombardment of ^{54}Fe. The solid symbols are the present results, the open symbols those of other authors.

8. Neutron Scattering Cross Sections of ^{59}Co

(A. B. Smith and P. T. Guenther)

Differential neutron elastic- and inelastic-scattering cross sections of ^{59}Co have been measured from 1-4 MeV at incident-energy intervals of $\approx$ 50 keV and with resolutions of $\approx$ 50 keV. The experimental results are being analyzed. Already it is evident that there is good agreement with similar results previously reported from this laboratory[1] and

considerable discrepancy with some aspects of ENDF/B-V.

[1]A. Smith et al., ANL/NDM-1 (1973).

9. Neutron Scattering Cross Sections of ^{45}Sc
(A. B. Smith and P. T. Guenther)

As a part of a continuing investigation of the neutron interaction with targets of small asymmetry, $\frac{(N-Z)}{A}$, the differential neutron scattering cross sections of ^{45}Sc were measured to incident-neutron energies of 4.0 MeV with sufficient detail to permit a reliable determination of the energy-averaged behavior. The data are now being analyzed.

10. Investigation of Vibrational-Rotational Band Interactions in the Even Isotopes of Tungsten.
(P. T. Guenther A. B. Smith)

New data have been measured for the inelastic scattering of fast-neutrons and the $(n;n'\gamma)$ process for the members of the β- and γ-vibrational bands in ^{182}W, ^{184}W, and ^{186}W. Given the improved precision of these cross sections a better definition of the coupling strength of these interactions is likely. This in turn will provide a better assay of the coupling schemes employed for model calculations for these nuclei and therefore the appropriate parameterization. Analysis is in progress.

11. Investigation of the Integral-Differential Discrepancy for $^{47}Ti(n,p)^{47}Sc$
(D. L. Smith, J. W. Meadows and W. Mannhart*)

Measurements of the integral reaction rate for $^{47}Ti(n,p)^{47}Sc$ in ^{235}U and ^{252}Cf standard fission-neutron spectra yield average cross sections which are systematically lower than values calculated from evaluated differential information. The discrepancies exceed the experimental errors. New differential measurements in the energy range 1.2 - 9 MeV have been performed at ANL and the processing of these data is nearly completed. New integral ^{252}Cf spectrum measurements for this reaction are in progress at PTB. All sample counting is related to a standardized PTB detector in order to eliminate the possibility of a systematic difference in counting procedures for the integral and differential results. When completed, the results from these measurements will be used to examine this integral-differential discrepancy problem anew.

*Physikalisch-Technische Bundesaustalt, Federal Republic of Germany.

12. Integral Measurements for $^{60}Ni(n,p)^{60}Co$, $^{58}Ni(n,p)^{58}Co$, $^{27}Al(n,p)^{27}Mg$, $^{27}Al(n,\alpha)^{24}Na$, $^{238}U(n,f)$ and $^{7}Li(n,n't)\alpha$ in a Standard $^{9}Be(d,n)^{10}B$ Neutron Spectrum
(D. L. Smith, J. W. Meadows, M. M. Bretscher and H. Liskien*)

Integral reaction rates for several activation reactions of interest for FBR and fusion energy applications have been measured in the previously characterized fast-neutron spectrum produced by 7-MeV deuteron bombardment of a thick Be target.[1] All sample counting is completed except for the ^{60}Co activity in the irradiated Ni samples. ^{60}Co counting has been delayed to allow substantial decay of the 71-day ^{58}Co activity, thereby reducing troublesome background. Data processing will be undertaken when all sample counting is over.

*CBNM-EURATOM, Belgium.
1 A. Crametz, H. H. Knitter and D. L. Smith, Antwerp Conference (1982).

B. FISSION PHYSICS

1. The ^{237}Np to ^{235}U Fission-Cross-Section Ratio
(J. W. Meadows)

The ^{237}Np to ^{235}U fission cross section ratio was measured at 63 discrete energies between 0.1 and 9.4 MeV using the $^{7}Li(p,n)^{7}Be$ and the $D(d,n)^{3}He$ reactions as neutron sources. The results are shown in Fig. B-1 The masses of the neptunium and uranium samples were determined by low-geometry alpha counting and the specific activities of the materials used. The specific activities of the uranium samples were based on; (1) isotopic analyses and evaluated half-lives,[1] (2) colorimetric analyses, and (3) isotopic dilution analyses. The neptunium specific activity was based on the specific activity and half-life measurement of Brauer et al.[2]

1 N. E. Holden, BNL-NCS-51320, Brookhaven National Laboratory (1981).
2 F. P. Brauer, R. W. Stromatt, J. D. Ludwick, F. P. Roberts and W. L. Lyons, J. Inorg. Nucl. Chem., 12, 214 (1960).

2. Fragment Angular Distributions and Total Kinetic Energies for the $^{238}U(n,f)$ Reaction
(J. W. Meadows)

A gridded ion chamber was used to measure the fission fragment angular distribution and average kinetic energy for the $^{238}U(n,f)$ reaction. The samples contained a small amount of ^{235}U and all measurements were made relative to ^{235}U thermal neutron induced fission. The kinetic energy measurements were restricted to those fragments in the angular range 0-60 deg. with

respect to the normal to the deposit. The ^{238}U deposits were fairly thick (0.15 to 0.20 mg U/cm^2) so energy loss in the deposits made the average kinetic energy measurements dependent on the fragment angular distributions. This was eliminated by dividing the cosθ-energy distribution into equal intervals in cosθ, averaging the fragment energy in each interval, then comparing that average with the average fragment energy in the corresponding interval for thermal neutron induced fission of the ^{235}U in the deposit. Corrections were also made for the isotopic composition of the samples, for the spectrum of the neutron source, and for neutron emission from the fragments.

Measurements were made over the energy range of 1.5 to 9 MeV and preliminary results for the average kinetic energy showed that it decreased linearly from 1.5 MeV to the second chance fission threshold at a rate of 0.30 ± 0.02%/MeV. At higher energies the behavior was consistent with a continued decrease in the average kinetic energy of first chance fission combined with a constant value for second chance fission.

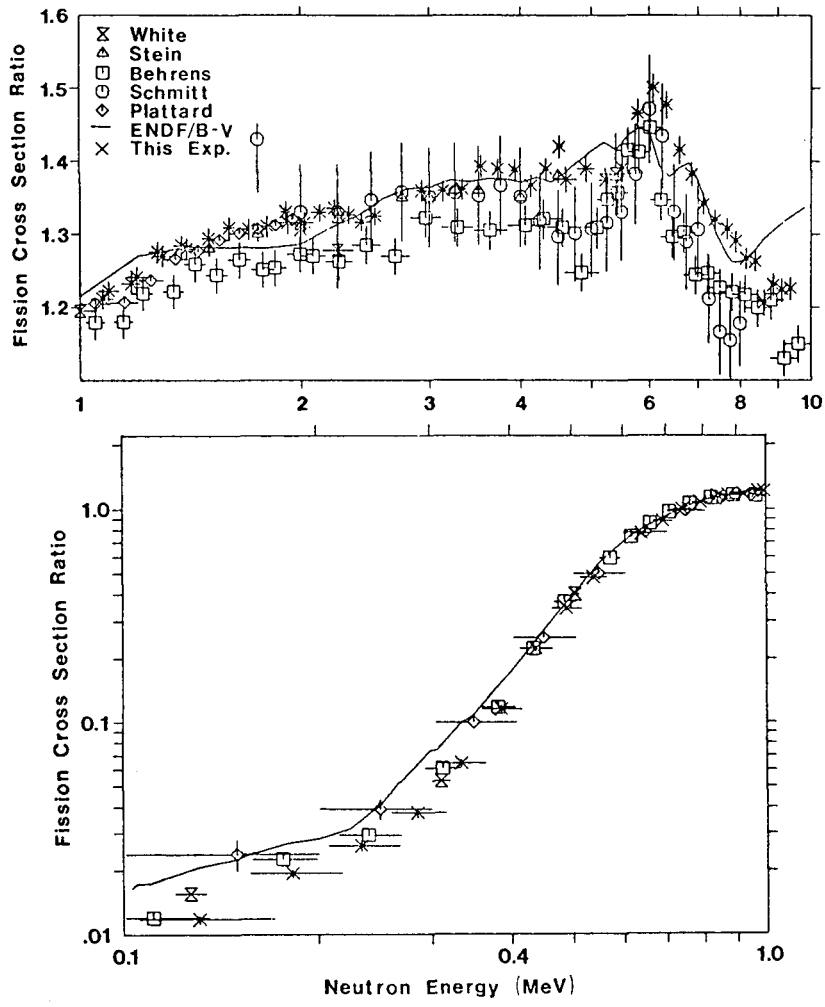

Fig. B-1. The $^{237}Np/^{235}U$ Fission-Cross-Section Ratio from 0.1 to 10.0 MeV.

3. Product Yields from Monoenergetic-Neutron-Induced Fission of ^{239}Pu
(J. E. Gindler, L. E. Glendenin, D. J. Henderson and J. W. Meadows)

Yields of 24 fission products were determined for the fission of ^{239}Pu induced with monoenergetic neutrons of energies 0.17, 1.0, 2.0, 3.4, 4.5, 6.1, and 7.9 MeV. Fission-product activities were measured with the high resolution (Ge-Li) γ-ray spectrometry of the neutron irradiated targets and with chemical separation of the fission product elements followed by beta counting. The results shown in Fig. B-2 exhibit a rapid increase of the near symmetric (valley) fission masses and a slow decrease of the most probable fission masses with increasing neutron energy. The fission yields with 14-MeV neutrons are shown for comparison by the dashed curve.

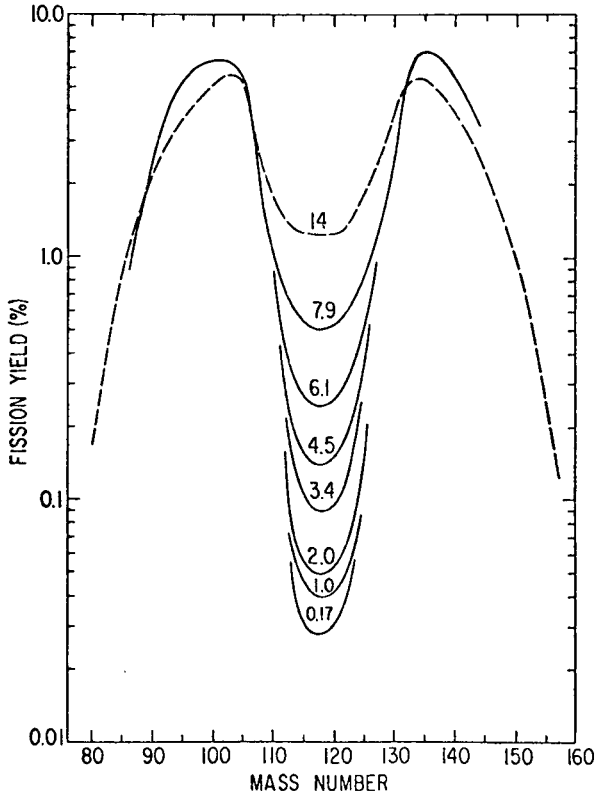

Fig. B-2. Mass Yields from Fission of ^{239}Pu Induced by Nuetrons with Energies of 0.17 to 14.0 MeV.

4. The Prompt-Neutron Spectrum of the Spontaneously-Fissioning ^{252}Cf
(W. P. Poenitz and T. Tamura*)

The prompt-fission neutron spectrum of ^{252}Cf was investigated in the energy range from 0.2 to 10 MeV. The spectrum was measured with Black Neutron Detectors which have well known efficiency. For the purpose of the present experiment, a liquid scintillator with higher hydrogen content and comparable or improved pulse-shape discrimination relative to NE 213 was

used together with the techniques outlined in the previous report. Corrections were applied and associated uncertainties accounted for a large variety of effects which may have been overlooked in many of the previously-reported fission-spectrum measurements.

Preliminary results, reported at the Antwerp Conference, indicate deviations from a Maxwellian toward a Watt spectrum shape. The average energy of the presently measured spectrum is somewhat higher than other recent results but substantially lower than that obtained in theoretical calculations by Madland and Nix. However, the spectrum-shape difference, relative to a Maxwellian spectrum shape of the same average energy, is in good agreement with the Madland and Nix prediction.

*Tohoku University, Sendai, Japan.

C. TECHNIQUES AND METHODOLOGY

1. Covariance Methodology
(D. L. Smith)

Communication of covariance analysis methods to the nuclear data research community must be given attention if these techniques are to be implemented in analyzing and reporting experimental results which will eventually be evaluated for the nuclear data files. Toward this end two recent tutorial papers have been prepared. One is currently available in report form[1] while the second has been submitted to a journal to be considered for publication.

[1] D. L. Smith, ANL/NDM-67, Argonne National Laboratory (1982).

2. Investigation of Some Potential Applications for Thick-Target Neutron Spectra in Nuclear Data Research
(D. L. Smith)

Thick-target neutron sources offer some unique possibilities for obtaining high neutron yield and extensive energy-range coverage. These spectra have been used for integral measurements, but the possibility of deriving differential cross sections from unfolding the results of a series of distinct integral measurements has not been widely exploited. The combination of measurement and evaluation functions in a unified least-squares approach has been investigated, and the results of this study appear in a recently issued report.[1]

[1] D. L. Smith, ANL/NDM-77, Argonne National Laboratory (1982).

3. Coupled Channels Optical Model Calculation of Neutron Cross Sections
(P. A. Moldauer)

The coupled channels program ECIS[1] has been modified to include the effects of compound-nucleus cross sections with width-fluctuation correction and Engelbrecht-Weidenmüller(E-W) transformation[2]. The modified program also includes compound scattering to uncoupled target states, capture and fission. Results of calculations for a variety of targets have been made, including a systematic study of the effects of the E-W transformation and the effects of the capture channels on scattering cross sections.

---

1 Courtesy J. Raynal, Saclay.
2 C. A. Engelbrecht, H. A. Weidenmüller, Phys. Rev. C8, 859 (1973).

D. EVALUATIONS, REVIEWS AND MEETINGS

1. Evaluation of the ^{238}U Neutron Total Cross Section
(A. B. Smith, W. Poenitz and R. Howerton*)

Experimental energy-averaged neutron total cross sections of ^{238}U were evaluated from 0.044 to 20.0 MeV using rigorous numerical methods. The evaluation results indicate that this neutron total cross section is known to better than ± 1% over wide energy regions. The uncertainties are somewhat larger below 0.2 MeV, near 8.0 MeV and above 15.0 MeV. The evaluation is consistent with that of ENDF/B-V to within the respective uncertainties but has the advantage of improved uncertainty specification including a detailed correlation matrix. The numerical values are given in the report ANL/NDM-74 (1982).

---

*Lawrence Livermore National Laboratory.

2. Reviews and Meetings

During the period a number of comprehensive reviews were prepared including:

i. Measurement Techniques for Radiative Capture,
W. Poenitz, to be published by Pergamon.

ii. ^{238}U and ^{232}Th Neutron Capture Cross Sections.
W. Poenitz, ANL-83-4 (1983).

iii. Neutron Capture Process in Fission Reactors,
W. Poenitz, to be published by Pergamon.

iv. ^{238}U Issues, Resolved and Unresolved, G. deSaussure* and A. Smith, Antwerp Conference.

v. The Nuclear Data of Major Actinide Fuel Materials, W. Poenitz and G. deSaussure*, to be published in Prog. in Nucl. Energy.

In addition to the above, the Proceedings of the NEANDC/NEACRP Specialists Meeting on Fast-Neutron capture Cross Sections is in press (editors, A. Smith and W. Poenitz). These proceedings consist of 570 pages of formal papers in a primary volume and a comprehensive supplement graphically summarizing the capture data discussed at the meeting. Copies of these two documents can be obtained from the National Technical Information Service under the document designations ANL-83-4 and ANL-83-4 SUPPLEMEMT.

*Oak Ridge National Laboratory.

BROOKHAVEN NATIONAL LABORATORY

The reactor-based neutron-nuclear physics research at BNL is composed of three categories: the study of nuclear structure with the (n,γ) reaction, the (n,γ) reaction mechanism and its application to pure and applied physics, and the spectroscopy of neutron-rich, fission product nuclides. These programs use the H-1 and H-2 beam ports of the HFBR. The tailored beam facility produces beams of thermal, 2- and 24-keV neutrons. A monochromator and chopper are used for resonance neutron studies. The TRISTAN on-line mass separator is used with a U-235 target to produce fission product nuclei. These facilities are operated in collaboration with a wide variety of collaborators from national laboratories and universities. In the following sections the complete program is outlined, and those sections of relevance to nuclear energy and other applications are described in detail.

A. SPECTROSCOPY OF FISSION PRODUCT NUCLIDES

1. Delayed Neutron Emission

The neutron capture cross sections of nuclei far from stability are of great interest for the development of fast-fission reactors and fission-fusion hybrids, and are of particular importance in the study of nucleo-synthesis. The energy region just above the neutron binding energy is generally the most critical, since those states participate most strongly in the capture process. Since the cross sections for nuclei far from stability cannot be measured by capture techniques, the inverse mechanism (neutron emission following β decay) offers the only feasible means of investigating the quality of theoretical predictions of the cross sections. The essential measurable quantities are the neutron level width (Γ_n) and the neutron energy (E_n) since these are difficult to predict.

Another application of delayed neutron spectroscopy is in the determination of complete β-strength functions. When the excitation energy of the β-decaying parent exceeds the neutron binding energy of the daughter, neutron spectroscopy becomes essential. In order to establish the relative β-feeding per energy interval, neutron γ-ray coincidence techniques are also necessary in order to unfold the singles neutron spectra into partial spectra for each final state. These studies can indicate the effects of small resonance-like structures in the Gamow-Teller giant resonance tail which may contribute strongly to β-decay properties.

a. Neutron Time-of-Flight

A time-of-flight (TOF) neutron spectrometer has been built and tested. This technique offers the best energy resolution at low energies (1-200 keV). However, because it is a coincidence technique, the efficiency tends to be low. Nevertheless, high resolution results have been obtained.

The best results have been achieved using a plastic scintillator β-telescope as the stop signal and a ^{6}Li glass scintillator as the neutron start signal. With this apparatus the absolute P_n of the 13 keV neutron peak in ^{95}Rb was measured to be (0.50 + 0.15)% which agrees well with the results of other investigators and with predictions using the gross theory of β decay and the spectrum shape. (Cornell/BNL)

b. Proton Recoil Spectrometer

Hydrogen-filled proportional counters potentially offer an alternative to the use of TOF spectroscopy for low energy neutrons, primarily due to the relatively high efficiency which these detectors can attain. The use of recoil detectors is limited by the complicated response function. Contributions from γ-ray and β-ray events generally will dominate the spectrum. To avoid this problem, two-parameter measurements of the pulse rise time and pulse height allow optimum application of pulse shape discrimination techniques to suppress the γ- and β-ray contributions. The detectors are calibrated for neutron response at the HFBR tailored beam facility. So far, delayed neutron spectra of ^{94,95,96}Rb have been collected, but exhibit excessive contamination from γ-ray events. In order to correct this further development work involving varying hydrogen gas pressures is ongoing. (INEL/BNL)

c. ^{3}He Counter Measurements

Cutler-Shalev type ^{3}He spectrometers have higher resolution than any other commercially available neutron detector. At neutron energies >20 keV the resolution is insufficient to determine widths of individual levels, but can be used to obtain an average level width for a relatively narrow group of levels. One such detector was used to do surveys of neutron emitting species made available by the surface ionization service at TRISTAN. Even though little acoustical and radiation shielding was used in these first tests a remarkable resolution, for this type of detector, of ≈13 keV for thermal neutrons, was obtained. Although the TOF technique has higher resolution, its low efficiency renders survey experiments too time consuming. Therefore, aside from the advantages of the Cutler Shalev detector for higher neutron energies, it is also of use in scanning the low energy regions for evidence of interesting structure that would be worthwhile to probe with greater resolution using the TOF approach. Such information has already been of use in the TOF study of ^{95}Rb mentioned above, and will be pursued in further studies. (McGill/Cornell/BNL)

d. Survey of Delayed-neutron Activities, Half Lives and P_n Values with the FEBIAD and Surface Ionization Sources

In order to survey neutron emitting isotopes and to deduce their gross properties (in particular, half lives and P_n values), it is advantageous to use an extremely high efficiency, low resolution neutron detector. Such a device, incorporating successive rings of neutron moderator and ^{3}He detectors, has been successfully used at TRISTAN to measure these quantities for all the delayed neutron emitters produced by both the Surface Ionization

and FEBIAD ion sources. For the FEBIAD source this survey study was also important in providing a general assessment of the activities produced.

The experiment was very successful, indicating neutron emissions from A=75-104, representing Cu, Ga, Br, Kr, and Rb precursors, and from A=121-149, representing Ag, In, I, Xe, and Cs precursors. Further analysis of the data may indicate still more precursors, such as Cd and Sn. If the results indicating the presence of ^{75}Cu are confirmed in later experiments, this will be the first observation of this isotope. It would be of high interest since it is five neutrons removed from the heaviest known Cu isotope. Upcoming experiments will study some of these nuclei in greater detail to extract specific Pn values. (PNW/BNL)

2. Q-values of Neutron-rich Isotopes

a. Evidence for Structure Effects in Nuclear Masses

Experiments to measure the Q-value for ^{88,94,96,98}Rb and ^{146,148}La were completed. The results were compared to three different types of mass formulae; those of Myers (liquid drop), Liran and Zeldes (semi-empirical approach), and Moller and Nix (Yukawa-plus-exponential macroscopic model). The best global fit is given by the Liran-Zeldes formula. Several trends are discernable: 1) agreement usually worsens at the mass extremes; 2) all three mass equations overestimate the stability of very neutronrich Rb isotopes (and of the La isotope to a lesser degree); 3) the effect of pairing appears to be treated incorrectly resulting in an odd-even staggering; and 4) the Myers and Moller-Nix formulae underestimate the binding in the shape transition region beyond the N=50 shell closure. For isotopes in the La region near N=90, an extensive survey of known masses, including the present results, suggests a correlation between spectroscopic data and mass data that may indicate possible corrections to the mass formulae. The spectroscopic data indicate that the lower Z elements (Ba,Ce) undergo a smooth transition from a vibrational to a rotational structure, whereas the higher Z ones (Nd,Sm) show a tendency toward a triaxial or γ-unstable structure before becoming rotational. The mass formulae give good agreement for the lower Z nuclei, but yield about a 1 MeV discrepancy for those higher ones which show the tendency toward triaxiality. It was suggested that perhaps including a tendency toward triaxial shapes (as suggested by the spectroscopic data) in the mass equations may improve the results. Q_β experiments will use the FEBIAD ion source to provide nuclides near the A=100 and N=90 regions of deformation as well as near closed shell regions. Effects of shape transitions on the ground state energy will be investigated. (Clark/Lafayette/BNL/Ames/Lafayette/Oklahoma/Maryland)

b. β Spectra

A E-ΔE coincidence spectrometer was used to attain β spectra nearly free of γ-ray contamination. The summed ΔE+E output gives the β energy and the requirement of a coincidence condition eliminates γ rays from the spectrum. Unfortunately, the response of this detector is complex due to electron scattering in the detectors. After carefully determining the

response function, several end point measurements have been accurately made. Ongoing experiments will attempt the more ambitious program of unfolding the complete β spectrum in order to measure β-feeding to specific final states. This is of importance in determining β-strength functions. (McGill/BNL)

3. Perturbed Angular Correlation Studies

The first perturbed angular correlation (PAC) experiments were performed at TRISTAN during FY 1982. The initial experiments used the integral PAC technique where the angular distribution is measured with the magnetic field in both the "up" and "down" directions. Later experiments have used the time-dependent PAC technique. The g-factors derived from the earlier experiments (especially ^{144,146}Ba) have been combined with existing experimental data for the neutron-rich Nd, Sn, and Gd isotopes and interpreted in terms of a simple IBA description involving constant values of the boson g factors. Earlier studies of the effects of the Z=64 subshell closure have suggested that assuming a sudden change in the proton boson number between N=88 and 90 gives better agreement for the energy levels of Ba-Sm nuclei than assuming a proton boson number which is independent of neutron number for each element. Under certain assumptions in the IBA formalism for magnetic moments, it is possible to show that a linear relationship is predicted between μ^{exp}/M_ν and M_π/M_ν where $M_\pi(M_\nu)$ is the matrix element of the angular momentum operator for proton (neutron) bosons. Calculations were carried out using two sets of parameters corresponding to the two assumptions above for proton shell structure, one where no sudden change of proton boson numberis included and a second set where the rapid change is incorporated. The predicted linear relationship is observed when the latter parameters are used and, for the former scenario, the discrepancies are larger for N=86 than N=88 indicating that the effect of the Z=64 gap is more important at N=86 and gradually dissipates toward N=90. Thus the g factor/magnetic moment measurements are a sensitive probe of the active number of valence protons and, moreover, they appear to even sample some of the details of the evolution of shell structure. Since these initial experiments, the technique has been utilized for studies of ^{98}Sr and ^{97}Zr, which are located in the crucial A≈100 mass region where another complex transition region occurs, and for ^{124}Sn, which lies just above the Cd isotopes that display exceptional level schemes due to the presence of intruder states. Thus far, only preliminary results for these three nuclei have been obtained. Further work is scheduled for the near future. The studies of ^{97}Zr and ^{124}Sn should be relatively straightforward. In the case of ^{98}Sr the short half life of the Rb parent necessitates the delay of this experiment until a new, faster tape collection and drive system is installed later in FY 1983. (BNL/Iowa State/Maryland)

4. Spectroscopic Studies of Nuclides Near Closed Shells

a. Multiplets in N=83 Isotones

For realistic nuclear forces, the splitting and displacement of low-lying $\pi g_{7/2}$ $\nu f_{7/2}$ and $\pi \ell_{5/2}$ $\nu f_{7/2}$ multiplets in the odd-odd N=83 isotones (^{146}Eu, ^{144}Pn, ^{142}Pr and ^{140}La) depend in a simple way on the occupancy of proton and neutron orbits. Paar has devised a convenient method

for analyzing these p-n multiplets near closed shells in terms of a quadrupole interaction from which a particularly simple parabolic relationship between E(I) and I(I+1) emerges. The resulting parabola opens down (i.e., maximum and minimum spin states the lowest) if the proton and neutron are both particles or both holes; it opens up (mid-spin lowest) if one is a particle and the other a hole. The effect of a dipole interaction is expected to be small but perhaps detectable: it is linear in I(I+1) and shifts the vertex of the parabola.

The data for the N=83 isotones were fitted to parabolas. A total of 50 levels have been fit in the four nuclides with an r.m.s. deviation of only 17 keV. The agreement is best for the lowest lying multiplet, indicating that there is little configuration mixing in that multiplet. The influence of the dipole interaction was found to be small even where quasi-particle blocking reduces the effects of the quadrupole term. Several 2^- and 3^- levels were not included in the fits, since they were clearly perturbed. The 3^- levels in ^{140}La, ^{142}Pr and ^{144}Pn lie close to the intersection of the gf and df parabolas; it seems that they interact and repel each other. (Maryland/Clark/BNL)

b. Configuration Mixing and Parabolic Structure in the N=85 Nucleus ^{142}La

The above treatment was extended to ^{142}La to investigate the effects of adding neutrons to the ^{140}La configuration and to higher-lying multiplets in ^{140}La and ^{142}Pr to investigate the effects of configuration mixing.

Using the results of fitting the N=83 parabolas, it was possible to project the low-lying level structure for ^{142}La. In this case, quasi-particle blocking effects [proportional to $(U^2_n - V^2_n)$] will cause the parabolas to become more shallow. The comparison of the calculated and experimental level density shows qualitative agreement. Thirteen low lying 0^-, 1^-, 2^- states and up to three 3^- states are predicted, as compared to thirteen observed low-lying 0^-, 1^-, 2^-, and3^- states and one 4^- state. The 4^- isomer is likely to be the bottom of one of the concave upward parabolas. A half-life of 1 μs is calculated for the 68 keV E2 single particle transition as compared to a measured half-life of 0.87 μs. Thus, the isomer can be viewed as a single particle transition from one multiplet to another. No transition is observed between the 4^- isomer and the 2^- ground state, corresponding to an E2 retardation of ≥ 50. Thus, it may be postulated that the ground state differs from the 4^- isomer in both its neutron and proton configuration. Higher-lying multiplets in ^{140}La and ^{142}Pr tend to be less steep than expected from the behavior of the lower-lying ones. This is interpreted in terms of configuration mixing. (Maryland/Clark/BNL)

c. Configurations of Low-lying Levels in ^{144}La

The low-lying negative parity levels in ^{144}La form a sequence of states that can be attributed to $\nu f_{7/2}\pi g_{7/2}$ and $\nu f_{7/2}\pi d_{5/2}$ configurations. In this case, the parabolas in ^{144}La should be inverted relative to those in ^{142}La, due to the increased occupancy of the $f_{7/2}$ neutron

orbitals. The gf parabolas should open down and the df parabolas open up. Analysis shows that while the levels do lie in the sequence suggested, the level structure is not well reproduced. The observed ground state spin of 3 is predicted when $\nu f_{7/2}\pi d_{5/2}$ is adopted as the ground state multiplet configuration. The low-lying positive parity, single particle states in ^{144}La can be constructed by coupling the ground state multiplet to the 1^- and 3^- states in the Ba core. An alternative, Nilsson orbital description, can also be considered. For deformations $\geq$0.25 (as suggested by ^{143}Cs) positive parity neutron orbitals from the $i_{13/2}$ shell model orbital may combine with positive parity proton orbitals to form states in ^{144}La. The 66-keV transition ($2^+ \rightarrow 1^+$) may be evidence of a rotational band head based on the 1^+ state. If this is so, then the band may have a $\pi 1/2^-$ [550] x $\nu 3/2^-$ [532] configuration. (Maryland/BNL/Clark)

5. Structure near the Z=64, N=90 Transitional Region

This region, containing a spherical-deformed transition, has long been of interest and remains a crucial testing ground for nuclear models. This is all the more so with the recent discovery of the shell gap of Z=64. Indeed, as a result of this, a new interpretation of the origin of deformation in this region, related to that now accepted for the A≈100 region, has been proposed in studies here. It avoids a potential paradox in the data and, moreover, suggests that the nuclei near Z=64 will show an incipient tendency toward triaxiality enroute to a full transition to an axial deformed shape for N$\geq$90. Further study of this region, and its systematics, are clearly of intense interest. They are pursued in a number of experiments at TRISTAN, described below, which ultimately will provide the desired systematics.

a. ^{142,144}Ce Angular Correlation Studies

Studies of these nuclei have continued this year. The ^{142}Ce studied was completed. A principal result is the suggestion that an anomalously low lying 2^+ level is rather more likely a 4^+ state. The resulting picture of ^{142}Ce is then much more amenable to a vibrational interpretation. The study of ^{144}Ce is continuing with emphasis on the higher lying states between 2 and 5 MeV. (Maryland/BNL/Clark/Iowa State/Oklahoma)

b. Decay of ^{146}La

An extended angular correlation experiment was performed to complete the necessary data for this level scheme. The data are quite complex and full analysis is continuing. (Iowa State/Maryland/Oklahoma/BNL)

c. Band Structure in ^{148}Ce

The onset of nuclear deformation in the rare earth region is known to occur at N=90 for even-even nuclides with Z>60. Recent studies (by the OSTIS separator group at the ILL) of the isotopes of barium (Z=56) show that this onset tends to occur at lower neutron number for Z<60. In order to examine the intermediate situation, namely for Z=58, the neutron-rich Ce

isotopes were studied through the decay of lanthanum obtained from the on-line isotope separator TRISTAN. The Ce isotopes show a complex structure. Some of the indicators suggest that ^{146}Ce (N=88) represents the onset of deformation (the 3^- and 1^- octupole states have crossed). However, angular correlation experiments performed in FY 1982 show that the level at 770 keV is a 0^+ state. Thus, the 0^+ state in Ce minimizes no earlier than at A=148 (N=90) and a minimum in 0^+ energy is often a signature of the onset of deformation. IBA-2 calculations, using parameters modified to reflect the strong subshell closure at Z=64, give good agreement with the experimental energy levels. However, the B(E2) values obtained with these parameters are in poor agreement with experiment. In any case the results show a very large mixing consistent with the idea of large rotation-vibration coupling at the edges of a deformed region. (BNL/Clark/Maryland/ISU)

d. The Decay of Low-spin ^{148,150,152}Pr to Levels in ^{148,150,152}Na

Singles, coincidence and half-life measurements were made in FY 1982 in an effort to determine a detailed level scheme for the Nd isotopes. The yields of the parent Pr ions are greatly enhanced with the use of a special graphite cloth ion source target. Unfortunately, as presently configured, such a target is not suitable or stable for long term studies of other nuclei. Therefore, the Nd studies will be repeated if an alternate approach to the ion source difficulties is successful. This new source will also utilize a graphite cloth but will act more as a thermal than as a surface ionization source. (Iowa State/Maryland/BNL)

e. ^{141}Ba

This level scheme, discussed in detail in last year's report, including the discussion in terms of Paar's cluster vibration calculations of neighboring nuclei, was completed this year. (Iowa State/Clark/Oklahoma/BNL)

f. The Decay of ^{145}Cs and ^{145}Ba

Studies of the level scheme of ^{145} Ba are surprisingly scarce, considering the very high yield of ^{145}Cs available at TRISTAN. However, with 89 neutrons, this nucleus is of considerable interest because it lies just at the "critical point" in the N=88-90 spherical to deformed transition region. Moreover, with Z=56, it should negotiate the transition region rather differently than the classic transitional isotopes of Sm and Gd which have proton number much closer to Z=64, where a major proton subshell occurs for certain neutron numbers. This contrasting behavior may shed light on a new understanding of the microscopic structure of this key region. In a short time period, sufficient data were taken to yield a very detailed level scheme for ^{145}Ba. The data analysis is not yet completed. The decay of ^{145}Ba to ^{145}La has also been studied. Detailed analysis of the data has shown that there are difficulties in separating the ^{145}Cs and ^{145}Ba activities. This problem will be resolved by further experiments. (Oklahoma/BNL/Sichuan University)

g. The Decay of ^{147}Cs and ^{147}Ba

TRISTAN was used to study the decays of ^{147}Cs and ^{147}Ba. Singles, coincidences, and multiscaling measurements were made. Half-lives were measured. Several γ rays previously assigned to the decay of ^{147}Cs were confirmed, and a number of ^{147}Ba γ rays were newly established. A tentative decay scheme for ^{147}Ba is proposed. Measurements were also taken on ^{147}La decay and the deduced level scheme shows some differences from previously proposed schemes. By using the BNL data, and the conversion electron data from studies at OSTIS, some multipolarities have been determined and some spin and parity assignments (or limits) have been made. However, since more definitive spin parity information will be required, the use of the Si(Li) electron spectrometer under construction will be necessary before the study can be completed. (BNL/Oklahoma)

h. The Decay of $^{144,146,148}Ba$ to Levels in $^{144,146,148}La$

The experiment on ^{144}La was completed during this period and submitted for publication. For $^{146,148}La$ data were taken to complete the experimental studies of these nuclei. The analysis of the data is nearly. (Maryland/Iowa State/BNL/Clark).

6. Structure in the Transitional Region Near A=100

a. ^{99}Rb and ^{99}Sr Decay

The high quality data obtained from the mass 99 experiments are being analyzed. The results show level schemes in greater detail than available anywhere else. The OSTIS group at ILL has also worked on those nuclides, but our level scheme differs substantially from their results. Specifically, the OSTIS study missed the second strongest gamma ray in the decay of ^{99}Sr and has very little information on the decay of ^{99}Rb. This work is nearly completed. (Oklahoma/Maryland/BNL)

7. Structure of Cd Nuclei

a. ^{122}Ag Level Scheme

With the FEBIAD source in use, a short experiment was performed to evaluate the possibility of studying the decay of ^{122}Ag. In this experiment, about 3 times as many gamma rays were observed than were previously known. The level of activity indicates that it should be possible to do angular correlation studies to determine the spins of the levels in the Cd daughters for many of the Ag isotopes. The even Cd (Z=48) nuclei lie just below the shell closure at Z=50 and comparison with the Sn nuclei is expected to give considerable insight into the effects of the proton-hole structure expected in Cd. Therefore, detailed experiments are in progress. (BNL/Clark/Iowa State)

b. ^{124}Ag Level Scheme

A short experiment to evaluate the yield of ^{124}Ag disclosed at least one gamma ray with a half life of about 125 n sec. This represents the first observation of ^{124}Ag decay. Detailed, longer experiments will be performed, when ion source improvements are expected to provide an improved yield. (BNL/Clark/Iowa State)

B. RESONANCE CAPTURE AND APPLICATIONS

1. Resonance Averaging in ^{239}Pu

Normally, one expects excellent averaging in tailored beam experiments on nuclei far from closed shells. One particularly striking exception, however, is known, namely, for the ^{239}Pu(n,γ)^{240}Pu reaction. However, one is dealing here with a fissile nucleus and so the Monte Carlo program for calculating resonance averaging fluctuations was modified to include a fission channel. In that case there is a strong dependence of fission width on resonance spin, and thus a strong effect of fission competition on the branching ratio for radiative capture. The calculated fluctuations agree well with experimental results, obtained from the 2 keV Sc filter. The ^{239}Pu shows good agreement of E1 strengths with the giant dipole extrapolation, and a single-particle energy dependence (E^3) for the M1 strengths. (BNL/ECN (Petten))

2. Applications of Neutron Capture

A number of surveys of applied radiative neutron capture were compiled in FY 1982. These included: a) a review of the fundamentals of the capture reaction for the Argonne Fast Neutron Capture Workshop in April; a review for the Winter ANS Meeting in Washington, November, 1982; and c) a review of applications for the American Physical Society Annual Meeting, January, 1983. In addition, editing and production of a monograph on "Radiative Neutron Capture" was carried out in FY 1982. (BNL)

C. NUCLEAR STRUCTURE WITH THE (n,γ) REACTION

The H-1 beam tube at the HFBR provides two beams used almost entirely for neutron capture γ-ray studies. These include the tailored beam facility, which provides beams of thermal, 2 and 24 keV neutrons, and the neutron monochromator, which provides energy-selected beams effective up to about 25 eV. These wide ranging beams provide a unique method of nuclear structure investigation due to the primarily nonselective character of the (n,γ) reaction. Indeed, in appropriate cases, all levels of a given spin-parity range in the final nucleus may be about equally populated without regard to the structure of the final state wave functions. This is primarily achieved with the use of the tailored beams, which provide resonance averaging of the primary transitions, and are absolutely indispensable in the construction of level schemes.

The primary transitions unambiguously fix level positions, which the secondary transitions cannot do, except by the inferential application of the Ritz Combination Principle.

1. Studies of Deformed Even-even Nuclei: Tests of the IBA

In the last several years a major advance in nuclear structure studies has been the development and testing of the IBA. Briefly, the basic problem of nuclear structure in heavy nuclei is the practical intractability of the shell model in the face of large numbers of valence nucleons. The familiar geometrical models attempt to overcome this difficulty by the macroscopic strategem of assuming an overall nuclear shape. The IBA offers an alternate scheme, at once more abstract and more general: it assumes an enormous truncation of the possible shell model configurations such that low lying excitations can be treated, in effect, in terms of bosons which represent pairs of fermions that are coupled to angular momentum 0 (s bosons) or 2 (d bosons). The complex Hamiltonian of the shell model is replaced by an extraordinarily simple one consisting of elementary (e.g., pairing and quadrupole) interactions between bosons. A particularly attractive feature is that three natural limiting symmetries, denoted group theoretically as SU(5), SU(3), and O(6), arise when one or another term in this Hamiltonian dominates. These symmetries correspond crudely to the familiar vibrator, rotor, and asymmetric rotor of the geometrical models but contain features unique to the IBA which have been empirically verified. Since intermediate situations are easily handled by adjusting the relative sizes of the various terms in the Hamiltonian, the IBA offers the very attractive possibility of treating vastly different nuclei within a single scheme. Tests of the model to date have centered primarily on even-even nuclei, in particular near the O(6) and SU(3) (deformed) regions. Many tests have been carried out at BNL using the (n,γ) reaction which, due to its inherent nonselectivity and general applicability, is ideally suited to testing a model that itself attempts to generate complete sets of low-lying, collective excitations over broad regions of nuclei. As an outgrowth of our initial study of the deformed nucleus ^{168}Er, with the IBA, a number of other projects have ensued. Several of these represent theoretical attempts to better understand the IBA itself, and its relationship to other models, while others are new but related empirical tests of the IBA. Still others deal with comparisons with traditional models.

a. (n,γ) Studies of ^{162}Dy and ^{164}Dy

The region of well deformed nuclei might well be considered one of the best understood in terms of nuclear structure. However, the recent applications of the IBA to this class of nuclei have revealed a number of new features which are at variance with the expectations of the simple harmonic geometrical model. One prerequisite for an improved understanding of deformed nuclei is the establishment of complete sets of collective excitations below the pairing gap in a number of nuclei, and a detailed empirical determination of the E2 matrix elements connecting these excitations. The (n,γ) reaction, in general, is ideal for such a purpose, since it can populate low spin states of widely different structure, and the specific combination of the high precision gamma and beta ray spectrometers (GAMS and BILL) at the ILL, and the

tailored beam and monochromator facilities at BNL, provides a unique experimental capability to study that reaction, as was demonstrated in the case of ^{168}Er. GAMS and BILL data on ^{162}Dy have, therefore, been taken at the ILL, and are currently being analyzed. A similar investigation of ^{164}Dy is planned for the coming year. Studies at BNL of both nuclei have been completed, and the results submitted for publication. In these studies, the quantitative interpretation of the resonance averaged data has been improved by use of a Monte Carlo analysis to establish criteria for J^{π} assignments. Further spin limitations have been imposed by the studies of primary transitions following capture in single resonances in both nuclei, using the neutron monochromator facility at BNL. The data can provide the ability to define complete sets of low spin states, and this known completeness has been used to establish a correspondingly complete band structure in each case. These results have already revealed a number of interesting features. For instance, it has been shown that there are no excited 0^+ bands in ^{164}Dy below 1630 keV, and that this fact has important implications for the application of the IBA or any other collective model to this nucleus. In addition, the data show that the lowest $K^{\pi}=4^+$ excitations are too high in energy to be of collective 2 γ-phonon structure. Coupled with a similar result in ^{168}Er, this would seem to support the suggestion of Soloviev that the main components of the two phonon excitations in deformed nuclei are shifted to higher energies and are considerably fragmented. In considering the negative parity structure, the complete set of collective octupole excitations was identified and so, combined with the results for ^{168}Er, extends the systematics of these excitations across the deformed region. (BNL/ILL/University of Manchester)

b. Systematics of $K^{\pi}=4^+$ Excitation in Deformed Nuclei

The Dy studies mentioned above, and similar ones in Er and Yb, have also identified or set lower bounds on the energies of $K^{\pi}=4^+$ excitations; this permits their systematics to be plotted for the first time. Walker et al. have recently analyzed the $K^{\pi}=3^+$ systematics. The combination of these two sets of results shows an interesting inversion of order with increasing mass: at low A the $K^{\pi}=4^+$ excitations are lowest, at high A, they rise in energy while the $K^{\pi}=3^+$ excitations fall. It is possible to give a simple interpretation of this feature in terms of the particle and hole character of the available two quasi-particle Nilsson states that can form 3^+ and 4^+ intrinsic excitations. Alternately, these results may provide information on the structure, behavior and role of a g-boson in the IBA. (BNL/University of Manchester)

c. Level Structure of ^{184}W

Average resonance capture data at neutron energies of 2 and 24 keV have been taken and analyzed, and preliminary results have been published. Curved crystal (GAMS) data have also been taken, and the analysis of these, and subsequent construction of the level scheme, is in progress. It may well be that, contrary to common opinion, the W isotopes are perhaps the best examples of near SU(3) nuclei. This possibility remains to be proved and the present data should provide an apt test. (BNL/Koln)

d. The $^{177}Hf(n,\gamma)^{178}Hf$ Reaction

A study of ^{178}Hf has been undertaken in collaboration with the University of Koln. Analysis of the 2 and 24 keV tailored beam spectra revealed the need for additional 24 keV data, which has been obtained this year and is currently being analyzed. Data from the GAMS and BILL spectrometers is being analyzed at Koln. (University of Koln/ILL/BNL)

2. Studies of Transitional and O(6)-like Nuclei

Since the discovery of the O(6) limit in ^{196}Pt and of an O(6)→Rotor transition in the Pt-Os region, a continuing program of studies in this mass region, and in others thought to exhibit similar structure, has been carried out. Recently these studies have been enlarged to also include other transitional regions, in particular the complex one near Z=64. Many of these studies are interpreted in terms of the IBA but other models and interpretations are brought to bear when appropriate and illuminating.

a. ^{188}Os and the O(6)→Rotor Transition Region

A number of years ago a detailed (n,γ) study of γ-ray transitions in ^{188}Os was carried out at BNL. Some of the results from the level scheme, primarily concerning 0^+ states, were published; these analyses provided a principal part of the initial motivation to look at IBA predictions for these and neighboring nuclei. In turn, this resulted in the discovery of the O(6) limit in ^{196}Pt and, thereby, in a host of other studies. However, the full level scheme was never published due to some remaining questions and the need for electron conversion data. Such data have now been recorded at the ILL. The E0 results have been published and are described in another paragraph. The remaining results are now being used to finalize the full ^{188}Os level scheme. It is expected that this work will be completed in FY 1983. (BNL/ILL/Clark)

b. E0 Transitions in ^{188}Os and ^{196}Pt

These experiments, carried out with the BILL spectrometer at the ILL in Grenoble, have been completed this year. The principal results, preliminarily noted in last year's report, are as follows. In the IBA, E0 transitions are directly related to the average number of d bosons in the initial and final states, and are thus a sensitive test of the wave functions. Studies of a good O(6) nucleus, ^{196}Pt, and a transitional one, ^{188}Os, were undertaken to see how these E0 transitions behaved and reflected the changes across a transition region (O(6)→SU(3)). Only mixed agreement with the model for $2^+\to2^+$ transitions was found. However, the most striking result was the empirical dominance, in ^{196}Pt, of the one ground state E0 transition allowed in the O(6) limit. In ^{188}Os, IBA calculations also predict only one strong $0^+\to0^+_g$ transition and, again, it is empirically observed. It is particularly interesting to understand the origin of this E0 strength. By expanding the wave functions for ^{188}Os in O(6) basis states, it is found that the transition originates precisely in the O(6) components of the two 0^+ states that led to the allowed transition in ^{196}Pt. Thus, the E0 strength

arises from the remnants of O(6) structure in ^{188}Os while earlier studies of E2 transitions show that they arise largely from the emerging SU(3) character of the levels. It is seen that E0 and E2 studies can be particularly useful in unraveling some of the rather detailed substructure of the wave functions. (BNL/ILL)

c. Nuclear Structure near Z=64

The effects of the Z=64 subshell closure on the structure of the transitional rare earth nuclei near N=90 has been the subject of considerable current interest, and a comprehensive series of (n,γ) studies of ^{148}Sm have been made, including tailored beam, $\gamma\gamma$ coincidence, and singles measurements using the neutron monochromator facility at BNL to populate the 3.4 eV resonance in ^{147}Sm. The data are currently being analyzed. (University of Manchester/BNL)

d. Nuclear Structure of ^{136}Ba

The nuclei in this region are similar to those in the Pt-Os region, in the sense that the underlying single particle structure consists of neutron holes and proton particles. In the IBA-2 framework, such a situation should give rise to an O(6)-like structure, and it is, therefore, of interest to look for the influence of such character in the structure of ^{136}Ba. The ^{135}Ba(n,γ)^{136}Ba reaction has been studied via tailored beam measurements at BNL, and with the GAMS spectrometers at ILL. In addition, low energy and primary γ rays following thermal neutron capture were studied at the neutron monochromator facility at BNL and these data have now been analyzed. Additional $\gamma\gamma$ coincidence data was taken at ILL during 1982. The analysis of these data is currently under way along with the construction of the level scheme and theoretical interpretation. (BNL)

3. Light Nuclei: Resonance Averaging for ^{55}Mn(n,γ)^{56}Mn

The concept of resonance averaging, using filtered beams at 2 and 24 keV, has been most successfully applied in the region for A>150, where the level spacings are small enough to give reasonably small intensity fluctuations. There are, however, advantages in the use of the technique even for light nuclides, where the averaging is much poorer. A case in point is ^{55}Mn(n,γ)^{56}Mn. In such cases the level scheme is relatively simple, the spectrum is correspondingly less complex and secondary γ rays at relatively high energies may be present. These may cause ambiguities in the level scheme developed from (n,γ) data, especially if only thermal neutron data are available. The filtered beam data at 2 and 24 keV were used in this case to separate primary and secondary γ rays by making use of the kinematic shift in the γ-ray energy. The shift was also used to discriminate against background and/or activation lines. As a result, a more reliable level scheme was developed for ^{56}Mn. (BNL)

4. Search for Single and Multi-j Supersymmetries

The extension of the IBA formalism to include the fermion degree of freedom has suggested the intriguing possibility of symmetries in the boson-fermion system, similar to those already predicted and observed for the even mass systems. Indeed, there exists, in theory, the possibility of a supersymmetry, which encompasses both the even and odd mass systems. Since a prerequisite for such a symmetry is that the even-even core of the odd mass system should itself exhibit one of the appropriate symmetries (SU(5), SU(3), or O(6)) the best region to search for such structures are those where the core exhibits such characteristics. Since few, if any, very good SU(5) or SU(3) nuclei exist (deformed nuclei are in fact not particularly good examples of the pure SU(3) symmetry), an O(6)-like region is suggested as the best place to search for a supersymmetry in nuclei. Initially, the theoretical predictions were worked out for a fermion in a j=3/2 orbit coupled to an O(6) core. Unfortunately, the shell model never provides an isolated j=3/2 orbit [there are always nearby $s_{1/2}$ (in a π=+ shell) or $p_{1/2}$ and $f_{5/2}$ (π=-) orbits]. Therefore, the group structure can describe only that subset of the empirical levels where the particle occupies a 3/2 orbit. In such a situation, the appropriate empirical probe is a particle transfer reaction that is sensitive to the shell model character of the 3/2 states observed. The earliest studies along these lines, utilizing, for example, results from (d,p), (t,p), and (p,t) studiescentered on the odd proton Ir and Au nuclei and revealed some resemblance between predicted and observed level sequence and selection rules, but also showed that a 3/2 x O(6) scheme had, at best, only approximate utility. Faced with this, recent group theoretical work has made substantial advances, and led to the prediction of a new supersymmetry corresponding to an O(6) core and a fermion that can occupy any of the j=1/2, 3/2, or 5/2 orbits. This situation is fortunate for it corresponds precisely to that occurring in the odd mass Pt isotopes and several studies have been launched to investigate this region.

The search for supersymmetries is being carried out for the following nuclides: ^{195}Pt, ^{197}Pt, ^{199}Pt, ^{131}Ba, ^{133}Ba, ^{135}Ba, ^{185}W, ^{187}W, and ^{169}Er. (BNL/ILL)

5. Other Studies of Odd Mass Nuclei

a. The ^{176}Lu(n,γ)^{177}Lu Reaction

The high ground state spin of ^{176}Lu, 7^-, allows the population of final states in the (n,γ) reaction which have much higher spin than normally feasible. However, the small amount of target material available precluded the use of resonance averaging, so that measurements have been made by populating a total of seven different single resonances in ^{176}Lu, using the neutron monochromator at BNL. These data have now been analyzed, and work is progressing to combine the seven spectra, with appropriate normalizations, so that an effective averaged spectrum is produced. Such a procedure should provide an improved capability to assign spins and parities, and allow the identification of a more complete set of final states. The secondary γ-ray spectrum following thermal neutron capture has been studied with the GAMS

spectrometers at ILL, and the analysis of these data is in progress. (University of Koln/ILL/BNL)

b. $^{190}Os(n,\gamma)^{191}Os$ Reaction

Earlier average capture data, as well as extensive Ge(Li) γ-γ coincidence studies at BNL, have been combined with data from the GAMS 1 spectrometer at the ILL. A detailed level scheme has been constructed but theoretical analysis has been delayed due to several puzzling features. The most prominent of these is the existence of five of the strongest transitions, which form a coincident cascade, but which cannot be incorporated into the existing level scheme. Delayed coincidence measurements have been carried out this year to see if these transitions can be placed in a cascade built on the $13/2^+$ isomer. Theoretically, this is unlikely because ^{191}Os is assumed to be prolate, not oblate as is ^{195}Pt; however, it is difficult to imagine other interpretations. The analysis of the new data is continuing. (BNL/ILL)

c. $^{124}Xe(n,\gamma)^{125}Xe$

Studies of ^{125}Xe via the $^{124}Xe(n,\gamma)^{125}Xe$ reaction at the Neutron Monochromator Facility have been completed. The results yield a rather complete level scheme giving spins and parities (or limits on these) for a large number of levels. (BNL)

d. The Nuclear Structure of ^{239}U

The γ radiation resulting from capture of 2 keV, 24 keV, and polarized neutrons on enriched ^{238}U has been studied. All levels with $J<5/2$ below 1.4 MeV have been identified, and unambiguous spin assignments based on a combination of resonance averaged capture spectra and circularly-polarized γ-ray analysis. Seventeen previously unobserved states have been identified, six of these with $J=5/2$. (ECN(Petten)/BNL)

6. Odd-odd Nuclei

a. ^{154}Eu

The odd-odd nucleus ^{154}Eu has been studied at the ILL with the GAMS and BILL spectrometers, and at the Technical University of Munich via the (d,p) reaction. Studies with the 2 keV neutron beam have been performed at BNL, as well as single resonance measurements on the neutron monochromator facility. All the data have now been analyzed, and a detailed level scheme has been constructed which incorporates about 86 levels below 600 keV in excitation energy. Almost all the possible low lying bands arising from the available two particle Nilsson configurations have been identified. A preliminary manuscript describing these results is currently in preparation. (Technical University of Munich/ILL/BNL/RIGA)

b. ^{108}Ag

Several years ago, in collaboration with physicists at several research institutes in Europe, work was carried out on the odd-odd nucleus ^{108}Ag. This consisted of studies of the γ rays from both individual resonance and average resonance capture. The level scheme has now been completed and submitted for publication. (BNL/University of London/Julich/ILL/Gatchina/Boris Kidric)

c. ^{134}Cs

As part of a collaborative effort involving Institut Boris Kidric in Belgrade, the PMF Institut in Zagreb, and the Institut for Kernphysik in Julich, studies have been carried out on the $^{133}Cs(n,\gamma)^{134}Cs$ reaction at the Neutron Monochromator Facility. The motivation for this work is to determine completely and reliably the complex low-lying level structure of odd-odd ^{134}Cs. New results obtained for neutron capture on resonances of 5.9 and 22.6 eV extend and improve results already obtained at the European Laboratories, particularly with respect to the assignment of level spins and parities. (ILL/BNL/Belgrade/Julich)

d. ^{238}Np

In a collaborative effort with Livermore, the University of Oregon, and the ILL, both individual and average resonance capture studies have been conducted on ^{238}Np. In this work a very large target of ^{237}Np was employed. The combination of the tailored beam and the individual resonance capture measurements is especially useful in this case, since, due to intensity limitations, the tailored beam results disclose only odd-parity final states, while the monochromator results give most (but not all) states of both parities, so that practically complete information on final states of both parities is obtained in the combined experiments. The experimental phase is essentially complete and the results partially analyzed. (LLL/ILL/University of Oregon/BNL)

D. FACILITY DEVELOPMENTS

1. The FEBIAD Source

The FEBIAD source was installed and successfully tested early in November 1982. It gave primary beams of Cu, Zn, Ga, Ge, As, Se, Br, Kr, Rb, Ag, Cd, In, Sn, Sb, Te, I, Xe and Cs in sufficient quantity to be competitive with other reactor based isotope separator facilities. For example, yields were 50-500 times higher than were available when TRISTAN was at Ames. Furthermore, as noted elsewhere in this report, initial experiments with this source have already observed a half-life for ^{124}Ag and have found some evidence for delayed neutrons emitted from ^{75}Cu.

2. Surface Ionization Sources

Several changes have been made to the surface ion source and extractor mechanism. By increasing the diameter of the extractor cone hole and moving it closer to the ion source, a factor of 4 increase in beam intensity was realized. By changing the target configuration from a graphite tube to a graphite cylinder with a large number of longitudinal holes, the beam intensity was increased by an additional factor of 5. Anticipated developments include modifying the ionizer to achieve a higher temperature, modifying target material and preparation procedures to increase the amount of uranium in the target and reduce the hold-up time to make it feasible to do better studies of short-lived isotopes.

The Ta-ionizer surface ionization ion source has been tested. This source produces Rb and Cs ions which are enhanced over the yields of Sr and Ba, making Rb and Cs experiments much easier due to the lower level of daughter activities. The output from the source is very high, yielding greater than 2×10^7 atoms/sec of ^{95}Rb. Gamma rays from ^{100}Rb were also observed. This source can also be operated in the negative ion mode to produce only I and Br. Operating this way, good yields of I and Br have been observed, but the larger beam divergence has prevented focus on an experimental station. New optical elements have been installed to resolve this problem. Two other types of negative ionizers will be tested in the near future: a LaB_6 ionizer and a thoriated tungsten ionizer. If necessary to obtain good yields, improvements in the magnet system used to deflect the electron beam will be implemented.

3. Perturbed Angular Correlation Facility/Superconducting Magnet

Perturbed angular correlation experiments have proved to be successful and because of their importance as a proton valence number probe, a vigorous program is anticipated. To study isotopes with shorter half lives, a new, faster, moving tape system is being designed. In order to carry out perturbed angular correlation studies in nuclei where the level lifetimes are short, a stronger magnetic field is necessary. This can best be achieved by acquiring a superconducting magnet. To this end, a superconducting magnet, capable of attaining fields of 6.5 T at 2.2°K, has been designed. It is similar to one recently purchased at Julich but incorporates certain improvements such as the capability for lower temperature (and increased field) operation and a much smaller source to detector distance. It consists of two split coils and an angled opening that allows 4 Ge(Li) detectors to view the source spot with minimum absorption. The capability of inserting additional Fe pole pieces will probably provide a further 10% field increase. Although the cryostat is an integral part of the system, the design is modular and allows different bottom flanges, liquid nitrogen casings, and moving tape through-tubes in order to accomodate a dual purpose. Specifically, by removing the optional Fe pole pieces, utilizing a through-tube with thin windows, and by inserting a hyperpure Ge detector in the central bore hole, it will be possible to carry out Q_β measurements with enormously increased efficiency and with low γ-ray background. Essentially, the field will act to spiral the electrons from the source to the detector. This dual purpose facility will be a major addition to the array of experimental techniques available at TRISTAN.

E. NATIONAL NUCLEAR DATA CENTER

1. Cross Section Evaluation Working Group (CSEWG) Activities

One meeting of CSEWG was held in May 1982 and one meeting of the Evaluation Subcommittee was held in November 1982. Release of revision 2 to ENDF/B-V was started. 28 materials $Z \leq 28$ were released in January 1983. Co, $^{107,109}Ag$, ^{10}B and 16 fertile/fissile isotopes will be released ≈ March 1983.

The schedule for ENDF/B-V is planned as follows. The formats should be fixed in Spring 1983 and the "standards" evaluation completed by Spring 1984.

A Report "Guidebook for the ENDF/B-V Nuclear Data Files" (EPRI NP-2510, ENDF-328) containing plots (300°) of all the cross section data in ENDF/B-V including the quantities η and α, RI, σ_{2200}, g, $\hat{\sigma}_f$ and σ_{14} Mev has been published and is available from EPRI.

A report "ENDF/B-V Cross Section Measurements Standards" (BNL-NCS-51619, ENDF-301) was distributed in October 1982.

A report "Benchmark Data Testing of ENDF/B-V" (BNL-NCS-31531, ENDF-311) was distributed August 1982.

The ENDF/B-V revision 2 Utility Code program tape (containing 10 codes) was distributed January 1983. The NNDC decided to discontinue distributing a different tape for DEC, CDC, and IBM computers. Instead, all machine dependent code have been incorporated into a single source file for each program. A small self documented program, SETMDC (distributed with the program tape) can be used to process each program source file and generate a source for compilation on the user's computer.

2. BNL-325 Volume I Part B

The evaluation of the resonance parameters, average resonance properties and thermal cross sections for the elements $Z=61-98$ has been completed and the results for $Z=61-80$ have been sent for review. It is expected that work on Part B will be finished by September 1983 and sent to Academic Press.

3. Nuclear Data Sheets

The NNDC has been producing the Nuclear Data Sheets at the rate of about an issue a month. Of these, nine issues a year are devoted to the nuclear structure evaluation and the remaining three for the publication of the Recent References.

The U.S. is part of an international network of evaluators contributing recommended values of nuclear structure information to the Evaluated Nuclear Structure Data file (ENSDF). Publication of the Nuclear

Data Sheets proceeds directly from this computerized file. In addition to the U.S., evaluations have been received or are anticipated from Germany, United Kingdom, USSR, France, Japan, Belgium, Kuwait, Sweden and Canada. International meetings of the network evaluators are sponsored by the IAEA and the last meeting was held at Zeist, the Netherlands in May 1982.

It is planned to bring out a new edition of the Nuclear Wallet Cards (last published in 1979) incorporating the new Wapstra mass evaluation expected to be finalized in early 1983. A computerized chart of nuclides called Computope Chart was distributed as a microfiche in 1982. This uses the data in the ENSDF, ENDF/B and the BNL-325 evaluation and can be updated/processed directly from these files without needing an independent evaluation. Since both these publications represent a subset of data extracted from the computerized ENSDF file, they are consistent and current with the Nuclear Data Sheets.

4. Data Request List

Requests for nuclear data in the 1981 Data Request List were reviewed, updated and critically examined for inclusion in the new 1983 Data Request List which is in press and will be ready for distribution in March 1983. A tape of the contents of the Data Request List was also sent to the IAEA, Vienna for inclusion in the WRENDA.

CROCKER NUCLEAR LABORATORY, UC DAVIS

A.

1. Measurement of $^{40}Ca(n,nx)$ with a Multiwire Chamber Proton Recoil Counter* (T.D. Ford,** F.P. Brady, J.L. Romero, and C.M. Castaneda)

We have collected data on ^{40}Ca using the (n,xn) reaction at E_n = 65 MeV, using the facility at Crocker Nuclear Laboratory, UC Davis. The detector, as previously reported, consists of two position sensitive multiwire chambers with a CH_2 converter and ΔE-E telescope for proton identification and energy measurement.

Figure A-1a shows the neutron beam profile from $^{7}Li(p,n)$ as measured with the detector for 60 MeV neutrons. The large error at higher energy reflects the poorer efficiency of the detector as energy increases.

Data were collected in the angular range 4 to 36 degrees from a 1 cm thick calcium target about 30 cm from the converter. The spectrum shown in Fig. A-1b represents the neutrons scattered between 7 and 9 degrees for approximately 7.5 hours of counting (including background). The full width at half maximum of the elastic peak is 3.9 MeV, or about 6%. We expected poorer resolution than in the case of (p,n) as we used a thick target and a large beamspot (2x4 cm) to increase the counting rate. Also this data must still be corrected for small gain shifts of the detector.

Data have been collected for C in the same angular and energy region and we plan to collect more ^{40}Ca data to enhance the statistics in the continuum region.

* Supported by the National Science Foundation (Grant PHY-8121003)

** Supported by Associated Western Universities Fellowship

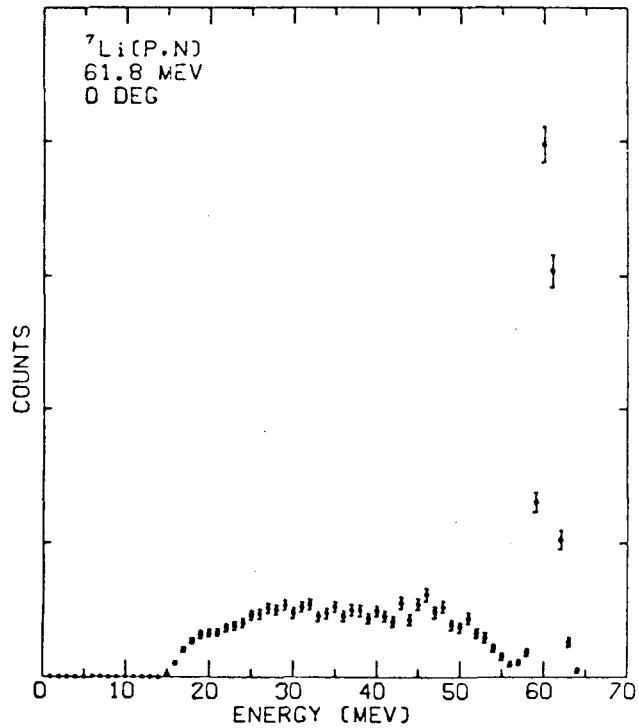

Figure A-1 (a) Spectrum from $^{7}Li(p,n)$ at 61.8 MeV, 0°.

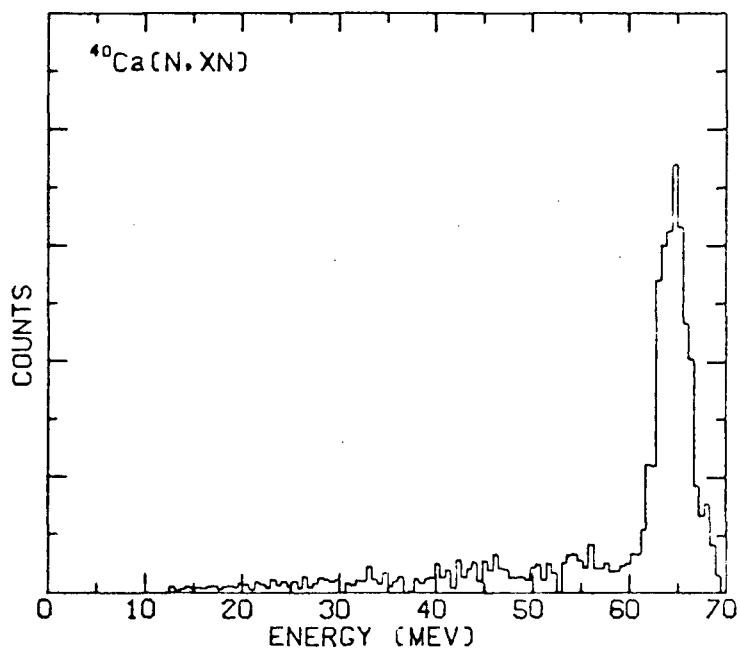

Figure A-1 (b) Spectrum from $^{40}Ca(n,n')$ at 65 MeV, 8°.

2. Precompound Analysis of $^{58-64}Ni(n,px)$ Reactions* (C.M. Castaneda, J.L. Ullmann,† F.P. Brady, and J.L. Romero)

In collaboration with M. Blann at Lawrence Livermore National Laboratory and N.S.P. King at Los Alamos National Laboratory we have compared calculations of proton angle-integrated cross sections using precompound models to the angle-integrated experimental results. In the later results, a strong isospin dependence is observed for close proton shell nuclei. The Ni isotopes is a good case to study since the isotopic spin changes by a factor of 4 in going from ^{58}Ni to ^{64}Ni. The models used: The Hybrid (H) and Geometric Dependent Hybrid (G.D.I.), which are based on the exciton model, assume that the equilibrium state in a compound nucleus is reached through two body residual interactions, which produce transitions among particle-hole configurations. None of these models, using the normal assumptions, are capable of reproducing the experimental results, as can be seeing in Figure A-2.

We have modified the Geometry Dependence Hybrid model to include the effect of the neutron skin which comes about by the neutron excess (N-Z). To calculate their neutron skin we have used the Droplet-model theory of Myers and Swiatecki. According to this theory the skin is the result of an equilibrium situation between the preference of bulk nuclear matter for symmetry and the nuclear surface energy which tends to suppress the excess neutrons at the surface. (The Coulomb energy also tends to destroy this neutron enrichment of the surface.) The end result is to shift the neutron density distribution outwards producing the neutron rich surface.

---

* Supported by the National Science Foundation (Grant PHY-8121003).

† Present address: Nuclear Physics Laboratory, University of Colorado, Boulder, CO 30309

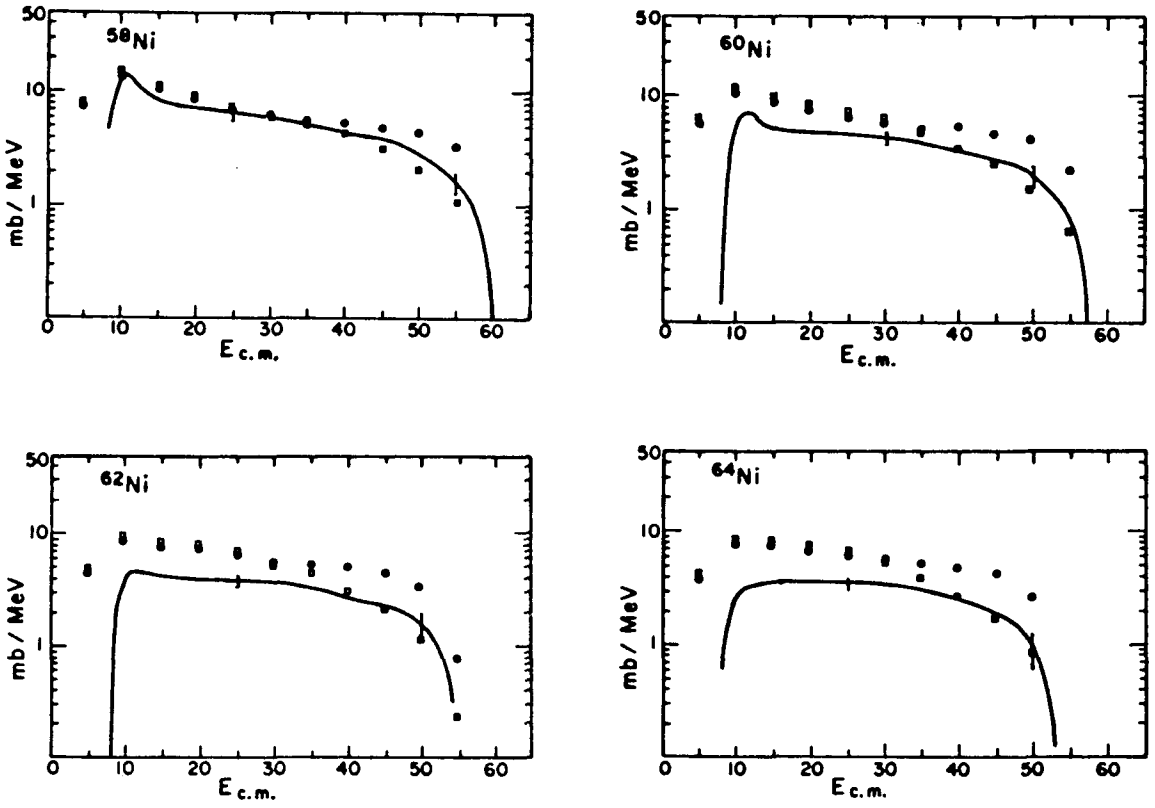

Figure A-2. GDH (●) and hybrid (□) calculations for ^{58}Ni; ^{60}Ni; ^{62}Ni, and ^{64}Ni, compared with experimental results. Solid curves resent the experimental spectra.

The results, shown in Figure A-3, of this modification to the GDH model are in the right direction producing a split in the angle-integrated cross section for the different Ni isotopes. This theoretical split is not enough yet to fully explain the experimental results, but it points to a direction in which to focus our future efforts.

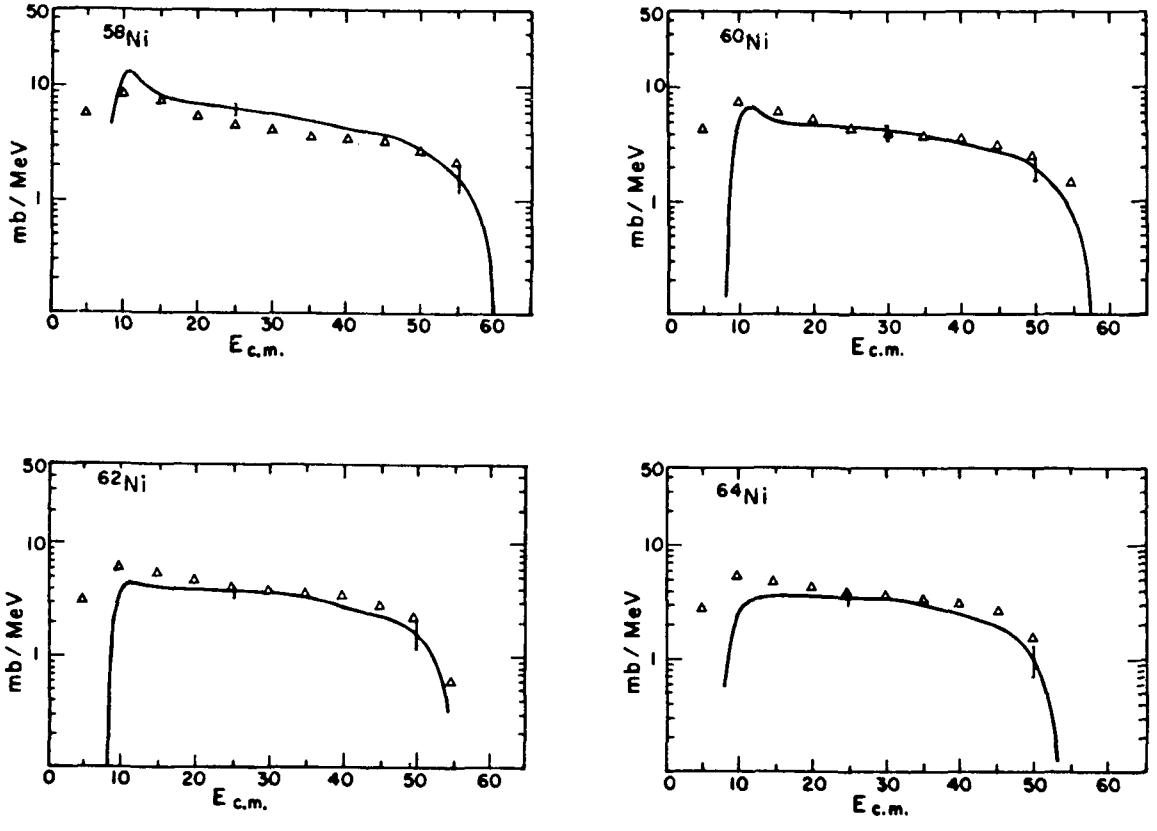

Figure A-3. GDH calculations using the neutron skin algorithm (Δ) compared with experimental results. Solid curves represent the experimental spectra.

3. Inclusive Hydrogen and Helium Spectra from Neutron-induced Reactions on C*. (T.S. Subramanian,** J.L. Romero, F.P. Brady, J.W. Watson***, D.H. Fitzgerald,† R. Garrett,†† G.A. Needham,# J.L. Ullmann,$ and C.I. Zanelli)

We have pursued the analysis of measurements of neutron-induced reactions on a project originally funded by the National Cancer Institute. In a collaboration with D. Brenner and R. Prael at Los Alamos National Laboratory, we are presently engaged in a detailed comparison with their model predictions of our measured double differential inclusive cross sections for the production of charged particles from tissue-resident elements at neutron energies of 27.4, 39.7, and 60.7 MeV. The particles detected include protons, deuterons, tritons, helium-3, and alphas, while the heavier fragments or recoils were not detected. Figure A-4 is a sample of our experimental results for 60.7 MeV neutrons incident on Carbon.

The theoretical model in Figure A-4 uses an intranuclear cascade code[1] which takes into account specific nuclear properties of Carbon, in particular, two nucleon and alpha clustering. It also allows excited nuclei to deexcite by Fermi break up mechanism. Comparisons with these calculations are in general favorable. It should be noted that, in order to improve statistics, the theoretical predictions have been averaged over 10° bins, which is considerably broader than the experimental angular resolution of around 3°. For secondary protons, deuterons and alphas, the calculation generally predicts too few high energy, direct particles at large angles. This is a direct consequence of the two-body interactions used in the intranuclear cascade code.

For comparison, the corresponding experimental results for proton-induced reactions on carbon obtained by Bertrand and Peelle[2] are also shown

---

* Supported by NCI Grant CA-16261 and NSF, Grants PHY71-03400 and PHY77-05301.

** The Radiation Oncology Center for Northern Illinois, Swedish American Hospital, Rockford, Illinois 61101.

*** Department of Physics, KSU, Kent, Ohio

† Department of Physics, UCLA, California

†† Department of Physics, University of Auckland, Auckland, New Zealand

Rocketdyne Division, Rockwell, Canoga Park, CA 91304

$ Nuclear Physics Laboratory, University of Colorado, Boulder, CO 80309

with a spline fit to the data. For the proton-induced data, charge symmetric reactions are compared, hence the (p,xt) and (p,x^{3}He) are, respectively, compared with the (n,x^{3}He) and (n,xt) reactions.

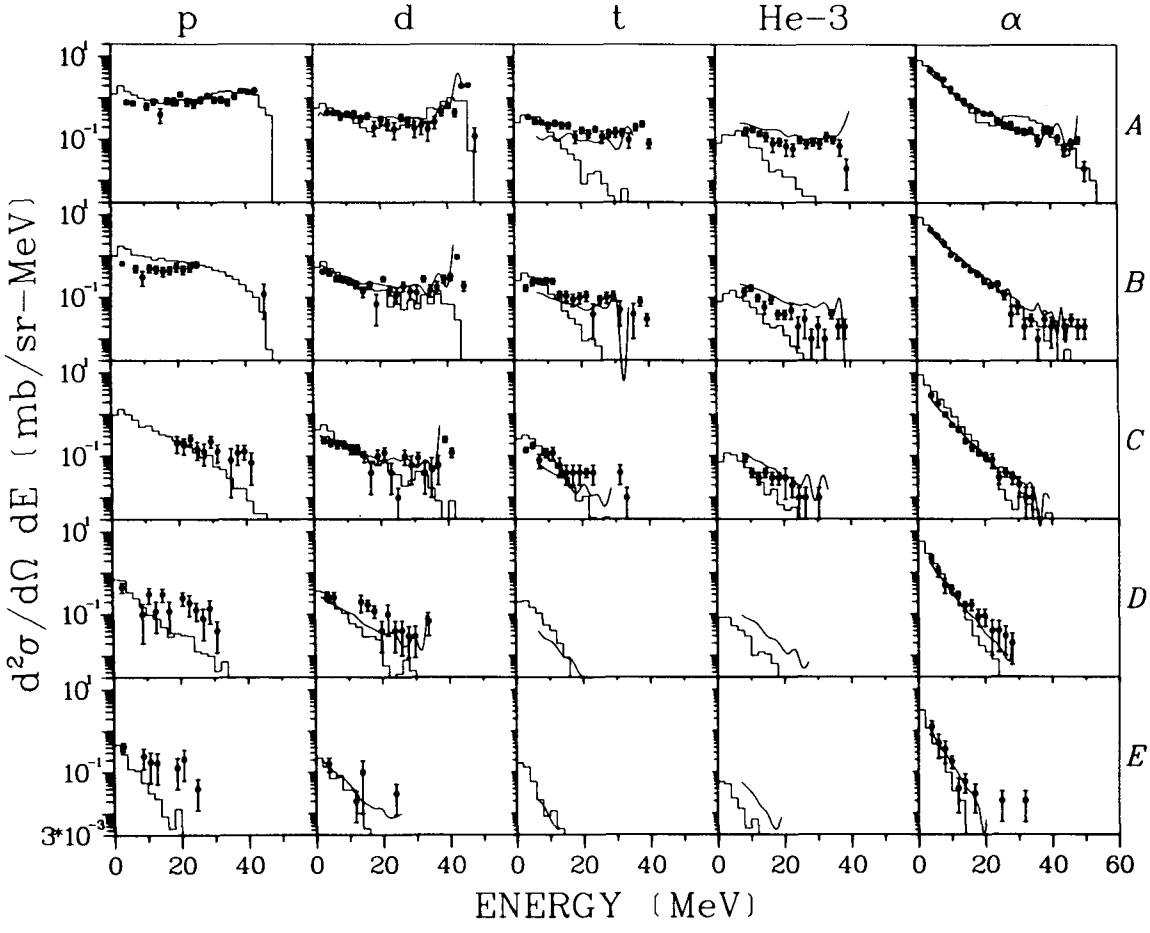

Figure A-4. Double differential cross sections for neutron on carbon at 60 MeV. See text. Key to angles: A = 20°, B = 40°, C = 65°, D = 90°, and E = 150°.

The agreement shown in Figure A-4 for all comparable particles and angles confirms the expected similarity between cross sections for reactions induced by protons and neutrons in self-conjugate nuclei. The corresponding theoretical predictions are also very similar, showing slight differences primarily due to the different particle separation energies.

---

[1] K. Chen, Z. Fraenkel, G. Friedlander, J.R. Groves, J.M. Miller, and Y. Shimamato, Phys. Rev. 166 (1968) 949.

[2] F.E. Bertrand and R.W. Peelle. Phys. Rev. C8 (1973) 3, 1045; ORNL-4799 (1973).

HANFORD ENGINEERING DEVELOPMENT LABORATORY

A. NUCLEAR DATA EVALUATION

1. Modification of ENDF/B-V Evaluation of ^{243}Am, ^{237}Np (F. M. Mann and R. E. Schenter)

Based on the recent data of Wisshak et al.(1), new Hauser-Feshbach calculations of the ^{243}Am (n,γ) reactions were performed. The ENDF/B-V evaluation which was based only on resonance parameter extrapolation was then modified.

The ENDF/B-V evaluation of ^{237}Np below 10-eV was replaced to obtain better agreement with experimental data.

2. Variance-Covariance Matrices for Fast Reactor Dosimetry Cross Sections (F. Schmittroth, F. M. Mann and R. E. Schenter)

A library of variance-covariance matrices for fast reactor dosimetry cross sections has been created. The library contains variance-covariance matrices for nearly 60 reactions in a multigroup format and was developed to support the FFTF Reactor Characterization Program. Fifty-three energy groups are used, and a code is available to convert to alternative multigroup structures. The available cross section covariance matrices include most important fast reactor actinide reactions, most common dosimeter cross sections, and other miscellaneous cross sections (e.g., krypton and xenon reactions important to gas-tagging). Several of the covariance matrices were processed directly from ENDF/B-V. Otherwise, new evaluations were made, either because the ENDF/B-V evaluations were deficient or because they were missing altogether.

B. DELAYED NEUTRON DATA

1. Compilation and Evaluation (F. M. Mann, R. E. Schenter, T. R. England* and W. B. Wilson*)

See LANL contribution B.7.

*Los Alamos National Laboratory

[1] K. Wisshak, F. Käppeler, G. Rupp, Proceedings of the Conference on Nuclear Data for Science and Technology, Antwerp, Belgium, 1982.

2. Calculation of the Population of Granddaughter States (R. E. Schenter, F. M. Mann, R. A. Warner** and P. L. Reeder**)

Using a statistical treatment of beta decay and the Hauser-Feshbach model of nuclear reactions (1), calculations were made and compared to experimental measurements using the SOLAR neutron counter (2) of the population of granddaughter (^{144}, ^{145}, ^{147}Cs and ^{95}Rb). Results show qualative agreement between calculation and experiment for all the optical models used and good quantitative agreement for the Moldauer (3), and Becchetti and Greenlees (4) potentials.

C. FFTF MEASUREMENTS

1. FFTF Shield Measurements (W. L. Bunch, L. L. Carter and F. S. Moore)

Reaction rate distribution measurements were made in accessible shield locations of the Fast Flux Test Facility reactor with the following: ^{58}Fe(n,γ), ^{54}Fe(n,p), ^{197}Au(n,γ), ^{59}Co(n,γ), ^{181}Ta(n,γ), ^{58}Ni(n,p). Samples are still being counted and data processed to establish reaction rates. Intercomparison of the reaction rates and attenuation calculations of the shields, composed primarily of steel and sodium, will provide a basis for evaluating the transport and reaction rate cross sections in various spectral environments.

2. Reaction Rate Measurements in FFTF (J. A. Rawlins, D. W. Wootan, F. Schmittroth and K. D. Dobbin)

Extensive reaction rate mapping was conducted during acceptance testing of the Fast Flux Test Facility (FFTF), a sodium cooled fast spectrum test reactor operated for DOE by Westinghouse-Hanford Company in Richland, Washington. Reaction rates measured at full reactor power (400 MW) in a central fuel assembly have been compared with calculation in a preliminary analysis. The neutron spectrum was calculated with three-dimensional diffusion theory using a 53 neutron energy group library based on ENDF/B-V data and normalized by a thermal-calorimetric calibration procedure.

**Battelle

[1] Mann, Dunn and Schenter, Phys. Rev. C25 (1982) 524.

[2] P. L. Reeder and R. A. Warner, Nucl. Inst. and Meth. 180 (1981) 173.

[3] P. A. Moldauer, Nucl. Phys. 47 (1963) 65.

[4] F. D. Becchetti, Jr. and G. W. Greenlees, Phys. Rev. 182 (1969) 1190.

Table C-1 lists the reaction rates measured to date, with C/E values and experimental uncertainties in parentheses. Appropriately neutron self shielded dosimeter cross sections were used to calculate reaction rates. The FERRET data adjustment code was used to assess consistency of measured reaction rates, calculated neutron spectra, and dosimeter cross sections. When either the $^{50}Cr(n,\gamma)$ or $^{233}U(n,\gamma)$ results were included in the analysis, their cross sections were adjusted upward approximately 20% and 60%, respectively. While the $^{50}Cr(n,\gamma)$ adjustments were comparable in magnitude with the cross section uncertainty, the $^{233}U(n,\gamma)$ adjustments were up to 3 times larger than the cross section uncertainty. It was concluded that there may be a problem with these two cross sections, and a FERRET analysis was made using only the remaining reaction rates. Notable spectrum adjustments included 10-15% upward adjustment in the region 7-MeV $<E_n<$17-MeV, and 10-30% upward adjustment in the range 10-eV $<E_n<$3-keV. Data from other fuel assemblies indicate similar results. The spectral adjustments in these regions are directly linked to the $^{55}Mn(n,2n)$ and $^{59}Co(n,\gamma)$ reactions. A consistency check in FERRET indicated a high probability that the data and a priori information were consistent.

Reaction rates measured in reflector and shield locations will also be compared with calculation. The response of non-threshold cross sections in out-of-core locations is completely different from in-core locations, so it is expected that simultaneous FERRET analysis of in-core and out-of-core reaction rate data will result in improved cross section knowledge of some dosimeters in the energy range 1-eV $<E_n<$1-MeV.

Table C-1

FFTF MID-CORE REACTION RATES

Reaction	Calculation/Experiment[$] (% Exp. Uncertainty)	
^{6}Li (n,tot ^{4}He)	0.956	(1.5%)
^{10}B(n,tot ^{4}He)	0.953	(1.5%)
^{45}Sc(n,γ)	1.117	(2.2%)
* ^{50}Cr(n,γ)	0.746	(2.4%)
^{58}Fe(n,γ)	1.017	(5.8%)
^{59}Co(n,γ)	0.861	(3.0%)
^{233}U(n,f)	1.008	(5.0%)
*^{233}U(n,γ)	0.562	(2.0%)
^{235}U(n,f)	1.020	(3.0%)
^{235}U(n,γ)	1.013	(2.0%)
^{239}Pu(n,f)	1.025	(3.0%)
^{239}Pu(n,γ)	1.044	(3.0%)
^{241}Pu(n,f)	1.060	(3.5%)
^{46}Ti(n,p)	0.944	(3.2%)
^{54}Fe(n,p)	1.026	(2.0%)
^{55}Mn(n,2n)	0.739	(2.2%)
^{58}Ni(n,p)	0.966	(2.2%)
^{237}Np(n,f)	1.033	(3.5%)
^{238}U(n,f)	1.004	(3.0%)
^{240}Pu(n,f)	1.064	(6.0%)
^{241}Am(n,f)	1.164	(16.%)

$ C/E values are prior to spectrum and cross section adjusment.

* Not used in adjustment.

IDAHO NATIONAL ENGINEERING LABORATORY

A. Nuclear-Structure And Decay-Data Evaluation Activities

1. The Use of Beta Strength-Function Data to Obtain Average Decay-Energy Values for Short-Lived Fission Products (C.W. Reich, R. L. Bunting)

In the course of our decay-data evaluation for the ENDF/B-V Fission-Product File, we became aware of measurements[1] of the beta-strength functions of a number of short-lived fission-product nuclides. Many of these were nuclides for which no other information on the emitted β or γ radiation was available. It seemed to us that data of this type could be used to provide average β- and γ-decay energies ($\langle E_\beta \rangle$ and $\langle E_\gamma \rangle$, respectively) for these nuclides, thus significantly expanding the base of "measured" data for ENDF/B-V. A method was developed to produce $\langle E_\beta \rangle$ and $\langle E_\gamma \rangle$ values from the measured β-strength-function data; and the resulting average decay-energy values were compared, where possible, with such information derived from other experiments (primarily decay-schemes studies). The results of this analysis have been published in Nuclear Science and Engineering 82, 132 (1982). The abstract of that paper is presented in the following.

In this paper, we point out that data from earlier experiments carried out to measure beta-strength functions for short-lived fission products can also be used to provide average beta- and gamma-decay energy values for these nuclides. In our evaluation of decay data for the ENDF/B-V fission product file, we have used this approach as a means of deducing average decay energy values for a number of these isotopes for which experimentally based average values would otherwise not have been available. The methods employed are discussed, and the results for the average beta-decay energies per decay, $\langle E_\beta \rangle$, are presented. Where available, $\langle E_\beta \rangle$ values deduced from decay scheme studies and from direct beta-spectrum measurements are given for purposes of comparison. Evidence is presented that suggests that the conventional decay scheme studies may not be a reliable source of average decay energy data for nuclides with large Q_β values. We propose that different types of experimental measurements, possibly involving total absorption techniques (of which the beta-strength work treated here might be considered as one example), may provide a better means of producing this important information.

2. Mass-Chain Evaluation for the Nuclear Data Sheets (R.L. Bunting, R. G. Helmer, C.W. Reich)

Through our participation in the International Nuclear Structure and Decay Data Evaluation Network, which has as one of its objecives the

---

[1] K. Aleklett, G. Nyman and G. Rudstam, Nucl. Phys. A246, 425(1975)

establishment and maintenance of a four-year cycle time for the Nuclear Data Sheets, we have the responsibility for the ten mass chains in the region $153 \leq A \leq 162$. Work on the A=160 and 161 mass chains is in progress. The evaluation of A=157 is in the prepublication review process. Work on the next two mass chains on our evaluation schedule, namely those with A=155 and 162, is planned to get underway later this year.

Our recommendation for the addition of a documentation record to the ENSDF Standard One-Card Formats was accepted and the description of this record now appears in the latest revision of the ENSDF formats manual.

B. APPLICATION OF NUCLEAR DECAY AND GAMMA-SPECTROSCOPY DATA

1. Emission Probabilities and Energies of Gamma-Ray Transitions from the Decay of ^{238}Pu (R.G. Helmer, C.W. Reich)

As a part of our laboratory involvement in the work of an internationally coordinated research program to measure and evaluate required nuclear decay data for selected transactinium isotopes, we are making precise (overall accuracy $\leq$1%) measurements of the emission probabilities (absolute intensities) of the prominent gamma-ray transitions from isotopes of U and Pu of particular importance for fission-reactor technology. The first two in this series of measurements involved the decay of ^{240}Pu and ^{239}Pu. These results have been published, as reported in our report last year to the U.S. Nuclear Data Committee. The third in this series involved the decay of ^{238}Pu. The abstract of a paper that has been submitted for publication on this work follows:

To aid in the precise quantitative assay of ^{238}Pu by means of γ-ray spectrometry, we have remeasured the emission probabilities of the γ radiation associated with its decay. The decay-rate calibration was based on a measurement of the α-emission rate by the National Bureau of Standards. The γ-ray emission rates and energies were measured with calibrated Ge spectrometers. The energy values obtained for the three prominent γ rays are 43.498$\pm$0.001, 99.853$\pm$0.003 and 152.720$\pm$0.002 keV and the respective γ -ray emission probabilities are 38.2$\pm$0.8, 7.43$\pm$0.08 and 0.936$\pm$0.010 photons per 10^5 decays.

2. Emission Probabilities and Energies of γ-Ray Transitions from the Decay of ^{233}U (C.W. Reich, R.G. Helmer, J. D. Baker, R.J. Gehrke)

As part of our laboratory effort to make precise ($\leq$1%) measurements of the emission probabilities of selected, prominent γ-ray transitions from the decay of isotopes of U and Pu important for fission-reactor technology, (see, e.g., contribution B.1, above, of this report), we have carried out measurements on a high-purity sample of ^{233}U. The emission rates of thirteen prominent γ rays from 29 to 320 keV were measured. The decay-rate calibration of the source material was based on the original calibration of

Table B-1. Emission Probabilities of Selected Prominent γ Rays From the Decay of ^{233}U

Nominal γ-Ray Energy (keV)	Emission Probability (γ/10^5 Decays) Detector		
	8-cm^3 Ge	114-cm^3 Ge	Average[d]
29.1	12.0 ±0.3[a]	--	12.0±0.3
42.4[b]	86.2 ±1.3[c]	--	86.2±1.3
54.7	18.2 ±0.3	--	18.2±0.3
119.0	4.06±0.05	4.07±0.06	4.06±0.04
120.8	3.31±0.04	3.32±0.03	4.32±0.03
135.3	2.29±0.02	2.33±0.02	2.32±0.02
146.3	6.51±0.05	6.62±0.06	6.57±0.06
164.5	6.20±0.05	6.26±0.06	6.23±0.05
208.2	2.25±0.03	2.31±0.02	2.29±0.03
245.3	3.60±0.04	3.63±0.04	3.62±0.03
291.3	5.34±0.05	5.40±0.05	5.37±0.05
317.2	7.75±0.07	7.77±0.06	7.76±0.07
320.6	2.92±0.04	2.88±0.03	2.90±0.03

[a] Includes a correction of 1% for presence of daughter γ ray.

[b] Decay-scheme studies indicate that this peak is a doublet.

[c] Includes a correction of 0.3% for presence of a daughter γ ray.

[d] Since the efficiencies of the two detectors are correlated, the uncertainty in the average is not allowed to be smaller than $\sqrt{\sigma(E)^2 + 0.4^2}$ %.

the material as well as a recent comparison with NBS-calibrated source of ^{235}U by isotope-dilution mass spectrometry. The resulting γ-ray emission probabilities are given in Table B-1. Gamma-ray energies have been determined for 32 peaks from 25 to 328 keV with uncertainties of from 1 to 11 eV.

3. Emission Probabilities and Energies of γ-Ray Transitions from the Decay of ^{235}U (R.G. Helmer, C.W. Reich)

Precise measurements of the emission probabilities of selected γ rays from the decay of ^{235}U are being carried out as a part of an activity to provide such data for a number of U and Pu isotopes important for fission-reactor technology (see the discussion in the preceding sections). The five prominent ^{235}U γ rays from 84 to 205 keV are those being measured in this study. These measurements were made on ^{235}U source material that was calibrated (in μmoles per gram of solution) by NBS. Because of the long half-life of ^{235}U and the large volumes of solution that had to be dried down to prepare suitable samples for the γ-ray counting, some of the sources were found to have a significantly nonuniform deposition of ^{235}U. This led to small, but significant, errors in using the standard detector-efficiency calibration curves (which had been measured using uniformly deposited sources). Measurements to permit the correction of the γ-ray emission probability data for the nonuniform source deposition are currently in progress.

4. γ-ray Emission Probabilities for the ^{232}U Decay Chain (R.J. Gehrke, V.J. Novick, J.D. Baker)

A number of studies and evaluations have been performed on various members of the ^{232}U decay chain, including several which report γ-ray intensity measurements. However, a comprehensive study including all members of the ^{232}U chain to provide a consistent set of γ-ray emission probabilities has not been reported.

This study was undertaken to obtain a consistent and precise set (i.e., uncertainty $<3\%$) of absolute intensities (emission probabilities) for a few γ rays throughout the entire ^{232}U decay chain.

For the ^{232}U γ rays at 57- and 129-keV, the respective emission-probability values were determined to be $P_\gamma = 0.200 \pm 0.004$ and 0.0686 ± 0.0007 γ rays per 100 decays of ^{232}U by 4π α-γ coincidence techniques. The γ-ray emission probabilities of the daughter activities were determined from (1) the relative intensities from a ^{232}U source in equilibrium with its daughter activities and (2) grow-in of the daughter activities from an initially pure ^{232}U source. The former values were normalized to the absolute intensity of the 583-keV γ ray and the latter were normalized to the above P_γ values. The emission probability of the 2614-keV ^{208}Tl γ ray was calculated from a measured α-branch intensity and its internal conversion coefficient to be (35.86 ± 0.06) γ rays per 100 decays of ^{228}Th and that of the 583-keV ^{208}Tl γ ray was determined from the decay scheme to be (30.52 ± 0.17) γ rays per 100 decays ^{228}Th. The adopted γ-ray emission pro-

babilities per 100 decays ^{228}Th, with γ-ray energies in parentheses are: ^{228}Th, $P_\gamma(84)=1.246\pm0.029$; ^{224}Ra, $P_\gamma'(241)=4.16\pm0.04$; ^{220}Rn, $P_\gamma'(549)=0.130\pm0.003$; ^{212}Pb, $P_\gamma'(238)=43.2\pm0.4$; ^{212}Bi, $P_\gamma'(727)=6.57\pm0.05$ and $P_\gamma'(39)=1.12\pm0.06$. P_γ is defined as the number of γ rays emitted per 100 decays of the parent (i.e., same) isotope; P_γ' is the number of γ rays emitted per 100 decays of the precursor, ^{228}Th, at equilibrium.

5. Emission Probability of the 316-keV γ Ray Emitted in the Decay of ^{146}Ce[1] (R.J. Gehrke)

In our survey of fission-product nuclear data, we ascertained that the data previously available on the decay of ^{146}Ce are not sufficient to provide accurate values for the γ-ray emission probability. In the most recent evaluation of mass 146 reported in the Nuclear Data Sheets[2], the transition intensities were normalized by assuming no β decay to the ground state or to the 12-keV state and by assuming that the 23-keV transition populating the 12-keV state is pure M1. This normalization led to a total intensity of ~103% and a 316-keV emission probability of 55 γ rays per 100 decays with no quoted uncertainty.

Because the chain yield for mass 146 is high in the thermal neutron fission of ^{235}U (i.e., 2.97%) and ^{239}Pu (i.e., 2.52%), the γ-ray emission probability of ^{146}Ce is important in a number of reactor-related applications. In a previous paper[3] we reported our 4π β-γ coincidence measurement of the emission probability of the 453-keV γ ray emitted in the decay of the daughter activity ^{146}Pr. With this value and the Ge γ-ray spectroscopic data obtained from following the growth and subsequent decay of ^{146}Pr from an initially pure ^{146}Ce source, we have determined the emission probability of the 316-keV γ ray to be 55.0±1.8 γ rays per 100 decays. The half-life was measured to be (13.16±0.05) min and the relative intensities of selected γ rays were also determined.

6. A 4π β-γ Coincidence System with Minimally Broadened Pulses (R.J. Gehrke, L.O. Johnson)

Over the past five years we have developed a 4π β-γ coincidence system which uses minimally broadened pulses and "quasi-extendable" dead times. The published abstract describing the performance characteristics of this system[4] follows.

---

[1] R.J. Gehrke, International Journal of Applied Radiation and Isotopes, accepted for publication.

[2] T.W. Burrows, Nucl. Data Sheets 14, 413 (1975).

[3] R.J. Gehrke and J.D. Baker, International Journal of Applied Radiation and Isotopes 31, 675 (1980).

[4] R.J. Gehrke and L.O. Johnson, Nuclear Instruments and Methods in Physics Research 204, 191 (1982).

The performance characteristics of a new type 4π β-γ coincidence system have been measured. In contrast with the conventional 4π β-γ circuitry which is based on a fixed pulse which (~2μs) and a non-extendable dead time, the pulse processing circuitry in this new system is based on a minimally broadened pulse (i.e., as narrow as 0.25 μs). In this system each pulse has a different pulse width, so that the dead times for the β- and γ-ray detectors are determined by summing the measured dead time attributed by each pulse in each channel. The β-γ coincidences are defined with an overlap coincidence circuit. This system is shown to be much less sensitive to mismatch in the coincidence timing than is the conventional system. In spite of the narrower pulse widths, no spurious β pulses are observed when the 4π proportional counter is operated near the center of its plateau. Disintegration rates were measured for calibrated sources with strength up to ~10^6 Bq. These data indicate that with this new system the disintegration rates of very intense sources (~10^6 Bq) and moderately intense sources ($<10^5$ Bq) can be determined with accuracies of ~4% and <0.1%, respectively.

7. Efficiency Calibration of a Ge Detector for 30-2800 keV γ Rays (R.G. Helmer)

As part of our effort to provide precise γ-ray emission-probability values from measurements with Ge detectors, we have carried out a precise efficiency calibration of an 8-cm^3 planar and an 114-cm^3 coaxial detector. The abstract of a paper which describes the calibration of the smaller detector follows:

As an illustration of the precision currently possible in γ-ray spectrometry, the calibration of a Ge detector for the measurement of emission rates of γ rays between 30 and 2800 keV is described. The estimated uncertainty in the resulting efficiency for point sources varies from 2% below 85 keV to 0.5% from 400 to 1400 keV. This calibration involved about 19 sources, 18 nuclides and 58 γ rays with energies from 14 to 2754 keV. These sources, obtained primarily from two metrology laboratories and our own laboratory, included both primary standards and secondary standards. Some deviations between the efficiency values from different nuclides and sources of the same nuclide are noted. The magnitudes of the necessary corrections and the various components of the uncertainty are discussed. An observed variation of the efficiency with time is illustrated and discussed.

8. Delayed Neutron Spectral Measurements (R.C. Greenwood, A.J. Caffrey)

The TRISTAN on-line mass separator at BNL is being used to measure spectra of delayed neutrons from individual fission-product isotopes. At the present time hydrogen gas-filled proportional counters are being used in order to facilitate measurement of the spectral structure down

---

[1] R.G. Helmer, Nucl. Instr. and Meth. 199, 521 (1982).

to a few keV. Analysis of the data for $^{93-96}$Rb confirms strong peaks in ^{95}Rb at 14 and 27 keV. This analysis has yielded the shapes of the delayed-neutron spectra from these Rb isotopes over an energy region of ~10 to 1200 keV. A recent set of measurements has been completed to extend these data sets to include ^{97}Rb and $^{143-145}$Cs.

C. NUCLEAR LEVEL-SCHEMES STUDIES

1. The Decay of ^{229}Th (R.G. Helmer, M.A. Lee,* C.W. Reich, I. Ahmad**)

As a part of our study of ^{233}U and its decay chain, we are studying the level scheme of ^{225}Ra, as observed in the decay of ^{229}Th, the daughter of ^{233}U. Measurements have been made of the γ-ray singles, γ -γ coincidence and α-γ coincidence spectra. A level scheme consistent with these data has been constructed. Additional measurements are planned to determine the multipolarities of selected γ-ray transitions, in order to provide definitive parity assignments for several of the observed levels.

2. Energy Separation of the Ground-State Doublet in ^{229}Th (C.W. Reich, R. G. Helmer)

Previous work[1] has suggested that the first excited state of ^{229}Th is the 3/2+[631] one-quasiparticle Nilsson state and that it lies quite close (<0.1 keV) to the 5/2 +[633] ground state. We have remeasured with high precision the energies of three γ-ray transitions and two energy differences in order to determine this energy separation more precisely. The revised upper limit on this excitation energy is 0.01 keV, assuming that the final states to which these transitions proceed are in fact those suggested in Ref. 1.

3. Level Scheme of ^{156}Gd Studied Using Neutron-Capture γ-Ray Spectroscopy (R.C. Greenwood, C.W. Reich)

A comprehensive study, utilizing neutron-capture γ-ray spectroscopy, of the level scheme of ^{156}Gd has been carried out. Research groups from Sweden and the Federal Republic of Germany and INEL were involved in this collaborative effort. The results of this work have now been published[2]; and the abstract of this paper is given below.

---

*Dickinson State College, Dickinson, N.D.

** Argonne National Laboratory

1 L.A. Kroger and C.W. Reich, Nucl. Phys. A259, 29 (1976).

2 A. Bäcklin, G. Hedin, B. Fogelberg, M. Saraceno, R.C. Greenwood, C.W. Reich, H.R. Koch, H. A. Baader, H.D. Breitig, O.W.B. Schult, K. Schreckenbach, T. von Egidy and W. Mampe, Nucl. Phys. A380, 189 (1982).

Levels up to 2.3 MeV in ^{156}Gd have been studied using the (n,γ) reaction. Energies and intensities of low-energy γ-rays and electrons emitted after thermal neutron capture have been measured with a curved-crystal spectrometer, Ge(Li) detectors and a magnetic electron spectrometer. The high-energy γ-ray spectrum has also been measured in thermal neutron capture and 2 keV resonance neutron capture. The neutron separation energy in ^{156}Gd was measured as S_n=8534.8±0.5 keV.

About 600 transitions were observed of which ~50% could be placed in a level scheme containing more than 50 levels up to 2.3 MeV excitation energy. Forty-two of these levels were grouped into 15 excited bands. In addition to the β-band at 1050 keV we observe 0^+ bands at 1168, 1715 and 1851 keV. Other positive-parity bands are: 1^+ bands at 1966, 2027 and 2187 keV; 2^+ bands at 1154 (γ-band) and 1828 keV; and 4^+ bands at 1511 and 1861 keV. Negative-parity bands are observed at 1243 keV (1^-), 1366 keV (0^-), 1780 keV (2^-) and 2045 keV (4^-). Reduced E2 and E0 transition probabilities have been derived for many transitions. The ground band, the β- and γ-bands and the 0^+ band at 1168 keV have been included in a phenomenological four-band mixing calculation, which reproduces well the experimental energies and E2 transition probabilities.

The lowest three negative-parity (octupole) bands, of which the 0^- and the 1^- bands are very strongly mixed, were included in a Coriolis-coupling analysis, which reproduces well the observed energies. The E1 transition probabilities to the ground band are also well reproduced, while those from the higher-lying 0^+ bands to the octupole bands are not reproduced. Absolute and relative transition probabilities have been compared with predictions of the IBA model and the pairing-plus-quadrupole model. Both models reproduce well the E2 transitions from the γ-band, while strong disagreements are found for the E2 transitions from the β-band. The IBA model predicts part of the decay features of the higher lying 2_2^+, 4_1^+ and 2_1^- bands.

D. SHORT-LIVED FISSION-PRODUCT STUDIES UTILIZING He-JET TRANSPORT AND ^{252}Cf SOURCES

1. Advanced System for Rapid Separation of Rare-Earth Fission Products (J.D. Baker, R.J. Gehrke, R.C. Greenwood, D.H. Meikrantz)

The following is an abstract of a paper published in the Journal of Radioanalytical Chemistry.

A microprocessor-controlled radiochemical system, which has been developed at the INEL, has been further advanced to separate individual rare-earth elements from mixed fission products in times of a few minutes. The system was composed of an automated chemistry system fed by two ~300 μg ^{252}Cf sources coupled directly by a He-jet to transport the fission products. Chemical separations were performed using two high performance

liquid chromatography columns coupled in series. The first column separated the rare-earth group by extraction chromotography using dihexyldiethylcarbamoylmethylphosphonate (DHDECMP) absorbed on Vydac C_8 resin. The second column isolated the individual rare-earth elements by cation exchange chromatography using Aminex A-9 resin with α-hydroxyisobutyric acid (α-HIBA) as the eluent. Significant results, which have been obtained to date with this advanced system, are the identification of several new nuetron-rich rare-earth isotopes including $^{155}Pm(T_{1/2} = 48+4$ s) and ^{163}Gd ($T_{1/2} = 68\pm3$ s). In addition a half-life of 41 ± 4 s is reported for ^{160}Eu.

2. Identification of a New Isotope, ^{165}Tb (R.C. Greenwood, R. J. Gehrke, J.D. Baker, D.H. Meikrantz, C.W. Reich)

The following is an abstract of a paper which has been accepted for publication in Physical Review C.

A previously unreported isotope, ^{165}Tb, has been identified, and its half-life has been measured to be 2.11 ± 0.10 min. This activity was observed in the Tb fraction separated, using a high-performance liquid chromatograph, from the fission products resulting from spontaneous fission of ^{165}Cf. Some 24 γ rays have been associated with the ^{165}Tb decay. New in the ^{165}Dy level scheme are excited states at 1337.1, 1400.2, 1773.1 and possibly 1813.7 keV, which are fed by β transitions with log ft values between 5.1 and 5.7. Configuration assignments for these states are discussed.

E. INTEGRAL REACTION-RATE AND CROSS-SECTION MEASUREMENTS

1. Capture and Fission Cross Sections for Actinides (R.A. Anderl)

Accurate neutron cross sections are required for a reliable prediction of the inventory of americium and curium isotopes in reactor fuels. The focus of our effort has been to measure fast integral cross sections for ^{241}Am and ^{243}Am in the fast neutron field of the Coupled Fast Reactivity Measurements Facility (CFRMF) and to utilize those integral data for testing evaluated cross sections.

The following is an abstract of a paper[1] on fast integral cross sections for ^{241}Am and ^{243}Am presented at the Kiamesha Lake ANS topical meeting.

This paper reports on integral capture and fission cross-section experiments for ^{241}Am and ^{243}Am in the fast neutron field of the Coupled

---

1 R.A. Anderl, N.C. Schroeder, Y.D. Harker, "Fast Integral Cross Sections for ^{241}Am and ^{243}Am," in Proceedings of the Topical Meeting on Advances in Reactor Physics and Core Thermal Hydraulics, Kiamesha Lake, N.Y., September 22-24, 1982, NUREG/CP_0034, Vol. 2, 1105 (1982).

Fast Reactivity Measurements Facility (CFRMF). The integral cross sections were derived from measurements of the $^{241}Am(n,f)$, $^{241}Am(n,\gamma)$ ^{242g}Am, $^{243}Am(n,f)$ and $^{243}Am(n,\gamma)$ ^{244g}Am integral reaction rates using gamma-spectrometric and isotope-dilution alpha-spectrometric (IDAS) techniques. Integral cross sections in barns obtained from this work are as follows: 0.450±6.2% for $^{241}Am(n,f)$, 1.22±3.5% for $^{241}Am(n,\gamma)$ ^{242g}Am, 0.353±6.1% for $^{243}Am(n,f)$ and 0.0976±4.8% for $^{243}Am(n,\gamma)$ ^{244g}Am. Conventional integral-testing analyses, based on ratios of calculated-to-measured spectrum-averaged cross sections, and least-squares-adjustment analyses were made to assess the consistency of these integral data with the corresponding cross sections on ENDF/B-V. The results of these studies are also reported here.

The least-squares-adjustment analysis reported in this paper indicated that, to achieve consistency between the measured integral data and the evaluated cross sections, the following cross section adjustments are required: $^{241}Am(n,f)$, ~10% down (0.2 MeV to 17 MeV); $^{241}Am(n,\gamma)$, ~30% up (0.1 keV to 17 MeV); $^{243}Am(n,f)$, ~13% down (0.2 Mev to 17 MeV) and $^{243}Am(n\gamma)$,~ 44% up (0.1 keV to 17 MeV). This analysis demonstrated the need for re-evaluating the ENDF/B-V fast capture and fission cross sections for these nuclides and for refining the associated covariance information on ENDF/B.

A paper[1] entitled "Actinide Integral Measurements in the CFRMF and Integral Tests for ENDF/B-V" was presented at the NEANDC/NEACRP Specialist Meeting on Fast-Neutron Capture Cross Sections. The following is an abstract for this paper.

Integral capture and/or fission rates have been reported earlier for several actinides irradiated in the fast neutron field of the Coupled Fast Reactivity Measurements Facility (CFRMF). These nuclides include ^{232}Th, ^{233}U, ^{235}U, ^{238}U, ^{237}Np, ^{239}Pu, ^{240}Pu, ^{242}Pu, ^{241}Am and ^{243}Am. This paper focuses on the utilization of these integral data for testing the respective cross sections on ENDF/B-V. Integral cross sections derived from the measured reaction rates are tabulated. Results are presented for cross-section data testing which includes integral testing based on a comparison of calculated and measured integral cross sections and testing based on least-squares-adjustment analyses.

Fission chamber measurements have been made in the CFRMF for ^{241}Am, ^{243}Am, ^{242}Pu and ^{235}U using two back-to-back NBS fission chambers and a fast data acquisition system developed by J.R. Smith for the ^{252}Cf $\bar{\nu}$ experiments. In a preliminary analysis of the data, fission-rate ratios relative to ^{235}U were determined for ^{241}Am, ^{243}Am and ^{242}Pu. Integral fission cross sections were derived from these ratios using a previously measured

---

1 R. A. Anderl, "Actinide Integral Measurements in the CFRMF and Integral Tests for ENDF/B-V," to be published in the Proceedings of the NEANDC/NEACRP Specialists Meeting on Fast Neutron Capture Cross Sections, Argonne National Laboratory, April 20-23, 1982.

integral value of 1538 mb±3.1% for ^{235}U fission. The results are: 463 mb for ^{241}Am; 356 mb for ^{243}Am; and 433 mb for ^{242}Pu. The uncertainties for these integral cross sections is ±4% or better. The fission chamber results for ^{241}Am and ^{243}Am corroborate the earlier radiometric values . The fission chamber result for ^{242}Pu is significantly different from an earlier radiometric measurement of 557 mb. The earlier measurement is suspect because of sample definition problems. A comparison of the "fission-chamber" integral cross section for ^{242}Pu to that calculated with ENDF/B-V yields a C/M of 1.10.

2. Capture Cross Sections for Fission Products (R.A. Anderl)

A review paper[1] entitled "Integral Measurements and Tests of Fission-Product Neutron Capture Cross Sections" was prepared for the NEANDC/NEACRP meeting. The following is an abstract for this paper.

This paper reviews the current status of measured integral data for fission-product fast-neutron capture and the application of those integral measurements for cross-section testing. The various types of integral experiments are described and an assessment is made of the utility of the measured data for testing cross sections. Although the integral data base is surveyed as completely as possible, specific emphasis is given to those integral data which have been published since the 1979 Bologna specialist's meeting on fission-product nuclei. As a second thrust of this paper, the utilization of measured integral data for cross-section adjustment and for conventional C/E testing is discussed. Specifically, the role of measured integral data for the ENDF/B-V evaluation of fission-product capture cross sections is addressed. A detailed discussion is presented of a study made to assess the consistency of the ENDF/B-V cross sections and the measured integral data from experiments in the Coupled Fast Reactivity Measurements Facility (CFRMF) and in the Experimental Breeder Reactor-II (EBR-II). We conclude the paper with a summary of the outstanding integral test discrepancies and point out the areas for improving consistency between integral data and evaluated cross sections.

---

1 R.A. Anderl, "Integral Measurements and Tests of Fission-Product Neutron Capture Cross Sections," to be published in the Proceedings of the NEANDC/NEACRP Specialists Meeting on Fast Neutron Capture Cross Sections, Argonne National Laboratory, April 20-23, 1982.

2 R.A. Anderl, Y.D. Harker, D.A. Millsap, JW Rogers, J.M. Ryskamp, "CFRMF Spectrum Update and Application to Dosimeter Cross-Section Data Testing," in the Proceedings of the Fourth ASTM-EURATOM Symposium on Reactor Dosimetry, Radiation Metrology Techniques, Data Bases, and Standardization, National Bureau of Standards, March 22-26, 1982, NUREG/CP-0029, Vol. 2, 623 (1982).

3. Cross Sections for Neutron Dosimetry (R.A. Anderl)

The following is an abstract of a paper which covers recent work related to improving the evaluation of cross sections of interest to reactor dosimetry.

The Coupled Fast Reactivity Measurements Facility (CFRMF) at the Idaho National Engineering Laboratory (INEL) is a Cross Section Evaluation Working Group (CSEWG) benchmark for data testing of dosimetry, fission-product and actinide cross sections important to fast-reactor technology. In this paper we present the results of our work in updating the CFRMF spectrum characterization and in applying CFRMF integral data to testing ENDF/B-V dosimeter cross sections. Updated characterization of the central neutron spectrum includes the results of neutronics calculations with ENDF/B-V nuclear data, the generation of a fine-group spectrum representation for integral data-testing applications, and a sensitivity and uncertainty analysis which provides a flux-spectrum covariance matrix related to uncertainties and correlations in the nuclear data used in a neutronics calculation. Our application of CFRMF integral data to cross section testing has included both conventional integral testing analyses and least-squares-adjustment analyses with the FERRET code. The conventional integral data-testing analysis, based on C/E ratios, indicates discrepancies outside the estimated integral test uncertainty for the ^{6}Li(n,He), ^{10}B(n,He), ^{47}Ti(n,p), ^{58}Fe(n,γ) ^{197}Au(n,γ) and ^{232}Th(n,γ) cross sections. The integral test uncertainty included contributions from the measured integral data and from the spectrum and cross sections used to obtain the calcuated integral data. Within the uncertainty and correlation specifications for the input spectrum and dosimeter cross sections, the least-squares-adjustment analysis indicated a high degree of consistency between the measured integral data and the ENDF/B-V dosimeter cross sections for all reactions except ^{10}B(n,He).

A. DECAY STUDIES OF FISSION PRODUCTS WITH TRISTAN AT THE HFBR AT BNL

The TRISTAN on-line isotope separator facility became operational at the High Flux Beam Reactor at Brookhaven National Laboratory in 1980. Using an integral target surface-ionization source combination, mass-separated beams of Rb, Sr, Cs, Ba, Ce, and Pr fission products are available for study of the above elements and their daughters. In late 1982 a multi-element FEBIAD plasma ion source was tested successfully and produced beams of a large number of other elements. Preliminary measurements made with this ion source are discussed below. Members of the Ames Laboratory group (Hill, Wohn, Wolf, Berant, and Yamamoto) have collaborated with a number of other users from BNL, Clark University, University of Maryland, and University of Oklahoma in a wide variety of measurements. Experiments have involved decay scheme studies using γ-ray spectroscopy, Q_β measurements with high-purity Ge detectors, and $\gamma\gamma$ angular correlations using a four Ge detector system. In addition Drs. A. Wolf and Z. Berant, one-year visitors from Israel, have installed a system for the measurement of "g factors" of nuclear excited states using the technique of perturbed angular correlations.

1. Evidence for the Decay of Neutron-Rich ^{152}Pr and ^{152}Ce (J. C. Hill, H. Yamamoto, and A. Wolf)

The previously unreported decay of ^{152}Pr to levels in ^{152}Nd has been studied. The ^{152}Pr half-life was measured to be 3.24 ± 0.19s, and its decay scheme was constructed based on γ singles and coincidence measurements. Excited states in ^{152}Nd at 72.58(2^+) and 236.61(4^+) were established and the E(4^+)/E(2^+) ratio of 3.26 is close to the rigid rotor value of 3.33. A γ transition observed at 285.0 keV probably results from the β^- decay of ^{152}Ce with a half-life of 3.1 ± 0.3s but that conclusion is tentative. The most likely J for the ^{152}Pr ground state is 3.

2. Decay of Mass-Separated ^{141}Cs to ^{141}Ba and Systematics of N=85 Isotones (H. Yamamoto *et al.*)

The study of the decay of 24.9s ^{141}Cs to levels in ^{141}Ba was reported last year. This material has been published[1] in Phys. Rev. C.

---

[1] Yamamoto, Wohn, Sistemich, Wolf, Walters, Chung, Gill, Shmid, Chrien, and Brenner, Phys. Rev. C 26, 1215 (1982).

3. Levels in ^{148}Ce from the Decay of Mass-Separated ^{148}La (R. L. Gill et al.)

The decay of ^{148}La was studied by γ-ray spectroscopy. A half-life of 1.05s for ^{148}La was determined from γ ray multiscaling measurements. The level scheme deduced incorporates 52 of 54 identified γ rays into a scheme with 28 levels. The decay scheme of ^{148}La is consistent with zero β branching to the ^{148}Ce ground state. The level scheme includes 0^+, 2^+, 4^+, members of the ground-state band, 0^+_β, 2^+_β, 4^+_β, 2^+_γ, 3^+_γ and 1^-, 3^- numbers of an octupole band. A manuscript on this material has been submitted to Phys. Rev. C.

4. Decay of ^{146}La and Band Structure in ^{146}Ce (F. K. Wohn et al.)

The decay of the low-spin isomer of ^{146}La to levels in even-even ^{146}Ce was studied by γ spectroscopy. More than 300 γ rays have been identified for this decay, which as a Q_β value of 6.4 MeV. No direct production of ^{146}La from the TRISTAN ion source has been established. Operation at low ion-source temperatures yields only ^{146}La from the β decay of even-even ^{146}Ba, hence the low-spin iosmer (6.27s) of ^{146}La can be isolated for study. Recent $\gamma\gamma(\theta)$ measurements have been analyzed. The ^{146}Ce levels deduced include 0^+, 2^+, 4^+, 6^+ members of the ground state band, 0^+_β, 2^+_β, 4^+_β, 2^+_γ, 3^+_γ, 4^+_γ and 1^-, 3^-, 5^- members of an octupole band. Comparison of our low-spin isomer decay with mixed low- and high-spin decays obtained at LOHENGRIN permits us to deduce the decay scheme for the $T_{1/2}$ = 10s high-spin isomer of ^{146}La.

5. Decay of ^{101}Y and the New Isotope ^{101}Sr (J. C. Hill et al.)

The TRISTAN Ta surface-ionization source was used to produce ^{101}Sr. The half-life of the new nuclide was roughly 100 ms and about 20 γ rays were observed. Levels were established in ^{101}Y at 128 and 262 keV which correspond to levels observed earlier in ^{99}Y from the decay of ^{99}Sr at 125 and 258 keV. Both probably are members of a $5/2^+[422]$ ground state Nilsson band. The decay of the ^{101}Y daughter was also observed with a half-life of about 450ms which is considerably smaller than an earlier published value of 1.1s. γ singles and coincidence measurements were carried out on the decay of both ^{101}Sr and ^{101}Y and analysis of the data is in progress.

6. Decay of the New Isotope ^{124}Ag (J. C. Hill et al.)

A survey in late 1982 with the multi-element FEBIAD ion source indicated that many elements not previously available at TRISTAN with surface ionization sources could be mass-separated and studied. In a short 8 hour run evidence for the new isotope ^{124}Ag was obtained. A very preliminary half-life of 250ms was measured. A γ ray observed at 613 keV probably is the transition from the 2_1^+ to the 0_1^+ ground state in ^{124}Cd. This compares with 569 keV for the corresponding level in

^{124}Cd and indicates a stiffening of the nucleus as the doubly-magic ^{132}Sn region is approached.

7. Surveys of Nuclides in Doubly-Magic Regions (J. C. Hill *et al.*)

The FEBIAD ion source makes possible studies of nuclei in the regions near doubly magic ^{132}Sn and ^{78}Ni. A survey of activity at A=135 indicated that ^{135}Te ($T_{1/2}$=19s) was produced in amounts available for detailed study. In a 30 minute survey all 3 γ rays known from previous decay studies of ^{135}Te were observed. ^{135}Te decays to levels in ^{135}I which is doubly-magic ^{132}Sn plus 3 protons. A survey at A=82 indicated production of ^{82}Ga($T_{1/2}\approx$0.6s) which will be a subject for future studies. It populates levels in ^{82}Ge which can be throught of as doubly-magic ^{78}Ni plus 4 protons.

8. Q_{β^-} Value Determinations for Neutron-Rich Rb and La Isotopes (D. S. Brenner *et al.*)

Beta-ray end-point energies for Rb and La fission products were measured with a hyperpure-Ge Q_β spectrometer. Coincidence measurements were used to establish β feedings and to verify level schemes for daughter nuclides. Q_β values have been determined to be 5313 ± 5 keV for ^{88}Rb, 10350 ± 100 keV for ^{94}Rb, 11550 ± 100 keV for ^{96}Rb, 12340 ± 150 keV for ^{98}Rb, 6380 ± 30 keV for ^{146}La and >5860 ± 100 keV for ^{148}La. This material has been published[2] in Phys. Rev. C.

9. Magnetic Moments of 2_1^+ States in the Neutron-Rich $^{144,146}Ba$ Isotopes (A. Wolf *et al.*)

The neutron-rich $^{144,146}Ba$ isotopes are of particular interest since they lie at the transition between vibrational and rotational like behavior. The g factors of the 2_1^+ states were measured using the integral perturbed angular correlation technique. Activities of the $^{144,146}Cs$ parents were obtained with the TRISTAN surface ionization source and moved on aluminized mylar tape to a position in a magnetic field of 22.4 kG. Coincidences were recorded by 4 Ge γ detectors in fixed positions with the B field alternately up and down. Values for $g(2_1^+)$ of 0.34 ± 0.05 and 0.28 ± 0.07 were obtained for ^{144}Ba and ^{146}Ba respectively. This material has been accepted for publication in Phys. Lett.

---

[2] Brenner, Martel, Aprahamian, Chrien, Gill, Liou, Shmid, Stelts, Wolf, Wohn, Rehfield, Dejbakhsh, and Chung, Phys. Rev. C, 26, 2166 (1982).

10. Magnetic Moment of the 1264-keV Level in ^{97}Zr (Z. Berant, et al.)

The g-factor of the $7/2^+$, 1264.4 keV level in ^{97}Zr populated via β^- decay of ^{97}Y was measured using the time-differential perturbed angular correlation method with a transverse magnetic field of 11.38 kG. Two NaI(Tl) detectors positioned at $\pm 135^o$ and 95°, 175° respectively to two large Ge detectors were used in the coincidence system. No attenuation of the anisotropy was observed due to the aluminized mylar tape. The result $g = +0.39 \pm .04$ is consistent with the Schmidt moment using $g_s^{free} = -3.83$ suggesting the configuration $g_{7/2}$ for the 1264.4 level. The observed half-life was 102.2 ± 2.5ns.

B. DECAY STUDIES AT THE KFA IN JÜLICH, GERMANY

One of us (Hill) spent a sabbatical year at the KFA Nuclear Research Center studying neutron-rich nuclei at the JOSEF separator and the JULIC cyclotron.

1. Levels in ^{102}Zr Populated in the Decay of ^{102}Y (K. Shizuma, et al.)

The β^- decay of ^{102}Y to levels in ^{102}Zr was investigated from sources produced in the thermal neutron induced fission of ^{235}U and separated using the gas-filled recoil separator JOSEF. Singles and coincident γ and X ray measurements were carried out. Only one β decaying level of ^{102}Y was observed with a half-life of 0.36 ± 0.04s. A total of 7 γ transitions were placed in a level scheme consisting of excited states in ^{102}Zr at 1523 (2^+), 478 (4^+), 731, 891, 965 (6^+), 1538, and 1823 keV. The 731-keV level may be 0^+ corresponding to the β bandhead, but additional measurements with cleaner sources will be needed in order to verify this assumption. This work was been submitted to Phys. Rev. C.

2. Identification and Decay of Neutron-Rich ^{36}P (J. C. Hill, H. R. Koch, and K. Shizuma)

The study of the decay of the new isotope ^{36}P reported last year has now been published[3] in Phys. Rev. C.

---

[3] Hill, Koch, and Shizuma, Phys. Rev. C 25, 3104 (1982).

UNIVERSITY OF KENTUCKY

A. NUCLEAR STRUCTURE STUDIES

1. Shape Transitional Nuclei. (Kleppinger, Khan, Yates)

The complex transition region between deformed rare earth nuclei and the spherical lead nuclei has been the subject of intensive study at the Van de Graaff Laboratory of the University of Kentucky for several years. This interest stems not only from evidence that this transition occurs through oblate, triaxial, and hexadecapole deformations but also from a belief that a truly unified description of nuclear structure must explain these transitions. The recent application of boson calculational techniques has led to renewed interest in the low-lying collective states of nuclei and to impressive successes in understanding these excitations. To test the current concepts of nuclear shape transitions and the models of collective nuclear motion, we have extensively utilized the (n,n'γ) reaction to examine the low-lying states of transitional nuclei in the osmium-platinum region,[1-3] taking advantage of the high energy resolution and good sensitivity of the (n,n'γ) technique, as well as its ability to place γ-rays correctly in the level scheme from threshold observations.

a. Even-Even Nuclei

In addition to the aforementioned studies[1-3] of ^{194}Pt and ^{198}Pt, we have recently completed studies of ^{190}Os, ^{192}Os, and ^{200}Hg by the (n,n'γ) reaction. Measurements of γ-ray excitation functions at incident neutron energies from 1.0 to 3.0 MeV and detailed γ-ray angular distributions were used for level placement and characterization. In many cases, the assignment of unique spin-parities was possible. Branching ratios have been extracted for comparison with the nuclear model predictions and cross sections for (n,n'γ) excitation at 2.5 have been computed by comparison with the well-known cross section of the 847-keV Fe γ ray. The significant conclusions from each of these studies are briefly summarized.

---

[1] Filo, Yates, Coope, Weil, and McEllistrem, Phys. Rev. C23, 1928 (1981).

[2] Yates, Khan, Mirzaa, McEllistrem, Phys. Rev. C23, 1993 (1981).

[3] Yates, Khan, Filo, Mirzaa, Weil, and McEllistrem, submitted to Nucl. Phys. A.

Our study of ^{192}Os and the resulting level scheme represents one of the most detailed characterizations of any nucleus in this region. The level scheme, now incorporating 54 low-spin ($J \leq 6$) states below 2.4 MeV, provides a wealth of new information. In addition to seeing all previously known low-spin levels, we have placed and assigned spins and parities to many new levels, including three below the pairing gap. The low-energy level structure of ^{192}Os is in reasonable accord with the predictions of IBA and BET. Ground, γ, and K = 4 rotational-like bands are observed, and there is evidence of triad structure built on the 0_2^+ excitation. Decay of the 0_3^+ excitation is inconsistent with predictions of both boson models. A seeming lack of definitive structure built on the 0_3^+ and 3_1^- states intimates a surprising deterioration of band structure in ^{192}Os at higher energies. An article[4] describing this work will soon be published.

While ^{190}Os has been previously studied[5,6] much more intensively than ^{192}Os, our work has produced much new information. We have placed more than ten new levels and have clarified a number of ambiguities in the level scheme. In the complex spectra ($\sim$200 γ rays below E_γ = 2 MeV) we observe evidence for the excitation of all known levels with $J \leq 6$. In contrast to ^{192}Os, the ^{190}Os nucleus appears to have a strong rotational character at all levels of excitation.

Perhaps one of the most thoroughly characterized[7] nuclei in the transitional region is ^{200}Hg. This fact has permitted us to make a useful evaluation of the capabilities of (n,n'γ) spectroscopy. Using a small sample ($\sim$10g) of ^{200}HgO we are able to confirm all previously known levels below 2 MeV. Our new data have allowed us to solve some long-standing problems in this nucleus and have provided a useful comparison with the other stable N=120 isotone, ^{198}Pt, which we had previously studied.

b. Odd-A Nuclei

With the suggestion[8] that dynamical supersymmetries may be present in complex nuclei and, in particular, in the platinum region, a number of experimental studies have focussed on this question. Gamma-ray excitation function and angular distribution data have been taken on both ^{191}Ir and ^{193}Ir.

---

4 E. W. Kleppinger and S. W. Yates, Phys. Rev. C27, in press.

5 Yates, Cunnane, Daly, Thompson, and Sheline, Nucl. Phys. A222, 276 (1974).

6 Casten, MacPhail, Kane, Breitig, Schreckenbach, and Cizewski, Nucl. Phys. A316, 61 (1979).

7 D. Breitig, R. F. Casten, and G. W. Cole, Phys. Rev. C9, 366 (1974).

8 F. Iachello, Phys. Rev. Lett. 44, 772 (1980).

The analysis of these data are progressing well and have exposed an exceptional, although not too surprising, similarity between these isotopes. While much remains to be done on these complicated level schemes we can report the identification of many new levels in both nuclei, some as low as 0.4 MeV excitation energy. Any comparisons of these data with the supersymmetry model (or other approaches such as the asymmetric rotor model) must await further analysis.

Some time ago we began an experimental study of ^{195}Pt as part of our systematic investigations of the Pt nuclei. The γ-ray spectra from the inelastic scattering reaction proved very complex at all but the lowest incident neutron energies. In a recent (n,γ) study of this nuclide, Warner et al.[9] identified all $J^{\pi} = 1/2^-$ or $3/2^-$ states below 1 MeV but were often unable to make a definitive spin assignment. Our angular distribution data, in particular, have made it possible for us to resolve many of their ambiguous spin assignments. Further work is still necessary before we can comment on the recently proposed[10] multi-j supersymmetry predictions for this region.

2. Deformed Nuclei. (Kleppinger, Yates)

An intriguing similarity of both the Bohr-Mottelson collective model and the interacting boson approximation (IBA) model is the prediction of two-phonon vibrational excitations. Although no such states have yet been clearly identified in deformed nuclei, their existence and character would have important ramifications for the nuclear models. Extensive spectroscopic information is essential for an adequate test of these representations of deformed nuclei.

The most comprehensive low-energy level scheme currently available for a deformed nucleus is certainly that of ^{168}Er. Using the ^{167}Er(n,γ)^{168}Er reaction, Davidson et al.[11] have built on previously known low-lying states of ^{168}Er and extended the level scheme to include 20 rotational bands below 2.2 MeV. We initiated a study of ^{168}Er using the (n,n'γ) reaction in order to: 1) search for possible two-phonon vibrations; and 2) test the nonselectivity of level population in the (n,n'γ) reaction.

Our γ-ray spectra and excitation functions indicate that all low-spin ($J \leq 6$) levels up to 2.0 MeV reported by Davidson et al.[11] have been excited.

---

[9] Warner, Casten, Stelts, Boerner, and Barreau, Phys. Rev. C26, 1921 (1982).

[10] Balentekin, Bars, Bijker, and Iachello, to be published.

[11] W. F. Davidson et al. J. Phys. G7, 455 (1981); 7, 843 (1981).

Furthermore, we have clear-cut evidence for an additional state at 1893 keV. This newly-placed level belies the completeness of the level scheme claimed previously[11] for this nucleus. While the decay pattern for this state is suggestive of an excitation composed of a γ vibration built on the lowest 0^+ excited state, no new low-lying candidates for two-phonon γ vibrations were observed. A companion study of ^{170}Er is presently underway. Comparisons of ^{168}Er and ^{170}Er level spectra should help ensure that possible local aberrations in the ^{168}Er spectrum are not interpreted as general features of this region or of deformed nuclei.

3. Spherical Nuclei

a. Structure of ^{146,148,149}Gd (Yates, Kleinheinz, & collaborators at LLNL and KFA-Juelich)

The realization[12] that ^{146}Gd has many of the properties of a "doubly magic" nucleus has generated intense interest in this mass region. During the latter half of 1981, S. W. Yates worked with Peter Kleinheinz and his group at the Kernforschungsanlage (KFA) Juelich, West Germany in studies of ^{148}Dy (a "two-proton" nucleus in comparison with the ^{146}Gd core) and ^{149}Dy by in-beam spectroscopic techniques. The high-lying yrast states of these nuclei were populated by α particle and heavy-ion reactions. The experiments included γ-ray singles excitation function studies, conversion electron singles measurements, γ-ray angular distributions, and γ-γ coincidence studies. Extensive new structural information which is readily interpreted in terms of the simple shell model has been obtained and preliminary reports[13,14] of this work have been given.

At the Max Planck Institute-Heidelberg, we (Yates and Kleinheinz) performed detailed ^{144}Sm(α,2nγ)^{146}Gd excitation function measurements in steps of 0.2 MeV to determine the feasibility of populating the non-yrast levels in ^{146}Gd. These measurements suggested a number of new ^{146}Gd non-yrast transitions, as well as their approximate location in the level scheme which can be deduced from the excitation function thresholds. With this information we, in collaboration with the nuclear chemistry group of LLNL, initiated a detailed (α,2n) study at the LANL Tandem Accelerator. From

---

[12] Kleinheinz, Lunardi, Ogawa, and Maier, Z. Phys. A284, 351 (1978).

[13] Julin, Yates, Soramel-Stanco, Lunardi, Kleinheinz, and Blomquist, Proc. Int. Conf. on High Angular Momentum Properties of Nuclei, Oak Ridge 1, 78 (1982).

[14] Julin, Yates, Lunardi, Soramel-Stanco, Kleinheinz, Chevallier, Chevallier, Haas, Khazrouni, Schulz, and Blomquist, Proc. Int. Conf. on High Angular Momentum Properties of Nuclear, Oak Ridge 1, 76 (1982).

extensive three-parameter γ-γ coincidence data (10^8 events), angular distribution data, and conversion electron measurements with a superconducting solenoid electron spectrometer an extensive set of non-yrast levels has been characterized. Most of these can be assigned as members of particle-hole multiplets and provide basic input data for shell model calculations in this region. The detailed analysis has progressed quite rapidly and a manuscript will be forthcoming.

b. $^{116,120,124}Sn(n,n'\gamma)$ Reactions. (Sa, Cao, Weil)

The analysis of the measurements on $^{124}Sn(n,n'\gamma)$ are nearing completion. The excitation functions of fifty-one gamma-ray production cross sections measured for $2.3 \leq E_n \leq 3.7$ MeV neutron energy have been converted to absolute cross sections by normalization to the well-known $^{56}Fe(n,n'\gamma_{847})$ cross section. From a preliminary analysis of the gamma-ray angular distributions measured at $E_n = 2.6$ and 3.5 MeV, it appears that spin-parity assignments can be given to twelve levels. Nine of these are levels which had no previous assignment. Limitations on the J^{π} of many other levels can also be set. Members of a vibrational 2-phonon triplet at $\cong$ 2.2 MeV excitation energy can now be identified.

The excitation functions of approximately forty gamma rays excited in the $^{116}Sn(n,n'\gamma)$ reaction were measured in the energy range $1.9 \leq E_n \leq 3.6$ MeV. More than twenty new gamma-ray transitions were noted in a preliminary analysis of the spectra. Angular distributions will be measured during the coming year, as will the excitation functions and angular distributions of the γ-rays from $^{120}Sn(n,n'\gamma)$.

4. <u>^{7}Be Decay Branching Ratio</u>. (Fisher, Hershberger)

The ^{7}Be beta decay branching ratio has been measured by direct observation of the number of ^{7}Be nuclei produced and the subsequent gamma emission following their decay. The total number of ^{7}Be nuclei produced by the $^7Li(p,n)^7Be$ reaction was counted using a 4-Pi neutron detector. The gamma branch was counted using a 120 cc Ge(Li) detector at a distance of 17 cm. The efficiency of the neutron detector is known to better than 3% for the neutron spectrum from this reaction. The efficiency of the gamma detector was calibrated with five separate sources and is known to better than 1% at 478 keV. Special care was given to the possibility of loss of ^{7}Be between activation and gamma counting, by using sandwich targets of 60 μg/sq-cm LiF on 500 μg/sq-cm aluminum backings covered with a layer of 130 μg/sq-cm gold or 80 μg/sq-cm aluminum. The activation was done at several proton energies with several targets. Preliminary results give (10.7±0.3) percent for the ^{7}Be decay branching ratio.

5. $^{56}Fe(n,n'\gamma)$ Reaction. (O'Brien, Sa, Weil)

For many years we have used the $^{56}Fe(n,n'\gamma)$ reaction for cross section normalization by measuring the yield of the 847-keV γ-ray. More recently we have found that it is also a useful reaction for energy calibration because of the many strong high energy (E_γ = 3-4 MeV) γ-rays that are emitted for neutrons in the energy range $3.5 \leq E_n \leq 4.5$ MeV. Gamma-ray excitation functions were measured for $3.6 \leq E_n \leq 4.5$ MeV, and also an angular distribution as E_n = 4.3 MeV, to learn more about the character of a triplet of states at 3.60 MeV excitation. Two of the states decay by ground state transitions. By direct comparison to the spectrum of a ^{56}Co source, one of these states has been identified as the 3601.9-keV state seen in the beta decays of ^{56}Co and ^{56}Mn. Significant Doppler shifts as a function of emission angle were observed for many of the γ-rays. From the Doppler shift measurements we will get new lifetime determinations for the states at E_x = 3449-, 4049- and 4100- keV excitation energy.

B. NEUTRON SCATTERING - ELASTIC AND INELASTIC

1. $^{187}Os(n,n)$ and (n,n') Cross Sections and Re/Os Nucleochronology. (Hershberger, Macklin*, Balakrishnan, Hill*, and McEllistrem)

Elastic scattering anisotropies for 60.5 keV neutron elastic scattering from $^{187,188}Os$ and the inelastic scattering cross section to the 9.75-keV excited level of ^{187}Os have been measured. These cross sections, together with the s- and p-wave strength functions, total cross sections, scattering length R', and neutron capture cross sections from the ground state for both isotopes, have been consistently treated in both potential and phase-shift analyses, so that the capture cross sections for capture from the first excited level of ^{187}Os could be determined with confidence. Our measurement of the (n,n') cross section gave a value of 1.13 b, much higher than had been expected if Re/Os nucleochronology[15] were to be reconciled with the relatively young galactic ages which seemed to be indicated by the U/Th chronology until 1983.

Thus our cross sections together with extrapolations of the expected stellar temperature of 30 keV require a galactic age of circa 18 Gyrs, rather than the 12 or 13 Gyrs indicated from U/Th chronology. However, private communication from F.-K. Thielemann of Karlsruhe indicates that a thorough review of decay rates for very heavy nuclei formed in nucleosynthesis leads to a U/Th age of about 20 Gyrs. Thus, following our measurements and interpretations and the work at Karlsruhe, nucleochronologies are once again in agreement, but at a much older galactic age than expected recently.

---

* Oak Ridge National Laboratory

[15] S. E. Woosley and W. A. Fowler, Ap. J. 233, 411 (1979).

2. ^{190}Os, ^{192}Os(n,n'). (Cao, Weil, Sa, Hanly, McEllistrem)

Measurements of neutron elastic and inelastic differential cross sections were made during the past year on ^{190,192}Os at E_n = 2.5 MeV and on ^{190}Os at E_n = 4 MeV. At the lower energy, inelastic scattering groups to the 2_1^+, 2_2^+, 4_1^+, 3_1^+ and 4_2^+ states were resolved, but at the higher energy only the inelastic scattering to the 2_1^+ state was measured with enough statistical accuracy to be useful. A coupled channels analysis of this data, along with previous measurements on ^{198}Pt and ^{192}Os in the energy range 1.5- 4.5 MeV is in progress. Previous measurements on ^{194}Pt at E_n = 2.5 and 4.5 MeV are being reanalyzed using the most recently determined value[16] of the 2_1^+ state quadrupole moment. It is hoped that the sensitivity of low-energy neutron scattering will provide some information about the non-axial excitations of these shape-transitional nuclei, and in particular their susceptibility to non-axial deformation. Previous work[17] with the Sm isotopes has shown that axial quadrupole deformations can be reliably extracted from neutron total, elastic, and inelastic scattering cross sections.

3. $^{116-124}$Sn(n,n) and Neutron-Excess Effects. (Harper, Weil, Godfrey)

The differential cross sections for elastic and inelastic neutron scattering from five even-A tin isotopes have been measured at 1.0, 1.6 and 4.0 MeV, as well as the total cross sections in the energy range $0.3 \leq E_n \leq 5.0$ MeV. The purpose of this was to investigate the effects of changing neutron excess in a sequence of isotopes with similar nuclear structure. The total cross section results have recently been published.[18] A reanalysis of the 1.0 and 1.63 MeV differential cross sections with the spherical optical model (SOM) has removed an energy dependent discrepancy in the real well depth neutron-excess dependence, and it is found to agree well with the global value. We find an imaginary well depth neutron excess dependence that is 2-3 times larger than the 12-14 MeV value often found in global fits. This work is about to be submitted for publication. Coupled channel fits with recent β_2 values for the first excited states are continuing, and are expected to give about the same result as the SOM for the real well, but a smaller neutron excess dependence for the imaginary well depth.

---

16 C. Y Chen, J. X. Saladin, and A. Hussein, B.A.P.S. 27, 705 (1982).

17 Lagrange, Lachkar, Haouat, Shamu, McEllistrem, Nucl. Phys. A345, 193 (1980).

18 R. W. Harper, T. W. Godfrey and J. L. Weil, Phys. Rev. C26, 1432 (1982).

4. $^{206,208}Pb(n,n')$ -- Collective Excitations. (Hanly, Weil, and McEllistrem)

Differential cross sections for elastic and inelastic scattering to several excited levels have been measured for 7 MeV neutrons incident on ^{208}Pb. The measurements show pronounced direct excitation not only for the 3^- first excited level, a well known octopole vibration, but also for two 5^- levels. The data also show especially strong excitation of a group of several unresolved levels near 4.5 MeV excitation energy. Additional, high resolution measurements of $(n,n'\gamma)$ production yields for incident neutron energies between 4 and 7 MeV provide the data needed to separate the strongly excited group near 4.5 MeV excitation into its components for different levels. Neutron scattering data have also been taken for 7 MeV neutrons incident on ^{206}Pb showing excitation of 3^- and 5^- levels and a collective group near 4.5 MeV excitation energy. However, the 4.5 MeV group in ^{206}Pb seems to be partially spread into excitation in neighboring excitation energy regions. It is not as strongly separated in strength from nearby excitations as is the case in ^{208}Pb.

Detailed comparison of 3^- and 5^- excitation strengths in these two nuclei should help relate the scattering potential absorptive strength in these two nuclei. The presently selected bombarding energy, 7 MeV, is near that at which other recent studies have suggested that nuclear structure influences on the scattering in Pb distort the elastic scattering cross sections' behavior from that characteristic of a scattering potential designed for the Pb mass region. Additional high resolution $(n,n'\gamma)$ data will be combined with additional neutron detection data for experiments with several Pb isotopes to explore the visibility of target excitations in elastic scattering cross sections at different incident energies and their consequent effects on determinations of scattering potentials.

C. PROTON STRENGTH FUNCTIONS

1. $88 \leq A \leq 130$ Mass Region. (Flynn, Gabbard, Hershberger, Laird*)

During the past year, much of the work on proton strength functions at sub-Coulomb bombarding energies has been analytical in nature. Using the programs GENOA (standard optical model), HELGA (Hauser-Feshbach model), CCHAN (Lane-model coupled channels), and ECIS (deformed-potential coupled channels), much work has been done to verify and gain a more detailed understanding of the anomalous, but systematic, variation of W, the imaginary part of the optical model (OM) potential, vs. A in the range $88 \leq A \leq 130$. This analysis has been based on (p,n), (p,p) and (p,γ) measurements done in this lab on eleven isotopes of Zr and Mo. An earlier analysis by Johnson et al.[19,20]

[19] C. H. Johnson, A. Galonsky and R. Kernell, Phys. Rev. Lett. 39, 1604 (1977)

which first demonstrated the anomaly was based almost entirely on (p,n) data alone. Measurements and their analysis at Kentucky have confirmed the existence of the W anomaly,[21,22,23]

Further study,[24] largely through the continuation of the systematic O.M. analysis of three zirconium isotopes and four molybdenum isotopes, has yielded new and/or more detailed information about the variation (with VR^2 approximately invariant) of the real part of the O.M. potential and the variation of the proton absorption (as reflected in the imaginary potential W) in these seven nuclei. The addition of a complete set of elastic (p,p) scattering measurements to the earlier (p,n) measurements has made this more detailed analysis possible. (See 3 and 4 below).

As postulated by Lane, et al.[25] and others, W is related to the transition rate (Fermi's Golden Rule #2) into the states of the compound nucleus and the other "states" which cause protons to disappear from the beam (absorption). Although these processes involve a complex array of reaction mechanisms, including compound nucleus formation and direct excitation of rotational and vibrational states, the qualitative description [$W = \text{const.} \ |\langle f|H'|i\rangle|^2 \ \rho(E)$] is generally understood.[25] The product of the level density and the square of the matrix element must be summed over all "types" of final states or intermediate states. The doorway (2plh) states are of special significance in the process of compound nucleus formation and theoretical computations normally treat transitions through these states.[26] Collective states are normally treated theoretically through use of deformed potentials (coupled channels). The density of states consisting of the incoming particle weakly coupled to the states in the target would also be interesting, but as yet we do not know of a good way to calculate this density.

---

[20] Johnson, Bair, Jones, Penny and Smith, Phys. Rev. C 15, 196 (1977).

[21] D. S. Flynn, R. L. Hershberger and F. Gabbard, Phys. Rev. C 20, 1700 (1979).

[22] R. L. Hershberger, D. S. Flynn and F. Gabbard, Phys. Rev. C 20, 896 (1979).

[23] Schrils, Flynn, Hershberger and Gabbard, Phys. Rev. C 20, 1706 (1979).

[24] D. S. Flynn, R. L. Hershberger and F. Gabbard, Phys. Rev. C 26, 1744 (1982).

[25] Lane, Lynn, Melkonian, and Rae, Phys. Rev. Lett. 2, 424 (1959). J. E. Lynn, Theory of Neutron Resonance Reactions, Clarendon Press, Oxford, Eng. (1969).

[26] S. M. Grimes, Phys. Rev. C 22, 436 (1980); B. Block and H. Feshbach, Ann. Phys. 23, 47 (1963).

* Eastern Kentucky University.

2. A ≅ 60 Mass Region. (Hershberger, Fisher, Gabbard)

Recently, we have begun a study of proton strength functions in the mass-60 region. Here the (p,n) contribution to the absorption cross section is not as dominant as in the mass-100 region. Hence, an analysis of the absorption cross section is much more dependent on experimental (p,p) and (p,γ) cross sections, and on the subsequent Hauser-Feshbach analysis.

3. Asymmetry Potential at Sub-Coulomb Proton Energies. (Flynn)

In the analysis of ^{90}Zr + p using the Lane model, the energy difference between the $3s_{1/2}$ single-particle resonance and the $3s_{1/2}$ isobaric-analog resonance can be related to the depth of the asymmetry potential, V_1. Using the observed energy difference of these two resonances results in a value of V_1 = 31.4 MeV at a proton energy of 3.5 MeV. This result is in excellent agreement with the analysis of Giannini *et al.*,[27] and suggests that the asymmetry potential is energy dependent with a variation from about 32 MeV at a proton energy of 3.5 MeV to about 17 MeV at a proton energy of 35 MeV.

4. Energy Dependence of the Proton-Absorptive Potential At Sub-Coulomb Energies. (Flynn, Hershberger, Gabbard)

An analysis of the proton-induced reaction cross sections for the isotopes of zirconium and molydenum reveal strong energy dependences which vary from one nuclide to the next in such a manner that at 7 MeV proton energy W is approximately independent of mass-number, whereas at 2 MeV proton energy the absorptive potential varies strongly with mass in the manner suggested by Johnson *et al.*[19] This variation is strongly correlated with the structure of the target nuclei.

5. Studies on the ^{79,81}Br(p,n) Reactions. (Fisher, Hershberger, Gabbard)

The feasibility of using ^{81}Br as a detector of the solar neutrino flux has made the measurement of the ^{81}Br(p,n) strength function and especially the ^{81}Br(p,n) threshold important. Preliminary measurements of these quantities have begun using targets of natural NaBr on aluminum backings, and further work is planned for the coming year using separated isotope targets.

---

[27] M. M. Giannini, G. Ricco, and Z. Zucchiatti, Ann. Phys. (N.Y.) 124, 208 (1979).

1. LAWRENCE BERKELEY LABORATORY

A. ISOTOPES PROJECT

(E. Browne, J.M. Dairiki, R.B. Firestone, C.M. Lederer, and V.S. Shirley)

The Isotopes Project is primarily responsible for the evaluation of nuclear structure and decay data in the A = 167-194 mass region. These evaluations are published in Nuclear Data Sheets, and the evaluated data are also entered into the Evaluated Nuclear Structure Data File (ENSDF) maintained by the National Nuclear Data Center (NNDC) at Brookhaven National Laboratory. During the past year evaluations of A = 189 and A = 190 were published in Nuclear Data Sheets; A = 169 and A = 187 are scheduled for publication in March 1983, and A = 192 is currently undergoing review. Mass chains A = 168, 171, 174, 181, and 183 are being evaluated at present.

Considerable progress has been made during the past year towards the production of the Radioactivity Handbook. This Handbook will provide recommended, evaluated decay data for applied users. Computer codes have been developed to enter data from ENSDF into the database management system DATATRIEVE and to establish necessary data links and pointers. Additional computer codes have been written for scientific checking, adoption of the best γ-ray properties independent of decay parent, and the calculation of x-ray and Auger-electron energies and intensities from internal conversion and electron capture decay.

These programs are now in place and they are discussed in detail below. At present, 64 mass chains (A = 200-263) have been incorporated into the database. Program development has begun to interactively generate output for publication. Final tables will be produced from DATATRIEVE with the UNIX document preparation system. The level scheme graphics program developed for the Table of Isotopes will be used.

The Panel on Basic Nuclear Data Compilations has requested that the Isotopes Project design a Nuclear Structure Handbook, based on ENSDF data. Preliminary Handbook specifications were presented to the Panel at its 1982 meeting at LBL; a more detailed proposal will be presented to the 1983 Panel meeting at Oak Ridge.

The Isotopes Project has taken a prominent role in promoting and advancing the science of nuclear data evaluation. For example, the DATATRIEVE system has made ENSDF data available, for the first time, to interactive searches at either local or remote computer terminals. This usage wll be actively promoted. The Isotopes Project also continues to provide input to the NNDC and its Subcommittee on Formats and Procedures directed at improving the style and scientific quality of ENSDF and the Nuclear Data Sheets and at making the evaluation process more efficient. One example is the computer program SPINOZA, described more completely below, which points out violations of physics rules in level schemes and suggests the best values of spins and parities for levels populated by γ rays and

decay. Also, systematics studies of nuclear structure data are continuing in an effort to provide a better basis for the adoption of the best nuclear data.

B. IMPLEMENTATION OF THE EVALUATED NUCLEAR STRUCTURE DATA FILE INTO DATATRIEVE

(R.B. Firestone and E. Browne)

The most comprehensive information on nuclear structure is contained in the Evaluated Nuclear Structure Data File (ENSDF). This computer file, which consists of about 500,000 records, is edited and maintained by the National Nuclear Data Center, Brookhaven National Laboratory, on behalf of the International Network for Nuclear Structure Data Evaluation. ENSDF is primarily used for the publication of mass-chain evaluations in the Nuclear Data Sheets, which serve the needs of a broad range of basic and applied users. The file may be used for studies of the systematics of nuclear properties, creation of horizontal evaluations, and the generation of specialized numerical files for complex calculations. At present these applications have been limited for the following reasons.

First, although the file has a simple structure of 80-character records with well-defined fields, the contents within these fields are not uniform; i.e., characters often appear mixed with numerical quantities. This requires elaborate computer decoding to extract the data and separate the numerical from the non-numerical quantities. Second, the file has about twelve record-types with different field definitions that are interconnected only by their sequential order in the file. For example, a "γ record", consisting of γ-ray information, always follows the "level record" containing the level properties corresponding to the deexcited level. This record organization makes the file inconvenient for use with database management systems that provide fast and efficient access to records. Finally, many connections among records are entirely missing from ENSDF. For instance, the terminal level of a γ transition is not in the file.

We have overcome these difficulties by converting the "numbers" in ENSDF into four distinct quantities. Each value is converted into a real number, its experimental uncertainty, an alphanumeric modifier (e.g., AP, LT, or IF), and the number of significant digits required to represent the number. The quantities associated with each record type were then stored in indexed files containing additional special identifier fields to interconnect the different files. For example, the file of γ-ray records also contains indices connecting each γ ray to the original ENSDF dataset identification, radioactive parent, and initial- and final-level records. These files have been stored in the VAX-11 780 computer at LBL and implemented into DATATRIEVE, a database management system provided by Digital Equipment Corporation.

We are using this database for the selective retrieval of data to present in the Radioactivity Handbook, for the generation of input data to calculate atomic x-ray and Auger-electron intensities, and to derive β-, β+, electron capture, conversion electrons, and γ-ray "binned" average energies

per decay. A project to match the nuclear energy levels populated in different reactions and decays with the "ADOPTED" levels reported in ENSDF is in progress. This will resolve a missing link in ENSDF and is indispensable for combining data from different experiments into a new "adopted" file. Although in some instances the matching procedure may require human intervention, we are minimizing this through extensive and reliable programming.

Currently 64 mass-chains (A = 200 to A = 263) have been implemented into the database, and we expect to install the entire ENSDF file within a year. We expect this numerical database to constitute a powerful research tool for theoreticians, experimentalists, and applied users.

C. X-RAY AND AUGER-ELECTRON INTENSITIES FROM K, L_1, L_2, AND L_3 ATOMIC SHELL VACANCIES PRODUCED BY NUCLEAR DECAY

(R.B. Firestone)

X-rays and Auger electrons are often the most intense radiations associated with nuclear decay. However, they are seldom accurately measured because of their low energies. The systematics and theory of atomic transitions are now known enough to reliably calculate x-ray and Auger-electron intensities arising fromn K, L_1, L_2, and L_3 atomic shell vacancies produced in nuclear decay.

Atomic vacancies are primarily produced in nuclear decay by internal conversion and electron capture decay. I have calculated the internal conversion atomic vacancies using the tables of Rosel et al.[1] and the electron capture vacancies using the tables of Bambynek et al.[2] To account for fluorescence-, Auger-, and Coster-Kronig processes I have used the tables of Krause et al.[3]

After determining the total intensity of all x-ray and Auger lines originating in each atomic shell, it is necessary to divide that intensity into the constituent lines associated with each vacancy. For x-rays, I accomplished this with a combination of the systematic data compiled by Salem et al.[4] and the theoretical calculations by Scofield.[5] I used the calculations of Chen et al.[6] to distribute the Auger intensity. Usually, values given by theory were as accurate as the experimental data.

Finally, I derived the x-ray energies from the atomic binding energies compiled by Bearden[7] and the Auger-electron energies from calculations by Larkins.[8] The ENSDF nuclear data file (DATATRIEVE version) has been selected as the source of input nuclear decay data, and the final atomic transition energies and intensities have been calculated with my computer code ATOMS. The statistical errors for all data are added in quadrature and are included with the final intensities. A comparison of experimental and calculated x-ray intensities from A = 252 nuclei is shown in Table 1. The complete set of calculated x-ray energies and intensities will appear in the Radioactivity Handbook.

TABLE 1. Comparison of Experimental and Calculated X-ray Intensities

Decay	Transition	Intensity Experiment	Intensity Calculation
^{252}Es α ^{248}Bk	K_{α_1}	0.0058 5	0.0047 8
	K_{α_2}	0.0037 3	0.0030 5
	K_{β_1}'	0.0023 2	0.0023 4
	K_{β_2}'	0.00082 8	0.00061 10
^{252}Es EC ^{252}Cf	K_{α_1}	4.7 4	4.3 8
	K_{α_2}	3.1 3	2.8 5
	K_{β_1}'	1.9 2	2.1 4
	K_{β_2}'	0.66 8	0.57 11
^{252}Cf α ^{248}Cm	L_{α_1}	2.8 3	2.5 4
	L_{α_2}	0.31 3	0.28 4
	L_{β_1}	2.6 2	2.2 4
	L_{β_2}	0.62 5	0.68 10
	L_{β_5}	0.16 3	0.16 2
	L_{γ_1}	0.70 6	0.55 10
	$L_{\gamma_{2,3}}$	0.020 4	0.016 1
	L_{γ_6}	0.15 3	0.11 2
	L	0.23 2	0.19 3

References

1. F. Rosel, et al., Atomic Data and Nucl. Data Tables 21, nos. 2-5 (1978)
2. W. Bambynek, et al., Rev. Mod. Phys. 49 (1977) 77
3. M.O. Krause, J. Phys. Chem. Ref. Data 8 (1979) 307
4. S.I. Salem, et al., Atomic Data and Nucl. Data Tables 14 (1974) 91
5. J.H. Scofield, Atomic Data and Nucl. Data Tables 14 (1974) 121 and Phys. Rev. A9 (1974) 1041
6. M.H. Chen, et al., Atomic Data and Nucl. Data Tables 24 (1979) 13
7. J.A. Bearden, Rev. Mod. Phys. 39 (1967) 78
8. F.B. Larkins, Atomic Data and Nucl. Data Tables 20 (1977) 338

D. SPINOZA: A COMPUTER CODE FOR THE SCIENTIFIC EVALUATION OF NUCLEAR DATA

(R.B. Firestone)

The computer code SPINOZA was designed to assist nuclear data evaluators in testing the consistency and scientific rigor of spin, parity, multipolarity, and other decay level-scheme assignments. This program accepts input data written in the Evaluated Nuclear Structure Data File (ENSDF) format and produces a complete tabular listing of the input data. SPINOZA also indicates, to the evaluator, scientific errors in the construction of a level scheme.

SPINOZA performs a reliable test of all level spins and parities. Beginning with states of known spin and parity, SPINOZA derives the spins and parities of all levels using the multipolarities of the interconnecting γ rays and the log*ft* values from ß-decay. All γ rays are considered to be stretched multipoles with the exception of those with an E2 multipolarity where an M1 admixture is assumed to be possible. However, the program has an option to consider E2 as a stretched transition. The γ rays of unknown multipolarity are presumed to be M1, E1, or E2. Other options allow M2 or eliminate E2 (e.g., in (n,γ) reactions). Log*ft* values are presumed to follow the selection rules of Raman.[1] If a transition is found to be inconsistent with all possible spin/parity values (as determined by other transitions), an error message is printed warning the evaluator that the transition cannot be placed. SPINOZA also differentiates between the spin/parity assignments derived from definite and less certain transitions. Finally, the program generates a listing of the possible spins and parities for each level.

In addition to deducing spins and parities, SPINOZA also verifies the level scheme intensity balances and produces a line-printer level scheme drawing. Future innovations will include a comparison of the transition probabilities with systematics. SPINOZA is expected to be an invaluable aid in the preparation of handbooks from the ENSDF file by maintaining the highest scientific standards.

Reference

1. S. Raman and N.B. Gove, Phys. Rev. C7 (1973) 1995

E. ACTINIDE PRODUCTION FROM THE REACTION OF ^{129}Xe WITH ^{248}Cm

R.B. Welch, K.J. Moody, D. Lee, K.E. Gregorich, P. Wilmarth, and G.T. Seaborg

We have measured the production cross sections for some actinide nuclides formed in the reaction of ^{129}Xe with ^{248}Cm at a projectile energy between 715 and 785 MeV (1.0 to 1.1 times the Coulomb barrier) in the target, to study the effect of using a more neutron-deficient projectile than those previously used by us in heavy-ion-induced reactions. These data are compared in Fig. 1 with the production cross sections for actinides from the similar reaction of ^{136}Xe with ^{248}Cm (ref. 1). The cross sections for

nuclides of a given element above the target ($Z > 96$) appear to be peaked about 2 mass units lighter for ^{129}Xe than for ^{136}Xe.

A ^{129}Xe beam was obtained by extraction of ^{129}Xe by the Abel injector of the SuperHILAC from a natural xenon source (26.4% ^{129}Xe) and accelerated to 1089 MeV by the SuperHILAC into our target system in S-Cave. After passing through a 1.8 mg/cm^2 havar window, 0.3 mg/cm^2 nitrogen cooling gas, and 2.3 mg/cm^2 beryllium target backing, the beam struck a 0.502 mg/cm^2 ^{248}Cm target, present as Cm_2O_3. The energy on target, as measured by a Si(Au) surface barrier detector, was 750 MeV, with a FWHM of 70 MeV.

The irradiation consisted of nine hours of approximately 250 electrical nanoamperes of $^{129}Xe^{+29}$ through the target. The reaction products were stopped in a gold catcher foil, and chemical procedures were used to create Cf, Es, and Fm alpha sources for counting. The procedures used are the same as those used by Moody et al.[1] for ^{136}Xe on ^{248}Cm.

Both of the ^{129}Xe and ^{136}Xe reactions were done at full energy of xenon out of the SuperHILAC and into the same target assembly and are approximately the same energy on target. As expected, the more neutron-deficient projectile (^{129}Xe) makes products that are more neutron deficient, in this case by about 2 mass units for a given Z. We intend to do another ^{129}Xe bombardment at the same energy to determine cross sections for neutron-deficient Cf, Es, and Fm isotopes, as well as any Bk and Am isotopes. We also intend to use different energies of ^{129}Xe and compare products with those from analogous ^{136}Xe reactions.

Reference

1. K.J. Moody, D. Lee, R. Welch, B.V. Jacak, R.M. McFarland, P.L. McGaugher, M.N. Nurmia, M. Perry, G.T. Seaborg, R.W. Lougheed, P.A. Baisden, and E.K. Hulet, Nuclear Science Division Annual Report 1979-80, LBL-11588, p. 87

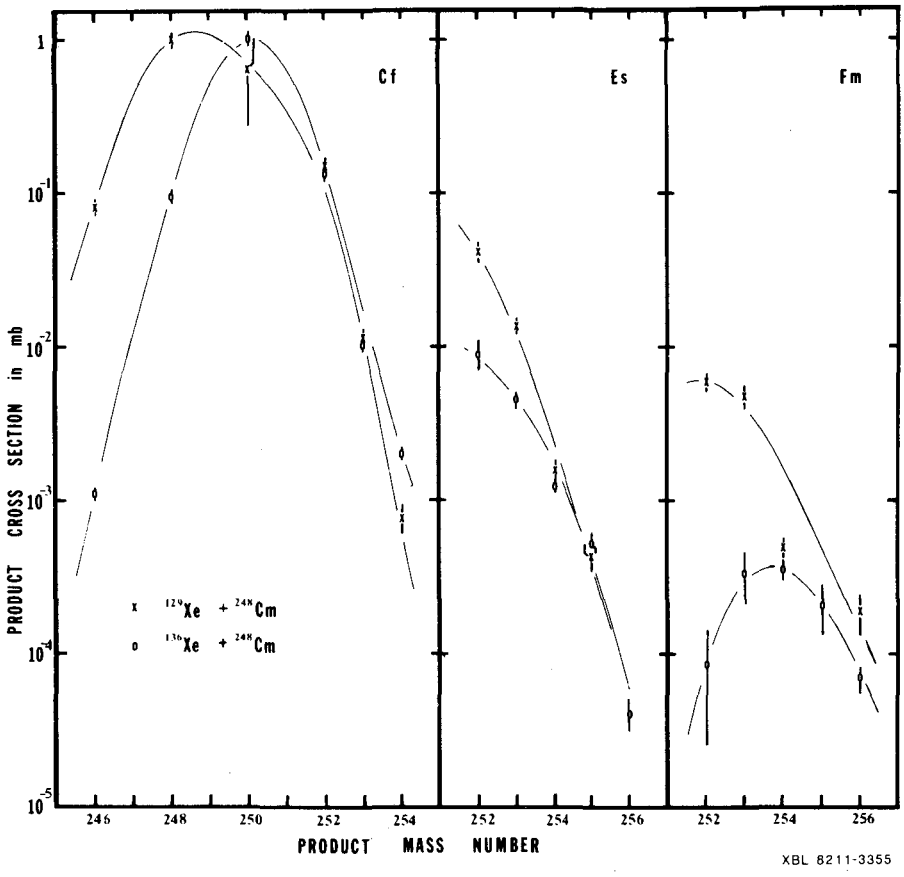

Fig. 1. Comparison of Cf, Es, and Fm product cross sections from 750 MeV ^{129}Xe + ^{248}Cm and ^{136}Xe + ^{248}Cm.

A. NUCLEAR DATA APPLICATIONS-MEASUREMENTS

1. Branching Ratio in the Decay of ^{7}Be (Mathews, Haight, Lanier and White)

Recently it has been suggested[1] that the ^{7}Be electron-capture branch to the ^{7}Li first excited state may be considerably larger than the presently adopted value of 10.4 ± 0.1%. This would imply lower cross sections for reactions producing ^{7}Be which have been determined by the 478-keV gamma rays from this decay. Particularly important is the ^{3}He(α,γ)^{7}Be reaction, a critical link in the p-p chain leading to the production of solar neutrinos. We have measured this branching ratio by implanting a ^{7}Be beam[2] into a silicon surface-barrier detector telescope and counting the subsequent gamma decays. We obtain a preliminary value of 10.7 ± 0.4% consistent with the adopted value.

2. Kerma Factor for Carbon at E_n = 14.1 MeV (Haight, Grimes,* Johnson,** and Barschall***)

The kerma factor (kinetic energy of charged particles per neutron/cm^2) for carbon has been determined at E_n = 14.1 MeV by measuring the C(n,α) cross section and the angular distribution of the alpha-particle emission spectra with a magnetic quadrupole charged-particle spectrometer. By combining these results with evaluated cross sections for elastic and discrete inelastic scattering, we infer the kerma factor to be $1.9 \pm 0.1 \cdot 10^{-11}$ Gy cm^2. This value is less than that in a recent compilation[3] by 15%.

---

* Present address: Ohio University, Athens, OH 45701.

** Present address: National Bureau of Standards, Washington, DC 20545.

*** Present address: University of Wisconsin, Madison, WI 53706.

1 C. Rolfs, BAPS, 27, 748 (1982).

2 R. C. Haight, G. J. Mathews, R. M. White, L. A. Aviles, and S. E. Woodard, Nucl. Instrum. and Methods (in press).

3 R.S. Caswell, J. J. Coyne, and M. L. Randolph, Radiation Research 83, 217 (1980).

3. Photoneutron Cross Sections with Monoenergetic Photons (Berman, Woodworth, Jury,* McNeill,** Pywell,*** Thompson****)

We have completed the analysis of our 1980 measurements at the LLNL Electron-Positron Linear Accelerator. The $^{15}N(\gamma,n)$ data (cross section and average photoneutron energy) are presented in Ref. 4, the $^{16}O(\gamma,n)$ data in Ref. 5, and the $^{28}Si(\gamma,n)$, $^{29}Si(\gamma,n)$, $^{30}Si(\gamma,n)$, and $^{30}Si(\gamma,2n)$ data in Ref. 6. Data have been obtained for ^{14}C in 1982, on a 35-Ci sample of elemental ^{14}C, in the giant-resonance region; and measurements are scheduled in early 1983 for the pygmy-resonance region on a combined sample of the above and a 50-Ci sample of $Ca^{14}CO_3$. This experiment will complete the series of total photoneutron cross-section measurements on the carbon, nitrogen, and oxygen isotopes performed at LLNL[4,5,7].

4. Neutron Differential Scattering Measurements in the Energy Range $14 \leq E \leq 38$ MeV (Hansen, Pohl, Wong, Poppe)

Elastic and inelastic differential cross sections have been measured for ^{93}Nb, ^{115}In, ^{140}Ce and ^{197}Au at 14.6 MeV. The purpose of these measurements is to fill wide gaps that exist in the data base of elastic neutron scattering. Together with our previously reported data,[8] these measurements will allow us to obtain a more complete comparison between measurements and calculations in the region $9 \leq A \leq 238$.

---

* Trent University, Peterborough, Ontario K9J 7B8, Canada.

** University of Toronto, Toronto, Ontario M5S 1A7, Canada.

*** University of Saskatchewan, Saskatoon, Saskatchewan S7N 0W0, Canada.

**** University of Melbourne, Parkville, Victoria 3052, Australia.

4 J. W. Jury *et al.*, Phys. Rev. C 26, 777 (1982).

5 B. L. Berman *et al.*, Phys. Rev. C 27, 1 (1983).

6 R. E. Pywell *et al.*, Phys. Rev. C (in press).

7 J. T. Caldwell *et al.*, Phys. Rev. Lett. 15, 976 (1965)--(^{16}O); S. C. Fultz *et al.*, Phys. Rev. 143, 790 (1966)--(^{12}C); B. L. Berman *et al.*, Phys. Rev. C 2, 2318 (1970)--(^{14}N); J. G. Woodworth *et al.*, Phys. Rev. C 19, 1667 (1979)--(^{18}O); J. W. Jury *et al.*, Phys. Rev. C 19, 1684 (1979)--(^{13}C); and J. W. Jury *et al.*, Phys. Rev. C 21, 503 (1980)--(^{17}O).

8 Hansen, Pohl, Poppe, Wong, Dietrich, BAPS 27, 721 (1982).

We have also started a program of high energy neutron elastic differential cross sections using the $^3H(d,n)^4He$ reaction and deuterons with energies $3 \leq E_d \leq 20$ MeV from the LLNL Cyclograaff facility. Preliminary measurements have been carried out for C, Fe and U at 26 and 29.5 MeV.

5. The Half-life of ^{77}Kr (Momyer, Fontanilla, Nagle, Prindle)

We produced about 8 x 10^5 Bq of ^{77}Kr for a half-life determination by irradiating enriched ^{78}Kr (99.1%) with 14 MeV neutrons at the Livermore ICT Facility. The decay of ^{77}Kr was followed in portions of the sample using thin-window, proportional counters for gross beta activity, Ge(Li) detectors for individual gamma rays (principally the 130-keV gamma), and a sodium iodide (NaI) detector for integral gamma count.

Useful data were obtained through more than ten half-lives and were analyzed for the ^{77}Kr half-life using an iterative least-squares program called Peanuts. The results are in Table A-1.

TABLE A-1. Peanuts' results for ^{77}Kr half-life

Sample	Counter	Half-life (minutes)	Error Estimate (%)
1	Beta # 1	71.219	.09
2	Beta # 1	71.245	.08
3	Beta # 2	71.129	.08
4	Beta # 2	71.128	.10
5	Ge(Li) #1	70.827	.10
6	Ge(Li) #2	71.158	.08
7	NaI	71.003	.10
	Average	71.101 ± 0.20%	

The error attached to the average is the standard deviation of a measurement estimated from the results. Our best value for the half-life of ^{77}Kr is 71.10 ± 0.14 minutes. The present literature value is 74.7 ± 0.7 minutes.[9]

6. Stellar Neutron Capture Rates for $^{86,87,88}Sr$ (Mathews, Becker, Howe)

Neutron capture cross sections from 1 to 200 keV have been measured for $^{86,87}Sr$ (and are underway for ^{88}Sr) using the Livermore electron linac as a neutron source. These cross sections are being utilized to study the s-process branching through ^{85}Kr as a monitor of the neutron capture rate during the s-process, and also to study the ^{87}Rb, ^{87}Sr chronometric pair as an independent measure of the age of

[9] I. Borchert, Zeit. Phys. 244, 338 (1971).

the galaxy. Preliminary analysis indicates a neutron-capture lifetime of 15 years for a 30 keV s-process, and a galactic age consistent with other chronometers.

7. Neutron Total Cross Cross Sections from 2.5 to 60 MeV (Phillips, White, and Camarda*)

Precision neutron total cross sections have been measured over a wide energy range for investigations of the optical model. We have completed measurements on four nuclei near mass-140, ^{139}La, ^{140}Ce, ^{142}Ce, and ^{141}Pr, and begun a study of the isotopes of calcium.

The first step in our analysis of these data was to obtain phenomenological optical model potentials which reproduce the energy dependence of the cross sections. We have also begun calculations of the optical potentials from a microscopic viewpoint using a folding model to infer the nuclear matter distributions from the data. We use two approaches to determine the effect of the nuclear medium on the force between nucleons: that suggested by Brieva and Rook,[10] which produces a density dependent interaction and that proposed by Jeukenne, Lejeune, and Mahaux,[11] which directly gives the optical potential. Preliminarily, we find better agreement with the second approach.

8. ^{142,143,144}Nd Neutron Capture Nucleosynthesis and the Origin of Meteoritic Isotopic Anomalies (Mathews, Käppeler**)

In order to better understand the origin of meteoritic abundance anomalies and the neutron capture nucleosynthesis of Nd isotopes, neutron capture cross sections have been measured for ^{142,143,144}Nd using the Kernforschungszentrum-Karlsruhe pulsed Van de Graaff proton beam to generate neutrons of 1-250 keV from the ^{7}Li(p,n) reaction. Stellarsynthesis, 30-keV Maxwellian-averaged capture cross sections of 62 ± 6, 298 ± 28, and 154 ± 8 mb have been derived for ^{142}Nd, ^{143}Nd, and ^{144}Nd respectively.

These new cross sections indicate the following: For ^{142}Nd, the cross section indicates an enhanced Nσ value for this nucleus in the s-process, which may result from alpha-particle recycling. The new higher ^{144}Nd cross section is more consistent than previous values with the expected mix of s- and r-process material for this isotope. The new cross sections tend to confirm the origin of Nd meteoritic anomalies to be due to a unique r-process-like event.

---

* Penn State University, Delaware County Campus, Media, PA 19063.

** Kernforschungszentrum Karlsruhe, Institut für Angewandte Kernphysik, Karlsruhe, Federal Republic of Germany.

10 F. A. Brieva and J. R. Rook, Nucl. Phys. A291, 317 (1977).

11 J. P. Jeukenne, A. Lejeune, and C. Mahaux, Phys. Rev. C 16, 80 (1977).

9. Measurement of the Half-life of ^{163}Ho (Baisden, Sisson, Niemeyer, Hudson, Bennett,* Naumann*)

In a continuing effort to explore the electron-capture (EC) decay properties of ^{163}Ho as a probe of neutrino mass, we have measured a half-life of 4570 ± 50 years (95% confidence level) for ^{163}Ho using isotope dilution mass spectrometry. This holmium isotope is of interest because its electron-capture Q-value (Q_{EC} = 2.6 ± 2.1 keV), though quite uncertain, is unusually small.[12] As a result, only EC from M (2.05 keV) or higher electron shells is energetically feasible, thus leaving only about 600 eV of energy for the emerging neutrino.

From the measured value of the half-life we infer an EC Q-value of 2.65 keV using known atomic physics factors and an estimate of the nuclear matrix element based on the systematics of EC ft values for the 7/2[523] to 5/2[523] electron capture transition of other Ho isotopes. The estimate of the nuclear matrix element is the dominant source of uncertainty in Q_{EC} and an uncertainty of ±30% in the matrix element corresponds to a Q_{EC} range of 2.45 to 2.90 keV.

10. Properties of Thermal-Neutron Fission of Long-Lived ^{236}Np (Lindner, Seegmiller**)

Approximately four nanograms of ^{236}Np ($^{237}Np/^{236}Np$ atom ratio = 0.272) and 60 nanograms of ^{235}U were irradiated in a stacked-foil arrangement for about seven hours in the core of the Livermore Pool-Type Reactor (LPTR). Following irradiation, no chemical separations were made; instead, the gamma-ray spectra were followed frequently for about six months, and the resultant gamma-ray photopeaks of all spectra were analyzed with the GAMANAL peak-shape fitting program.[13]

Thirty-seven fission products were identified from the decay of the observed photopeaks. The fission-product mass-yield curve was constructed by two independent methods: a) by comparison of the ^{235}U and ^{236}Np fission product photopeak intensities together with the published

---

* Princeton University, Princeton, NJ 08540.

** Present address: Kirtland Air Force Base, Albuquerque, NM 87117.

12 C. M. Lederer and V. S. Shirley, Eds., Table of Isotopes, 7th ed., Wiley, New York (1978).

13 R. Gunnink and J. B. Niday, Lawrence Livermore National Laboratory, Livermore, CA, UCRL-51061 (1971).

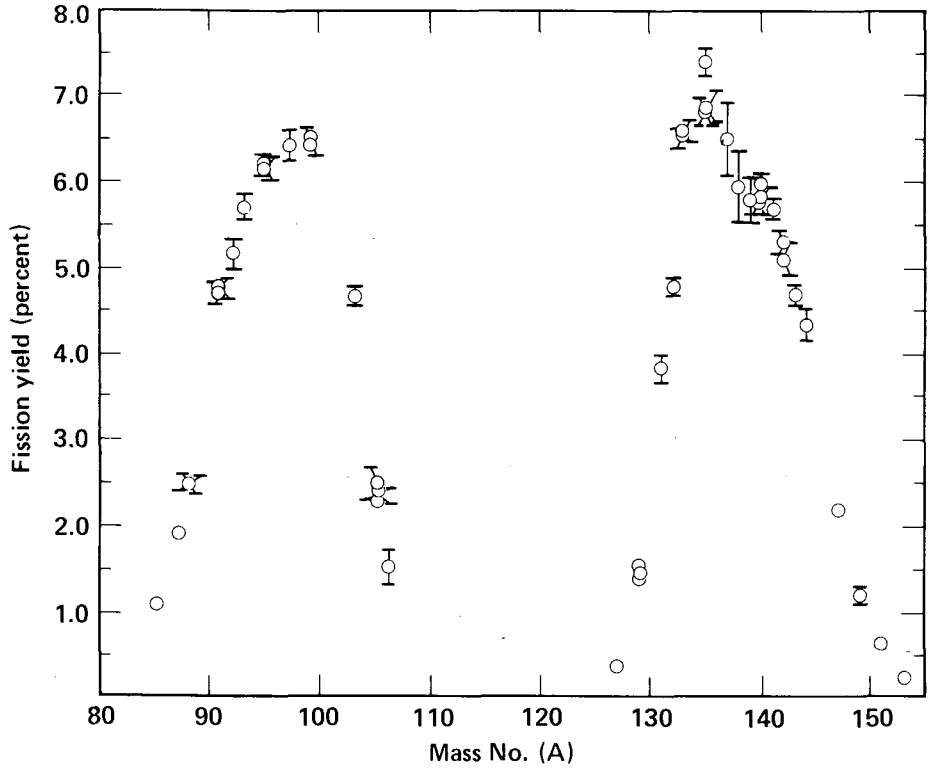

Fig. A-1. Fission-product yield vs. mass for long-lived ^{236}Np.

fission yields[14] of ^{235}U (R-value method); and b) from interpretation of the absolute intensities of the photopeak decay data. The agreement was generally good. The mass-yield curve for ^{236}Np fission obtained by method (a) is shown in Fig. A-1. It appears to show little, if any, of the "fine structure" characteristic of ^{235}U. The shape more closely approximates that of ^{239}Pu thermal fission than that of ^{235}U.

---

[14] B. F. Rider, NEDO-12154-3C ENDF322 (1981).

We have carefully examined the data for independent yields in the isobaric pairs ^{92}Sr - ^{92}Y, ^{105}Ru - ^{105}Rh, ^{131}Sb - $^{131}Te^m$, ^{133}I - ^{133}Xe, ^{135}I - ^{135}Xe, and ^{140}Ba - ^{140}La. No evidence for independent yields of ^{92}Y, ^{105}Rh, ^{135}Xe, or ^{140}La could be found within the calculated uncertainties of the data.

Independent yields of $^{131}Te^m$ and ^{133}Xe were a larger fraction of the chain yield for ^{236}Np than for ^{235}U. These yields, together with a 20-fold higher fission yield for the shielded nuclide ^{136}Cs found in ^{236}Np fission, indicate that, in some modes at least, neutron evaporation--and hence nuclear excitation--is more pronounced in ^{236}Np thermal fission than in ^{235}U.

We have also calculated the thermal fission cross section of ^{236}Np by two methods: a) by comparison with ^{235}U fissions and the known fission cross section of that nucleus, and b) by comparison with the known ^{237}Np (n,γ) cross section, the observed ^{238}Np, and the known isotope ratio $^{237}Np/^{236}Np$ of the sample. These results are shown in Table A-1.

TABLE A-1. Thermal Fission Cross Section

Comparison Method	Cross Section (b)
$^{235}U(n,f)$	$1.90 \cdot 10^3$ (± 7.6%)
$^{237}Np,(n,\gamma)^{238}Np$	$1.74 \cdot 10^3$ (± 2.9%)

Our values may be compared to that of Gindler, et al.,[15] who reported a thermal fission cross section of $(2.54 \pm 0.46) \cdot 10^3$ barns. The cross sections used for $^{235}U(n,f)$ and $^{237}Np(n,\gamma)$ are valid only for a truly thermalized neutron spectrum. The extent to which the spectrum in the core of the LPTR differed from an ideal thermal spectrum introduces uncertainties not reflected in the above estimates. Thus the agreement among the three reported values seems generally satisfactory.

---

[15] Gindler, Glendenin, Krapp, Fernandez, Flynn, and Henderson, J. Inorg. Nucl. Chem. 43, 445 (1981).

11. Revised Branching Ratios in ^{237}U and ^{238}Pu Decays (Ruhter, Camp)

The gamma-ray branching intensity value used for the ^{238}Pu, 152.68-keV gamma ray is reported to be $(9.56 \pm 0.20) \times 10^{-6}$.[16] We have remeasured[17] this value to be $(9.32 \pm 0.08) \times 10^{-6}$. Several other references[18,19] also report a reduction in this branching intensity.

The gamma-ray branching intensity value used for the ^{237}U 164.58-keV gamma-ray is reported to be $(4.53 \pm 0.10) \times 10^{-7}$.[16] This value has been remeasured and determined to be $(4.67 \pm 0.04) \times 10^{-7}$.[19,20]

---

16 R. Gunnink, J. Evans and A. Prindle, "A Reevaluation of the Gamma-Ray Energies and Absolute Branching Intensities of ^{237}U, $^{238,239,240,241}Pu$, and ^{241}Am," UCRL 52139 (1976).

17 W. Ruhter and D. Camp, "A Portable Computer to Reduce Gamma-Ray Spectra for Plutonium Isotopic Ratios," UCRL 53145 (ISPO-134) (1981).

18 J. Fleissner, J. Lemming, and J. Yarvis, "Study of a Two-Detector Method for Measuring Plutonium Isotopics," Proceedings of the ANS Conference, Analytical Methods for Safeguards and Accountability Measurements of Special Nuclear Materials, NBS 528 (1978).

19 H. Ottmar, "Results from an Interlaboratory Exercise on the Determination of Plutonium Isotopic Ratios by Gamma Spectrometry," KfK 3149, ESARDA 1/81 (1981).

20 W. Ruhter, to be published.

12. Levels of ^{244}Cm Populated by the Beta Decay of 10-hour ^{244g}Am and 26-minute ^{244m}Am (Hoff, von Egidy,* Lougheed, White** Börner,*** Schreckenbach,*** Warner,**** Barreau*****)

We have measured gamma ray and conversion-electron spectra for the ^{244}Am beta decay isomers in ^{243}Am targets undergoing neutron capture in the High Flux Reactor of the Institut Laue-Langevin at Grenoble. Six new gamma transitions are assigned to the beta decay of 26-min ^{244m}Am, including a prominent E0 transition (984.92 keV) that depopulates an excited 0^+ state in ^{244}Cm. This is the first observation of an excited 0^+ state in ^{244}Cm. The experimental observations for this transition are four electron peaks from conversion in the K, L_I, M_I, and N_I shells of curium. The observed ratio of L_I/K conversion = 0.21 ± 0.03 agrees well with theoretical values of 0.184[21] and 0.195.[22] Consistent with the placement of this E0 transition is the observation of a 941.95-keV gamma ray that is assigned as an E2 transition populating the 43-keV 2^+ level. Four other transitions, all with energies above 1 MeV, are assigned to the de-excitation of new levels in ^{244}Cm at 1084 and 1106-keV (see Fig. A-2).

The experimental value for the ratio of reduced transition probabilities from the 984.91-keV level, $X \equiv B(E0;\ 0_2^+ \rightarrow 0_1^+)/B(E2;\ 0_2^+ \rightarrow 2_1^+) = 2.1^{+1.3}_{-0.7}$, is larger than other experimental X values for 0_2^+ states in the actinide region, the average of which is 0.25. Rasmussen[23] has demonstrated that for collective vibrations of deformed nuclei (beta vibrations), one expects values of X = 0.2. On the other hand, larger values of X have been determined experimentally and produced in calculations for more highly excited 0^+ states in the actinides. The 984.91-keV level in ^{244}Cm is apparently the first excited 0^+ state in ^{244}Cm since we can set limits of no more than 10-15% of the observed beta decay to lower-lying 0^+ states (except the ground state). This level is distinctive because of its large X value relative to other 0_2^+ states in the actinide region. A more detailed description of its nature will require additional experimental and theoretical treatment.

---

* Physik-Department, Technische Universität München, 8046 Garching, Federal Republic of Germany

** Western Oregon State College, Monmouth, OR 97361.

*** Institut Laue-Langevin, 38042 Grenoble, France

**** Physics Department, Brookhaven National Laboratory, Upton, NY 11973.

*****Centre d'Etudes Nucléaires de Bordeaux-Gradignan, France.

21 D. A. Bell, C. E. Aveledo, M. G. Davidson, and J. P. Davidson, Can. J. Phys. 48, 2542 (1970).

22 R. S. Hager and E. C. Seltzer, Nucl. Data Tables A6, 1 (1969).

23 J. O. Rasmussen, Nucl. Phys. 19, 85 (1960).

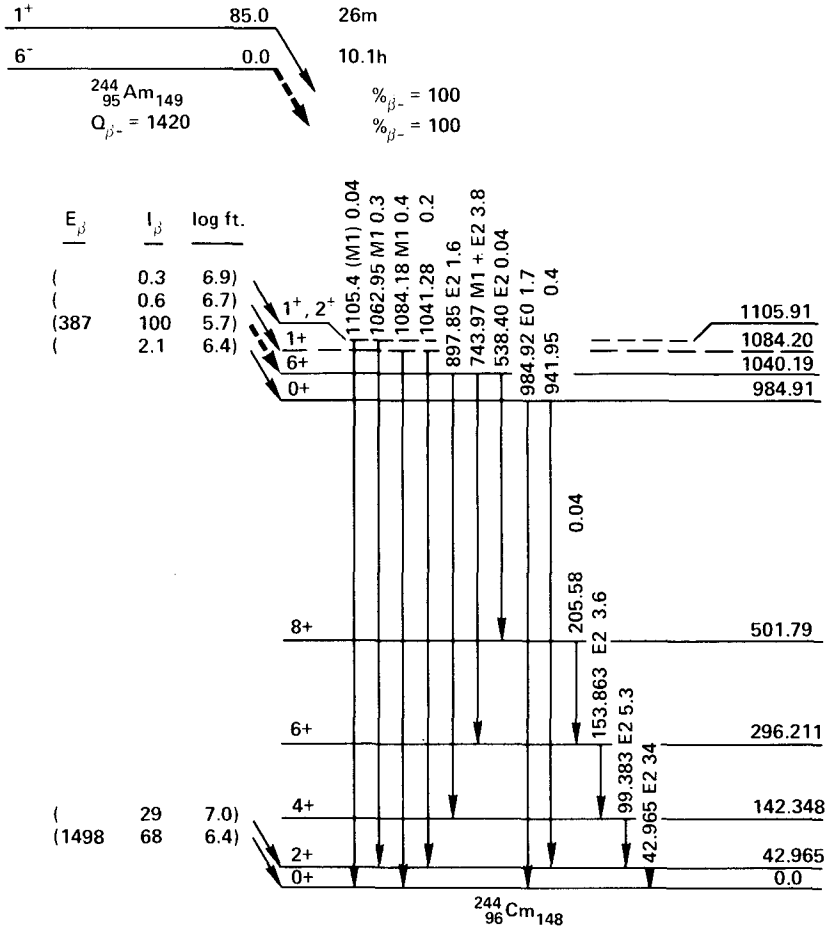

Fig. A-2. Levels of ^{244}Cm from gamma transitions accompanying beta decay of ^{244}Am isomers. Transition intensities ($I_\gamma + I_{ce}$) per 100 neutron captures are listed following gamma-ray energies and multipolarities.

B. NUCLEAR DATA APPLICATIONS-CALCULATIONS

1. Systematic Test of Microscopic Optical Models for Nucleon Scattering in the Range 7-60 MeV (Dietrich, Hansen, Phillips, Pohl, Poppe, Wong, Petrovich,* Mellema,** Finlay**)

In order to improve our ability to calculate elastic neutron scattering on targets for which direct measurements are difficult or impossible, we have undertaken a systematic study of microscopic optical models that relate nucleon scattering to the nuclear density and a realistic nucleon-nucleon interaction. The two principal models that have been tested in the range 7-60 MeV are those of Brieva and Rook[1] (BR), and Jeukenne, Lejeune, and Mahaux[2] (JLM). In both of these models, the results of nucleon-scattering calculations in nuclear matter at various densities are applied to finite nuclei by making a local-density approximation. The models have been tested against 14-MeV neutron angular distributions and total cross sections over a wide mass range and also neutron data on ^{54}Fe, ^{56}Fe, and ^{208}Pb in the range 7-26 MeV; new angular distributions in the range 20-26 MeV were measured on ^{208}Pb and the Fe isotopes in collaboration with Ohio University. The isospin properties of the models have been tested by including proton-scattering data in the analysis. Total neutron cross sections in the range 5-60 MeV for ^{140}Ce have also been calculated and compared with experiment (see Sec. A.7).

When the strengths of the calculated real and imaginary potentials are adjusted with normalizing parameters, it is found that both models yield reasonable comparisons with the shapes of the angular distribution data. In nearly all cases, the normalizing parameters lie in the ranges 1.0 ± 0.1 and 1.0 ± 0.3 for the real and imaginary potentials, respectively. The energy- and mass-dependence of the imaginary normalizing parameter is much weaker for the JLM than the BR model. Total neutron cross sections are reproduced more accurately by the JLM than the BR model; however, this is partly due to an extra parameter in the JLM model that adjusts the r.m.s. radius of the potentials. The comparison of neutron and proton scattering on ^{208}Pb shows that, when Coulomb effects are treated properly, the BR model is isospin consistent; i.e., at each energy the same normalizing parameters apply to scattering of both projectiles. Figure B-1 shows a comparison of the calculated and measured[3] elastic scattering cross sections at 14.6 MeV.

---

* Florida State University, Tallahassee, FL 32306.

** Ohio University, Athens, OH 45701.

1 F. A. Brieva and J. R. Rook, Nucl. Phys. A291, 299,317 (1977).

2 J. P. Jeukenne, A. Lejeune, and C. Mahaux, Phys. Rev. C 16, 80 (1977).

3 L. F. Hansen, B. Pohl, and C. Wong, Lawrence Livermore National Laboratory report UCID-18987 (1982).

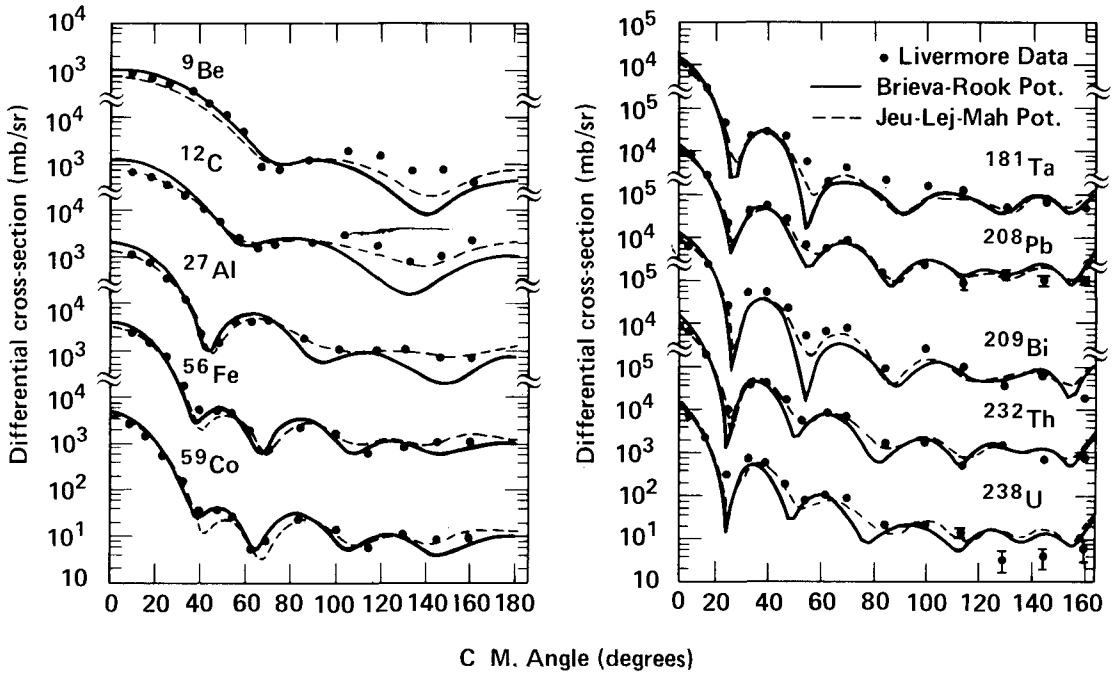

Fig. B-1. Comparison between the 14.6 MeV neutron elastic scattering measurements and calculations carried out with the JLM, and BR microscopic optical potentials.

2. Lanczos Method Shell-Model Calculations of Gamow-Teller Strength Functions (Bloom, Mathews, Aron, Fuller,* Hausman**)

A method has been developed for calculating the Gamow-Teller (GT) strength function for complex nuclei based on the Livermore system of vector method codes. The essence of the technique is to construct a collective GT state vector, |CGT>, by applying the GT operator to the parent ground state. A basis of daughter states is then constructed by applying a suitable two-body operator (e.g. double isospin flip, spin flip or $\vec{J}^2$) to the |CGT>. Finally this basis is diagonalized via a suitable number of Lanczos iterations with a Hamiltonian which includes a realistic finite-range nucleon-nucleon force. The GT strength function is then projected out of these daughter states.

---

* Enrico Fermi Institute, Univ. of Chicago, Chicago, IL 60637.

** Los Alamos National Laboratory, Los Alamos, NM 88545.

We have calculated the GT strength function for ^{90}Zr. In this calculation ground-state correlations were introduced via a pairing Hamiltonian, and the basis of daughter states (12,535 uncoupled Slater determinants) was generated by successive operations with the $\vec{T}^2$ and $\vec{J}^2$ operators. The experimental structure and widths are well reproduced for excitation energies < 16 MeV. In addition there is evidence for strength at high energies (16-25 MeV) which may have been observed experimentally but, at the moment, is tentatively assigned to L = 1. Similar calculations have also been done which allow for 2-particle, 2-hole excitations in ^{56}Fe and ^{54}Fe.

Calculations have also been done for nuclei of interest in astrophysics. For example, the GT electron-capture rates for nuclei near ^{58}Fe have been calculated. The new rates significantly decrease the rate of neutronization during gravitational collapse of a massive star. This has led to successful computations[4] of core-bounce supernovae scenarios. Efforts have also been underway to calculate the GT beta-decay rates of very neutron-rich heavy nuclei such as ^{95}Rb and ^{130}Cd which are of interest in r-process nucleosynthesis.

3. Explosive Nucleosynthesis and Direct Radiative Capture Rates (Mathews, Dietrich, Mengonni,* Thielemann,** and Fowler***)

In explosive astrophysical environments involving rapid neutron (r-process) or proton (rp-process) capture, the capture reactions may involve low Q values ($\sim$1 MeV), and few (or no) compound nuclear resonances. In this case, the nuclear statistical-model assumptions usually applied are not valid and the reaction rates may be more appropriately described by a direct radiative capture (DRC) mechanism. We have made global calculations of DRC rates for neutron and proton reactions with nuclei far from the line of beta stability. One such comparison is shown in Fig. B-2 which shows DRC Maxwellian averaged neutron capture cross sections compared with two different Hauser-Feshbach estimates. The calculations include nuclei near beta stability, out to, and beyond the r-process peak at A = 130, N = 82. Near the r-process path the DRC cross sections become comparable to or greater than the statistical-model estimates and hence should be included in network calculations. Since the DRC rates can also be taken as a lower limit, we utilize this limit to infer a critical neutron density of $\rho_n > 1.5 \times 10^{-20}$ cm^{-3} above which $(n,\gamma) \rightleftarrows (\gamma,n)$ equilibrium is guaranteed in the r-process at any temperature.

---

* Kernforschungszentrum Karlsruhe, Institut für Angewandte Kernphysik, Karlsruhe, Federal Republic of Germany.

** Max Planck Institut für Astrophysik, Garching, Federal Republic of Germany.

*** California Institute of Technology, Pasadena, CA 91125.

[4] T. A. Weaver, S. E. Woosley, and G. M. Fuller, BAAS 14, 957 (1983).

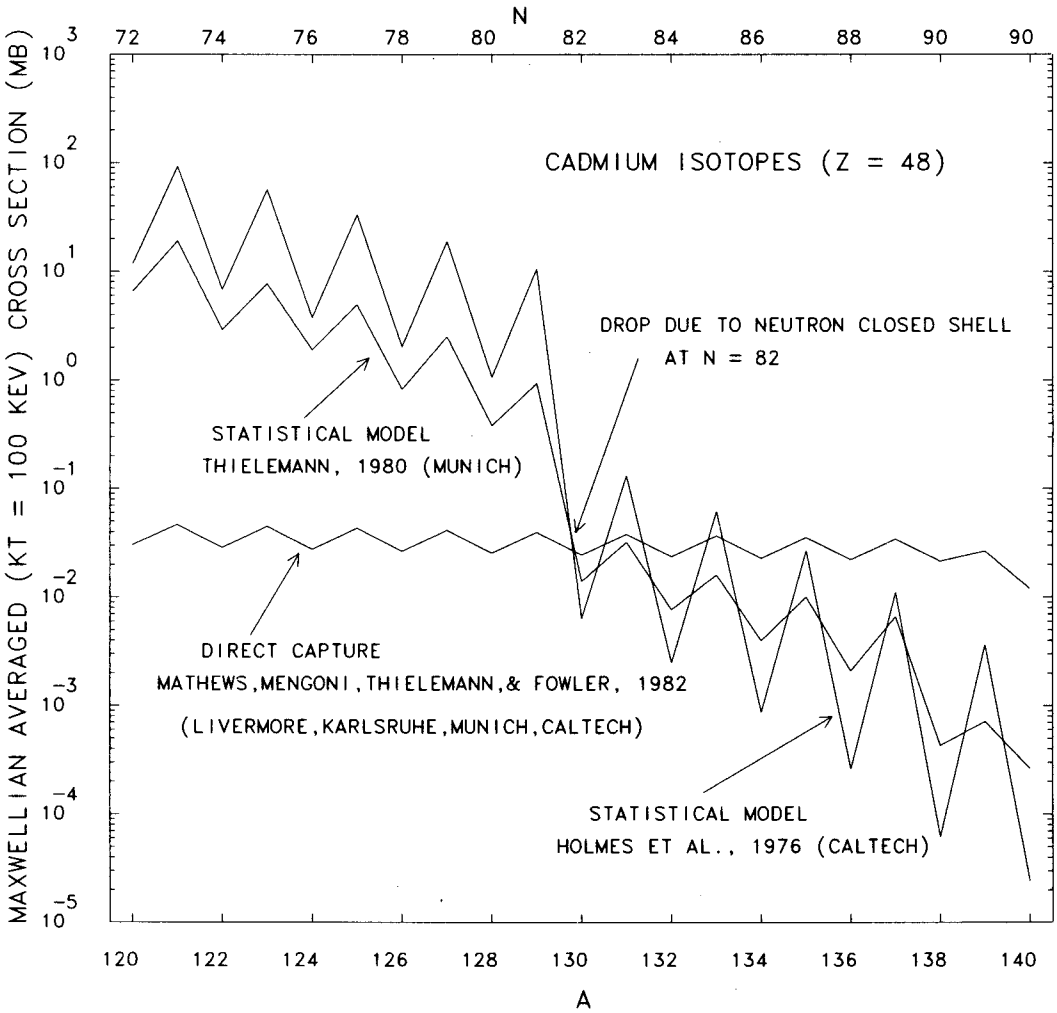

Fig. B-2. Maxwellian-averaged neutron-capture cross sections for cadmium isotopes calculated with the direct radiative capture model and two Hauser-Feshbach, statistical models.

4. Calculation of Fission Cross Sections (White)

We have completed a computer code, FISCAL, employing Hauser-Feshbach theory, to calculate the fission cross sections over the energy region of the fission neutron spectrum, from ∿100 keV to ∿5 MeV. In this energy region many of the fissile actinides have 'macroscopic' structure as seen, for example, in the $^{235}U(n,f)$ and $^{245}Cm(n,f)$ cross sections around 1 MeV neutron energy. We have applied the code to these two nuclei to investigate this structure around 1 MeV as well as the general shape and magnitude of the fission cross section in the energy range from 100 keV to 5 MeV. The code allows flexible input of neutron transmission coefficients, discrete levels and level density representations of both the residual and compound nuclei. Also included are

discrete levels and level density representations of fission transition states at both barriers of a double-humped fission barrier. Results and conclusions of our calculations of the $^{235}U(n,f)$ and $^{245}Cm(n,f)$ cross sections have been reported.[5]

C. NUCLEAR DATA APPLICATIONS-EVALUATIONS

1. Evaluated Data Libraries (Howerton)

During the past year ENDL82, ACTL82, and ECPL82 were prepared and distributed. ENDL82 is the 1982 version of the LLNL Evaluated Neutron Data Library. ACTL82 is the 1982 version of the LLNL Evaluated Neutron Activation Data Library. ECPL82 is the 1982 version of the LLNL Charged Particle Data Library.

Considerable modifications are made to all these data files. Complete evaluations for six new materials were added to ENDL ($^{74,75}As$, $^{88,89}Y$, ^{233}Pa, ^{237}Pu); over two hundred activation cross sections were added to ACTL; six new reactions and Maxwell-averaged average energies for residuals and reacting particles were added to ECPL. Since ENDL now contains explicit energy distributions for all secondary particles ($Z \leq 2$, $A \leq 4$), it is possible to check for total energy imbalances. A code (GAMCHK) was written to do the checking and total photon production cross sections were assumed to be the source of any imbalance. The photon production cross section was modified to insure total energy balance within 10% if the imbalance was greater than 100 keV. If the imbalance was less than 100 keV, it was ignored.

Documentation of the code (OMEGA) is in the final stages and will be published before mid-1983. OMEGA controls nine codes that update, plot, list in convenient form, make calculational constants for Sn, Diffusion and Monte Carlo codes and produce standard data files of the calculational constants using the appropriate evaluated data file.

---

[5] R. M. White and J. C. Browne, Proc. Int. Conf. on Nuclear Data for Science and Technology, Antwerp, Belgium (1982) (to be published).

LOS ALAMOS NATIONAL LABORATORY

A. NUCLEAR DATA MEASUREMENTS

1. Low-Energy Fusion Cross Sections (N. Jarmie, R. Brown, R. Hardekopf)

During the past year we have completed our measurements for the D(t,α)n reaction. We have obtained integrated cross sections at 16 energies from 8.3 to 78.1 keV (equivalent deuteron bombarding energy), corresponding to plasma temperatures kT in the range of about 1 to 20 keV. Most of the cross sections were measured to an accuracy of 1.4% absolute, with the error rising to 4.8% at the lowest energy. The energy variation of the cross section is consistent with the reaction proceeding through the well known $3/2^+$ resonance.

We have combined our data with 4 other data sets from the literature and have obtained an excellent single-level fit to the data up to a deuteron bombarding energy of 250 keV. This fit was then used to generate reactivities for a Maxwellian D+T plasma up to a temperature kT of 20 keV. At the higher plasma temperatures, our reactivities are in good agreement with those of Greene;[1] however, below temperatures of a few keV, Green's values become significantly lower than ours. A more recent evaluation by Hale[2] agrees better with our results at low temperatures, but does not agree as well at higher temperatures.

We are presently measuring cross sections for the D(d,p)T and D(d,^{3}He)n reactions and expect to obtain data in the deuteron bombarding energy range from 117 keV to about 15 or 20 keV. We do not expect the errors to be quite as small as for the D+T reaction, because the D+D cross sections are several hundred times smaller. After these measurements are completed, we plan to spend some time investigating the D(t,γ) reaction before proceeding to work on the T(t,α)nn reaction. The D(t,γ) process has the potential for being an important plasma diagnostic reaction, but its low-energy cross section is virtually unknown.

---

[1] S. L. Greene, UCRL-70522 (1967)

[2] G. M. Hale and D. C. Dodder, Proc. Conf. on Neutron Cross Sections and Technology, Washington, DC, 1975 (NBS Special Pub. 594), p. 650.

2. Triton-Triton Interactions (D. Drake, G. Haouat,* M. Drosg,** N. Jarmie)

We have begun a program to measure triton-triton reactions and, as a first step, have measured angular distributions of t-t elastic scattering from 6 to 13-MeV incident tritons. We plan to measure the ^{3}H(t,α)2n reaction over the same energy range and eventually extend these measurements to lower energy.

---

* Centre d'Études de Bruyères-le-Châtel, Montrouge, France.

**University of Vienna, Vienna, Austria.

3. Neutron-Induced γ-Ray Production at WNR (S. Wender, G. Auchampaugh)

Using the WNR pulsed neutron source and a set of four large BGO (Bismuth Germanate) scintillators, we have measured the excitation function for the production of 4.4-MeV γ-rays via the $^{12}C(n,n'\gamma)^{12}C$ reaction from threshold to 100 MeV. The 90° excitation function for 4.4-MeV γ-rays is shown in Fig. A-1. This technique provides a powerful method for measurement of neutron-induced γ-ray production.

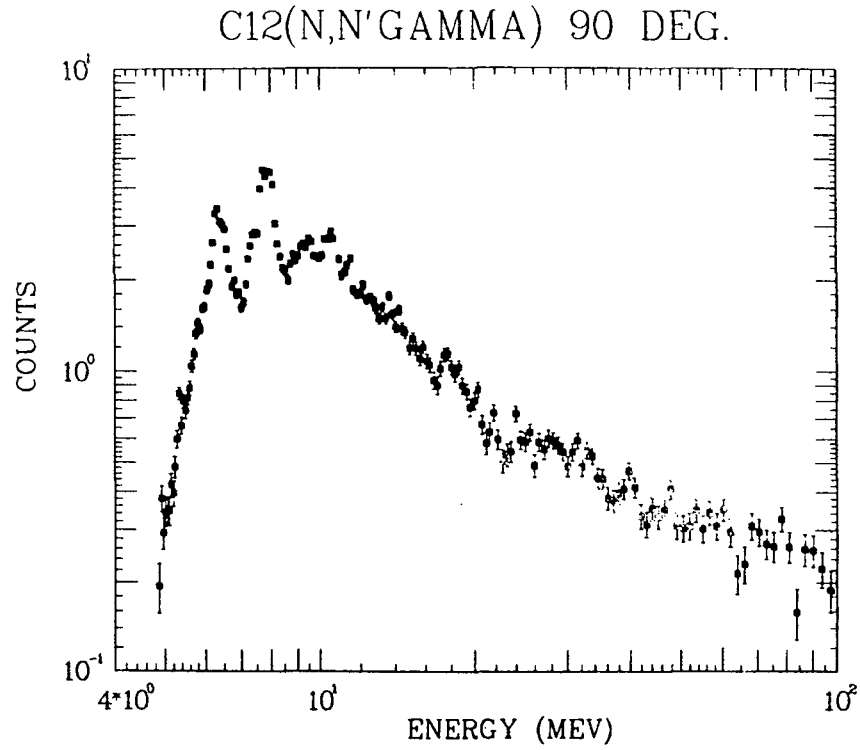

Fig. A-1. Excitation function for production of 4.4-MeV gamma-rays from the $^{12}C(n,n'\gamma)$ reaction at 90°.

4. Fission Angular Distribution Measurements in Neutron-Induced Fission of ^{232}Th, ^{235}U, and ^{238}U (M. Moore, G. Auchampaugh, C. Olsen, C. Goulding*, N. Hill**, R. White†)

Fission-fragment angular-distribution and kinetic-energy measurements have been completed with a 5-m flight path at WNR for neutron-induced fission of ^{232}Th, ^{235}U, and ^{238}U. The measurements were carried out with double-sided gridded ionization chambers in which the cathodes consisted of virtually backless conducting foils on which the fissionable material had been deposited by vacuum evaporation as the tetrafluoride. The angular distributions were determined in two different ways: (1) by measuring the time required for the centroid of charge to pass the grid, a technique described by Auchampaugh and Hill,[1] and (2) by comparing the cathode pulse height to the sum of the anode pulse heights, similar to the method of Knitter and Budtz-Jorgensen.[2] Data were obtained as a function of neutron time of

flight in the range of 1-30 MeV. The objective of the experiment is to study changes in the kinetic energies and angular distributions in the threshold region and near the onset of second-and third-chance fission.

---

* E.G. & G., Los Alamos, New Mexico
**Oak Ridge National Laboratory
† Lawrence Livermore National Laboratory

[1] G. Auchampaugh and N. Hill, presented at the Baltimore American Physical Society meeting, April 1983.

[2] H. -H. Knitter and C. Budtz-Jørgensen, Proc. Int. Conf. Nuclear Data for Science and Technology, Antwerp, Beligium, Sept. 6-10, 1982, to be issued.

5. Intermediate Structure in the Fission of ^{235}U+n below 100 keV (M. Moore, F. Corvi*, H. Weigmann*)

An earlier analysis of Keyworth's[1] polarized-neutron and polarized-target spin determinations of fission of ^{235}U+n below 25 keV[2] suggested that the average fission widths of intermediate structure are correlated, i.e., that there is a common doorway. High resolution capture and fission cross section measurements done at Gelina[3] have permitted a new study of this question, showing that the earlier conclusion was not correct. We have analyzed the combined data of Corvi et al.[3] and Keyworth et al.[1] by Monte-Carlo simulation employing the same model used earlier[2] to describe subthreshold fission of n+^{244}Pu. The results suggest that the structure in suprathreshold fission of ^{235}U+n can be adequately described by such a model, and that fission occurs through well-defined Class II states even at energies well above both humps in the double-humped barrier.

---

* CBNM, Geel, Belgium

[1] G. Keyworth et al., Proc. Conf. on Neutron Cross Sections and Technology, Washington, DC, 1975 (NBS Special Pub. 425, V2), p. 576.

[2] M. Moore et al., Phys. Rev. C18, 1328 (1978).

[3] Corvi et al., Proc. Conf. Nuclear Data for Science and Technology, Antwerp, Belgium, September 6-10, 1982, to be issued.

6. Resonance Structure of ^{237}Np+n (M. Moore, G. Auchampaugh, J. Moses, C. Olsen)

High resolution total and fission cross-section measurements on ^{237}Np were carried out at ORELA and WNR, respectively, as part of a study of the nature of the coupling between Class I and Class II states in subthreshold fission of ^{237}Np+n. The existence of the high resolution data enabled us to re-analyze the 1974 polarized neutron-and-polarized-target measurements of Keyworth et al.,[1] and to assign spins to many more of the resonances than was possible in the earlier work, where the resonance structure was not so well defined. One result of the present analysis is

clearly anomalous: many more of the subthreshold fission clumps seem to have a component of both spins than would be expected if the spacing distribution in the second well follows the usual statistical behavior of independent Gaussian Orthogonal Ensembles.

---

[1] G. Keyworth et al., Proc. Conf. on Neutron Cross Sections and Technology, Washington, DC, 1975 (NBS Special Pub. 425, V2), p. 576.

7. Backbending in ^{244}Pu (M. Moore, W. Spreng*, H. Embing*, E. Grosse*, R. Kulessa**, R. S. Simon*, H. Wollersheim*, M. Mutterer†, J. P. Theobald†, D. Schwalm††)

The phenomenon of backbending, a dramatic change in the spectrum of states in the ground-state rotational band, has been observed in deformed nuclei in the lanthanides but not in the actinide region. Theoretical calculations suggested that, for most of the actinides so far studied, the residual interaction between band crossings is so strong that backbending cannot occur, but that ^{242}Pu and ^{244}Pu might be in a region where it would be permitted. We looked for backbending by bombarding thin targets of these isotopes with a ^{208}Pb beam at the G.S.I. in Darmstadt, thereby Coulomb-exciting the collective bands built on the ground states of ^{242}Pu and ^{244}Pu. Preliminary results of a run carried out in June 1982 were inconclusive. Since that time, additional data have been analyzed, and there is now clear evidence for a pronounced upbending of the spectrum in ^{242}Pu and a sharp backbending in ^{244}Pu.

---

* G.S.I., Darmstadt
** Univ. of Krakow
† T.H., Darmstadt
†† Univ. of Heidelberg

8. Simulations of Nuclide and Gamma-Ray Production by Cosmic Rays (R. C. Reedy)

A number of experiments are being done with colleagues in the Federal Republic of Germany and in the U.S. to understand the interactions of energetic cosmic rays with matter and the nuclides and gamma rays made by these interactions. In Mainz, FRG, a DT generator was the source of neutrons from 14 MeV to thermal energies that irradiated targets of Mg, Al, SiO_2, Fe, and concrete; interpretation of the measured fluxes of gamma rays emitted from these targets is in progress. With colleagues in Cologne and Mainz, a proposal has been prepared to measure gamma rays emitted from various targets irradiated with neutrons of energies up to 45 MeV made by the d + Be reaction at the Isochroncyclotron in Jülich, FRG. The gamma rays escaping from the front surfaces of various thick targets irradiated by 2.1-GeV protons were measured at LBL with coworkers from JPL and UCSD, using monitor foils to determine the particle fluxes inside the targets. Additional thick-target bombardments are planned for Berkeley and Los Alamos.

The gamma-ray fluxes measured in these three experiments will be used to help plan for and analyze data from gamma-ray spectrometers that hopefully will be flown to the moon, Mars, or asteroids. Rotating targets of stone spheres of various radii will be irradiated with 600-MeV protons at CERN, and the radionuclides and noble gases produced in various foils will be measured in Cologne and Mainz, respectively. The depth-versus-concentration profiles of these products will be used in interpreting the cosmic-ray production of nuclides in meteorites.

9. Neutron Production, Fertile-to-Fissile Conversion, Fission, and Neutron-and Charged-Particle Production Cross Section Measurements (G. Russell, J. Gilmore, M. Meier, R. Prael, H. Robinson)

Using the spallation process initiated by medium-energy (500-800 MeV) protons, several laboratories throughout the world are building and designing intense thermal and epithermal neutron sources. Some consideration is also being given to using high-intensity, medium-energy particle accelerators to convert fertile materials to fissile materials (accelerator breeder). In both these applications, computational tools are used extensively in concept design and performance evaluation. At Los Alamos, we are performing benchmark measurements to test the validity of the Monte Carlo codes used to calculate spallation reactions.

We have measured the total neutron captures occurring in a 2-m-diameter by 2-m-high water-bath for a variety of thick targets bombarded by 800-MeV protons. These integral experiments evaluate the net effects of neutron production and transport. We have measured the axial distribution of the fertile-to-fissile conversion (^{232}Th to ^{233}U and ^{238}U to ^{239}Pu) inside thick targets bombarded by 800-MeV protons, and integrated this distribution over the target volume to obtain the total conversion. We have measured the axial distributions of fission and spallation products and integrated these distributions to obtain nuclide production. We have also determined the total number of fissions occurring in the targets. More detailed discussions of these measurements are given in Los Alamos reports LA-UR-80-1360, LA-UR-80-2943, and LA-UR-81-1815.

We are extending our experimental program to include measurements of absolute neutron and charged-particle spectra emitted from thin targets bombarded by 800-MeV protons. The spectra will be measured at several angles to the proton beam, will span the energy range 0.1-800 MeV, and will be converted to production cross sections.

B. NUCLEAR DATA EVALUATION

1. Fusion Cross Sections for Polarized Particles (G. M. Hale, D. C. Dodder, and P. W. Keaton)

Recently, a suggestion by M. Goldhaber led R. Kulsrud and collaborators at the Princeton Plasma Physics Laboratory to propose using polarized particles to modify fusion cross sections.[1] Polarizing the projectile and target changes both the angular distribution and integral for the cross section of a fusion reaction. Polarizing d and T so that their spins are parallel, for instance, enhances the integrated cross section for the T(d,n) reaction by a factor of as much as 1.5. In addition, Kulsrud's study shows it is plausible that polarized particles in a plasma will maintain their polarization for a relatively long time in the presence of a strong magnetic field.

We have provided the Princeton group with cross sections for polarized d-T and d-d reactions, calculated with the Los Alamos R-matrix code, EDA. These calculations are based on comprehensive studies of reactions in the ^{4}He and ^{5}He systems, using EDA's capability to analyze and predict data for interacting particles in any combination of polarization states. For the case of parallel spins in the d+T reaction, we calculate an enhancement factor for the integrated cross section at low energies very close to the theoretical maximum of 1.5. The situation for the d+d reactions, where enhancements as large as a factor of 3 are theoretically possible, is more complex.

Results of our calculations for the d+d reactions are summarized in Table B-1. The quantity $\sigma_{m,n}$ is the integrated cross section for the deuterons in pure spin states, having projections m and n, respectively, along the center-of-mass momentum direction of the incident deuteron. Since the deuterons are identical, $\sigma_{m,n} = \sigma_{n,m}$, and reflection invariance implies $\sigma_{\bar{m},\bar{n}} = \sigma_{m,n}$, so there are only four independent combinations, (m,n) = $(\bar{1},\bar{1})$, (1,0), (1,-1), and (0,0). The unpolarized integrated cross section, σ_0, is related to the sum of the polarized cross sections by

$$\sigma_0 = 1/9(2\sigma_{1,1} + 4\sigma_{1,0} + 2\sigma_{1,-1} + \sigma_{0,0})$$

Table B-1 lists the unpolarized cross sections σ_0 and the ratios $\frac{\sigma_{m,n}}{\sigma_0}$ for the four independent (m,n) combinations at deuteron energies between 100 and 500 keV for both d+d reactions.

---

[1] Kulsrud, Furth, Valeo, and Goldhaber, "Fusion Reactor Plasmas with Polarized Nuclei," PPL-1912 (1982); see also, "Polarized Plasmas May Prove Useful for Fusion Reactors," Physics Today, p. 17 (August 1982).

According to these calculations, the best configuration for enhancing the cross section is (1,0) and the best one for suppressing it is (1,-1) with (1,1) a close second. The results are moderately energy-dependent and somewhat reaction-dependent, with the maximum enhancement (~ 1.6) well below the theoretical limit. The reason for this is that a number of transitions are important in the low energy d+d reactions, in contrast to the single $J^{\pi} = 3/2^{+}$ transition that completely dominates the d+T reaction at low energies. However, the increased complexity of the d+d reactions, coupled with the relative scarcity of reliable polarization data at low energies, makes the results of Table B-1 much less certain than those for the T(d,n) reaction. We are attempting to improve the reliability of the d+d predictions by including more recent low-energy polarized d+d data in the four-nucleon analysis, but we point out that the most directly useful measurements, involving polarized deuterons incident on polarized deuterons, have not yet been done.

TABLE B-1. Polarized Cross Sections for the d-d Reactions*

A. D(d,p)†

E_d(keV)	σ_0(mb)	$\frac{\sigma_{1,1}}{\sigma_0}$	$\frac{\sigma_{1,0}}{\sigma_0}$	$\frac{\sigma_{1,-1}}{\sigma_0}$	$\frac{\sigma_{0,0}}{\sigma_0}$
100	16.05	.949	1.146	.672	1.175
200	33.68	.776	1.334	.550	1.011
300	45.14	.672	1.468	.448	.889
400	53.18	.603	1.562	.371	.803
500	59.18	.554	1.626	.320	.749

B. D(d,n)†

E_d(keV)	σ_0(mb)	$\frac{\sigma_{1,1}}{\sigma_0}$	$\frac{\sigma_{1,0}}{\sigma_0}$	$\frac{\sigma_{1,-1}}{\sigma_0}$	$\frac{\sigma_{0,0}}{\sigma_0}$
100	15.87	.745	1.289	.668	1.020
200	35.60	.573	1.491	.535	.820
300	49.70	.479	1.621	.436	.687
400	60.08	.421	1.706	.367	.600
500	67.99	.382	1.762	.321	.546

*From Los Alamos ^{4}He system R-matrix analysis, 8/79

†Sum rule for cross sections

$$1/9(2\sigma_{1,1} + 4\sigma_{1,0} + 2\sigma_{1,-1} + \sigma_{0,0}) = \sigma_0$$

2. Generalized Fokker-Plank Theory for Charged-Particle Elastic Scattering (G. M. Hale and A. Andrade)

Current treatments of the slowing-down of ions in plasmas due to small-angle elastic scattering generally consider only Rutherford scattering and neglect the nuclear plus Coulomb-nuclear interference contribution to the cross section, σ_{NI}. Using the exact Legendre polynomial expansion for σ_{NI},[1] we have included it in the Fokker-Plank equation, and found analytic expressions for the integrals over the scattering angle.

In a test case for deuterons injected into a plasma of "cold" tritium, chosen because the Fokker-Plank equation could be solved analytically, the slowing-down contribution from σ_{NI} is comparable to the ion-ion Rutherford contribution, but both are dominated by the ion-electron slowing down. We are presently looking at more realistic cases, with Maxwellian distributions of background ion velocities, to assess the relative importance of the σ_{NI} contribution at small angles.

---

[1] G. M. Hale, D. C. Dodder, and J. C. DeVeaux, "Charged Particle Elastic Cross Sections," Proc. Int. Conf. on Nuclear Data for Science and Tech., Antwerp, 1982 (to be published, 1983).

3. Cross Section Calculations for n+^{169}Tm (P. G. Young, E. D. Arthur, and C. Philis*)

We have carried out a final adjustment of our deformed optical model analysis[1] of n+^{169}Tm reactions using recent measurements of elastic and inelastic neutron scattering from ^{169}Tm by Haouat and Patin.[2] Prior to these measurements, the only ^{169}Tm data available for our analysis were s- and p-wave neutron strengths (S_0,S_1), potential scattering radii (R'), and neutron total, (n,γ), and (n,xn) cross sections. We therefore relied on the neighboring nucleus ^{165}Ho for the angular distribution data used in our earlier analysis.

The coupled-channel code ECIS was used for the deformed optical model calculations. The measured distributions were corrected for compound nucleus contributions and the unresolved 8.4-keV first excited state of ^{169}Tm using parameters from our previous analysis. At the same time that a minimum χ^2 relative to the elastic angular distributions was sought, we attempted to improve agreement with measurements of S_0, S_1, and R' for low neutron energies and to maintain good agreement with measurements of the total cross section.

The parameters that resulted from our this analysis are listed in Table B-2. A comparison between Haouat and Patin's measurement at 0.57 MeV and angular distributions calculated with parameters from both the previous and present analyses is given in Fig. B-1. The new analysis results in a small reduction in χ^2 for the elastic angular distribution measurements and

improves overall agreement in calculated values of S_0, S_1, R' with experiment (particularly S_1). Additionally, the new parameters lead to improved calculations of (n,2n) and (n,3n) cross sections near the thresholds for these reactions, and result in calculated total and (n,γ) cross sections that agree with experiment roughly as well as the previous analysis.

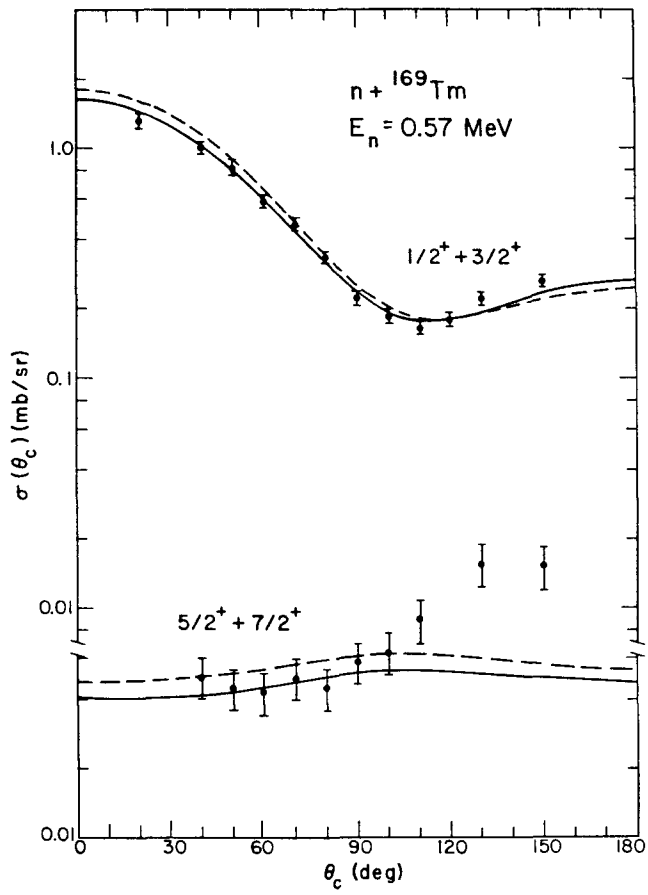

Fig. B-1. Comparison of calculated and measured[2] neutron angular distributions to several states in ^{169}Tm at an incident neutron energy of 0.57 MeV. The solid curve represents results from the present analysis; the dashed curve indicates the analysis of Ref. 1.

---

* Centre d'Études de Bruyères-le-Châtel, Montrouge, France.

1 Young, Arthur, Philis, Nagel, and Collin, "Analysis of n+^{165}Ho and ^{169}Tm Reactions," Proc. Conf. Nuclear Data for Science and Technology, Antwerp, Belgium, September 6-10, 1982, to be issued.

2 G. Haouat and Y. Patin, Bruyères-le-Châtel, personal communication, 1982.

TABLE B-2. Deformed Optical Model Parameters for n+^{169}Tm*

			r	a
V	$= 47.0 - 0.26\ E$		1.29	0.60
W_{VOL}	$= -1.8 + 0.2\ E$	$E > 9$ MeV	1.29	0.60
V_{SO}	$= 6.0$		1.29	0.60
W_{SD}	$= 2.5 + 0.6\ E$	$E < 7.5$ MeV	1.29	0.48
	$= 7.0 - 0.03(E-7.5)$	$E \geqq 7.5$ MeV	1.29	0.48
β_2	$= 0.31$	$\beta_4 = -0.01$		

* All well depths are in MeV and geometrical parameters in fm.

4. New Calculations of n+^{239}Pu Reactions with Emphasis on Inelastic Scattering (E. D. Arthur)

We have calculated neutron cross sections on ^{239}Pu for incident energies between 0.01 and 20 MeV using coupled-channel, Hauser-Feshbach, and preequilibrium nuclear models. The ECIS deformed optical model code was used to calculate direct-reaction contributions to inelastic cross sections and to provide neutron transmission coefficients for use in the GNASH and COMNUC statistical model codes. Fission cross sections were calculated using improved fission models recently implemented in these Hauser-Feshbach codes. Improvements in the fission model included a multi-barrier (2 or 3) description of the fission channel for each compound nucleus, allowance for separate transition state spectra to be specified at each barrier, and provision of state density enhancement factors that account for symmetry conditions existing at a given barrier.

The calculation of fission cross sections on actinide nuclei at higher neutron energies involves sizable multi-chance fission contributions, particularly for $E_n > 5$-6 MeV. To aid in the determination of fission barrier prameters and multi-chance fission contributions to the total ^{239}Pu fission cross section, we employed a technique in which charged-particle direct-reaction fission probability data was analyzed using models identical to those used for our neutron cross section calculations. This technique explicitly accounts for differences in compound nucleus spin populations produced in charged-particle and neutron-induced reactions, and eliminated other sources of ambiguity in barrier parameter determinations.

The results of these calculations were used in a revision to the present ENDF/B-V evaluation for ^{239}Pu in which particular emphasis was placed on improvement of neutron inelastic scattering cross sections and

angular distributions. To check our calculations, we compared them to recent sources of differential elastic and inelastic scattering data for ^{239}Pu, one of which is shown in Fig. B-2. The data there are new Argonne measurements[1] in which the total cross section for inelastic scattering from levels above a given excitation energy was determined. The solid curve represents our calculated results, while the ENDF/B-V evaluation is shown by the dashed curve. The major cause for the difference between these curves appears to be the neglect in the ENDF/B evaluation of direct-reaction contributions to inelastic scattering from low-lying levels occupying the ground-state rotational band of ^{239}Pu. Further differences in the evaluated total inelastic cross section appear in Fig. B-3 where the solid curve represents our evaluation and the dashed curve, ENDF/B-V. The differences below 3 MeV again result from the inclusion of direct-reaction contributions in our calculations, while those above 7 MeV are also attributable to direct-reaction and preequilibrium mechanism effects.

---

[1] Allan B. Smith, P. T. Guenther, and R. D. McKnight, "On the Neutron Scattering Cross Sections of ^{232}Th, ^{233}U, ^{235}U, ^{238}U, ^{239}Pu, and ^{240}Pu," presented at the Nuclear Data for Science and Technology Int. Conf., Antwerp, Belgium, September 1982.

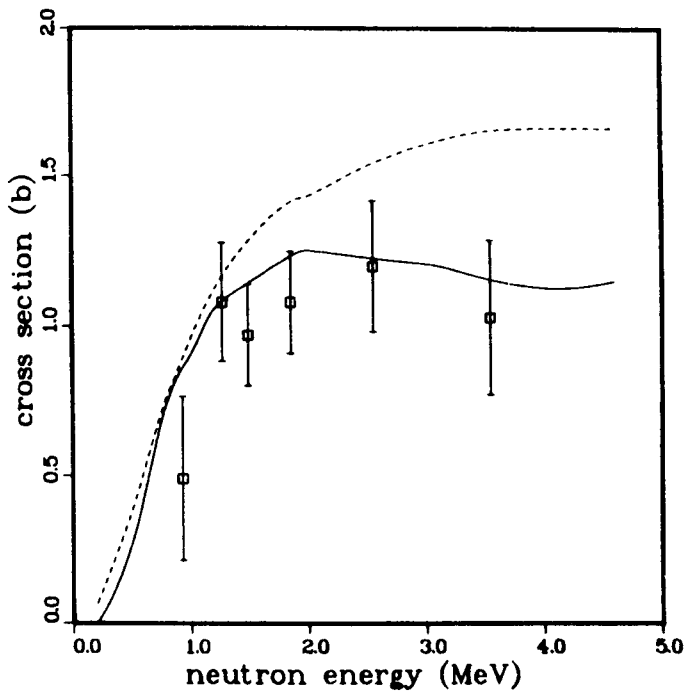

Fig. B-2. Comparison of our calculated results (solid curve) to new Argonne data[1] for inelastic scattering to levels lying above a given excitation energy. The dashed curve is ENDF/B-V.

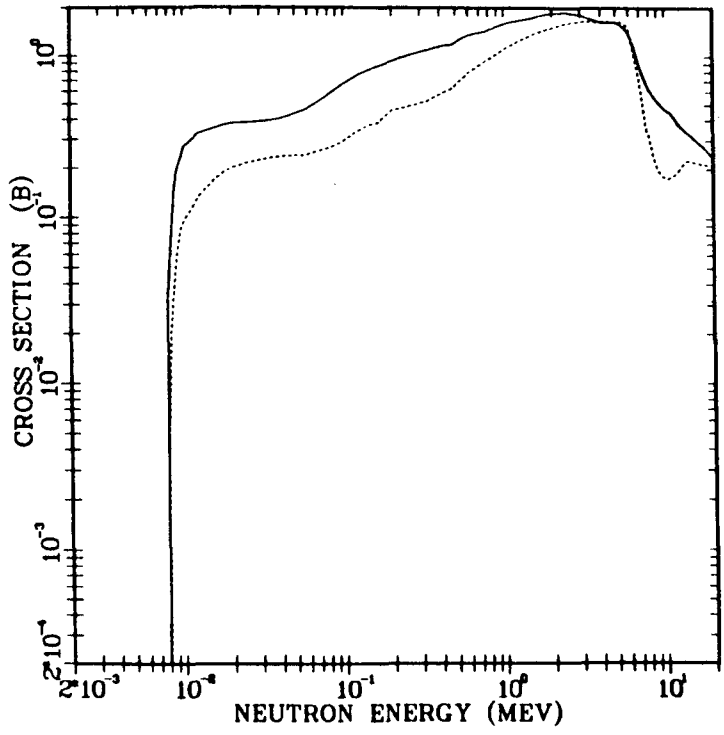

Fig. B-3. Comparison of the total inelastic cross section resulting from our evaluation (solid curve) to that given by ENDF/B-V (dashed curve).

5. Prompt Neutron Spectrum and Average Prompt Neutron Multiplicity for the Spontaneous Fission of ^{252}Cf (D. G. Madland and J. R. Nix)

We have performed a new calculation[1] of the prompt fission neutron spectrum and average prompt neutron multiplicity for the ^{252}Cf(sf) reaction, using a recently developed theory by Madland and Nix.[2] Because of increased accuracy requirements due to the use of this reaction as a standard, we have performed our calculations with greater accuracy than previously.[2,3] In particular, we have calculated the integral for the average energy release without approximation and with the use of more recent mass sources. We then optimized the nuclear level-density parameter by performing a least-squares adjustment to a specific experimental spectrum. Our calculated spectrum is shown compared to the experimental data of Boldeman et al.[4] in Fig. B-4. The average energy of the calculated spectrum is $\langle E \rangle = 2.168$ MeV. The calculated value of the average neutron multiplicity is $\bar{\nu}_p = 3.783$.

---

[1] D. G. Madland and J. R. Nix, "Calculation of the Prompt Neutron Spectrum and Average Prompt Neutron Multiplicity for the Spontaneous Fission of ^{252}Cf," presented at the Int. Conf. on Nuclear Data for Science and Technology, Antwerp, Belgium, September 6-10, 1982 (proceedings to be published).

[2] D. G. Madland and J. R. Nix, "New Calculation of Prompt Fission Neutron Spectra and Average Prompt Neutron Multiplicities," Nucl. Sci. Eng. 81, 213 (1982).

[3] D. G. Madland, "Calculation of the Prompt Neutron Spectrum and $\bar{\nu}_p$ for the Spontaneous Fission of ^{252}Cf," Trans. Am. Nucl. Soc. 38, 649 (1981).

[4] J. W. Boldeman, D. Culley, and R. J. Cawley, Trans. Am. Nucl. Soc. 32, 733 (1979).

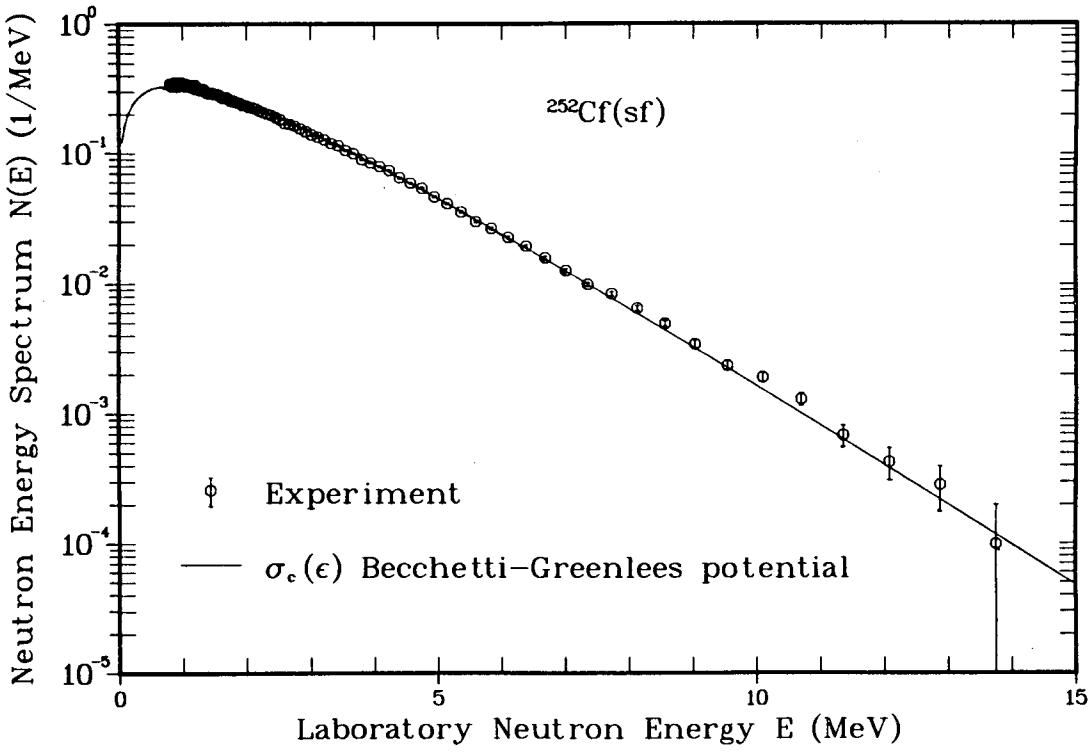

Fig. B-4. Prompt fission neutron spectrum for the spontaneous fission of ^{252}Cf. The solid curve gives the spectrum calculated as described in Ref. 1. The experimental data are from Experiment #7 of Boldeman et al.[4]

6. Compilation of Fast-Neutron-Induced Gamma Rays (C. E. Moss)

Energies and relative intensities for gamma rays produced by fast neutron interations with 77 elements have been compiled and tabularized for convenient use in nuclear safeguard applications.[1]

[1] C. E. Moss, "Gamma Rays from the Interactions of Reactor Fast Neutrons Ordered by Increasing Gamma-Ray Energy," Los Alamos report LA-9604-MS (1982).

7. Delayed Neutron Pn Values and Spectra (T. R. England, W. B. Wilson, R. E. Schenter,* and F. Mann*)

Work on precursor evaluation of measured data augmented with model calculations of emission probabilities (Pn)[1 2] and spectra[3] has continued. Pn values were revised,[2] and 29 measured spectra were augmented with 76 model-code values.[3] Aggregate time-group and total equilibrium spectra were calculated for 11 fissionable nuclides at one or more neutron fission energies. These were compared where possible with the more limited evaluations of measured spectra.[4] A comparison of the total ^{238}U calculated and evaluated measured spectra following fast fission is given in Fig. B-5 and time-group 1 in Fig. B-6. The normalization is to a unity integral between 0 and 1 MeV; however, the measured spectra actually cover the range of 70 keV to 1.2 MeV and the calculation, the range of 0 to ~ 5 MeV. (The final ENDF/B-V evaluation was extrapolated linearly to 0 from ~ 70 keV, as is evident on the figure). Calculated spectra below ~ 100 keV show significant peaks of importance for fast reactor control and safety; all time group comparisons show even larger deviations from aggregate measurements. We anticipate that measurements of individual precursor spectra that are in progress and capable of measuring the low energy range will show even larger deviations at low energies from the current ENDF/B-V evaluations.

---

* Hanford Engineering Development Laboratory, Richland, WA

[1] England, Schenter, and Schmittroth, "Delayed Neutron Calculations using ENDF/B-V Data," Proc. ANS/APS int. Conf. Nucl. Cross Sections for Technology, Knoxville, Tenn. (October 22-26, 1979). [NBS Special Publication 594, issued September 1980.]

[2] Mann, Schreiber, Schenter, and England, "Compilation of Neutron Precursor Data," presented at the Int. Conf. on Nuclear Data for Science and Technology, Antwerp, Belgium, September 1982. (LA-UR 82-1339).

[3] Mann, Dunn, and Schenter, "Beta Decay Properties from a Statistical Model," Trans. Am. Nucl. Soc. 39, 880 (1981). [See also Phys. Rev. C, 25, No. 1, 524 (January 1982).]

[4] England, Wilson, Schenter, Mann, "Aggregate Delayed Neutrons and Spectral Calculations Using Preliminary Precursor Data Evaluated for Inclusion in ENDF/B-VI," presented at the American Chemical Society Meeting, Las Vegas, Nevada, May 28, 1982 (LA-UR 82-841). [Accepted for publication in Nucl. Sci. Eng.]

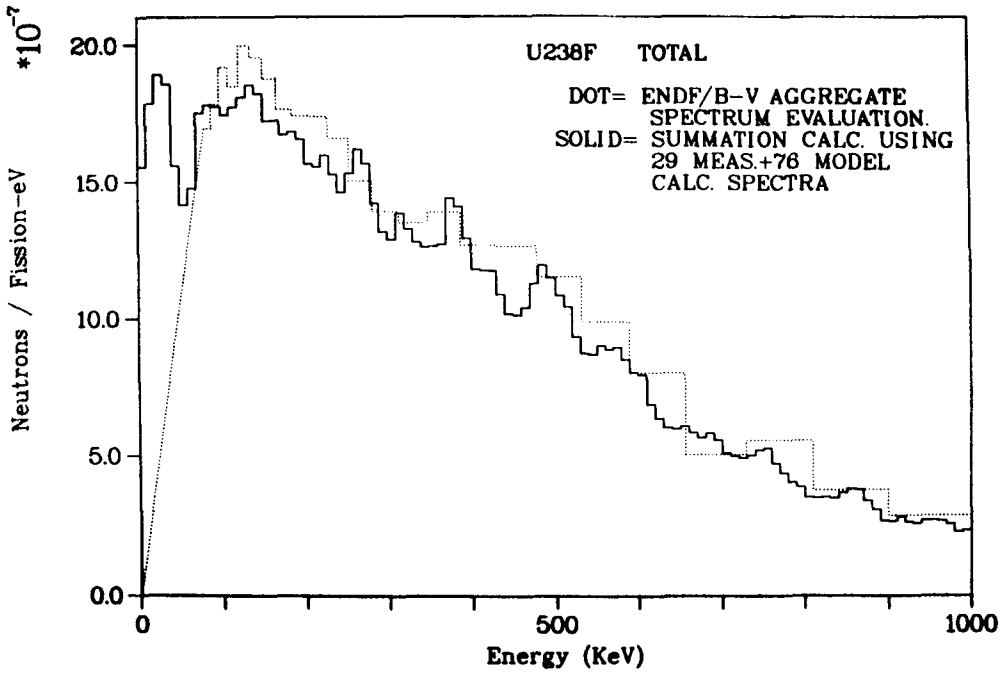

Fig. B-5. ^{238}U normalized delayed neutron spectra (total).

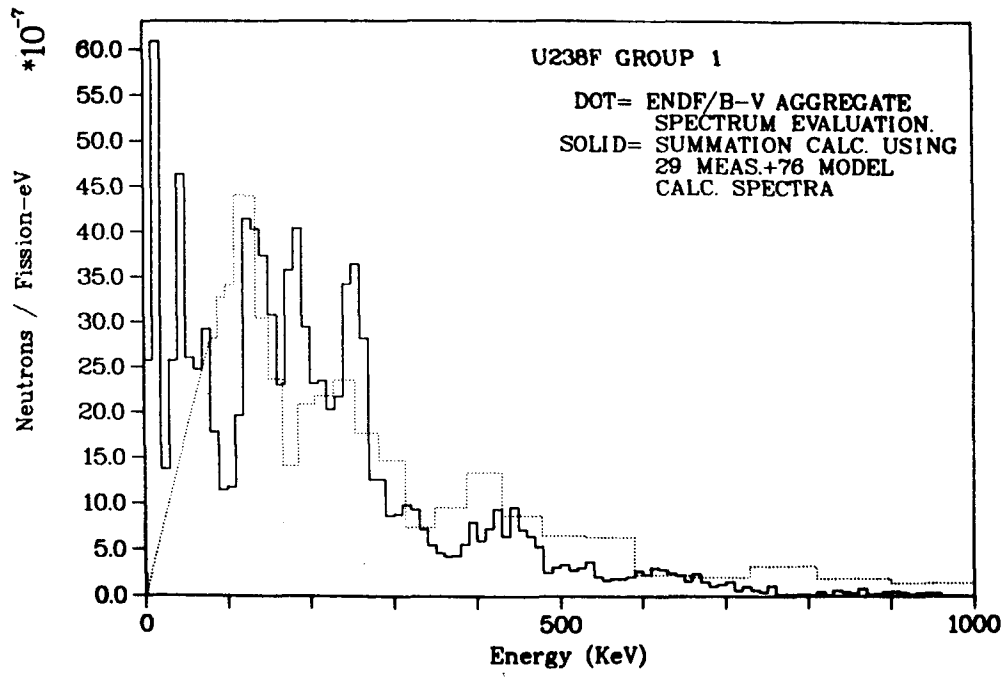

Fig. B-6. ^{238}U normalized delayed neutron spectra (Group 1).

UNIVERSITY OF LOWELL

A. NEUTRON CROSS SECTION MEASUREMENTS FOR ^{232}TH AND ^{238}U

(L.E. Beghian, G.H.R. Kegel, G.P. Couchell, J.J. Egan, A. Mittler, S.Q. Li, C.A. Ciarcia, J.Q. Shao and G. Goswami)

1. Ground State Rotational Band

We have measured the neutron scattering cross sections via the time-of-flight technique at 125° for the 0^+ ground states (elastic) and first two excited states (2^+,4^+) in Th-232 and U-238 at neutron energies in the range 200-500 keV. The extension of these measurements up to 900 keV is currently underway thereby, in the case of U-238 overlapping our 900-3100-keV measurements previously reported[1]. Careful attention has been paid to data reduction and multiple scattering corrections, which are significant at low energies, using computer codes developed at this laboratory.

2. States Above 650 keV in Excitation

We have undertaken these measurements in three steps corresponding to optimization of the time-of-flight spectrometer for three scattered neutron energy regions, (i) 200-400 keV, (ii) 400-800 keV, (iii) 800-1400 keV. The first two phases of the experiment are almost complete and step three will begin shortly.

The measurements in the first phase were made at 50-keV intervals for states up to 1300 keV, at bombarding energies in the region 0.9 to 1.5 MeV. The second phase measurements were made at 100-keV intervals on the same states in the bombarding energy range 1.2 to 2.0 MeV. Excitation function work has been completed for both of these outgoing neutron energy regions and angular distributions are currently being measured at selected energies, beginning at 1.2 MeV where the compound nucleus cross section is dominant. We shall then proceed to 1.5 MeV where incipient direct interaction effects are perceived for states near 700 keV in excitation.

In the third phase of the experiment where the spectrometer is optimized for the detection of 800 to 1400-keV neutrons we shall be able to investigate the behavior of the cross sections in a region where the direct interaction contribution dominates. These measurements are complementary to our already completed (n,n'γ) work and will provide an excellent test of reaction mechanism theories. Samples of our results are shown in Figs. A-1, A-2 and A-3.

---

[1] L.E. Beghian, G.H.R. Kegel, T.V. Marcella, B.K. Barnes, G.P. Couchell, J.J. Egan, A. Mittler, D.J. Pullen and W.A. Schier, Nucl. Sci. and Eng. 69, 191 (1979).

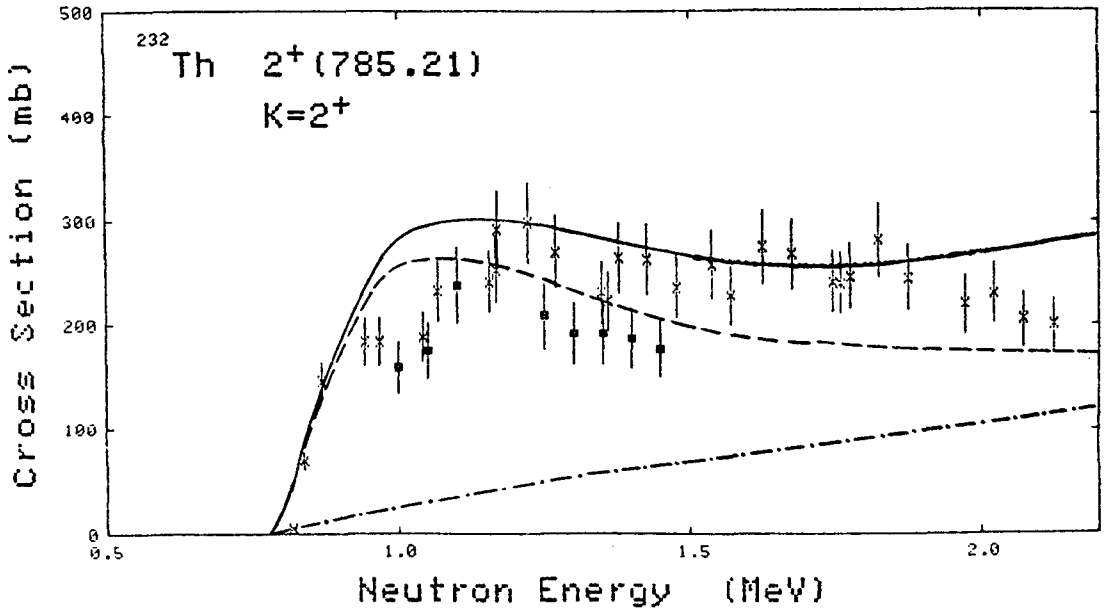

Fig. A-1. Inelastic scattering excitation function for the 785-keV, 2^+ state in Th-232 with (n,n'γ) data shown as crosses and (n,n') as solid dots. See text for explanation of the curves.

Figure A-1 shows our (n,n'γ) and (n,n') data for the 785-keV state in Th-232. The dashed curve is a theoretical compound nucleus calculation, the dot-dash curve represents the calculated direct interaction contribution while the solid curve is the combination of both. (See Section B of this report for details of these calculations).

Figure A-2 shows a similar excitation function for the 829-keV, 3^+, state in Th-232. Here the direct interaction contribution is small and the compound nucleus predominates. Our results shown in Figs. A-1 and A-2 are in reasonable agreement with the (n,n') data of McMurray et. al.[2]

---

[2] W.R. McMurray, I.J. van Heerden, E. Barnard and D.T.L. Jones, Southern Universities Nuclear Institute Annual Research Report, SUNI-41, 4 (1975).

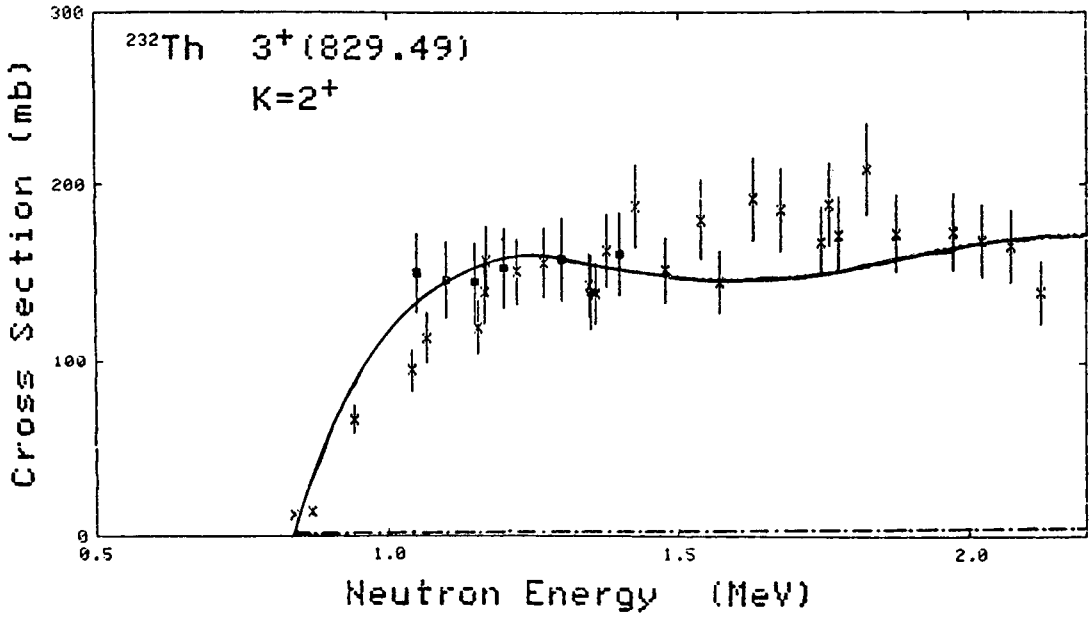

Fig. A-2. Inelastic scattering excitation function for the 829-keV state in Th-232.

Figure A-3 shows the angular distribution of the 785-keV state at 1200-keV incident neutron energy, an energy at which the compound nucleus is predominant. Figure A-3 also shows how the data for this level were extracted from the doublet which includes two 774-keV levels.

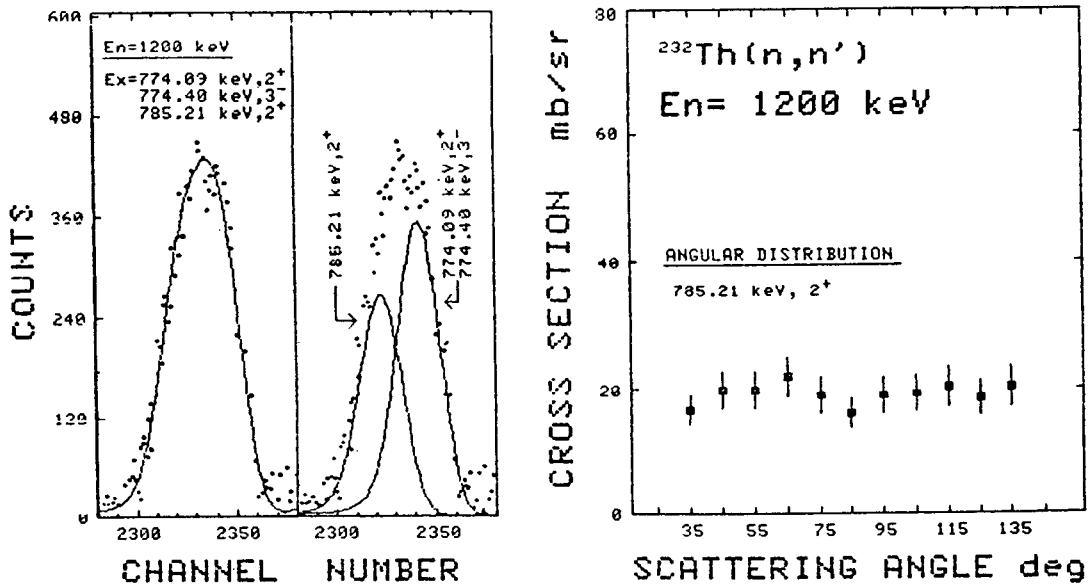

Fig. A-3. Resolving 774,885-keV doublet at E_n=1200 keV (left). Angular distribution of 785-keV level at E_n=1200 keV (right).

3. Data Analysis

Because of the high level density encountered above 650 keV in Th-232 and U-238 we have developed special computer assisted unfolding techniques. The method was outlined in our 1982 Report to the DOE but it has now been successfully applied to very complex spectra. An example is shown in Fig. A-4 where the solid lines are the unfolded peaks due to individual states labeled by their excitation energy in keV.

Neutron scattering data must be corrected for neutron absorption, for finite scatterer size effects and for neutron multiple scattering. Our approach has been to use an order-of-scattering expansion rather than a Monte Carlo calculation. A description of the first order scattering code was published in 1981.[3]

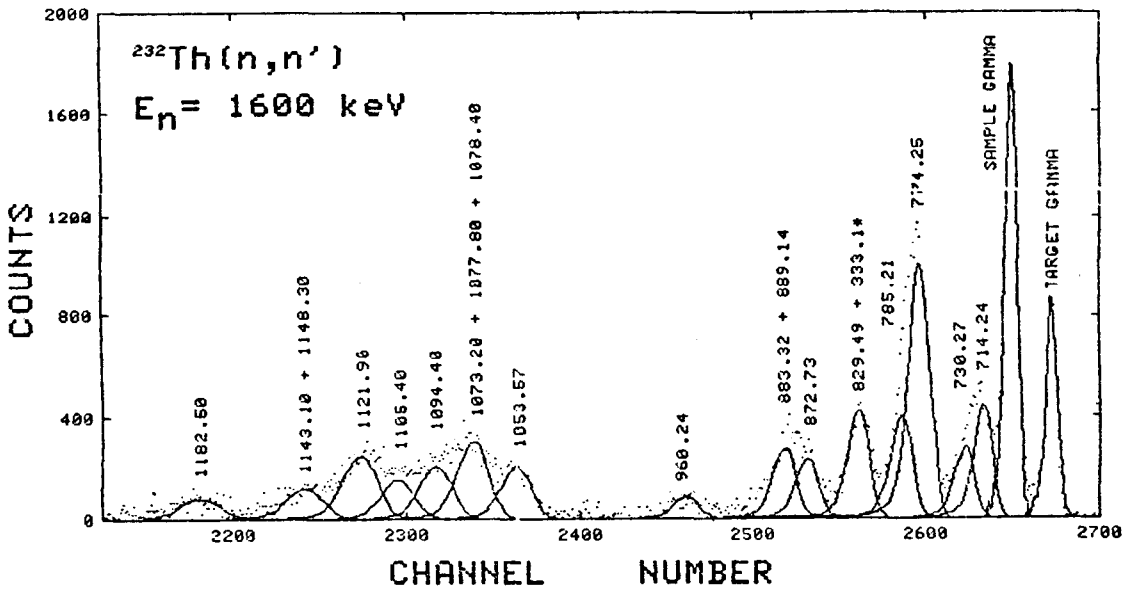

Fig. A-4. Portion of the background subtracted time-of-flight spectrum taken at E_n=1600-keV showing the region containing peaks corresponding to levels from 714 to 1182 keV.

The second order code which has been in use for some time has recently been revised to improve its accuracy and to make it applicable to cylindrical as well as disk scattering geometries. In addition we have been able to considerably reduce the running time of the code.

---

[3] G.H.R. Kegel, Computer Physics Communications, 24, 205 (1981).

B. THEORETICAL UNIFIED STATISTICAL S-MATRIX CALCULATIONS OF ANGLE-INTEGRATED NEUTRON INELASTIC SCATTERING CROSS SECTIONS FOR TH-232, U-238, PU-240 AND PU-242 (E. Sheldon and D.W.S. Chan)

Consolidating the previous sets of computations to derive angle-integrated cross sections for the inelastic scattering of fast neutrons in the 0.8 to 3.5-MeV range for even-mass actinide nuclei from the unified statistical S-matrix formalism of Tepel, Weidenmuller et al.[1], when higher collective (quadrupole or octupole vibrational) states are populated, the program "NANCY"[2] has been applied to obtain detailed level excitation functions for Th-232, U-238, Pu-240 and Pu-242. A consistent set of optical potential and deformation parameters, as proposed by the Bruyeres group, has been employed throughout, and the findings have been presented in a series of publications[2-7], comparing the calculated data with (n,n') level cross sections determined from (n,n') and (n,n'γ) measurements. In refs. 2 & 3, the calculations were performed in "standard" (CN + DI) formalism for Th-232 and U-238 vibrational levels, together with some preliminary "unified" computations as presented in the previous report. In ref. 4, the unified computations were extended to embrace the 21 principal vibrational states in Th-232 and 17 in U-238 up to excitation energies of about 1200 keV; satisfactory fits were obtained to data derived by the Lowell group from (n,n'γ) measurements in most instances, but discrepancies with the evaluated ENDF/B-V data file became evident, a finding also substantiated by the Bruyeres group.[8] These comparisons were carried further in ref. 5, while in ref. 6 the data were extended to include (a) experimental cross sections derived from (n,n') measurements by the Lowell group, (b) experimental cross sections for scattering to rotational levels in the ground-state band of Th-232, U-238, Pu-240 and Pu-242, as derived by various groups from (n,n') and (n,n'γ)

---

[1] J.W. Tepel, H.M. Hofmann and H.A. Weidenmuller, Phys. Letters 49B, 1 (1974); H.M. Hofmann, J. Richert, J.W. Tepel and H.A. Weidenmuller, Ann. of Phys. (NY) 90, 391 & 403 (1975); H.M. Hofmann, T. Mertelmeier, M. Herman and J.W. Tepel, Z. Phys. A 297, 153 (1980).

[2] D.W.S. Chan, Ph.D. Thesis, University of Lowell, 1981 (unpublished).

[3] D.W.S. Chan, J.J. Egan, A. Mittler and E. Sheldon, Phys. Rev. C26(3), 841 (1982).

[4] D.W.S. Chan and E. Sheldon, Phys. Rev. C26(3), 861 (1982).

[5] E. Sheldon and D.W.S. Chan, in Fast Neutron Scattering on Actinide Nuclei, Proceedings of an OECD/ECDE - NEANDC Specialists' Meeting, Paris, Nov. 1981 (OECD/ECDE, Paris, 1982), p. 169.

[6] E. Sheldon, in Proceedings of the International Conference on Nuclear Data for Science and Technology, Antwerp, 6-10 Sept., 1982 (in publication).

[7] E. Sheldon, contributed paper to the International Conference on The Neutron and Its Applications, Cambridge, 13-17 Sept., 1982 (to be published in J. Phys. G - Nucl. Phys., 1983).

[8] G. Haouat, J. Lachkar, Ch. Lagrange, J. Jary, J. Sigaud and Y. Patin, Nucl. Sci. Eng. 81, 491 (1982).

measurements, together with (c) the corresponding theoretical excitation curves, and (d) calculated level excitation functions for Pu-240 and Pu-242 vibrational states. Due to space restrictions, only a selection of data could be presented in ref. 6; the totality of data, corrected to take account of competition from other neutron inelastic scattering channels, radiative capture and fission channels, was presented in ref. 7. The numerical results have also been communicated to the National Neutron Cross Section Center for archiving.

As our experimental group has now commenced (n,n') angular distribution measurements on Th-232 and U-238, the program "NANCY" is being modified to provide differential cross-section output, as well as to include explicit provision for continuum, radiative-capture, and fission competition. Currently, angular distribution calculations for the lowest vibrational levels in Th-232 and U-238 are being performed with the CN code "CINDY"[9] and the DI code "KARJUP"[10] at various incident neutron energies between 1 and 2 MeV to furnish appropriate data for comparison with the forthcoming experimental and unified theoretical investigations.

C. DELAYED NEUTRON ENERGY SPECTRA OF FISSIONABLE ISOTOPES

(G.P. Couchell, W.A. Schier, D.J. Pullen, N.M. Sampas, R. Tanczyn, Q. Sharfuddin, M. Haghighi)

In this project we are studying delayed-neutron spectra following neutron induced fission of U-235, Pu-239 and U-238. Fission is induced by fast neutrons produced using the University of Lowell Van de Graaff Accelerator or by thermal neutrons using the University of Lowell nuclear reactor. Delayed neutrons are detected using ^{6}Li-loaded glass scintillators as well as Pilot U plastic scintillators. The time-of-flight technique is used to determine energies of delayed neutrons and to greatly suppress background events. Fast transfer of fission fragments to a low-background environment is achieved using a helium-jet gas transfer system. Each composite spectrum can be decomposed into its various six-group components by using a tape transport system to select delay- and dwell-times following fission.

Special emphasis will be placed on the determination of delayed-neutron spectra at low energies, i.e., below 200 keV, where other measurements show large discrepancies. This region is of importance since fast reactor transient behavior is particularly sensitive to variations in the lower-energy region of the delayed-neutron spectrum.

---

[9] E. Sheldon and V.C. Rogers, Computer Phys. Commun. 6, 99 (1973).
[10] H. Rebel and G.W. Schweimer, Kernforschungszentrum Karlsruhe Report KFK-1333, 1971 (unpublished).

Details of the experimental arrangement were included in the 1982 Report to the DOE Nuclear Data Committee, DOE/NDC027/U. The complete assembly, including the fission chamber with a U-235 foil, the helium jet and tape transport systems with helium recirculation, and the TOF spectrometer with beta-pileup rejection, has been operated to measure preliminary TOF spectra employing both ¼-in thick Pilot U plastic and ^{6}Li-glass scintillators as neutron detectors. The spectrometer was run with a single beta detector and a slow tape speed giving a delay-time-after-fission range of 0.4 to 27 seconds. These measurements, therefore, yielded spectra that were approximately "near-equilibrium".

Flight paths of 41- and 13-cm were chosen for the plastic and glass scintillators, respectively, to allow the measurement of high-energy neutrons up to 2 MeV with the plastic scintillators and low-energy neutrons down to 10 keV with the glass scintillators. Typical time-of-flight spectra obtained with each type scintillator are shown in Fig. C-1.

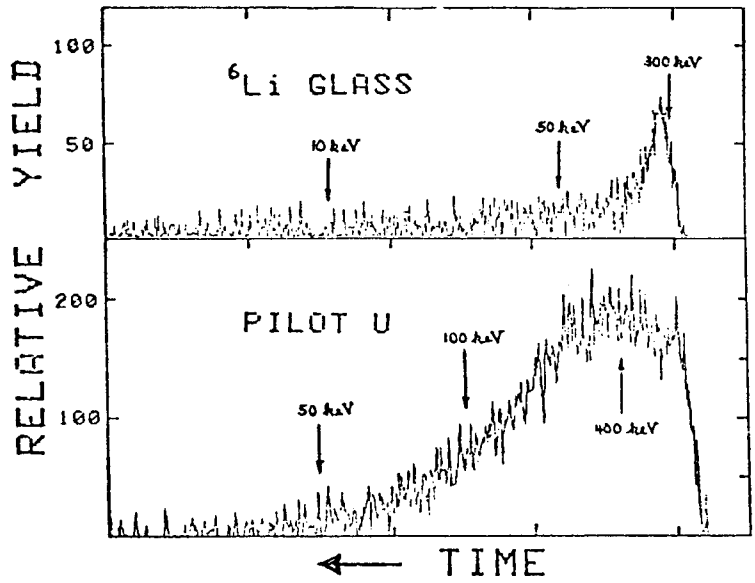

Fig. C-1. Delayed neutron time-of-flight spectra using ^{6}Li glass at 13 cm and Pilot U at 41 cm flight paths. Isotropic backgrounds have been subtracted and the spectra truncated at the beta-pileup shoulder.

Prior to converting the TOF spectra to energy spectra, relative detection efficiencies were measured and the time-response functions to monoenergetic neutrons were studied for both detectors. These measurements were made with our standard TOF system[1], utilizing pulsed and bunched

---

[1] L.E. Beghian, G.H.R. Kegel, B.K. Barnes, G.P. Couchell, J.J. Egan, P. Harihar, T.V. Marcella, A. Mittler, D.J. Pullen and W.A. Schier, Nucl. Sci. Eng. 69, 191 (1979).

(< 1 ns) proton beam bursts on thin ^{7}Li targets. Neutron flux was normalized with a U-235 fission chamber detector. The time response of the detectors to monoenergetic neutrons shown in Fig. C-2 are approximately characterized by a peak with an exponential tail. We observed that this tail was essentially independent of flight path both in magnitude (a fixed

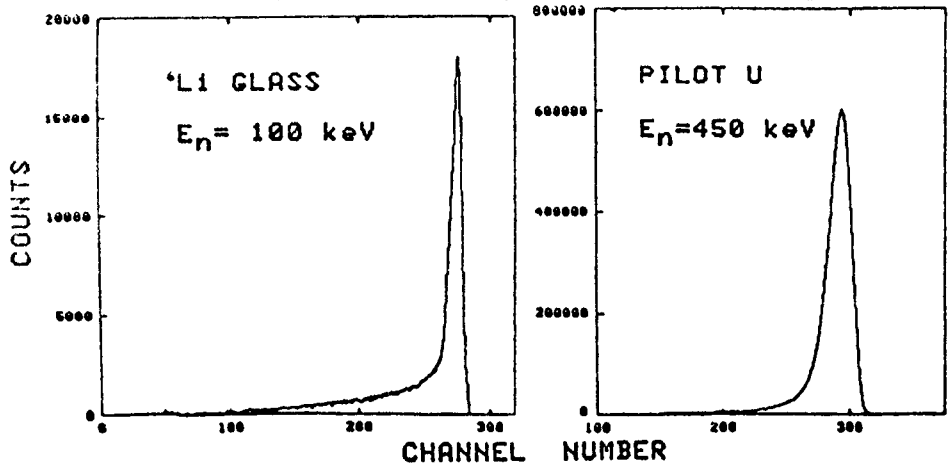

Fig. C-2. Response functions of ^{6}Li glass and Pilot U plastic scintillators to nearly monoenergetic neutrons.

per cent of the peak) and time duration at a given energy. Furthermore, the decay time constant of the exponential tail was approximately independent of the incident neutron energy. In the delayed-neutron measurements, it is important to subtract tail neutrons because they are superimposed on low-energy neutrons, particularly in the region E_n < 100 keV. These tails are believed due primarily to the lucite couplers between the scintillators and the phototubes, which we have subsequently replaced with fused silica couplers.

We have written a computer program which subtracts these tails from the delayed-neutron spectra through an iterative process using the approximation that the tail shape is energy independent, while accounting for the measured tail area/peak area ratio function. The spectra are then converted to an energy scale and corrected for neutron detection efficiency.

The corrected delayed-neutron spectra obtained from these preliminary studies are shown in Fig. C-3, in which the data points corresponding to the Pilot U and ^{6}Li-glass measurements are represented by different symbols. Of particular interest in this composite are the substantial number of neutrons appearing in the spectrum below 100 keV, a region of considerable ambiguity in published delayed-neutron data.

A refinement made to the neutron spectrometer after these preliminary measurements were completed was the replacement of the lucite couplers between the 5" phototubes and ^{6}Li-glass scintillators by silica-glass couplers. This substitution reduced neutron moderation by the couplers and

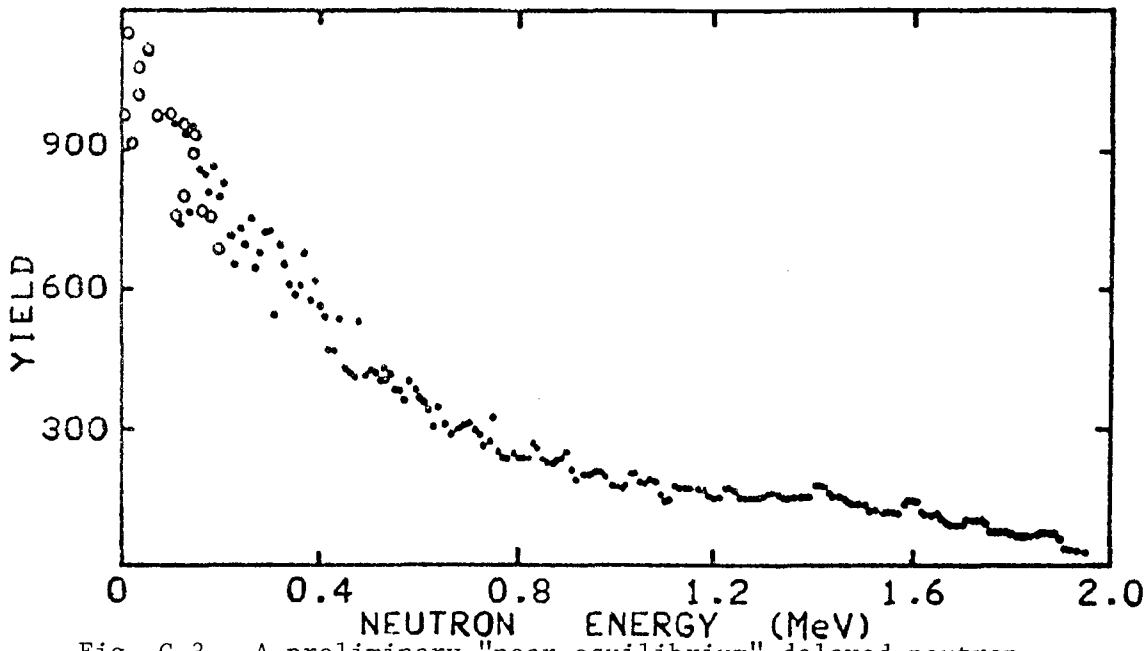

Fig. C-3. A preliminary "near-equilibrium" delayed-neutron energy spectrum measured with Pilot U (solid points) and ^{6}Li-glass (open circles) neutron detectors in the time-of-flight spectrometer.

thus resulted in approximately a 50% reduction in tail area of the monoenergetic neutron time response function.

Recently more definitive time-of-flight studies of U-235 delayed-neutron spectra have been started. Neutrons were detected by 4 ½"-thick Pilot U plastic scintillators 4½" in diameter, using a flight path of 50 cm. Correlated betas were detected by 1" x 0.5" and 3" x 0.5" Pilot U scintillators, each 0.040" thick. The two beta detectors allow the simultaneous study of two delay time intervals following fission. At present measurements of fast neutron induced fission of U-235 have been made for the following pairs of time intervals: 0.44 - 0.65 s, 0.73 - 1.35 s; 0.73 - 1.35 s, 1.6 - 3.4 s, 4.2 - 9.7 s; 4.2 - 9.7 s, 12.0 - 28.5 s; 12.0 - 28.5 s, 35.3 - 85 s. Note that each pair of time intervals has one interval in common with the adjacent pair, thus allowing normalization of each spectrum to the same relative fission yield.

Background-subtracted time-of-flight spectra for each time interval are shown in Fig. C-4. Variations in the spectra are discernible for different time intervals. Excellent agreement was observed between spectra corresponding to common time intervals from adjacent time pairs. The conversion of these spectra into neutron energy spectra, and their subsequent decomposition into individual delayed-neutron groups (a 6-Group analysis will be initially performed) are now underway. These studies will be repeated using 4 ^{6}Li-glass scintillators in place of Pilot U. The second series of measurements will be sensitive to the low energy portion, 10 keV $\leq E_n \leq$ 400 keV, of each spectrum.

Similar studies will be undertaken shortly using thermal neutrons from our 1-Mw reactor to induce U-235 fission. Comparison of the corresponding thermal vs. fast neutron measurements should provide information regarding the energy dependence of delayed-neutron spectra.

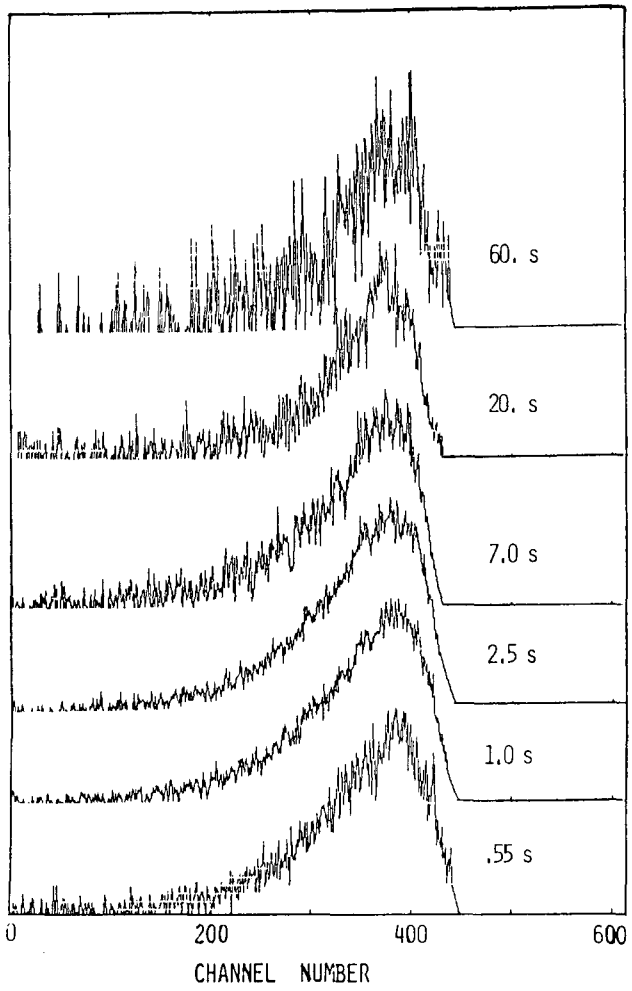

Fig. C-4. Delayed-neutron TOF spectra from fast neutron induced fission of U-235. Spectra are labeled according to the mean delay time following fission. Measurements were made using four ½"-thick by 4½" diameter Pilot U plastic scintillators 50 cm from the delayed-neutron source.

THE UNIVERSITY OF MICHIGAN
Department of Nuclear Engineering

A. INTRODUCTION

We have continued the development of our experimental facilities for the measurement of 14 MeV neutron cross sections in a well-shielded, low-albedo laboratory. Initial measurments of the fission cross sections of U-235 and Pu-239 are now completed, and extension of similar measurements to U-233, Np-237, and U-238 are well underway. Additional measurements on some (n,p), (n,alpha), and (n,2n) reaction cross sections have also begun, concentrating in materials of interest in fusion technology, neutron dosimetry, and neutron diagnostics. Several of these measurements are being carried out in collaboration with Dr. J.C. Robertson of the University of New Mexico.

As a follow-up to our earlier measurement at 23 keV, we are also planning measurements of the Th-232 capture cross section at additional energies between 140 and 964 keV provided by our set of photoneutron sources. These experiments will combine our well-established facilities for the activation and calibration of photoneutron sources with high-sensitivity gamma counting techniques now under development.

B. FISSION CROSS SECTION MEASUREMENTS AT 14 MeV (M. Mahdavi, G. F. Knoll, K. Zasadny)

The fission cross-sections of U-235 and Pu-239 have been measured at a neutron energy of 14.63 MeV. A 150 KV accelerator, installed on a low mass floor at the center of a large laboratory, provided a source of D-T neutrons under conditions of low scattering.

Fission events were accumulated with the target foils and detectors positioned inside a vacuum chamber and at various distances from the neutron source. Fission fragments passing through a limited solid angle aperture were registered on polyester track-etch films. The masses of the foil deposits were previously determined by microbalance weighings and confirmed by thermal fission and alpha counting.

The angular distribution of fission fragments for U-235 and Pu-239 were measured in a separate experiment. In this case the fission fragments were detected by a polyester track-etch film which was shaped to cover a 110° arc on a sphere of 5.08 cm radius centered on the deposit. Results of these measurements are reported in the following section.

The neutron flux was measured relative to $^{56}Fe(n,p)^{56}Mn$ and $^{27}Al(n,\alpha)^{24}Na$ reaction cross-sections. The Mn-56 and Na-24 activities were measured in a $4\pi\beta$ gas flow proportional counter. The absolute efficiencies were separately measured using a $4\pi\beta$-γ coincidence counting technique. The room scattered

flux contribution to the total flux was determined from different source-detector spacing runs. The precise neutron energy was directly measured using a silicon surface barrier detector.

The cross-sections obtained for U-235(n,f) and Pu-239(n,f) reactions were 2.070±.046 and 2.44±.092 b respectively and a ^{239}Pu(n,f)/^{235}U(n,f) cross-section ratio of 1.179±.028. These results are compared with other measurements in the same energy region in Figures B-1 and B-2.

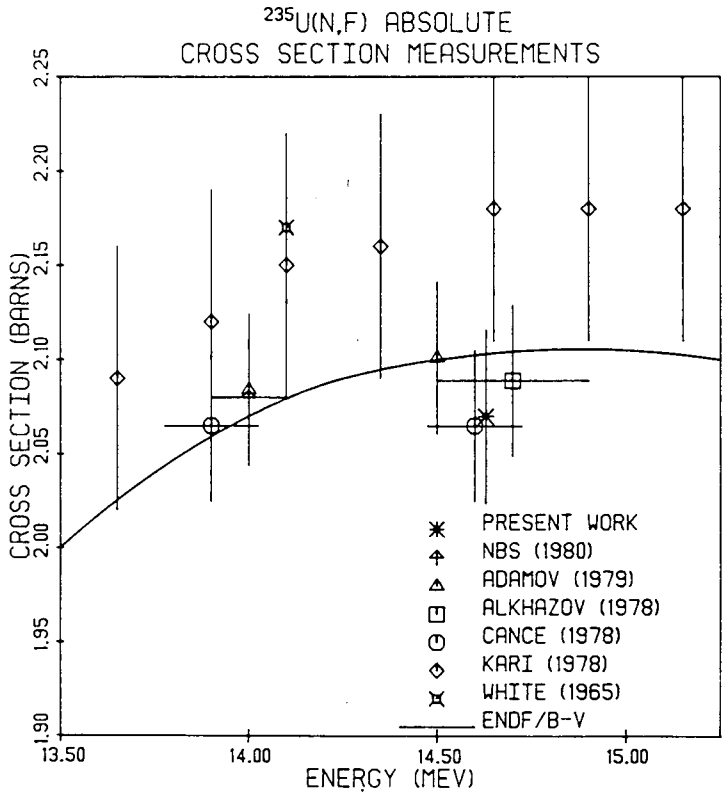

Fig. B-1. Absolute U-235 (n,f) cross section measurements.

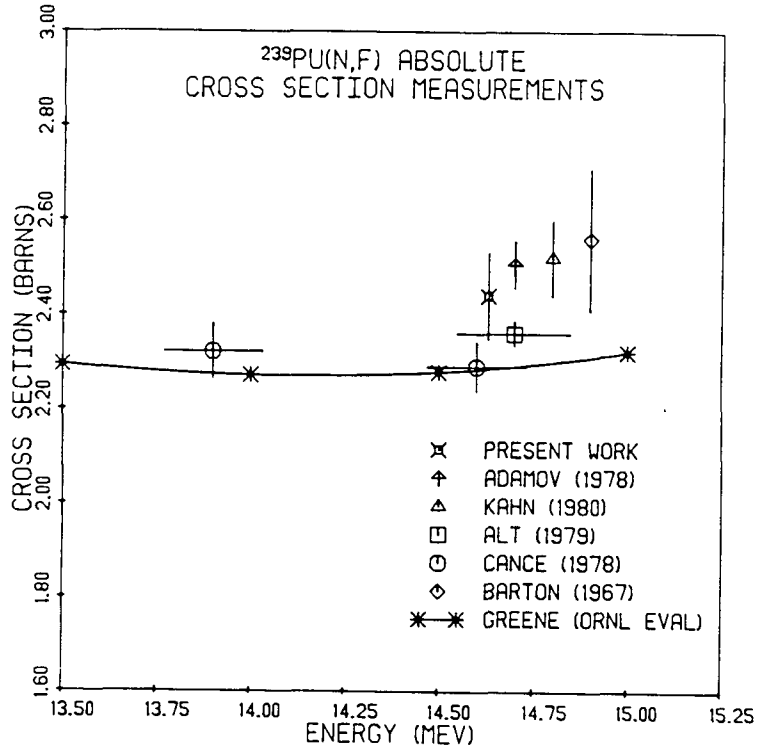

Fig. B-2. Absolute Pu-239(n,f) cross section measurements.

A similar set of measurements is nearing completion on the fissionable isotopes U-233, Np-237, and U-238. All but the last of these involve target foils with masses that have been well documented through their use in our previous photoneutron measurements.

C. FISSION FRAGMENT ANGULAR DISTRIBUTION MEASUREMENTS OF ^{235}U AND ^{239}Pu

(M. Mahdavi, G. Knoll, K. Zasadny)

A precise knowledge of fission fragment angular distribution is required in our fission cross-section measurements because the fission fragments are detected in limited solid angle. Sensitivity calculations have shown that a 2 percent change in the value of anisotropy will vary the corresponding cross-section in this work by 1 percent. Using 14 MeV neutrons, we have measured the absolute values of anisotropy for ^{235}U and ^{239}Pu targets. The same target foils used for cross-section measurements were employed in

anisotropy measurements. The deposits have diameters of 2.76 cm, but in this application the active diameters were restricted to .64 cm by means of a mask. The detector consisted of .102 mm polyester film (dupont cronar) mounted behind a semicircular screen aperture of radius of curvature 5.08 cm. The aperture limited the active detection area of the film to a height of 1.905 cm and a maximum angle of 110 degrees. The U-235 or Pu-239 targets were mounted at the center of the semicircular detector and tilted to 45 degrees with respect to the neutron beam to minimize the energy loss of fission fragments in the target. The experimental rig consisting of the target and detector were enclosed in a thin wall aluminum vacuum chamber. The chamber was then evacuated to the pressure of 10^{-2} torr. via a mechanical pump.

After a typical exposure of about 5 hours, the polyester film detector was etched in a 6.25 N solution of KOH at 68° for approximately 4.5 hours. A grid was then ruled on the film. The grid size (.889mm X .889mm) was chosen so that each vertical grid corresponds to 1° angular spread at the target. The fragment tracks were then counted at average angles of 0°, 15°, 30°, 60°, 75° and 90° with respect to the neutron beam. At each angle, angular spreads of up to $\pm 5°$ ($\pm$ five vertical grids) were used.

In order to account for angular nonuniformities in the fragment detection system, a separate measurement was carried out using thermal neutrons for which the yield is assumed to be isotropic. These results were used to normalize the observed distribution at 14 MeV.

The data were then fit with the expression,

$$Y(\theta) = 1 + A \cos^2\theta \quad .$$

Results obtained at a neutron energy of 14.63 $\pm$ .015 MeV are as follows:

	Y(0°)/Y(90°)
U-235	1.426 $\pm$ .024
Pu-239	1.295 $\pm$ .024

A paper describing these measurements will appear on the program of the June, 1983, meeting of the American Nuclear Society. Similar measurements on U-233, Np-237, and U-238 are in progress.

D. OTHER NEUTRON-INDUCED REACTIONS AT 14 MeV (K. Zasadny, Y. Lai, G. Knoll)

We have begun a program to develop experimental techniques for (n,p), n,alpha) and (n,2n) reaction cross section measurements at 14 MeV. Feasibility studies are underway for alternative techniques to measure the absolute neutron flux employing proton recoil monitors and/or dual thin scintillation detectors. The long term goals of these measurements remain to apply our techniques to the measurements of (n,alpha),(n,p), and (n,2n) reactions of technological interest, and in the determination of several

tritium breeding reactions of particular importance in fusion feasibility studies.

E. THORIUM CAPTURE CROSS SECTION MEASUREMENTS (S. Wilderman, G. Knoll)

The results of our measurement of the capture cross section in Th-232 at 23 keV were presented at the Specialists Meeting on Fast Neutron Capture held at Argonne National Laboratory in April of 1982. The measurements yield a cross section about 10 percent higher than recent evaluations in this energy range. Because of its large technological significance, a discrepancy of this magnitude is of major consequence. A careful reexamination of all factors in this measurement, including questions of the energy spectrum of the source raised at the conference, have confirmed our original conclusions. Because the measurement was designed to depend only on a very small number of ratio measurements to yield the absolute value of the cross section, we have strong confidence in the result.

In order to shed further light on this question, we are investigating the feasibility of extending the same techniques to other energies using three additional photoneutron sources. Because these sources are very much weaker than the antimony-beryllium source used in the original measurement, we will need to devise much more sensitive counting techniques. One possibility is the substitution of close-geometry sodium iodide counting for the germanium detector spectroscopy employed in the previous measurement. We need to gain about two orders of magnitude in efficiency, and on paper it appears feasible to accomplish that objective with this substitution. We will need to look closely at the question of radiochemical purity of the separated sample since the sodium iodide spectroscopy will not allow clean separation of any potential impurities. This evaluation is now underway and if the results prove positive we will proceed with the measurements of the thorium capture cross section at 140, 265, and 964 keV.

A. NEUTRON DATA MEASUREMENTS AND DETECTORS

1. Absolute Measurements of the $^{235}U(n,f)$ Cross Section for Neutron Energies from 0.3 to 3.0 MeV (A. D. Carlson, J. W. Behrens)

Recently the data taking phase was completed for these measurements of the ^{235}U fission cross section. The experiment was performed at the NBS Neutron Time-of-Flight facility. The neutron flux was determined with a "black neutron detector" located at the 200 m experimental station. On the same beam line at 69 m from the neutron target, a well-characterized[1] ^{235}U fission chamber with deposits of $\sim$ 100 $\mu g/cm^2$ was used to measure the reaction rate. The backgrounds for both detectors were reduced to negligible levels. The data accumulated during this experiment were stored in a two-parameter (time-of-flight and pulse height) format on magnetic disk for both detectors. The data from the individual experimental runs are now being analyzed for cross section values and consistency. A measurement of the efficiency of the black neutron detector at 2.6 MeV using the associated particle technique is planned. Monte Carlo calculations of the efficiency of this detector have been verified[2] experimentally below 0.9 MeV. The 2.6 MeV measurement will allow a test of the calculations near the end of the energy region of this experiment.

2. An Absolute Measurement of the ^{235}U Fission Cross Section for Neutron Energies from 2 to 6 MeV (M. S. Dias,* R. G. Johnson, A. D. Carlson, O. A. Wasson)

As an application of the dual thin scintillator (DTS) neutron detector described in Section (A-6), the ^{235}U fission cross section was measured at the NBS Neutron Time-of-Flight facility. This measurement uses the same physical and electronic setup as used in the experiment described in the previous section. The only change was the replacement of the large plastic scintillator (black detector) by the DTS detector as the neutron flux monitor. The data obtained in this measurement over the neutron energy range of 2 to 6 MeV are presently being analyzed. Since the measurement was designed to test the DTS detector, only moderate statistical precision was obtained for the fission chamber. The data will be grouped in broad ($\Delta E/E$ = 15%) energy bins.

---

* Ph.D. student from the Instituto de Pesquisas Energéticas e Nucleares - São Paulo - Brazil.

[1] O. A. Wasson and M. M. Meier, Nucl. Instrum. Methods 190, 571 (1981).

[2] M. M. Meier, Proceedings of a Symposium on Neutron Standards and Applications, NBS-SP 493, 221 (1977).

3. Absolute $^{235}U(n,f)$ Cross Section at 2.6 MeV (K. C. Duvall, Li Linpei,** O. A. Wasson)

A measurement of the $^{235}U(n,f)$ cross section at 2.6 MeV using the time-correlated associated-particle technique with the $^{2}H(d,n)^{3}He$ reaction continues at the 3 MV Van de Graaff laboratory. The neutron yields in this challenging experiment are nearly three orders of magnitude less than in our recently published[3] measurement at 14 MeV which used the more prolific $^{3}He(d,n)^{4}He$ reaction. Titanium-deuteride targets have been obtained from separate suppliers to compare target quality in terms of neutron yield, surface contamination, and deterioration. Extensive measurements have shown that the desired 1% accuracy in the cross section determination cannot be achieved with present techniques due to the surface conditioning of the presently used TiD targets. Future measurements will employ electrostatic separation instead of foil absorption to separate reaction products from the elastically scattered deuteron beam.

4. Measurement of ^{235}U Fission Cross Section Using a ^{252}Cf Neutron Source (I. G. Schröder, Li Linpei)

A new measurement of the ^{235}U fission cross section using a ^{252}Cf neutron source is in progress. The major sources of error in an earlier NBS experiment[4] are reduced by improved techniques. The improvements include the ^{252}Cf neutron source strength, the mass scale of the NBS fissionable isotope mass standards, calculations of the neutron scattering from the fission chamber, and the determination of the room-return neutron background in the facility. All of these measurements will reduce by a factor of two the 2.4% (1σ) error assigned to the previous cross section measurement.

5. Fission Cross Section Measurements in Reactor Physics and Dosimetry Benchmarks (J. A. Grundl, D. M. Gilliam)

Fission cross sections for eight fissionable isotopes of importance for nuclear technology have been measured in two fission neutron spectra and one fission-neutron-driven standard neutron field. New measurements for ^{240}Pu, ^{241}Pu, ^{233}U, and ^{232}Th accompany revised values from earlier determinations for ^{239}Pu, ^{235}U, ^{238}U, and ^{237}Np. (Table A-1).

** Visiting scientist from National Institute of Metrology, Beijing, Peoples Republic of China.

[3] Wasson, Carlson, Duvall, Nucl. Sci. Eng. 80, 282 (1982).

[4] Heaton, Grundl, Spiegel, Gilliam, Eisenhauer, "Absolute ^{235}U Fission Cross Section for ^{252}Cf Spontaneous Fission Neutrons," Proceedings of a Conf. on Nuclear Cross Sections and Technology, NBS Special Publication 425, U.S. Dept. of Commerce, Washington, DC (1975).

The starting point for all of these measurements is an absolute cross section measurement for ^{252}Cf fission spectrum neutrons. This absolute cross section is determined from a neutron source strength, a source-to-detector distance, and an absolute fission rate. Relative fission cross section measurements for the Intermediate-Energy Standard-Neutron Field (ISNF) are put on an absolute scale by employing a flux transfer procedure from the ^{252}Cf source. For ^{235}U fission spectrum neutrons, cross section ratios measured in a cavity fission source are normalized to the ^{235}U fission cross section measured in the ^{252}Cf fission neutron field. Two fission cross sections for ^{239}Pu fission spectrum neutrons, derived from earlier ratio measurements designed to compare ^{235}U and ^{239}Pu fission neutron spectra, are included for completeness. Errors are given at one standard deviation. These benchmark measurement results are intended to provide integral normalizations and a test of differential neutron cross section data.

Table A-1. Fission Cross Sections for Reactor Physics and Dosimetry Benchmarks

Isotope	ISNF (mb)	Fission Spectra [a]	
		^{252}Cf (mb)	^{235}U (mb)
^{232}Th	38.4 ± 1.2	89.4 ± 2.7	--
^{233}U	2424 ± 65	1893 ± 48	--
*^{235}U	1606 ± 35	1216 ± 19	(b)
*^{238}U	149.0 ± 3.6	326 ± 6.5	309 ± 8
*^{237}NP	829 ± 22	1366 ± 27	1344 ± 54
*^{239}Pu	(b)	1824 ± 35	1832 ± 55
^{240}Pu	824 ± 23	1337 ± 32	--
^{241}Pu	2152 ± 108	1616 ± 80	--
$^{235}U/^{238}U$	10.78 ± 1.1%	3.73 ± 1.2%	3.94 ± 2.0%
$^{235}U/^{239}Pu$	0.866 ± 1.0%	0.666 ± 0.9%	0.664 ± 2.5%
$^{237}Np/^{238}U$	5.56 ± 1.7%	4.19 ± 1.5%	4.35 ± 3.0%

[a] Two cross sections for the ^{239}Pu fission spectrum derived from ^{235}U and ^{239}Pu fission spectra comparison experiments are $\sigma_f(^{238}U) = 319 \pm 0.09$; and $\sigma_f(Np) = 1346 \pm 44$ mb.

[b] Neutron fluence transfer reactions are $\sigma_f(^{235}U, \chi_{25})/\sigma_f(^{235}U, \chi_{Cf}) = 1.000 \pm 0.004$ (2 SD), and $\sigma_f(^{239}Pu, ISNF)/\sigma_f(^{239}Pu, \chi_{Cf}) = 1.018 \pm 0.006$ (2 SD).

* Previous work.

6. Development of a New Absolute Flux Detector for MeV Neutrons
(M. S. Dias, R. G. Johnson, O. A. Wasson)

A neutron flux detector for use in the 1-15 MeV energy range has been built to be used for cross section experiments in the NBS Positive Ion Van de Graaff and Linac accelerators. A dual thin scintillator (DTS) configuration yields a proton recoil spectrum which approaches the ideal thin scintillator response. The detector consists of two thin plastic scintillators optically separated from each other and independently coupled to phototubes (Fig. A-1). In this configuration the escape of protons is eliminated experimentally and the multiple scattering correction is low. The detector has been calibrated at 2.44 MeV and 14.1 MeV, using the associated particle technique with the NBS Positive Ion Van de Graaff as a neutron source. Theoretical calculations of the detector efficiency and pulse height distributions were performed using a Monte-Carlo code in order to extend the detector efficiency to other energies between 1 and 15 MeV.

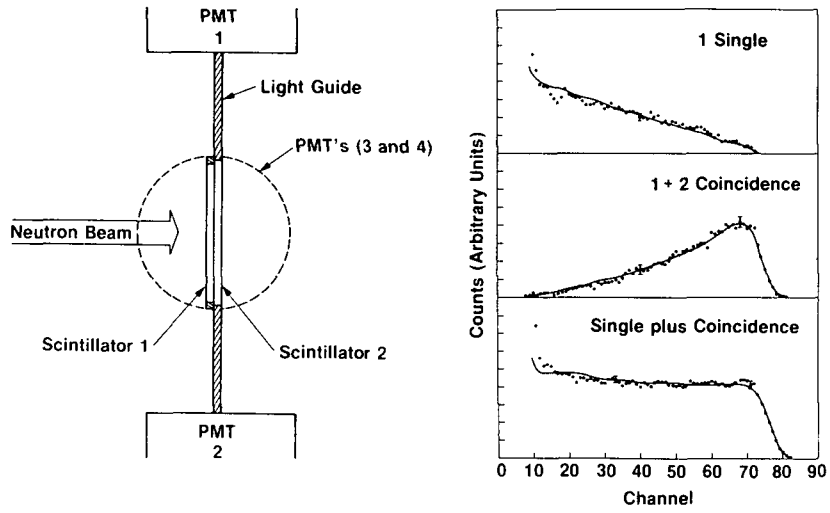

(a) (b)

Fig. A-1. (a) Dual thin scintillator detector geometry.

(b) Detector response for 14 MeV neutrons. The measured responses are indicated by the dots while the solid curve shows the calculated response.

7. Spent Fuel Assay (J. W. Behrens, R. G. Johnson, R. A. Schrack)

Neutron transmission measurements have been made for samples of high burnup (25,000 MWd/te) power reactor fuel. Two samples (each approximately 2.5-cm thick and 1.0 cm in diameter) were used; one cut from the center of a fuel rod and the other from an end. The transmissions of these samples were measured from 0.8 to 45 eV at the NBS Neutron Time-of-Flight facility using a 20-m flight path and a ^{6}Li-glass detector. From the data we have identified the resonances for 11 actinides and 5 fission products. Using ENDF/B-V files as a basis set for these 16 isotoptes the transmission data were fit with an interactive computer code. The results of this fitting are shown in Table A-2. Differences in isotopic abundance as a result of the flux difference (approximately a factor of two) between the center and end of the fuel rod are clearly evident. These measurements demonstrate a method for spent fuel analysis with both isotopic discrimination and high precision. The method is adaptable to industrial use[5] and would be valuable to programs for improved fuel utilization, transport and storage of spent fuel, reprocessing, safeguards, and determining the value of spent fuel.

Table A-2. Isotopic Abundance in Samples of Spent Fuel

Isotope	Abundance x 10^5 (atoms/b)	
	Center Cut	End Cut
U-234	1.481 ± 0.060	1.265 ± 0.038
U-235	37.67 ± 0.85	63.57 ± 0.65
U-236	15.79 ± 0.42	9.12 ± 0.14
U-238	4765. ± 27.	4256. ± 16.
Pu-238	3.74 ± 0.76	2.52 ± 0.43
Pu-239	26.26 ± 0.60	16.98 ± 0.36
Pu-240	10.64 ± 0.15	4.572 ± 0.043
Pu-241	4.94 ± 0.33	1.37 ± 0.22
Pu-242	1.512 ± 0.033	0.202 ± 0.016
Am-241	5.52 ± 0.22	2.68 ± 0.13
Am-243	0.705 ± 0.058	0.197 ± 0.031
TC-99	9.94 ± 0.27	4.02 ± 0.19
ND-145	3.10 ± 0.27	1.67 ± 0.18
Xe-131	3.382 ± 0.063	1.595 ± 0.020
Cs-133	7.63 ± 0.29	3.46 ± 0.19
Sm-152	0.694 ± 0.013	0.330 ± 0.006

[5] C. D. Bowman et al., Neutron Transmission Analysis of Reactor Spent Fuel Assemblies, World Conference on Neutron Radiography, 7-10 December 1981, San Diego, California.

8. Resonance Neutron Radiography Analysis of Waste Material for U-235 Content (R. A. Schrack)

The ability of Resonance Neutron Radiography to determine the amount and distribution of any isotope independent of the matrix in which it is embedded has been applied to the problem of waste assay. Vermiculite has been used as a substitute for incinerator ash as the matrix material. A two-liter plastic container was filled with vermiculite and then innoculated with successively larger amounts of uranium. Table A-3 shows the comparison of weights of uranium as measured by RNR. Measurements were also made of non-homogeneous samples with results of similar precision.

Table A-3. Measurement Comparisons of U-235 Content in Two Liters of Vermiculite

Sample	By Weighing	By Radiography
1	0.9577±.0001	1.053±0.17
2	2.9011±.0001	3.085±0.22
3	9.2196±.0001	9.009±0.23

9. Lithium-6 Gel Neutron Detector (R. A. Schrack, R. G. Johnson, B. M. Coursey)

The need for a large or a fast detector for low energy neutrons has prompted a detector development program. Lithium glass detectors are expensive and difficult to make in large sizes. We have initiated a program to make a detector using ^{6}Li in an organic scintillator. An aqueous solution of $LiC\ell$ and an organic scintillator have been combined using a suitable detergent to produce a stable gel. Tests have been made to determine the light transmission of the multiphase mixture and a suitable optical cell has been fabricated. A detector 6" in diameter and 1 cm thick has been produced. It has a calculated efficiency of 9% for 10 eV neutrons. The detector will be directly coupled to a 5" diameter photomultiplier for tests.

10. Multichannel Plate Neutron Detector (R. A. Schrack. R. G. Johnson)

The ability of the multichannel plate detector to provide high resolution two-dimensional images with good neutron energy resolution was demonstrated using samples of gold, tungsten, and rhodium stacked together. Figure A-2a shows the image of the stack obtained with x-ray radiography. The same image is obtained with thermal neutron radiography. Using time windows placed on the three resonances, we can obtain three separated images corresponding to the distributions of the gold, tungsten, and rhodium. Figure A-2b shows the separated radiographs. Since all isotopes have a unique neutron resonance structure, one may thus selectively image the distribution of any desired isotopte in a complex matrix.

a)

b)

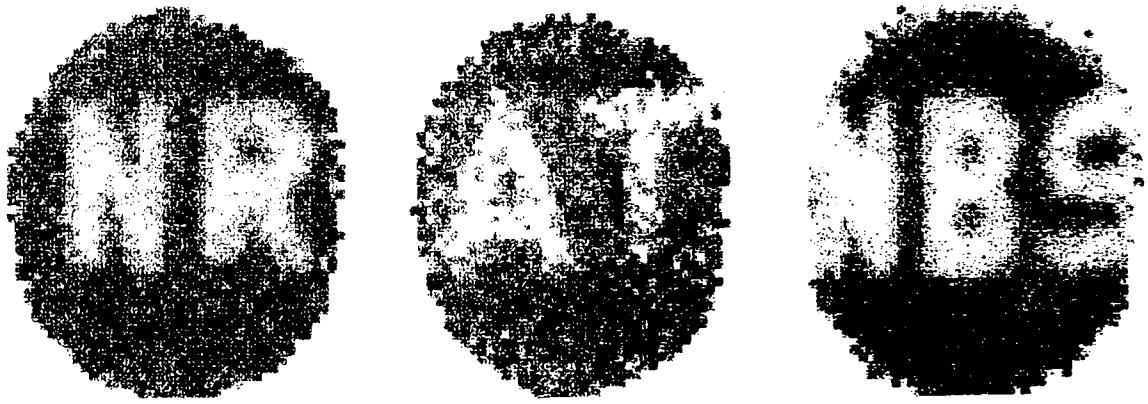

RHODIUM TUNGSTEN GOLD

Fig. A-2. a) X Ray of sample containing gold, tungsten, and rhodium.

b) Neutron radiographs of sample.

11. Development of a ^{3}He-Based, Gas Scintillation Detector for Neutron Standards Use in the keV Energy Range (J. W. Behrens)

A program of detector development and measurement has been started to establish the ^{3}He(n,p) reaction as a useful standard in the keV range. Presently there is no single reaction which is suitable for flux measurements throughout the keV range (0.5 to 2000 keV). Both ^{6}Li(n,α) reaction and ^{10}B(n,α) reaction change so rapidly or become so small in the higher energy region that neither is suitable at higher energies. For ^{235}U(n,f) the structure below 100 keV causes the reaction to be useless for standards purposes. However, the ^{3}He(n,p) reaction is smooth throughout and is relatively flat from 300 to 3000 keV. The NBS is presently designing a ^{3}He-based, gas scintillation detector with geometry suitable for standards measurements and accurate cross section measurements.

12. Inferred MeV Fission Cross Sections for Unmeasured Actinides (J. W. Behrens)

During the past decade considerable effort has been spent in extending the measurements of fission cross sections of the actinides in the MeV range. Measured data now exist for over 24 nuclides. This set is now sufficiently large to justify an attempt to infer the fission cross section for unmeasured nuclei from the systematics of neighboring nuclei. Two papers[6,7] have recently been published on this subject and a talk was presented at the 1982 Cambridge Conference.[8] Figure A-3 shows present results for 12 isotopes of plutonium. Closed squares represent measurements;[9] whereas, open circles represent fission cross sections inferred from systematics. Similar results can be obtained for the isotopes of thorium through americium using the currently available experimental data sets.

13. ^{232}Th:^{235}U Fission Cross Section Ratio Measurement in the MeV Region (J. W. Behrens, J. C. Browne,† E. Ables††)

Final results are published[10] on the fission cross-section ratio for ^{232}Th relative to ^{235}U in the neutron energy range from 0.7 to 30 MeV. The measurement was conducted at the Lawrence Livermore National Laboratory 100 MeV electron linac. Our measurement provides a fission cross-section ratio that fills gaps in the MeV range where past experimental data were lacking.

---

† Los Alamos National Laboratory, Los Alamos, NM.

†† Lawrence Livermore National Laboratory, Livermore, CA.

6 Behrens, Bull. Am. Phys. Soc. 27, 459 (1982).

7 Behrens, Trans. Am. Nucl. Soc. 43, 722 (1982).

8 Behrens, Int. Conf. Neutron and Its Applications, September 13-17, 1982, Cambridge, England.

9 Behrens et al., Nucl. Sci. Eng. 66, 205 (1978); Nucl. Sci. Eng. 66, 433 (1978); Nucl. Sci. Eng. 68, 128 (1978).

10 Behrens, Browne, Ables, Nucl. Sci. Eng. 81, 512 (1982).

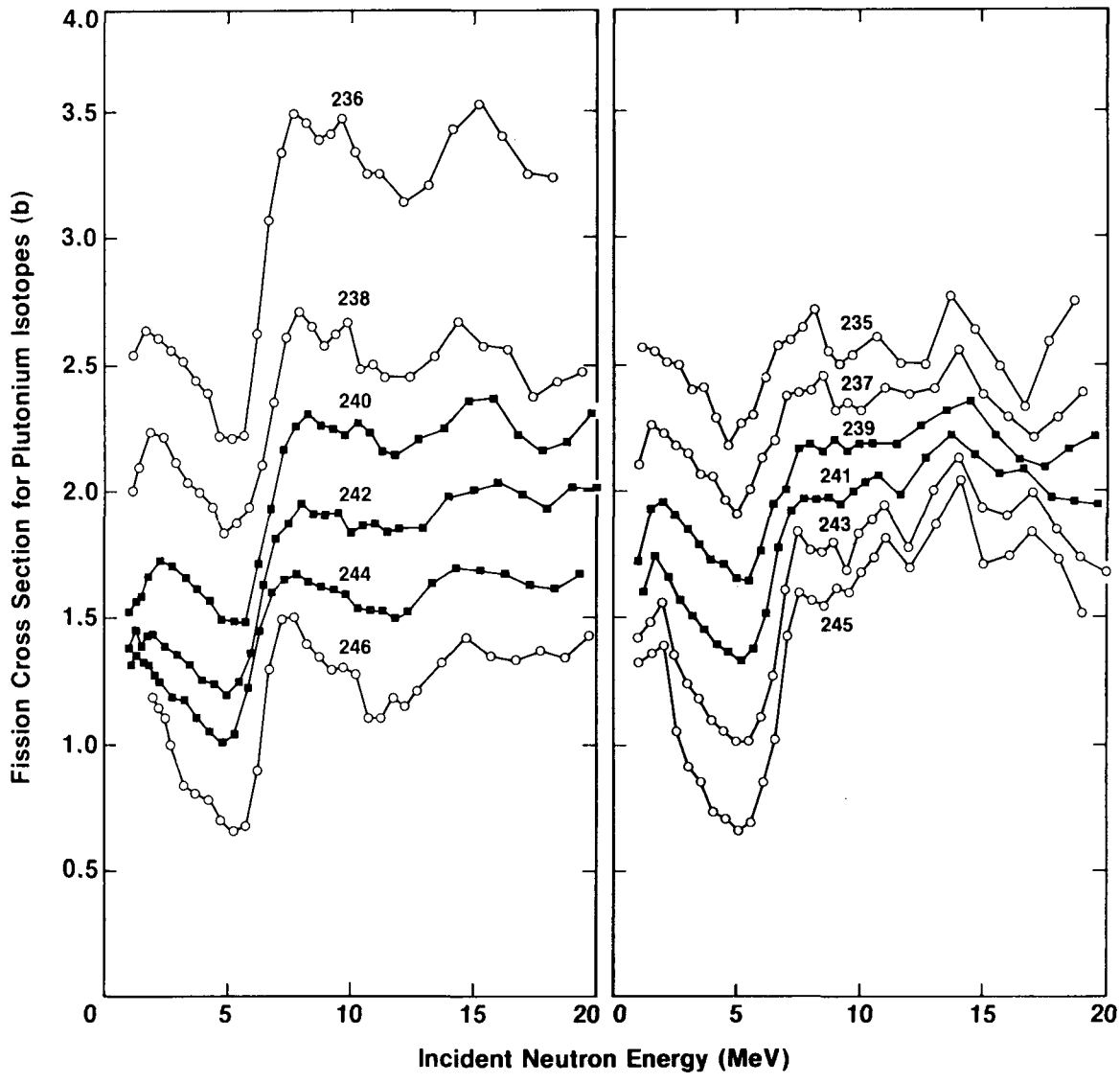

Fig. A-3. Fission cross sections for various Pu isotopes. Closed squares represent measurements while the open circles represent cross sections inferred from systematics.

B. NEUTRON PHYSICS

1. The Influence of Neutron-Induced Electronic Excitations in Atoms and Molecules on Neutron Moderation (R. G. Johnson and C. D. Bowman)

The excitation of electronic states in atoms and molecules by neutron-nucleus scattering has been studied theoretically.[11] Although the probabilities for such excitations are small, the phenomena are interesting in both the basic and applied sense. As an applied problem the possible influence on neutron moderation has been estimated.

In Ref. 11 it is shown that on the average the probability for excitation of atomic electrons is proportional to the incident neutron energy. Then assuming an average energy loss equal to the atomic ionization energy, the effect of electronic excitations can be included in neutron moderation problems as a small increase in the average logarithmic energy decrement, $\overline{\xi}$. Estimating this increase for typical light atoms an increase in $\overline{\xi}$ of the order of 10^{-4} is found.[12] For molecules increases in $\overline{\xi}$ of the same order of magnitude can be expected. Consequently the influence of neutron-induced electronic excitations on neutron moderation can be neglected in most applications.

C. DATA COMPILATION

1. Photon and Charged Particle Data Center (M. J. Berger, E. G. Fuller, H. Gerstenberg, J. H. Hubbell, S. M. Seltzer)

New tabulations of electron and positron stopping powers and ranges have been published[13,14,15] and proton stopping power tables are in progress.

---

[11] Lovesey, Bowman, and Johnson, Z. Phys. B47 (1982) 137.

[12] C. D. Bowman and R. G. Johnson, Neutron-Induced Atomic Excitations and Neutron Moderation, Int. Conf. on Nucl. Data for Sci. and Tech. 6-10 September 1982, Antwerp, Belgium.

[13] S. M. Seltzer and M. J. Berger, Evaluation of Collision Stopping Power of Elements and Compounds for Electrons and Positrons, Int. J. Appl. Rad. & Isotopes, 33, 1189 (1982).

[14] S. M. Seltzer and M. J. Berger, Procedure for Calculating the Radiation Stopping Power for Electrons, Int. J. Appl. Rad. & Isotopes, 33, 1219 (1982).

[15] M. J. Berger and S. M. Seltzer, Stopping Power and Ranges of Electrons and Positrons, NBSIR 82-2550 (1982).

The 1973-1981 photonuclear data index supplement is now published,[16] and the Center's accumulation of abstracted photonuclear data sheets is being prepared for publication. Improved primarily-theoretical tables of photon attenuation and energy-absorption coefficients for energies 1 keV to 20 MeV are now published,[17] and further evaluation of this new data set is in progress using the Center's recently-computerized data base of measured photon attenuation coefficients.[18] This Center has also collaborated with a group at Göttingen in preparing tables of relativistic Hartree-Fock-Slater modified atomic form factors.[19]

2. Kerma Factors for Neutron Energies Below 30 MeV (R. S. Caswell, J. J. Coyne, and M. L. Randolph (ORNL))

Neutron energy transfer to matter is frequently described in terms of "kerma factors" based on neutron nuclear data. The term "kerma factor" is used to distinguish these data from "energy transfer coefficients" which give equivalent information but are defined less conveniently for use with neutron fields. In an earlier publication[20] kerma factors were calculated for 19 elements and 15 compounds and mixtures based on ENDF/B-V neutron cross sections below 20 MeV, and much less reliable extrapolations in the region 20-30 MeV. These tables have now been extended to 44 other compounds and mixtures[21] generally of interest to dosimetry and biology.

---

[16] E. G. Fuller and H. Gerstenberg, Photonuclear Data Index, 1973-1981 (Suppl. 2 to NBS Spec. Publ. 380) NBSIR 82-2543 (1982).

[17] J. H. Hubbell, Photon Mass Attenuation and Energy-Absorption Coefficients from 1 keV to 20 MeV, Int. J. Appl. Rad. & Isotopes, 33, 1269 (1982).

[18] H. Gerstenberg and J. H. Hubbell, Comparison of Experimental with Theoretical Photon Attenuation Cross Sections Between 10 eV and 100 GeV, Proc. Int. Conf. on Nuclear Data for Science and Technology, Antwerp, Belgium, Sept. 6-10, 1982) (in press).

[19] Schaupp, Schumacher, Smend, Rullhusen and Hubbell, Small-Angle Scattering of Photons at High Energies: Tabulations and Relativistic HFS Modified Atomic Form Factors, J. Phys. Chem. Ref. Data (in press).

[20] R. S. Caswell, J. J. Coyne, and M. L. Randolph, Kerma Factors for Neutron Energies Below 30 MeV, Radiation Research 83, 217-254 (1980).

[21] R. S. Caswell, J. J. Coyne, and M. L. Randolph, Kerma Factors of Elements and Compounds for Neutron Energies Below 30 MeV, Int. J. Appl. Radiation Isot. 33, 1227-1262 (1982).

A. CROSS SECTION MEASUREMENTS

1. Capture and Total Cross Sections

a. Neutron Capture in the 1.15-keV Resonance of Iron*
(R. L. Macklin)

b. Application of New Techniques to ORELA Transmission Measurements and Their Uncertainty Analysis: The Case of Natural Nickel From 2 keV to 20 MeV** (D. C. Larson, N. M. Larson, J. A. Harvey, N. W. Hill, and C. H. Johnson)

The neutron transmission through a 2.54-cm sample of natural nickel has been measured for neutron energies between 2 keV and 20 MeV. The Oak Ridge Electron Linear Accelerator (ORELA) was used to provide the neutrons which were detected at the 200-m flight path by a NE-110 proton recoil detector. A selective gating system was utilized to minimize background effects due to large light-level events which produce phototube afterpulsing and long decay-constant light emission in the detector. A detailed discussion of the development of this system is given. An analysis of systematic uncertainties in the measurement is presented, and a covariance matrix is developed for this measurement. The experimental results are compared with the total cross section in the ENDF/B-V file for nickel.

c. Resonance Parameters of ^{60}Ni + n From Measurements of Transmission and Capture Yields from 1 to 450 keV † (C. M. Perey, J. A. Harvey, R. L. Macklin, F. G. Perey, and R. R. Winters‡)

High-resolution transmission and capture measurements of ^{60}Ni-enriched targets have been made at the Oak Ridge Electron Linear Accelerator (ORELA) from a few eV to 1800 keV in transmission and from 2.5 keV to 5 MeV in capture. The transmission data from 1 to 452 keV were analyzed with a multi-level R-matrix code which uses the Bayes' theorem for the fitting process. This code provides the energies and neutron widths of the resonances inside the 1- to 452-keV region as well as a possible parameterization for outside resonances to describe the smooth cross section in this region. The capture data were analyzed from 2.5 to 452 keV with a least-squares fitting code using the Breit-Wigner formula. Average parameters for the 30 observed s-wave resonances were deduced. The average level spacing D_0, was found to be equal to 15.2 ± 1.5 keV; the strength function, S_0, equal to (2.2 ± 0.6) x 10^{-4}; and the average radiation width, $\bar{\Gamma}_\gamma$, equal to 1.30 ± 0.07 eV. The

---

*Nucl. Sci. Eng. 83, 309 (1983).
**Abstract of ORNL/TM-8203 (1983).
†Submitted to Physical Review C.
‡Denison University, Granville, Ohio 43203.

staircase plot of the reduced level widths and the plot of the Lorentz-weighted strength function averaged over various energy intervals show possible evidence for doorway states. The level densities calculated with the Fermi-gas model for $\ell = 0$ and for $\ell > 0$ resonances were compared with the cumulative number of observed resonances, but the analysis is not conclusive. The correlation coefficient, ρ, between Γ_n^0 and Γ_γ is equal to 0.53 ± 0.18. The average capture cross section as a function of the neutron incident energy is compared to the tail of the giant electric dipole resonance prediction.

d. Neutron Transmission and Capture Measurements and Analysis of ^{60}Ni from 1 to 450 keV* (C. M. Perey, J. A. Harvey, R. L. Macklin, R. R. Winters,** and F. G. Perey)

High-resolution transmission and capture measurements of ^{60}Ni-enriched targets have been made at the Oak Ridge Electron Linear Accelerator (ORELA) from a few eV to 1800 keV in transmission and from 2.5 keV to 5 MeV in capture. The transmission data from 1 to 450 keV were analyzed with a multi-level R-matrix code which uses the Bayes' theorem for the fitting process. This code provides the energies and neutron widths of the resonances inside the 1- to 450-keV region as well as a possible parameterization for outside resonances to describe the smooth cross section in this region. The capture data were analyzed with a least-squares fitting code using the Breit-Wigner formula. From 2.5 to 450 keV, 166 resonances were seen in both sets of data. Correspondence between the energy scales shows a discontinuity around 300 keV which makes the matching of resonances at higher energies difficult. Eighty-nine resonances were seen in the capture data only. Average parameters for the 30 observed s-wave resonances were deduced. The average level spacing D_0 was found to be equal to 15.2 ± 1.5 keV, the strength function, S_0, equal to $(2.2 \pm 0.6) \times 10^{-4}$ and the average radiation width, $\overline{\Gamma}_\gamma$, equal to 1.30 ± 0.07 eV. The staircase plot of the reduced level widths and the plot of the Lorentz-weighted strength function averaged over various energy intervals show possible evidence for doorway states. The level densities calculated with the Fermi-gas model for $\ell = 0$ and for $\ell > 0$ resonances were compared with the cumulative number of observed resonances, but the analysis is not conclusive. The average capture cross section as a function of the neutron incident energy is compared to the tail of the giant electric dipole resonance prediction.

e. Neutron Resonance Parameters of ^{68}Zn + n and Statistical Distributions of Level Spacings ^{30} and Widths† (J. B. Garg,‡ V. K. Tikku,‡ J. A. Harvey, J. Halperin, and R. L. Macklin)

---

*Abstract of ORNL-5893, ENDF-330 (November 1982).
**Denison University, Granville, Ohio 43203.
†Phys. Rev. C 25(4), 1808 (April 1982).
‡State University of New York, Albany, New York 12222.

f. Overlapping β Decay and Resonance Neutron Spectroscopy of Levels in ^{87}Kr* (S. Raman, B. Fogelberg, J. A. Harvey, R. L. Macklin, P. H. Stelson, A. Schröder**, and K.-L. Kratz**)

Energy levels in ^{87}Kr have been studied, with special emphasis on the unbound region, using two different methods. The first method comprises neutron capture and transmission measurements on an enriched gas target of ^{86}Kr using neutron time-of-flight techniques. In this way, neutron widths were determined for 39 resonances below 400 keV and capture areas for 14 resonances below 90 keV. The second method is a decay study of 56-s ^{87}Br in which a level scheme for ^{87}Kr has been established that shows 126 levels in the bound and 12 levels in the unbound region. A detailed comparison between the neutron resonance, the γ-ray decay, and available delayed neutron results has been made. Almost a one-to-one correspondence exists between the currently observed p-wave resonances below 250 keV and levels in ^{87}Kr studied through delayed neutron emission. The overall β-strength distribution derived from the present data shows broad resonance like structures. However, no marked selectivity is observed in the β decay to individual levels in the unbound region of ^{87}Kr. The neutron capture cross section of ^{86}Kr is found to be about 5 mb for 30-keV neutrons with a Maxwellian energy distribution. The future of delayed neutron spectroscopy as a new tool for obtaining level-density information is discussed.

g. Neutron Capture Cross Sections of the Silver Isotopes ^{107}Ag and ^{109}Ag from 2.6 to 2000 keV† (R. L. Macklin)

h. Cross Sections of the ^{169}Tm(n,γ) Reaction from 2.6 keV to 2 MeV‡ (R. L. Macklin, D. M. Drake,¶ J. J. Malanify,¶ E. D. Arthur,¶ and P. G. Young¶)

i. ^{178,179,180}Hf and ^{180}Ta(n,γ) Cross Sections and Their Contributions to Stellar Nucleosynthesis§ (H. Beer,△ R. L. Macklin)

j. Neutron-Capture Cross Sections of the Tungsten Isotopes ^{182}W, ^{183}W, ^{184}W, and ^{186}W from 2.6 to 2000 keV▲ (R. L. Macklin, D. M. Drake,▽ and E. D. Arthur¶)

---

*Submitted to Phys. Rev. C.
**Institut für Kernchemie, Universität Mainz, D-65 Mainz, Germany.
†Nucl. Sci. Eng. 82, 400-407 (1982).
‡Nucl. Sci. Eng. 82, 143-50 (1982).
¶Los Alamos National Laboratory, P. O. Box 1663, Los Alamos, New Mexico 87545.
§Phys. Rev. C 26(4), 1404 (1982).
△Kernforschungszentrum Karlsruhe GmbH, Institut für Angewandte Kernphysik, D-7500 Karlsruhe, Federal Republic of Germany.
▲Submitted to Nucl. Sci. Eng.
▽Los Alamos National Laboratory, Los Alamos, New Mexico 87545.

2. Scattering and Reactions

a. ^{187}Os(n,n') Inelastic Cross Section at 34 keV* (R. L. Macklin, R. R. Winters,** N. W. Hill, and J. A. Harvey)

A measurement of the ^{187}Os inelastic neutron cross section to the $3/2^-$, 9.75-keV excited state with 34 ± 2 keV incident neutrons gives 1.5 ± 0.2 b. Pulsed neutron time of flight and a short anisotropic iron-aluminum filter allowed separation of the inelastic yield from the $1/2^-$ ground-state elastic yield at 24 keV. The influence of the result on r-process galactic age calculations via the Re-Os decay chronometer is discussed and the need for further theoretical calculations is emphasized.

b. ^{206}Pb Level Structure from ^{206}Pb(n,n'γ) Measurements† (J. K. Dickens)

A study of gamma-ray data produced by neutron inelastic scattering from a lead sample enriched in the isotope ^{206}Pb has resulted in placements, or tentative placements, of 146 gamma rays as transitions among 112 known or postulated levels of the ^{206}Pb level structure.

c. Gamma-Ray Decay of Levels in ^{63}Cu and ^{65}Cu‡ (J. K. Dickens)

Gamma-ray decay of levels in the stable copper isotopes ^{63}Cu and ^{65}Cu has been studied using ^{63,65}Cu(n,n'γ) reactions for incident neutron energies between threshold and 6 MeV. Of the 257 gamma rays or gamma-ray groups observed for neutron interactions with ^{63}Cu, 137 have been placed or tentatively placed among 88 levels in ^{63}Cu up to an excitation energy of 5.9 MeV. Similarly, of 335 gamma rays or gamma-ray groups observed for neutron interactions with ^{65}Cu, 127 have been placed among 100 levels in ^{65}Cu up to an excitation energy of 5.8 MeV, including new decay data for >70 excited states of ^{65}Cu.

d. Gamma-Ray Production Due to Neutron Interactions with Copper for Neutron Energies Between 0.7 and 10.5 MeV¶ (G. G. Slaughter and J. K. Dickens)

Differential cross sections for 22 gamma rays produced by neutron interactions with elemental copper having energies, E_γ, between 0.36 and 2.5 MeV have been measured for neutron energies, E_n, between 0.7 and 10.5 MeV for $\Theta_\gamma = 90°$ using a Ge(Li) detector system. The present data are compared with previously reported measurements; agreement with earlier reported data is generally good for $E_n < 3$ MeV and generally poor for $E_n > 4$ MeV.

---

*Submitted to The Astrophysical Journal.
**Denison University, Granville, Ohio 43203.
†Abstract of ORNL/TM-8137 (1982).
‡Accepted for publication in Nucl. Phys.
¶Submitted to Nucl. Sci. Eng.

e. Neutron-Induced Gamma-Ray Production in ^{57}Fe for Incident-Neutron Energies Between 0.16 and 21 MeV* (Z. W. Bell, J. K. Dickens, D. C. Larson, and J. H. Todd)

Interactions of neutrons with the iron isotope ^{57}Fe have been studied by measuring gamma-ray production cross sections for incident-neutron energies between 0.16 and 21 MeV. Neutrons produced by the Oak Ridge Electron Linear Accelerator impinged upon a metallic iron sample enriched to 93% in the isotope ^{57}Fe. The resulting gamma radiation was detected using a 100-cm^3 Ge(Li) detector placed at 125 deg with respect to the neutron beam line. A complete description of the experiment is given. Absolute gamma-ray production cross sections were measured for gamma rays corresponding to the $^{57}Fe(n,n'\gamma)^{57}Fe$, $^{57}Fe(n,\gamma)^{58}Fe$, $^{57}Fe(n,\alpha)^{54}Cr$, $^{57}Fe(n,2n)^{56}Fe$, and $^{57}Fe(n,p)^{57}Mn$ reactions. The cross section for the $^{57}Fe(n,2n)^{56}Fe$ reaction exceeds 1 b for $E_n \sim 15$ MeV, and the cross section for the $^{57}Fe(n,p)^{57}Mn$ reaction exceeds 0.2 b for $E_n \sim 9$ MeV. A new excited state is postulated for ^{57}Mn to account for observed data. Several new transitions are reported for decay of levels in ^{57}Fe. Measured cross sections are compared with data obtained from the current ENDF/B evaluation.

3. Actinides

a. Yields of Short-Lived Fission Products of Thermal-Neutron Fission of Thorium-229** (J. K. Dickens, J. W. McConnell, and K. J. Northcutt).

b. Yields of Fission Products Produced by Thermal-Neutron Fission of ^{229}Th† (J. K. Dickens and J. W. McConnell)

c. Fission Product Yields for Thermal-Neutron Fission of Curium-243‡ (David G. Breederland)

Cumulative fission yields for 25 gamma rays emitted during the decay of 23 fission products produced by thermal neutron fission of ^{243}Cm have been determined. Using Ge(Li) spectroscopy, 33 successive pulse-height spectra of gamma rays emitted from a 77-ng sample of ^{243}Cm over a period of approximately two and one-half months were analyzed. Reduction of these spectra resulted in the identification and matching of gamma-ray energies and half-lives to specific radionuclides. Using these results, 23 cumulative fission-product yields were calculated. Only those radionuclides having half-lives between 6 hours and 65 days were observed. Prior to this experiment, no fission-product yields had been recorded for ^{243}Cm.

---

*Accepted for publication in Nucl. Sci. Eng.
**Nucl. Sci. Eng. 80, 455-61 (1982).
†Phys. Rev. c 27, 253 (1983).
‡Abstract of ORNL/TM-8168 (1982).

d. Electron Spectra from Decay of Fission Products* (J. K. Dickens)

Electron spectra following decay of individual fission products ($72 \leqslant A \leqslant 162$) are obtained from the nuclear data given in the compilation using a listed and documented computer subroutine. Data are given for more than 500 radionuclides created during or after fission. The data include transition energies, absolute intensities, and shape parameters when known. An "average" beta-ray energy is given for fission products lacking experimental information on transition energies and intensities. For fission products having partial or incomplete decay information, the available data are utilized to provide best estimates of otherwise unknown decay schemes. This compilation is completely referenced and includes data available in the reviewed literature up to January 1982.

e. A Measurement of the Average Number of Prompt Neutrons from Spontaneous Fission of Californium-252** (R. R. Spencer, R. Gwin, and R. Ingle)

f. Measurement of the ^{241}Am Neutron Fission Cross Section† (J. W. T. Dabbs, C. H. Johnson, and C. E. Bemis, Jr.)

g. Measurement of the ^{232}Th(n,f) Subthreshold and Near-Subthreshold Cross Sections‡ (R. B. Perez, G. de Saussure, J. H. Todd, T. J. Yang,¶ and G. F. Auchampaugh§)

A measurement of the ^{232}Th(n,f) cross section for incident neutron energies between 100 eV and 1.6 MeV has been performed at the ORELA electron linear accelerator. The weak subthreshold fission cross section found in this measurement confirms the model of a low first barrier in the triple-humped fission barrier which has been theoretically predicted for the (^{232}Th + n) system. However, the appearance of a series of plateaus in the near-threshold fission cross section region presents a challenge to current barrier calculations in the ^{233}Th compound nucleus.

h. Comparison of Measured and Calculated ^{238}U Capture Self-Indication Ratios from 4 to 10 keV△ (R. B. Perez, G. de Saussure, J. T. Yang, J. L. Munoz-Cobos, and J. H. Todd)

From 4 keV to 149 keV the ^{238}U cross sections are represented in ENDF/B-V by unresolved-resonance parameters (URP). The purpose of this presentation is to enable the calculation of resonance self-protection as a

---

*Abstract of ORNL/TM-8285 (1982).
**Nucl. Sci. Eng. 80, 603-29 (1982).
†Nucl. Sci. Eng. 83, 22-36 (1983).
‡Submitted to Nucl. Sci. Eng.
¶Institute of Nuclear Research, Taiwan, Republic of China.
§University of California, Los Alamos National Laboratory, Los Alamos, N.M.
△Accepted for presentation at June 1983 ANS meeting.

function of temperature and dilution. Since the URPs are not defined unambiguously by the cross-section data, it is important that the unresolved representation be tested with appropriate experiments, such as capture self-indication ratio (SIR) measurements. In this paper we compare ^{238}U capture SIR measurements in the 4- to 10-keV energy range with calculations done with ENDF/B-V and with recently published resolved resonance parameters.

i. ^{238}U Self-Indication Ratio Measurements in the Resonance Region* (J. T. Yang,** J. L. Munoz-Cobos,† G. de Saussure, R. B. Perez, and J. H. Todd)

An accurate knowledge of the ^{238}U resonance parameters and of the $^{238}U(n,\gamma)$ cross section in the resolved resonance region is required for the calculation of several parameters in both thermal and fast reactors. Block et al. at RPI have demonstrated the usefulness of self-indication ratio measurements to test the adequacy of resonance parameters. The purpose of this paper is to compare a set of self-indication ratio measurements, performed over a wide range of ^{238}U sample thicknesses, with a calculation based on the ENDF/B-V evaluated data over the resolved resonance region.

j. The Radiative Capture Yield of Thorium-232‡ (R. B. Perez, G. de Saussure, R. L. Macklin, J. Halperin, and N. W. Hill)

k. ^{238}U, Issues Resolved and Unresolved¶ (G. de Saussure and A. B. Smith§)

The interaction of 1 eV to 20 MeV neutrons with ^{238}U is discussed with emphasis on recently resolved and remaining issues relevant to both application need and physical understanding.

The apparent inability of older ^{238}U evaluations to predict the measured ^{238}U capture rate in thermal critical lattices has stimulated several recent precise measurements of the ^{238}U cross sections, reanalysis of older data, and improved evaluations. The uncertainty in the evaluated value of the parameters of the first few large resonances is now estimated to be smaller than 2% for the neutron widths and smaller than 3% for the capture widths. The recent evaluations predict satisfactorily the ^{238}U capture rate in thermal critical lattices. In the region from 1.5 to 4 keV there are differences of the order of 15%, sometimes larger, between the values of the neutron widths of the main resonances reported by several experimenters or obtained by different evaluators. These systematic discrepancies have been examined by several authors but are not yet fully understood and deserve further research.

*ANS Topical Meeting, Kiamesha Lake, N. Y., Sept. 22-24, 1982, NUREG/CP-0034 vol. 2, p. 1084 (1982).
**Department of Nuclear Engineering, University of Tennessee, Knoxville, Tenn.
†Universidad Politechnica de Valencis, Spain.
‡Nucl. Sci. Eng., 80, 189-198 (1982).
¶Nuclear Data for Science and Technology, Sept. 6-10, 1982, Geel, Belgium.
§Argonne National Laboratory, Argonne, Illinois.

Above 4 keV there are only sparse results of resonance analysis and most evaluations adopt a statistical treatment of the resonance structure. However, an inspection of good resolution data suggest that the energy and neutron width of the most prominent resonances could be determined with reasonable accuracy at least up to 10 keV. Since these large levels control the resonance self-protection effect it appears that it would be desirable to include them explicitly in evaluations. Recent work indicates that the statistical treatment adopted in many evaluations may not account properly for resonance self-shielding. Some factors affecting the determination of the average properties of the resonance parameters will be discussed.

Above the inelastic-scattering threshold, energy-averaged neutron total, scattering, capture and fission cross sections are reviewed in a unified manner integrating measurement, calculation and evaluation. (n,n') and (n,2n') energy-transfer mechanisms are addressed including pre-equilibrium contributions. Particular attention is given to neutron capture, stressing precisions consistent with applied need. Fission properties are discussed including: prompt and delayed fission-neutron spectra and nubar, and fragment yields and energetics. Physical understanding is assayed with attention to compound-nucleus and direct-reaction mechanisms, and applications impact is illustrated in the context of fast-breeder-reactor performance.

1. Neutron Fission Cross Sections of Pu-239 and Pu-240 Relative to U-235* (L. W. Weston and J. H. Todd)

The ratios of the neutron fission cross sections, $\sigma_f(240)/\sigma_f(239)$, $\sigma_f(240)/\sigma_f(235)$, and $\sigma_f(239)/\sigma_f(235)$ have been measured simultaneously with a multiplate ionization fission chamber using the Oak Ridge Electron Linear Accelerator as a neutron source over the neutron energy range from 5 keV to 20 MeV. The Pu-240 ratio data are in overall agreement with ENDF/B-V with exceptions in relatively narrow neutron energy regions. Below 150 keV and from 10 to 20 MeV, the present Pu-239/U-235 fission ratios indicate significant discrepancies when compared to ENDF/B-V. These ratios are important for thermal and fast reactor applications.

m. Review of Fast-Neutron Capture Cross Sections of the Higher Plutonium Isotopes and Am-241** (L. W. Weston)

The fast-neutron capture cross sections of Pu-240, 241, 242, and Am-241 are reviewed. These nuclides are important to core physics of reactors that contain Pu-239. There have been several significant measurements of these cross sections in recent years. These measurements were instigated by the need for these cross sections for reactor calculations involving high burn-up and build-up of the higher actinides. These recent measurements have satisfied the urgent need for these cross sections in the context of the accuracy needed relative to those of the major fissile isotopes. Problems that exist in the experimental measurements and their evaluation are discussed.

*Accepted for publication in Nucl. Sci. Eng.
**To be published in Proc. NEANDC/NEACRP Specialists Meeting on Fast Neutron Capture Cross Sections, ANL, April 20-23, 1982.

n. Resolved Resonance Parameters for Uranium-238 from 4 to 6 keV* (D. K. Olsen and P. S. Meszaros)

o. ^{238}Measurement Plans (R. B. Perez)

Plans for 1983 are measurement of the U-238 transmission at 77K and 150 m, measurements of capture and self-indication ratios on U-238 at 150 m. Goals are to contribute to resolution of systematic discrepancies in resonance parameters above 1 keV and to extend resolved resonance treatment of U-238 to 10 keV.

4. Experimental Techniques

a. Neutron Flux Measurements at the 22-Meter Station of the Oak Ridge Linear Accelerator Flight Path No. 8** (Z. W. Bell, J. K. Dickens, J. H. Todd, and D. C. Larson)

The measurement of the ORELA flux at neutron energies from 0.16 MeV to 31 MeV is described. The techniques of fitting calculated responses to measured responses and the method of calculating the covariance matrix are detailed. A sample flux and listings of the codes are presented.

b. Counting Anticoincidences to Reduce Statistical Uncertainty in the Calibration of a Multiplicity Detector† (R. W. Peelle and R. R. Spencer)

c. A Digital Pulse-Pair Detecting Circuit‡ (Z. W. Bell, J. W. McConnell, and E. D. Carroll)

A completely digital pulse-pair detecting circuit is described. The inspection interval ranges from approximately 100 ns to 1.3 ms in steps of 20 ns. Tests of the circuit indicate reliable operation at input rates up to 25 MHz.

d. ISOLR - An Isometric Plotting Package for Use with ORPLOT¶ (Z. W. Bell)

An isometric plotting package is described. It is written entirely in FORTRAN and is designed to work in conjunction with ORPLOT, a general purpose plotting package in use at the ORELA PDP-10. The isometric plotter supports views from any point in space, logarithmic scales, and hidden lines.

---

*Nucl. Sci. Eng. 83, 174-81 (1983).
**Abstract of ORNL/TM-8514 (in preparation).
†Nucl. Instr. Meth. 00 (1983).
‡Accepted for publication in Nucl. Instr. Meth.
¶Abstract of ORNL/TM-8192 (1982).

5. Integral Measurements

a. Calculated Neutron and Gamma-Ray Energy Spectra from 14-MeV Neutrons Streaming Through an Iron Duct: Comparison with Experiment* (R. T. Santoro, R. G. Alsmiller, Jr., J. M. Barnes, G. T. Chapman, and J. S. Tang)

b. Comparison of Measured and Calculated Neutron and Gamma Ray Energy Spectra Behind an In-Line Shielded Duct** (R. T. Santoro, R. G. Alsmiller, Jr., J. M. Barnes, G. T. Chapman, J. S. Tang)

Integral experiments that measure the transport of ∿14 MeV neutrons through a 0.30-m-diameter duct having a length-to-diameter ratio of 2.83 that is partially plugged with a 0.15 m diameter, 0.51 m long shield comprised of alternating layers of stainless steel type 304 and borated polyethylene have been carried out at the Oak Ridge National Laboratory. Measured and calculated neutron and gamma-ray energy spectra are compared at several locations relative to the mouth of the duct. The measured spectra were obtained using an NE-213 liquid scintillator detector with pulse shape discrimination methods used to simultaneously resolve neutron and gamma-ray events. The calculated spectra were obtained using a computer code network that incorporates two radiation transport methods: discrete ordinates (with P_3 multigroup cross sections) and Monte Carlo (with continuous point cross sections). The two radiation transport methods are required to account for neutrons that singly scatter from the duct to the detectors. The calculated and measured neutron energy spectra above 850 keV agree within 5 to 50% depending on detector location and neutron energy. The calculated and measured gamma-ray energy spectra above 750 keV are also in favorable agreement, ∿5 to 50%, depending on detector location and gamma-ray energy.

c. Comparison of Measured and Calculated Neutron and Gamma-Ray Energy Spectra Behind an In-line Shielded Duct† (R. T. Santoro, R. G. Alsmiller, Jr., J. M. Barnes, G. T. Chapman, and J. S. Tang)

d. The ORNL Integral Experiment to Provide Data for Evaluating Magnetic-Fusion-Energy Shielding Concepts. Part I: Attenuation Measurements‡ (G. T. Chapman, G. L. Morgan,¶ and J. W. McConnell)

Integral experiments to measure the energy spectra of neutrons and gamma rays due to the transport of approximately 14-MeV $T(d,n)^4He$ neutrons through laminated stainless-steel and borated-polyethylene shield configurations have been performed at the Oak Ridge National Laboratory. An NE-213 detector and conventional pulse-shape-discrimination circuitry were

*Nucl. Sci. Eng. 80, 586-602 (1982).
**Abstract of ORNL/TM-8258 (1983).
†Submitted for publication in J. Fusion Eng.
‡Abstract of ORNL/TM-7356.
¶Los Alamos Scientific Laboratory, Los Alamos, New Mexico 87545.

used to record the pulse-height distributions from which the energy spectra were derived. Descriptions of the facility and experimental techniques are given in this paper along with tables and curves showing the results of the measurements.

B. DATA ANALYSES

1. Theoretical Calculations

a. Experience in Using the Covariances of Some ENDF/B-V Dosimetry Cross Sections: Proposed Improvements and Addition of Cross-Reaction Covariances* (C. Y. Fu and D. M. Hetrick)

b. New Developments in the Unresolved Range** (R. B. Perez and G. de Saussure)

c. Sensitivity of Computed Uranium-238 Self-Shielding Factors to the Choice of the Unresolved Average Resonance Parameters† (J. L. Munoz-Cobos, G. de Saussure, and R. B. Perez)

d. Representation of the Neutron Cross Sections of Several Fertile and Fissile Nuclei in the Resonance Regions‡ (G. de Saussure and R. B. Perez)

e. Meeting Cross-Section Requirements for Nuclear-Energy Design¶ (C. R. Weisbin, G. de Saussure, and R. T. Santoro)

f. Process Studies in the Light of New Experimental Cross Sections: Distribution of Neutron Fluences and r-Process Residuals§ (F. Kappeler,△ H. Beer,△ K. Wisshak,△ D. D. Clayton,▲ R. L. Macklin, and Richard A. Ward▽)

g. Major Questions About Derivation of Variance-Covariance Information for Nuclear Data Evaluations▼ (R. W. Peelle)

The uncertainties in and correlations among evaluated nuclear data must also be evaluated to permit estimation of data-related uncertainties in design quantities and to focus future studies to improve the data. This paper summarizes the major questions that now arise in trying to obtain

*Proceedings of the Fourth ASTM-EURATOM Symposium on Reactor Dosimetry, NUREG/CP-0029, Vol. 2 (1982).
**Specialists' Workshop Entitled: "^{238}U Capture in Fast Reactors," Teton Village, Wyoming, June 22-24, 1982.
†Nucl. Sci. Eng. 81, 55-65 (1982)
‡Ann. Nucl. Energy, Vol. 9, 79-94, 1982.
¶Ann. Nucl. Energy, Vol. 9, 615-673, 1983.
§The Astrophysical Journal, 257, 821-846 (1982).
△Kernforschungszentrum Karlsruhe GmbH, Institut fur Angewandte Kernphysik.
▲Max-Planck-Institut fur Kernphysik, Heidelberg; and Rice University.
▽Max-Planck-Institut fur Physik und Astrophysik, Munchen
▼Nuclear Data for Science and Technology, Sept. 6-10, 1982, Geel, Belgium.

numerical files of this uncertainty information ("covariance data"), and points toward likely answers. Covariance data must be sufficient to construct the variance-covariance matrix of the evaluated cross sections.

Up to now the most important question has usually been how to combine differential data that are discrepant or for which experiment uncertainties are incompletely reported. Evaluators must be thoughtfully bold in discarding or reweighting data sets; therefore authors may wish to report covariance data on some prior experiments to assure their continued use.

On other questions, (1) covariance data may be required in more detail for use in future evaluations than for use in engineering applications, (2) it is yet unclear whether few-group covariance representations for structural materials will be adequate for both core physics and deep penetration shielding analysis, (3) data evaluations performed with the aid of nuclear theory must also include output covariance data based at least on the covariance matrix of the model parameters, and (4) a consensus is still lacking on the role of integral data in the evaluation of nuclear cross sections and their uncertainties.

2. ENDF/B Related Evaluations

a. Evaluated Neutron-Induced Cross Sections for ^{40}Ca from 20 to 40 MeV* (D. M. Hetrick, C. Y. Fu, and D. C. Larson)

Nuclear model codes were used to compute cross sections for neutron-induced reactions on ^{40}Ca for incident energies from 20 to 40 MeV. The input parameters for the model codes were determined through analysis of experimental data in this energy region. Computed cross sections along with emission spectra for each product were combined into an Evaluated Nuclear Data File (ENDF) using the proposed format for charged-particle reactions. Discussion of the models used, the resulting calculations, and the final evaluated data file are included in this report.

b. Summary of ENDF/B-V Evaluations for Carbon, Calcium, Iron, Copper, and Lead and ENDF/B-V Revision 2 for Calcium and Iron** (C. Y. Fu)

This report, together with documents already published, describes the ENDF/B-V evaluations of the neutron and gamma-ray-production cross sections for carbon, calcium, iron, copper, and lead and the ENDF/B-V Revision 2 evaluations for calcium and iron.

---

*Abstract of ORNL/TM-8290, ENDF-326 (September 1982).
**Abstract of ORNL/TM-8283, ENDF-325 (1982).

c. Neutron Scattering Cross Sections of Carbon Below 2 MeV for ENDF/B-V* (C. Y. Fu and F. G. Perey)

d. Comparison of the ENDF/B-V and SOKRATOR Evaluations of ^{235}U, ^{239}Pu, ^{240}Pu, and ^{241}Pu at Low Neutron Energies,** (G. de Saussure and R. Q. Wright)

The U.S. and U.S.S.R.'s most recent evaluations of ^{235}U, ^{239}Pu, ^{240}Pu, and ^{241}Pu are compared over the thermal region and over the first few resonances. The two evaluations rest on essentially the same experimental data base and the differences reflect different approaches to the representation of the cross sections or different weightings of the experimental results. It is found that over the thermal and resolved ranges the two evaluations are very similar. Some differences in approaches are briefly discussed.

---

*ENDF/B-V Cross Section Measurement Standards, BNL-NCS-51619, ENDF-301 (October 1982).

**Presented at the Joint IAEA/NEA Consultants Meeting on Uranium and Plutonium Resonance Parameters, Vienna, Austria, Sept. 28 - Oct. 2, 1981.

A. NEUTRON SCATTERING

1. Structure of ^{12}B from Measurement and R-Matrix Analysis of $\sigma(\theta)$ for $^{11}B(n,n)^{11}B$ and $^{11}B(n,n')^{11}B^*$ (2.12 MeV) and Shell Model Calculations.* (Koehler, Knox, Resler, Lane and Millener**)

Differential cross sections for neutrons elastically scattered from ^{11}B and inelastically scattered to the first excited state $^{11}B^*$ (2.12 MeV) have been measured at 13 incident energies for $4.8 \leq E_n \leq 7.6$ MeV. These new data have been analyzed together with previously published cross sections for $0 \leq E_n \leq 7.5$ MeV using a multilevel-multichannel R-matrix program to determine J, π, E_λ and $\gamma_{\lambda c}$ for several states in ^{12}B. The shell model was used to calculate states in ^{12}B as well as spectroscopic amplitudes for reactions leading to these states. The results of this model calculation have been compared to those of the R-matrix analysis. Much of the structure observed in the experimental work is predicted by the model for $E_x \lesssim 7$ MeV. The data have also been compared to continuum shell model calculations. A paper describing this work has been published in Nucl. Phys. A394 (1983) 221.

2. Elastic and Inelastic Scattering of 20-26 MeV Neutrons from ^{12}C.*** (Meigooni, Finlay, Randers-Pehrson†, Brient, Marcinkowski††, Kurup and Mellema)

Elastic and inelastic scattering of 20.8 and 26 MeV neutrons from ^{12}C was studied at the Ohio University beam swinger time-of-flight spectrometer. The low background and high efficiency of the new spectrometer permit the observation of scattering to α-particle unstable states above 9 MeV. Complete differential cross sections for the ground state, the 2^+ (4.43 MeV) and 3^- (9.63 MeV) have been measured. Partial angular distributions or upper limits for the 0^+ (7.65) state and for more highly excited states have been obtained. Results have been analyzed together with the earlier measurements made with conventional techniques at 24 MeV.

---

* Work supported by the U.S. Department of Energy.

** Permanent address: Brookhaven National Laboratory, Upton, New York.

*** This investigation was supported by Grant Number CA25193, awarded by the National Cancer Institute, and by NSF Grant Number PHY 8108456.

† Present address: Columbia University Nevis Laboratory, Irvington, NY.

†† Permanent address: Institute for Nuclear Research, Warsaw, Poland.

3. Deep Inelastic Scattering of 22 and 24 MeV Neutrons from ^{12}C.*
(Petler, Meigooni, Finlay, Brient, Islam and Annand)

Elastic and inelastic scattering of 20-26 MeV neutrons from ^{12}C has been studied at Ohio University beam swinger time-of-flight spectrometer.[1] The low background of this spectrometer system permits the observation of scattering to the states above 7.6 MeV which subsequently decay by α-emission. The states 0^+ (7.65 MeV), 3^- (9.64 MeV), 1^- (10.84 MeV), 2^- (11.83 MeV), 1^+ (12.71 MeV), 2^- (13.35 MeV), 4^+ (14.08 MeV), 1^+ (15.11 MeV) and 2^+ (16.11 MeV) have been observed for incident neutron energies of 22 and 24 MeV. Measurements were performed at 12° intervals from 20° to 152° and partial differential cross sections have been extracted for several states. The total cross sections for these states have been compared with the results of B. Antolković et al.[2]

4. Differential Elastic and Inelastic Neutron Scattering from ^{13}C.**
(Resler, Koehler, Knox, Randers-Pehrson*** and Lane)

Differential cross sections for the $^{13}C(n,n)^{13}C$ and $^{13}C(n,n')^{13}C^*$ (3.09 MeV) reactions have been measured at a total of 59 incident neutron energies from 4.5 to 11 MeV. In one experiment which used the Ohio University swinger time-of-flight system, measurements were made at 37 incident energies from 7.5 to 11 MeV. Neutrons produced via the D(d,n) reaction were incident on a scattering sample of 40.75 grams of ^{13}C enriched to 98% located 20.5 cm from the neutron source. The detector was located 4.2 m from the sample and was one 4" thick by 8" diameter NE213 liquid scintillator coupled to an RCA-4522 photomultiplier. At each energy measurements were made at 11 angles between 15° and 160°. Both the elastic and inelastic angular distributions show considerable changes in shape with energy indicating compound nuclear structure in ^{14}C.

5. Differential Elastic and Inelastic Neutron Scattering from ^{18}O.**
(Koehler, Resler, Knox, Randers-Pehrson***, Lane and Auchampaugh†)

Differential cross sections were measured at 35 energies between 5.5 and 7.3 MeV for the $^{18}O(n,n)^{18}O$ and $^{18}O(n,n')^{18}O^*$ (1.98 MeV) reaction at 9 to 12 angles from 20° to 160°. In this energy region there are

---

* This investigation was supported by Grant Number CA25193, awarded by National Cancer Institute and by NSF Grant Number PHY-8108456.

** Work supported by U.S. Department of Energy.

*** Present address: Columbia University Nevis Laboratory, Irvington, NY.

† Permanent address: Los Alamos National Laboratory, Los Alamos, NM.

1 A.S. Meigooni et al., Bull. Am. Phys. Soc. 27 (1982) 544.

2 B. Antolković et al., Proc. Int. Conf. on Nuclear Data for Sci. and Tech., Antwerp (1982), to be published.

several broad resonance structures in the total cross section. Both the elastic and inelastic angular distributions show considerable changes in shape with energy. In particular, the Legendre polynomial expansion coefficients for the elastic cross section reveal that angular momentum channels up to and including f-waves are resonant over at least part of the region studied. These facts suggest the possibility that we may be seeing the effects of states involving the major strength of the $f_{7/2}$ shell in ^{19}O. No previous differential elastic neutron scattering measurements for ^{18}O have been reported at these energies. There have been no previous reports of differential inelastic neutron scattering from ^{18}O besides our measurements.

6. Neutron Scattering from ^{26}Mg.* (Tailor**, Rapaport, Finlay and Randers-Pehrson***)

Elastic and inelastic cross sections have been measured for 24 MeV neutrons incident on ^{26}Mg using the time-of-flight technique. These cross sections and existing proton data were analyzed in terms of a Lane consistent optical potential. Distorted-wave and coupled-channel calculations have been carried out. Deformation parameters for the first 2^+ state (1.81 MeV) and the second 2^+ state (2.94 MeV) derived from both the (n,n') and (p,p') data have been used to obtain the ratio of neutron and proton transition matrix elements $M_n(E2)$ and $M_p(E2)$ for these states. Comparison of results for $M_n(E2)/M_p(E2)$ with those obtained from pion work, from electromagnetic (EM) rates and theoretical evaluations have been made. A paper describing this work has been accepted for publication in Nuclear Physics.

7. Excitation of M1 States by Neutron Scattering. (Alarcon, Wang and Rapaport)

The excitation of giant GT resonances via (p,n) reactions[1] at intermediate energies has prompted the study of excitation of giant M1 resonances by scattering of light projectiles. This resonance is strongly excited in 200-MeV forward-angle inelastic proton scattering[2] but no evidence was found for it in the inelastic scattering of 24-MeV protons.[3] The discrepancy may be understood in terms of the features of the central nucleon-nucleon effective interaction. If the excitation of the M1 resonance is mainly a neutron excitation then for proton scattering there is a destructive interference between the V_σ and $V_{\sigma\tau}$ terms of the interaction. At the

---

* Supported in part by the National Science Foundation.

** Present address: University of North Carolina, Chapel Hill, NC.

*** Present address: Columbia University Nevis Laboratory, Irvington, NY.

1 C. Gaarde et al., Nucl. Phys. A369 (1981) 258.

2 C. Djalali et al., Nucl. Phys. A388 (1982) 1.

3 F.E. Cecil et al., Nucl. Phys. A232 (1974) 22.

lower bombarding energy the transition matrix element is very small, because $V_\sigma \approx V_{\sigma\tau}$. At higher energies, $V_{\sigma\tau}$ appears significantly greater than V_σ[4] and thus M1 states are observable. On the other hand for neutron inelastic scattering there is a constructive interference and thus M1 states should be observed. Recently Cecil and Peterson have reported[5] microscopic calculations for the excitation of the M1 resonance in ^{90}Zr with 23 MeV neutrons.

In a preliminary experiment we have measured the forward angle scattering of 26 MeV neutrons of ^{51}V and ^{nat}Zr using the Ohio University time-of-flight facility. Monoenergetic neutrons were produced via the T(d,n) reaction. Scattered neutrons were observed at θ_L = 7.5°, 10° and 15° using a 4" thick, 8" in diameter detector filled with NE-213 liquid scintillator located at a flight path of 9 m. An energy resolution less than 600 keV was obtained. Neutron yields at θ_L = 10° in ^{51}V and ^{nat}Zr in the region of the reported M1 states are consistent with the microscopic calculations. However, there is not an observable clear enhancement of the cross section in this region as is observed in the (p,p') reaction at higher energies. The identification of the observed cross section with M1 states needs further evaluation.

8. Analysis of Fast Neutron Scattering from ^{54}Fe and ^{56}Fe.* (Mellema, Finlay, Randers-Pehrson**, Dietrich***, and F. Petrovich†)

Precision elastic and inelastic differential cross section data for neutron scattering on ^{56}Fe at 26 MeV and on ^{54}Fe at 20, 22 and 26 MeV have been taken using the new, higher resolution beam-swinger time-of-flight spectrometer at Ohio University. Analysis, which also includes previous data, has been carried out using both phenomenological and microscopic approaches. The aim for elastic scattering has been to study the energy dependence of the optical model potentials and also to study their isospin dependence by comparison with proton elastic scattering data. Preliminary analysis of the inelastic scattering has also been carried out using a collective model and DWBA calculations, and comparisons have been made with similar analyses on proton inelastic scattering.

---

* Work supported by the National Science Foundation and by the Department of Energy, W-7405-Eng-48.

** Present address: Columbia University Nevis Laboratory, Irvington, NY.

*** Permanent address: Lawrence Livermore National Laboratory, Livermore, CA.

† Permanent address: Florida State University, Tallahasee, FL.

[4] N. Anantaraman et al., Phys. Rev. Lett. 46 (1981) 1318.

[5] F.E. Cecil and R.J. Peterson, Phys. Rev. Lett. 47 (1981) 1566.

9. Elastic and Inelastic Scattering of 8 and 10 MeV Neutrons from Even Isotopes of Se.* (Kurup, Finlay and Delaroche**)

Differential cross sections for neutron scattering from ^{76,80}Se have been measured with special emphasis on the excitation of the second, third and fourth excited states. The data have been analyzed in terms of collective models using a coupled-channels formalism. Predictions based on the asymmetric rotor model fit to the Se($\vec{p}$,$\vec{p}$) reaction[1] are in remarkable agreement with the neutron scattering data and may be interpreted as evidence for neutron excitation of γ-vibrational bands in medium mass nuclei.

10. Neutron Scattering from ^{208}Pb and ^{209}Bi at Energies 4 to 6 MeV. (Annand and Finlay)

Differential elastic and inelastic cross sections have been measured at energies 4.0, 4.5, 5.0, 5.5 and 6.0 MeV for the nuclei ^{208}Pb and ^{209}Bi in the angular range 10-160° using the Ohio University Beam Swinger Time of Flight facility.[2] Forward of 35° the elastic cross sections are very similar in both isotopes, while in ^{208}Pb at larger scattering angles the cross section is consistently larger. While this is not unexpected at the lower energies where the ^{208}Pb compound elastic cross section should be larger, the effect persists up to 6 MeV where compound nucleus effects in both isotopes ought to be negligible. Cross sections have also been measured for the 2.61 MeV 3^- state of ^{208}Pb and the 0.90 $7/2^-$ and 1.61 $13/2^+$ states of ^{209}Bi. The ^{209}Bi $7/2^-$ and $13/2^+$ excitations appear to be essentially compound in nature with negligible strength above 5.5 MeV.

11. Performance of a Large-Volume Liquid Scintillator.* (Polster***, Annand and Finlay)

Energy resolution in neutron time-of-flight experiments can usually be improved by increasing the flight path. In order to achieve optimum resolution and still retain detection efficiency at the Ohio University Beam Swinger time-of-flight spectrometer, a large (11 ℓ) liquid scintillator was constructed and tested both on- and off-line. Pulse height uniformity, pulse shape discrimination and coincidence timing uniformity were tested off-line with radioactive sources. Neutron time-of-flight performance was evaluated by studying the ^{11}B(d,n)^{12}C reaction at E_d = 7.52 MeV. Performance of the large-volume detector has been compared with conventional detectors.

---

* Supported in part by the National Science Foundation.

** Permanent address: Centre d'Etudes de Bruyeres-le-Chatel, France.

*** Participant, Ohio University Undergraduate Research Internship Program.

1 Delaroche, Clegg and Varner, Bull. Am. Phys. Soc. 27 (1982) 460.

2 R.W. Finlay et al., Nucl. Instr. and Meth. 198 (1982) 197.

B. (n,z) REACTIONS

1. Differential Cross Sections for the $^6Li(n,t)\alpha$ Reaction Cross Section for $2 \leq E_n \leq 3.5$ MeV.* (Knox, Randers-Pehrson**, Koehler, Resler, Lane and Rodricks)

Measurements of the differential cross section for the $^6Li(n,t)\alpha$ reaction have been made at four incident neutron energies between 2.0 and 3.5 MeV. These measurements were made with the Ohio University triplet quadrupole spectrometer and used the $T(p,n)^3He$ reaction as the neutron source. The ^6Li radiator was a 0.8 mg/cm^2 ^6LiF target evaporated on a gold backing. Background measurements were made with a similar BaF_2 target. Measurements of both alpha and triton yields were made at laboratory angles of 0°, 20°, 40°, 60° and 70°. Triton yields were also obtained at 120°. The resulting differential cross sections do show changes in shape, particularly when compared to the earlier measurements of Overley et al.[1] at lower incident energies, indicating possible new structure information for the ^7Li system.

2. (n,z) Measurements on ^{58}Ni, ^{60}Ni and Stainless Steel.* (Graham, Grimes, Randers-Pehrson** and Ahmad)

Measurements of the (n,p) and (n,α) cross sections for ^{58}Ni and 316-Stainless Steel have been carried out at bombarding energies of 9.5 and 11 MeV. These show larger cross sections but similar characteristics to those reported previously at 8 MeV. Both the (n,p) and the (n,α) spectra appear to be predominantly due to compound nuclear processes. At 11 MeV the proton spectrum from ^{58}Ni shows a significant yield for energies below the Coulomb barrier, apparently due to the (n,n'p) process. Measurements of the $^{60}Ni(n,p)$ and (n,α) spectrum at 11 MeV have also been made. This proton spectrum shows little yield in the sub-Coulomb region.

Deuteron emission cross sections were too small to measure at 8 and 9.5 MeV ($\lesssim$ 1 mb integrated over angle and energy) but are larger than this limit at 11 MeV.

The large negative Q value for the (n,d) reaction restricts the excitation energy of the residual nucleus to small enough values that the spectrum consists of resolved peaks. These are probably populated in direct reactions.

---

* Work supported by the U.S. Department of Energy.

** Present address: Columbia University Nevis Laboratory, Irvington, NY

1 Overly, Sealock and Ehlers, Nucl. Phys. A221 (1974) 573.

At 11 MeV, the measured (n,p) and (n,α) spectra could have contributions from these reactions induced by the d(d,n) break-up neutrons. These backgrounds were estimated with a separate measurement using neutrons from the ^{3}He(d,n) break-up reaction.[1] These backgrounds were not found to be important at lower energies.

Hauser-Feshbach calculations are being made for the reactions on ^{58}Ni and ^{60}Ni to compare with the measurements. Spectra for the ^{60}Ni(n,p) and ^{60}Ni(n,α) reactions will also be measured at 8 and 9.5 MeV during the next year.

C. (p,n) REACTIONS

1. ^{89}Yt(p,n,γ) Angular Correlation. (Brient, Egun, Tsukamoto)

The ^{89}Yt(p,n-γ) reaction is being used to study the neutron-gamma angular correlations by observing the γ's in coincidence with the zero degree neutrons. The system includes a 20 cm diameter by 10 cm thick NE213 neutron detector with pulse shape discrimination at zero degrees and a neutron flight path of 5 meters. The 66 cm^3 Ge(Li) detector at 13 cm from the target detected γ's in coincidence with neutrons leading to states in ^{89}Zr at 0.588, 1.095, 1.451, 1.628 1.743 and 1.834 MeV. The individual time-of-flight neutron spectra in coincidence with each photo-detected gamma from the residual state are simultaneously stored, along with background spectra. The coincidence spectra are gated by both a fast digital coincidence (10 nsec-FWHM) and a time-of-flight gamma gate.

D. ANALYSIS AND MODEL CALCULATIONS

1. An R-Matrix Analysis of the ^{7}Li System.* (Knox and Lane)

Differential cross sections for neutron elastic scattering from ^{6}Li and for the ^{6}Li(n,t)α reaction, ^{6}Li+n neutron polarization data and total neutron cross section data were analyzed by means of a multilevel multichannel R-matrix program for energies between thermal and 4 MeV. Six states in ^{7}Li were included in the analysis with the ℓ = 0 contributions represented by unbound $J^\pi = 1/2^+$ and $3/2^+$ states. This set of states is consistent with existing model calculations for ^{7}Li. Very good fits to all available data were obtained and the results are consistent with thermal cross section measurements for ^{6}Li.

---

* Work supported by the U.S. Department of Energy.

1 Grimes, Grabmayr, Finlay, Graham, Randers-Pehrson and Rapaport, Nucl. Inst. and Meth. 203 (1982) 269.

2. Optical Model and Coupled-Channel Analysis of 20-40 MeV Neutron Scattering from ^{12}C.* (Meigooni, Petler and Finlay)

The energy dependence of neutron interactions with ^{12}C in the interval from 20 to 40 MeV have been investigated in terms of both optical model and coupled-channel representations. Neutron elastic and inelastic scattering cross sections have been measured at 20.7, 22, 24 and 26 MeV at the Ohio University Beam Swinger Facility.[1] Additional measurements[2] from Michigan State University using the same swinger magnet are included in the analysis. An improved representation of neutron cross sections in this energy interval has direct application to important problems in neutron dosimetry and radiotherapy.

3. An Optical Model Analysis of Neutron Scattering. (Rapaport)

Neutron elastic scattering data in the range $A > 16$, $7 < E < 30$ MeV are analyzed using a standard local optical model potential. The obtained parameters are compared with similar optical model parameters derived from proton elastic scattering. Empirical values for the Coulomb correction term, isospin dependence and energy dependence are obtained. The results have been compared with theoretical calculations. A paper describing this work has been published in Physics Reports 87 (1982) 25.

4. Shell Model Calculations. (Grimes, Lane, Resler, Koehler and Knox)

Work on shell model calculations in the p shell and sd shell was continued. A calculation for ^{15}O using no core was found to yield reasonable spectra and spectroscopic factors only after the PMM interaction strength was reduced to 25% of its original value. The size of the reduction was somewhat larger than expected, but it is well known that truncation effects in shell model calculations can require significant changes in the interaction strength as the basis size is changed. We now plan to use these single particle energies and two body matrix elements to calculate the spectra of $^{19}O(n+^{18}O)$ and $^{14}C(n+^{13}C)$ to compare with R-matrix analyses.

We have also (in collaboration with S.D. Bloom of Livermore and H. Vonach of Vienna) carried out studies of the effects of truncation in moment-method calculations of level densities in ^{28}Si. A reduction of about 35% in the strength of the two-body interaction was needed when the basis was expanded from sd to $sdf_{7/2}$. Thus, truncation effects may be seen either

---

* This investigation was supported by Grant Number CA25193 awarded by the National Cancer Institute, DHHS.

1 R.W. Finlay et al., Nucl. Instr. and Meth. 198 (1982) 197.

2 R.P. DeVito, private communication.

as the number of levels or the number of active nucleons is changed. A paper on the level density of ^{28}Si has been prepared and submitted for publication.

5. Test of the Isospin Properties of a Microscopic Optical Model for Nucleon Scattering on ^{208}Pb.* (Dietrich**, Finlay, Kurup, Mellema, Randers-Pehrson***, Petrovich†, Carr†, Love†† and Kelly†††)

A local microscopic folding-model optical potential[1] has shown reasonable success in qualitatively reproducing the elastic scattering of nucleons from nuclei over a wide mass range. The present work further tests the model by comparing neutron and proton scattering on the same nucleus (^{208}Pb). For making this comparison, new neutron elastic-scattering angular distributions have been measured with the Ohio University beam-swinger facility[2] at 7.2, 20 and 24 MeV; older data at 11 and 25.7 MeV from the same laboratory are also included. Proton data in the range 24.1-61.4 MeV are the same as in the analysis of Ref. 3. In the calculations, the central interaction of Ref. 1 and the Elliott spin-orbit interaction from Ref. 4 were used. The nuclear density, equivalent to that inferred[5] from 800-MeV proton scattering, contains a neutron skin. The energy at which the interaction was evaluated for protons was not modified by the Coulomb potential as it is in Ref. 1; within the nucleus the Coulomb potential is largely compensated by the nuclear symmetry potential. The calculations were compared to the data by least-squares fitting of normalizing parameters λ_V and λ_W for the real and imaginary central optical potentials, respectively. These parameters, along with the reduced chi-squared, are shown below. Except for 45-MeV protons, for which the calculations are too oscillatory $\gtrsim 100°$, the fits are visually reasonable with χ^2 typically greater than for

---

* Work performed under the auspices of the U.S. Department of Energy by Lawrence Livermore National Laboratory under contract #W-7405-Eng-48, and Ohio University (National Science Foundation).

** Permanent address: Lawrence Livermore National Laboratory, Livermore, CA.

*** Present address: Columbia University Nevis Laboratory, Irvington, NY.

† Permanent address: Florida State University, Tallahasee, FL.

†† Permanent address: University of Georgia, Athens, GA.

††† Permanent address: Massachusetts Institute of Technology, Cambridge, MA.

1 F. Brieva and R. Rook, Nucl. Phys. A291 (1977) 317; H. von Geramb et al., in Lecture Notes in Physics, Vol. 89, p. 105, Springer, 1979.

2 R.W. Finlay et al., Nucl. Inst. and Meth. 198 (1982) 197.

3 W.T.H. van et al., Phys. Rev. C10 (1974) 307.

4 G. Bertsch et al., Nucl. Phys. A284 (1977) 399.

5 L. Ray et al., Phys. Rev. C18 (1978) 1756 and Phys. Rev. C18 (1978) 2641.

phenomenological potentials by a factor of ≈ 4. The neutron skin reduces the back-angle difficulties found earlier for protons, and is also required for good agreement with σ(reac) ($\approx 5\%$). Neutron σ(tot) are too high by $\approx 4\%$. Below 20 MeV, the imaginary potentials are significantly less surface-peaked than phenomenological ones. We conclude that the effective interaction of Ref. 1 yields a consistent treatment of p and n scattering on ^{208}Pb. This is not the case if the usual Coulomb correction is used, as then λ_W is systematically higher for protons than for neutrons by $\approx 40\%$, even though the quality of the fits is only slightly degraded.

NEUTRONS				PROTONS			
E(MeV)	χ^2/N	λ_V	λ_W	E(MeV)	χ^2/N	λ_V	λ_W
7.2	12.6	0.98	0.69	24.1	60.0	1.10	0.99
11.0	16.9	0.99	0.77	26.3	37.4	1.10	1.08
20.0	24.4	1.04	1.03	30.3	20.9	1.13	1.17
24.0	16.0	1.07	1.02	45.0	174.0	1.10	1.05
25.7	41.2	1.04	1.03	61.4	12.4	1.17	0.88

PACIFIC NORTHWEST LABORATORY

A. DELAYED NEUTRON STUDIES

1. Sr, Y, Ba, and La Precursors (P. L. Reeder and R. A. Warner)

The surface ionization source at the TRISTAN on-line isotope separator facility efficiently ionizes Rb and Cs. Sr and Ba are ionized somewhat less efficiently and Y and La are mainly produced by beta decay. Delayed neutron precursors among these elements were studied by measuring neutron and beta growth and decay curves at masses 97-99 and 146-148. The growth and decay curves were analyzed with the least squares fitting code MASH to obtain half-lives and neutron emission probabilities (P_n) as given in Table A-1.

The P_n values are quite small (<1%) for Sr, Y, Ba, and La precursors in contrast to a published set of measurements[1] and are consistent with a recent set of measurements at OSTIS.[2] We did not see a 2.1 s component in the neutron decay curve at mass 98 corresponding to an isomer of ^{98}Y as was reported in Ref. 1. The mass chain beginning with ^{98}Rb is illustrated in Figure A-1 where the delayed neutron branches from this work are emphasized. At mass 97, we report a 1.17 s component in the neutron decay curve which corresponds to ^{97m}Y. This isomer had not been identified as a precursor previously.

The large P_n for ^{148}Ba reported in Ref. 1 had a potential impact on the fission yield of ^{148}Nd which is commonly used to determine nuclear fuel burnup. If ^{148}Ba had a P_n of 23.9 ± 2.1% as reported, this would alter the cumulative fission yield of ^{148}Nd by 1-3% for fissioning systems of interest. The present results show that no such correction is necessary.

The existence of delayed neutron emission from ^{148}La is in conflict with a recent mass excess measurement for ^{148}La.[3] If the new mass excess for ^{148}La is correct, then delayed neutron emission is energetically forbidden. Our results have been submitted for publication.[4]

---

1 G. Engler and E. Ne'eman, Nucl. Phys. A367, 29 (1981).

2 Gabelman, Munzel, Pfeiffer, Crawford, Wollnik, and Kratz, Z. Phys. A308, 359 (1982).

3 Brenner, Martel, Aprahamian, Chrien, Gill, Liou, Shmid, Stelts, Wolf, Wohn, Rehfield, Dejbakhsh, and Chung, Phys. Rev. C. 26, 2166 (1982).

4 P. L. Reeder and R. A. Warner, "Delayed Neutron Precursors at Masses 97-99 and 146-148", November 1982, PNL-SA-11065, submitted to Phys. Rev. C.

TABLE A-1. Half-lives and Emission Probabilities of Sr, Y, Ba, and La Delayed Neutron Precursors.

Precursor	Half-life (s)	P_n (%)
^{97}Sr	0.417 ± 0.005	0.007 ± 0.006
^{98}Sr	0.66 ± 0.07	0.11 ± 0.02
^{99}Sr	0.274 ± 0.004	0.17 ± 0.05
^{97g}Y	3.76 ± 0.08	0.019 ± 0.002
^{97m}Y	1.17 ± 0.05	0.029 ± 0.010
^{98g}Y	0.51 ± 0.01	0.16 ± 0.03
^{98m}Y	(2.1 s isomer was not seen)	
^{99}Y	1.47 ± 0.02	0.48 ± 0.10
^{146}Ba	2.18 ± 0.11	<0.006
^{147}Ba	0.91 ± 0.03	0.055 ± 0.010
^{148}Ba	0.594 ± 0.003	0.055 ± 0.009
^{146}La	6.0 ± 0.4	<0.004
^{147}La	4.48 ± 0.08	0.013 ± 0.011
^{148}La	1.46 ± 0.03	0.067 ± 0.011

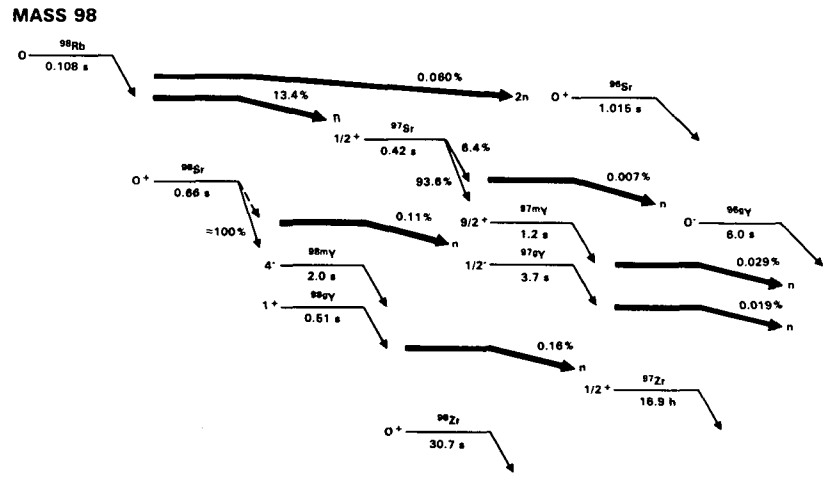

FIGURE A-1. Mass Chain Beginning with ^{98}Rb Showing Delayed Neutron Branches.

2. Delayed Neutron Yields from FEBIAD Ion Source (P. L. Reeder R. A. Warner, R. L. Gill)

In November 1982, a survey was made of delayed neutron count rates at each mass number produced by the new FEBIAD ion source at TRISTAN. Saturation count rates for 100 s intervals were measured for both neutrons and betas simultaneously. The net count rates are shown in Figure A-2. The FEBIAD ion source ionizes more elements than the surface ionization source and thus greatly increases the number of precursors available for study. The survey was obtained at a relatively low power level and the yield of the very short-lived precursors was reduced due to long diffusion times. With increased power, the prospects are very good for observing new precursors among the Cu, Ga, Ag, and In elements.

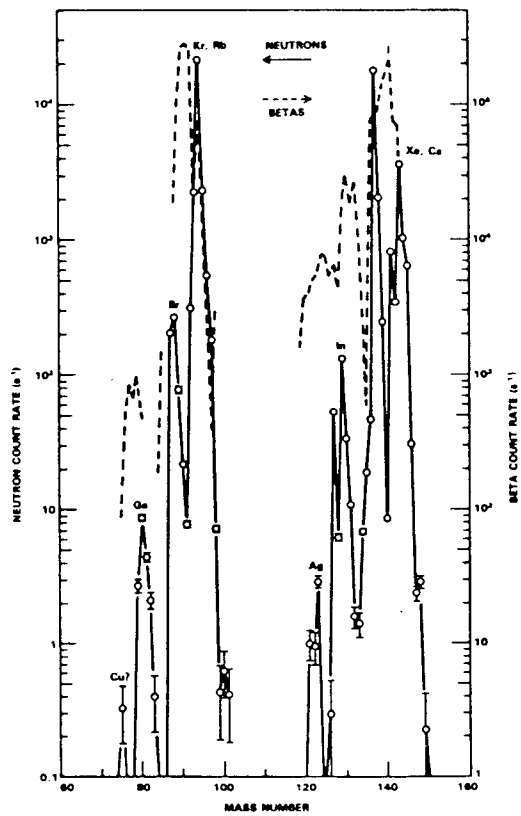

Figure A-2. Beta and Delayed Neutron Count Rates with FEBIAD Ion Source. Rates are Uncorrected for Counter Efficiencies ($n \approx 0.5, \beta \approx 0.17$).

3. Neutron Emission Probabilities of Ag and In Precursors
(P. L. Reeder, R. A. Warner, and R. L. Gill)

Simultaneous neutron and beta growth and decay curves were measured at masses 120-124 and 127-130 to obtain P_n values of Ag and In precursors. These data were analyzed with the least squares fitting code MASH. All the P_n values were normalized to the P_n for ^{127m}In.[5] Our results for a single set of measurements are given in Table A-2. The data for Ag have been submitted for publication.[6] The 19.6 s isomer of ^{128}In was seen in two experiments with different cycle times. A long half-life isomer of ^{128}In ($t_{1/2} \approx 12s$) was seen in previous work but could not be reproduced.[5]

Table A-2. Half-lives and Emission Probabilities of Ag and In Delayed Neutron Precursors.

Precursor	Half-life(s)	P_n(%)
^{120}Ag	1.25 ± 0.03	<0.003
^{121}Ag	0.91 ± 0.06	0.076 ± 0.003
^{122}Ag	0.57 ± 0.03	0.186 ± 0.006
^{123}Ag	0.30 ± 0.01	0.55 ± 0.02
^{124}Ag	0.54 ± 0.08	>0.1
^{127g}In	1.096± 0.003	≤0.002
^{127m}In	3.69 ± 0.05	0.68 ± 0.06[a]
^{128}In	0.82 ± 0.03	0.047 ± 0.002
^{128}In	19.6 ± 2.8	0.9 ± 0.3
^{129g}In	0.61 ± 0.01	0.030 ± 0.014
^{129m}In	1.15 ± 0.02	4.35 ± 0.14
^{130}In	0.36 ± 0.05	1.19 ± 0.14
^{130}In	0.62 ± 0.07	10. ± 8.

[a] Ref. 5. Used for normalization.

5 Lund, Hoff, Aleklett, Glomset, and Rudstam, Z. Phys. A294, 233 (1980).

6 P. L. Reeder, R. A. Warner, and R. L. Gill, "Half-lives and Emission Probabilities of Delayed Neutron Precursors $^{121-124}Ag$," December, 1982, PNL-SA-11100, submitted to Phys. Rev. C.

4. New Precursor — ^{124}Ag (P. L. Reeder, R. A. Warner, R. L. Gill)

At mass 124, simultaneous neutron and beta growth and decay curves were measured using the new FEBIAD ion source at a power level 10% above that used for the initial survey. A neutron activity with a half-life of 0.54 ± 0.08 s was clearly seen. This component could not be unambiguously identified in the beta growth and decay curve due to the overwhelming abundance of Cd and In activities. The neutron activity is assigned to Ag since Cd and In are energetically forbidden to be precursors at this mass number.

B. HALF-LIVES OF Cd ISOTOPES BY BETA DECAY MEASUREMENTS (P. L. Reeder and R. A. Warner)

The beta decay curves obtained as part of the P_n experiments for Ag and In precursors include Cd activities among the complex mixtures of isobars. The MASH program was used to find the best half-lives for Cd isotopes at masses 122-124, and 127 as shown in Table B-1. The half-life for ^{123}Cd has not been reported previously. The 0.4 s activity at mass 127 is very weak and the assignment to ^{127}Cd is only tentative until additional evidence is obtained.

TABLE B-1. Half-lives of Cd isotopes.

Mass No.	Half-life (s)
122	5.10 ± 0.13
123	2.07 ± 0.03
124	1.2 ± 0.1
127	≈0.4

UNIVERSITY OF PENNSYLVANIA

A = 16-17

This review has been published as Nuclear Physics A375 (1982) pp. 1-168.

F. Ajzenberg-Selove and G. C. Marshall

A = 18-20

This review has been published as Nuclear Physics A392 (1983) pp. 1-216.

F. Ajzenberg-Selove and G. C. Marshall

A = 5-6, A = 7-8, A = 9-10

A preprint of these reviews have been sent out to 120 colleagues as PPP 3-82 (September 1982), PPP 4-82 (December 1982) and PPP 1-83 (March 1983). We plan to submit A = 5-10 to Nuclear Physics in July 1983 and to begin at that time the review of A = 11-12.

F. Ajzenberg-Selove and G. C. Marshall

RENSSELAER POLYTECHNIC INSTITUTE

A. Nuclear Data

1. Fission Cross Section Measurements of ^{244}Cm, ^{246}Cm and ^{248}Cm at RINS

(Block, Stopa, Harris, Maguire, Jr.*, Slovacek**, Dabbs***, Dougant, Hofft, Lougheedt)

The fission cross sections of ^{244}Cm, ^{246}Cm AND ^{248}Cm have been measured from 0.1 to 80,000 eV using the Rensselaer Polytechnic Institute LINAC as a pulsed neutron source and the RINS spectrometer. Results were normalized to the ^{235}U ENDF/B-V broad-bin-averaged fission cross section.[1] Fission widths were determined for the resolved low-energy resonances. These results are presented in reference 2.

The measured fission cross sections have been compared with the ENDF/B-V evaluated data and these results are shown in Figures A1 to A3. The ENDF/B-V data have been broadened to the resolution of the RINS system. this resolution is well represented by an energy-dependent Gaussian function which has been determined by Little et al.[3] In general, the agreement between the measured and evaluated data is poor. Below 20 eV there were no prior fission measurements, so the evaluated data are at best only a rough estimate of the cross section and thus gross discrepancies are not unexpected. There is also the possibility of 'contamination' at very low energies from the small amounts of odd curium isotopes in the samples, so the measured fission data below about 1 eV may be lowered somewhat when corrections are applied. However, since we do not have information on the fission cross sections of all the odd curium isotopes, these corrections must await future measurements. For all energies above ~20 eV, we note that the ^{244}Cm evaluated data are in resonable agreement with the measurement near the reasonances in the 20 to 40 eV regions, but the evaluated data underpredict the measurement from 100 eV to 20 keV. In addition, the measured cross section falls monotonically with energy above 10 keV and there is no evidence for the broad peak shown in the evaluated data near 20 keV. The situation is similar for the ^{246}Cm data shown in Figure A2. Again, the peaks near 20 and 90 eV are closely reproduced by the evaluated data, but in general the evaluated data fall significantly below the measured data elsewhere. In particular, the evaluated data are two orders of magnitude smaller than the measurement above 10 keV. For the ^{248}Cm data shown in Figure A3 the agreement is good at the peak of the 76-eV resonance, and at the shoulder near 10 keV. However, the evaluated data fall well below the measured data between 100 eV and 8 keV. In summary, we recommend that the fission cross sections of these curium isotopes be re-evaluated in the 1 eV to 100 keV energy range.

The RINS spectrometer cannot resolve individual curium resonances above ~200 eV. The cross sections for these three curium isotopes are plotted in figure A-4, and we observe several peaks in the ^{244}Cm and ^{246}Cm curves between ~200 eV and several keV. We suspect that these are probably unresolved clusters of strongly fissioning resonances. For ^{248}Cm we observe

a broad peak or plateau near 10 keV. In addition, the ^{244}Cm and ^{246}Cm fission cross sections decrease smoothly with energy and with about the same slope above a few keV, whereas the ^{248}Cm cross section decreases more slowly with energy and is strongly affected by the peak near 10 keV.

The ^{244}Cm and ^{246}Cm data in the 0.2-to-few-keV region are suggestive of intermediate structure. However, it is interesting to note that based on the theoretical calcualtions of Howard and Möller[4] the neutron binding energy is higher than the outer barrier (which is ~1 MeV lower than the inner barrier) and therefore, one does not expect to see strong intermediate structure effects in the fission cross section. In the ^{248}Cm fission cross section, the peak or plateau at ~10 keV could also result from clusters of resonances unresolved by the RINS resolution which may be the result of intermediate structure.

---

* Now at Westinghouse Electric Corporation, Pittsburgh, PA.

** Knolls Atomic Power Laboratory

*** Oak Ridge National Laboratory

† Lawrence Livermore National Laboratory

---

[1]M.R. Bhat, "Evaluation of ^{235}U Neutron Cross Section and Gamma Ray Production Data for ENDF/B-V," March 1980, BNL-NCS-51184 (ENDF-248).

[2]C.R.S. Stopa, H.T. Maguire, Jr., D.R. Harris, R.C. Block, R.E. Slovacek, J.W.T. Dabbs, R.J. Dougan, R.W. Hoff and R.W. Lougheed, "Fission Cross Section Measurements of ^{244}Cm, ^{246}Cm, and ^{248}Cm, "Proc. of ANS TopicalMeeting on Advances in Reactor Physics and Core thermal Hydraulics," September 22-24, 1982, Kiamesha Lake, N.Y., NUREG/CP-0034, Vol. 2, page 1090.

[3]R.C. Little, H.M. Fisher, B. Alam, D.R. Harris, R.D. Block and R.E. Slovacek, "Monte Carlo Modeling of the Neutronics of a Lead Slowing Down Time Assay Device," Trans. Am. Nucl. Soc., 43, 119 (1982).

[4]W.M. Howard and P. Möller, At. Data & Nucl. Data Tables, 25, 219 (1980).

2. Neutron Spectrum Measurements of ThO_2, (Feigenbaum*, Block, Harris, Becker, Malaviya, Hayashi**, Yamamoto***)

Neutron time-of-flight spectrum measurements of ThO_2 were performed at the RPI Gaerttner Linac Laboratory; the experimental apparatus and procedure have been previously described.[1,2] Neutron spectrum measurements[3-5] were

performed from 3.616 keV to 14 MeV for the thoria assembly, and from 724.3 keV to 14 MeV for the bare photoneutron target. A ^{10}B-Vaseline NaI (B-V) detector was used to measure intermediate-energy neutrons, and a proton-recoil organic-liquid (P-R) scintillator was used to measure fast neutrons; the B-V detector was not able to measure the bare target photoneutron spectrum because of bremsstrahlung-induced saturation. The bare target photoneutron spectrum below 0.7243 MeV was represented by a Maxwellian curve with a nuclear temperature of 0.8 MeV.

The results of the thoria neutron spectrum measurements are plotted as thick-lined histograms in Figure A5. The measured neutron spectrum was collapsed into 46 energy groups and plotted as a function of flux per unit energy versus energy. The neutron spectra measured with the B-V and P-R detectors were combined into a single spectrum by performing a least-squares ratio fit of the two spectra over their respective energy overlap range.

The reactor physics code DTF-IV (Ref. 6), a one-dimensional, discrete-ordinates, multigroup transport code, was used to simulate the integral measurements. DTF-IV calcualtions were performed using a 49-group structure, S_{16} quadrature, and a P_8 scattering approximation of the ENDF/B-V cross sections of thorium, hydrogen, oxygen, and tantalum; bench-mark comparisons were made to the DTF-IV calcualtions performed in Japan using ENDF/B-IV cross sections and S_8 quadrature. The group constants used in DTF-IV were generated using the computer code SUPERTOG-III-JR (Ref. 7). A weighting function of 1/E was used to generate group constants for hydrogen, tantalum, and thorium, and a $1/(E\sigma_T)$ weighting function was used for oxygen; the values of σ_T used in the oxygen weighting function are a weighted summation of σ_T for ThO_2.

The measured and calculated thoria spectra were normalized to each other by a least-squares ratio fit and were plotted onto Figure A5 as a set of histograms. There is generally good agreement between these two sets of histograms. In particular, the dip in the measured neutron spectrum in group 26 (387.7 to 467.6 keV), which contains the oxygen resonance, is accurately reproduced in the calculation. The plots do indicate, however, an underprediction of neutrons between 3.46 and 0.724 MeV, and an overprediction of neutrons between 300 and 59.5 keV. One explanation for these results is that there may be too much moderation (e.g., by inelastic scattering) predicted in thorium between 3.46 and 0.724 MeV. This is similar to what was reported by Parvez and Becker for ^{238}U (Ref. 9).

In summary, data and methods appear to be sufficient to make reasonably accurate predictions of spectra in thoria. Should further interest be displayed in thorium, further investigations would be useful to eliminate the modest discrepancies observed.

---

* Now at American Electric Power

** Kyoto University, Research Reactor Institute

*** Kyoto University, Research Reactor Institute

---

[1]B.K. Malaviya, N.N. Kaushal, M. Becker, E. Burns, A. Ginsberg, and E.R. Gaerttner, "Experimental and Analytical Studies of Fast Neutron Transport in Iron." Nucl. Sci. Eng., 47, 329 (1972).

[2]N.N. Kaushal, B.K. Malaviya, M. Becker, E. Burns, and E.R. Gaerttner, "Measurement and Analysis of Fast Neutron Spectra in Uranium Depleted in the Uranium-235 Isotope," Nucl. Sci. Eng., 49, 330 (1972).

[3]H. Nishihara, I. Kimura, K. Kobayashi, S.A. Hayashi, S. Yamamoto, and M. Nakagawa, "Measurement and Analysis of Neutron Spectrum in Spherical Pile of Thoria," J. Nucl. Sci. Technol., 14, 426 (1977).

[4]R.C. Block, M. Becker, D.R. Harris, B.K. Malaviya, S.A. Bokharee, R.W. Emmett, P.S. Feigenbaum, S.H. Levinson, H.T. Maguire, Jr., S.A. Hayashi, and S. Yamamoto, "Neutron Spectrum Measurements upon a Spherical Assembly of Thoria," Proc. Conf. Nuclear Cross Sections for Technology, Knoxville, Tennessee, October 22-26, 1979.

[5]P.S. Feigenbaum, R.C. Block, D.R. Harris, M. Becker, B.K. Malaviya, S.A. Hayashi, and S. Yamamoto, "Neutron Spectrum Measurements of ThO_2," Trans. Am. Nucl. Soc., 43, 721 (1982).

[6]K.D. Lathrop, "DTF-IV, A Fortran-IV Program for Solving the Multigroup Transport Equations with Anisotropic Scattering," LA-33373, Los Alamos National Lab (1965).

[7]R.Q. Wright, N.M. Green, J.L. Lucius, and C.W. Craven, Jr., "SUPERTOG, A Program to Generate Fine Group Constants and Pn Scattering Matrices from ENDF/B," ORNL-TM-2679, Oak Ridge National Lab (1969); see also, Y. Taji, T. Okada, K. Minami, and S. Miyasaka, "SUPERTOG-Jr., A Code Generating Transport Group Constants, Energy Deposition Coefficients and Atomic Displacement Constants with ENDF/B," Japan Atomic Energy Research Institute.

[8]R. W. Emmett, "Analysis of Tantalum Target Photoneutron Production Spectrum Using Monte Carlo Simulation Techniques," Masters Thesis, Rensselaer Polytechnic Institute (August 1980).

[9]A. Parvez and M. Becker, "An Assessment of ENDF/B-IV Data for Uranium-238," Nucl. Sci. Eng., 62, 571 (1977).

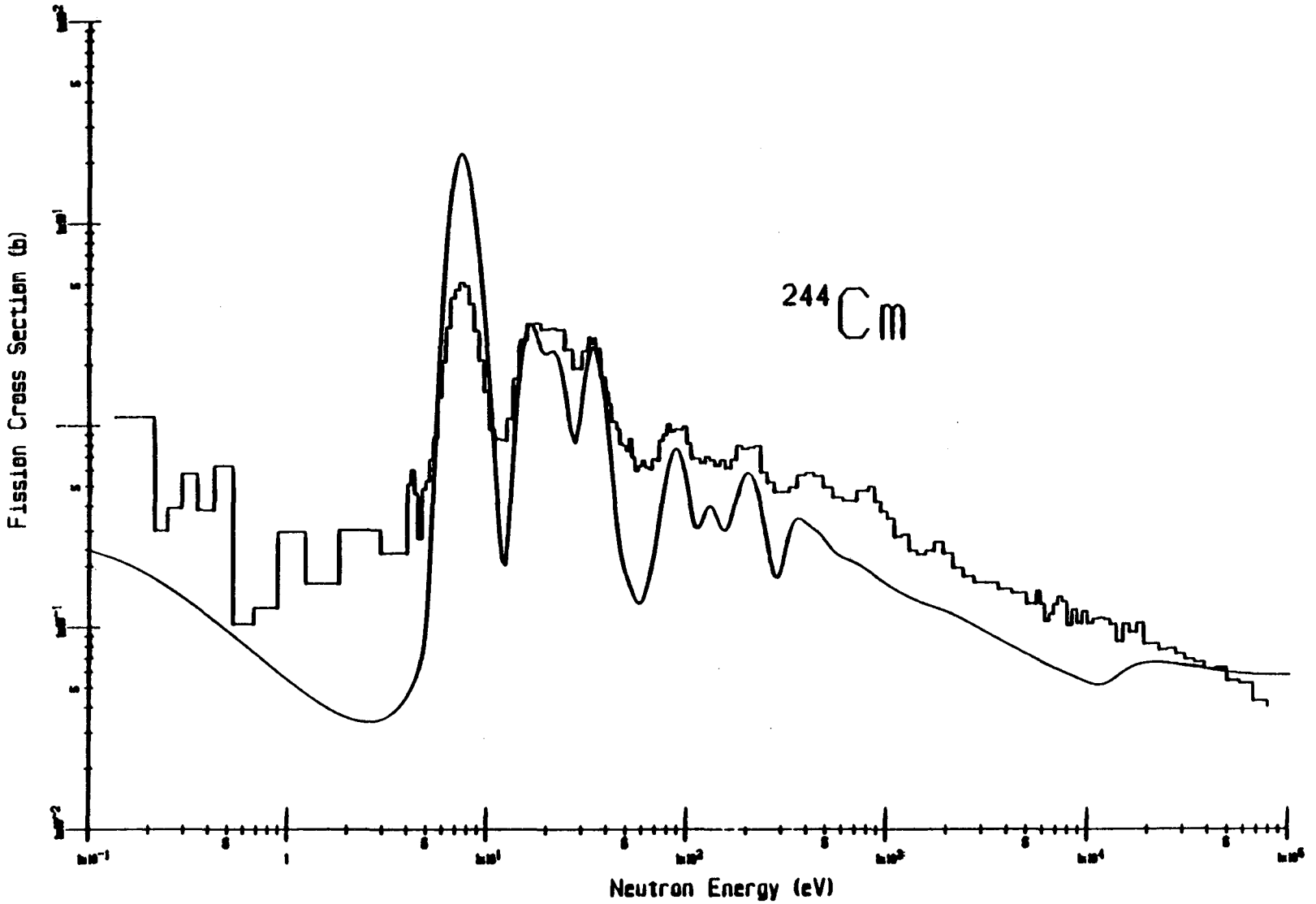

Figure-A1 The measured ^{244}Cm fission cross section (histogram) compared with the ENDF/B-V evaluated data (smooth curve)

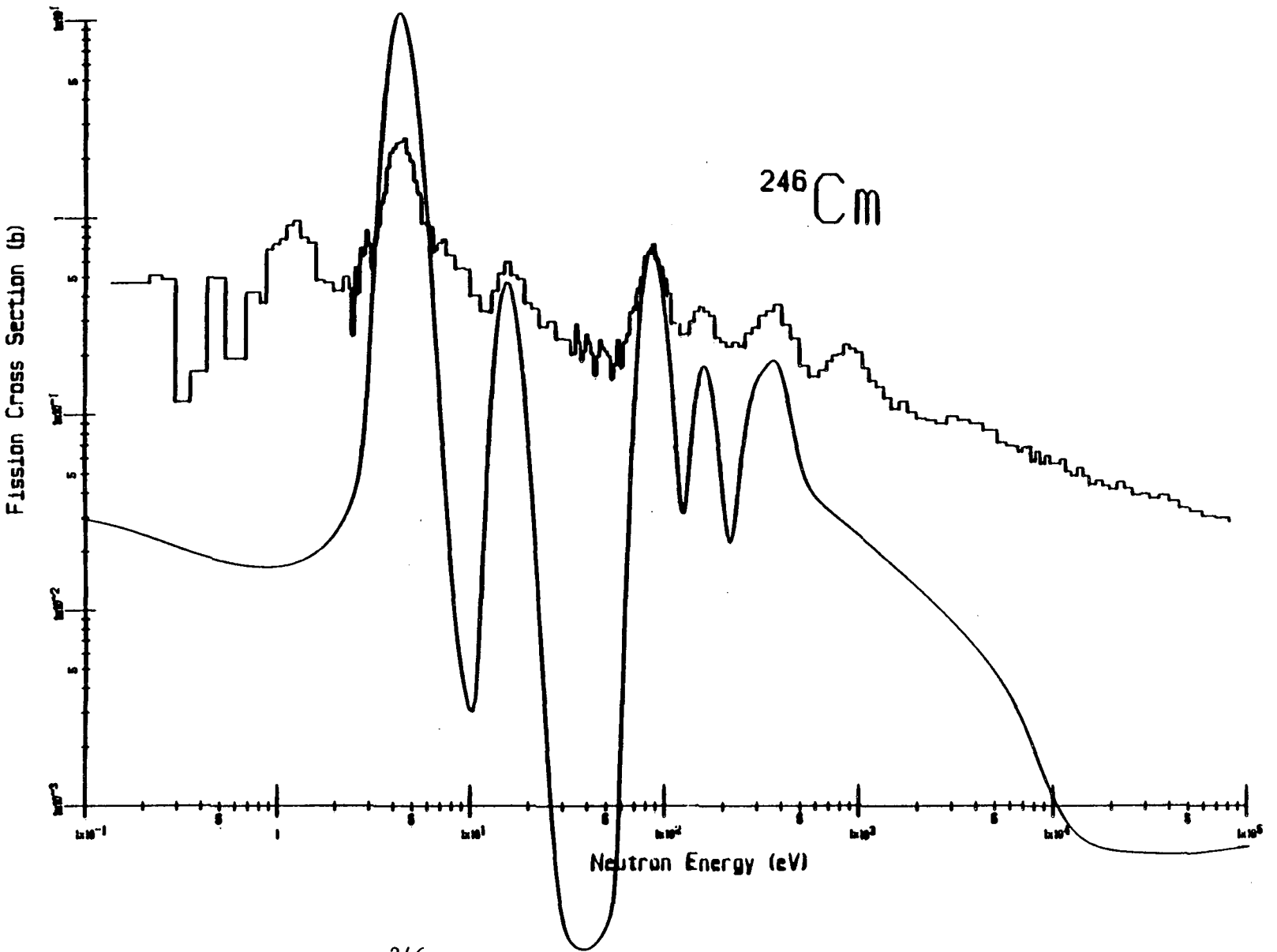

Figure-A2 The measured ^{246}Cm fission cross section (histogram) compared with the ENDF/B-V evaluated data (smooth curve)

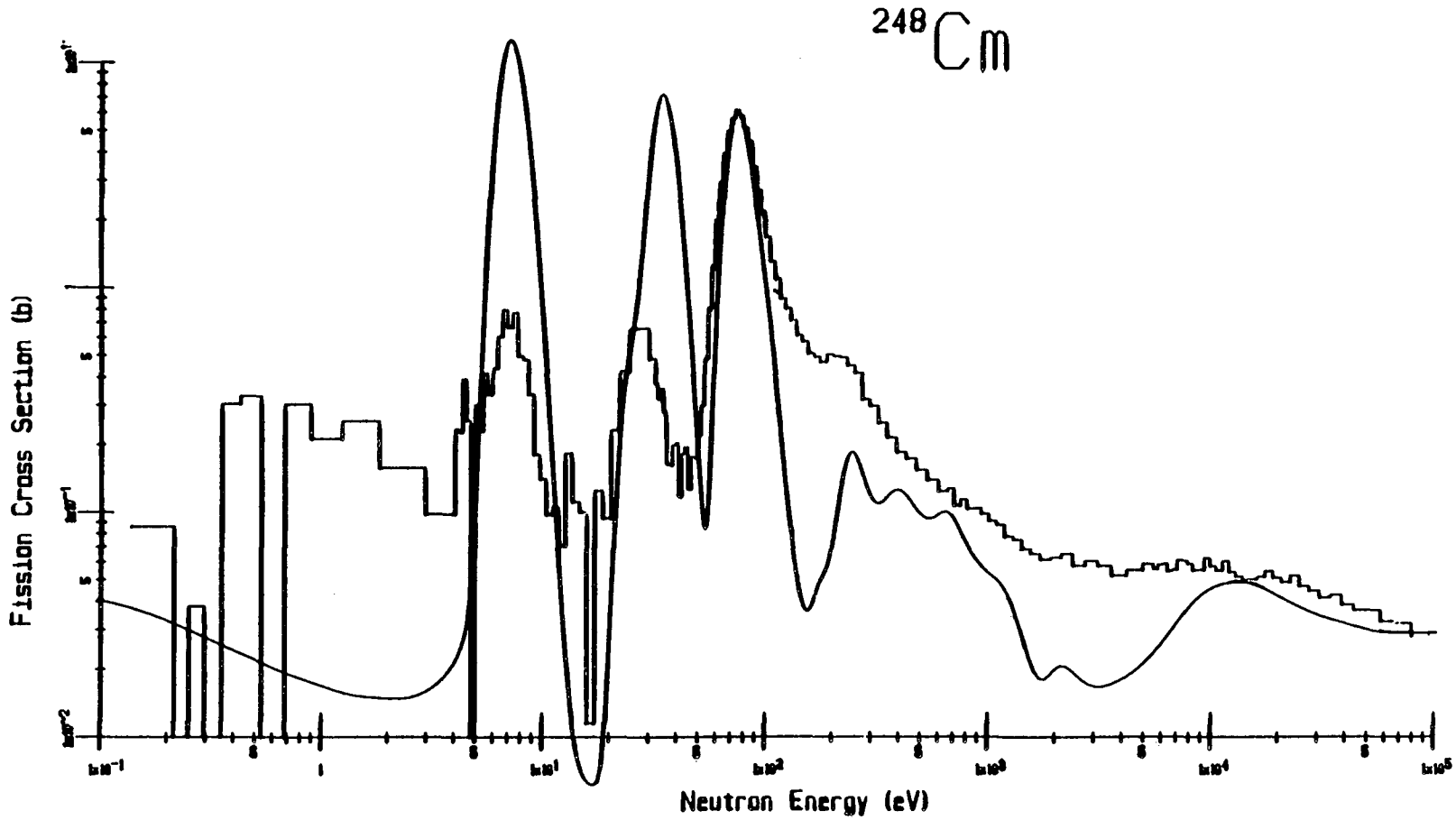

Figure-A3 The measured ^{248}Cm fission cross section (histogram) compared with the ENDF/B-V evaluated data (smooth curve)

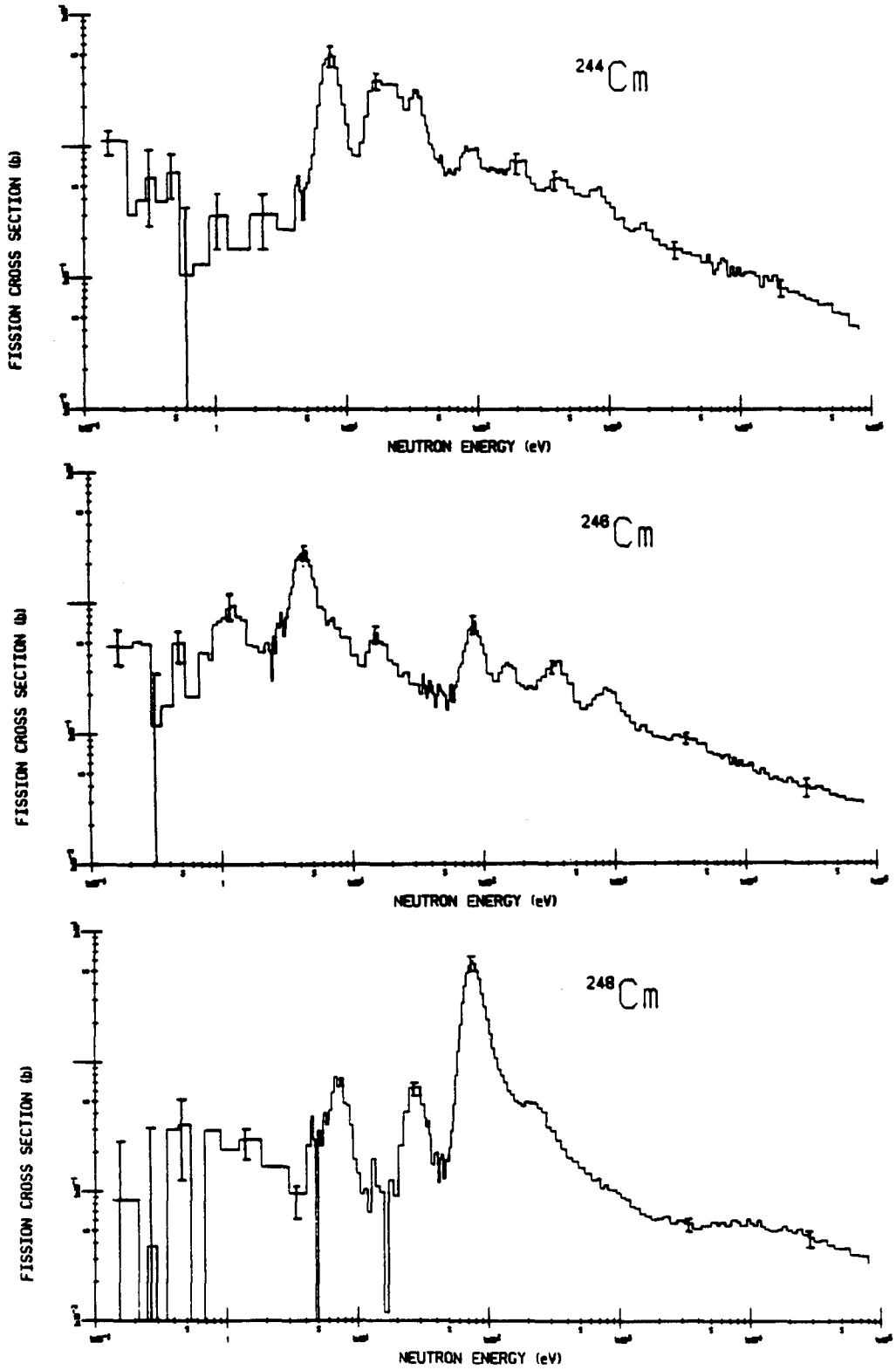

Figure A4 Fission cross section vs. neutron energy for the curium isotopes

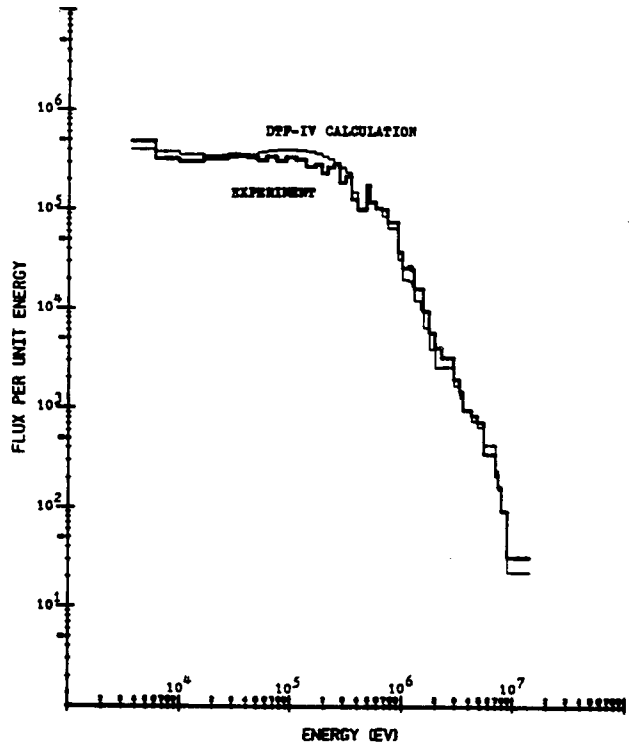

Figure A5. A Comparison of measured and calcualted neutron spectra data for the thoria assembly.

A. NEUTRON PHYSICS

1. Helium Generation Cross Sections for 14.8-MeV Neutrons

(D. W. Kneff, B. M. Oliver, R. P. Skowronski, and Harry Farrar IV)

Neutron-induced helium generation is a major consideration in the development of materials for fusion reactor components. Rockwell International is engaged in two programs to measure total helium generation cross sections for fast neutrons. The Department of Energy's Office of Basic Energy Sciences (OBES) is sponsoring the measurement of the cross sections of a large range of separated isotopes and their associated pure elements for fast (8-15 MeV) monoenergetic neutrons. The Office of Fusion Energy is supporting cross section measurements of other fusion-related materials in the ~14.8-MeV T(d,n) neutron field, plus helium generation cross section measurements in the broad energy spectra used for fusion materials irradiation testing.

The OBES cross section measurements are made by irradiating small (~10-20 mg) samples of a wide range of pure elements and separated isotopes in a nearly monoenergetic neutron spectrum. The amount of helium generated in each sample is subsequently measured by high-sensitivity gas mass spectrometry. The neutron fluence distribution for the irradiation volume is mapped using a comprehensive set of radiometric plus helium accumulation neutron dosimeters, and then combined with the helium generation measurements for multiple samples of each material to deduce cross sections. Absolute fluence normalization is based on the $^{93}Nb(n,2n)^{92m}Nb$ cross section; the fluence mapping is the dominant source of uncertainty (~5-8%) in the cross section measurements. Helium measurement uncertainties are typically ~1-3%.

Irradiations performed to date have utilized the ~14.8-MeV neutron spectra from the T(d,n) Rotating Target Neutron Sources-I and -II (RTNS-I,II) at the Lawrence Livermore National Laboratory (LLNL). Rockwell's previous 14.8-MeV cross section measurements have been summarized in earlier Reports to the DOE Nuclear Data Committee.[1-3] A detailed paper covering our previous and current cross section measurements is in preparation.

Since the last report, cross sections have been measured for Li, ^{6}Li, ^{7}Li, B, ^{10}B, ^{11}B, C, F, Al, Ti, Y, and Ta from RTNS-II. The Li,

---

[1] Kneff, Oliver, Nakata, and Farrar, BNL-NCS-27800, p. 181 (1980)

[2] Kneff, Oliver, Nakata, and Farrar, BNL-NCS-29426, p. 155 (1981)

[3] Kneff, Oliver, Nakata, and Farrar, BNL-NCS-31052, p. 144 (1982)

^{6}Li, ^{7}Li, and F cross sections were derived from irradiated samples of LiF, ^{6}LiF, ^{7}LiF, and PbF_2, respectively. Additional samples of ^{6}LiF, ^{7}LiF, and PbF_2 were also irradiated in a subsequent RTNS-I experiment. The preliminary ^{6}Li and ^{7}Li cross sections derived from this latter work, a scoping experiment performed in conjunction with LLNL, indicate some cross section inconsistencies with the RTNS-II data. The results are being used to design a new RTNS-II irradiation experiment to resolve these inconsistencies.

Helium analyses have also been performed for O (as PbO, Nb_2O_5), Cr, and most of the separated isotopes of Ti and Cr. Cross sections have not yet been determined from these results, however, pending a precise measurement of the oxygen content of each material. Oxygen impurities in the Ti and Cr isotopes must be measured because of the large helium generation cross section of oxygen (~400 mb) at ~14.8 MeV.

Sample preparation and helium analysis work is in progress for Be, N, Mn, Ag, W, and selected separated isotopes of Sn, W, and Pb that have been irradiated in RTNS-II. The analysis of a few of these materials awaits completion of a new high-sensitivity constant-temperature sample furnace that is now under construction. Future work will include some additional measurements at 14.8-MeV (including further work on ^{6}Li and ^{7}Li), and cross section measurements at a different neutron energy.

TRIANGLE UNIVERSITIES NUCLEAR LABORATORY

A. NEUTRON CROSS SECTION EXPERIMENTS

1. Brief Overview (R. C. Byrd, J. Dave, C. E. Floyd, P. P. Guss, C. R. Gould, G. Honore, C. Howell, K. Murphy, H. Pfutzner, R. Pedroni, F. O. Purser*, L. W. Seagondollar, J. Templon, G. Tungate**, R. L. Walter, J. P. Delaroche***)

The focus of the neutron scattering program at TUNL has been to measure and analyze differential cross-sections and/or analyzing powers for elastic and discrete-inelastic scattering from elements across the periodic table. The energy range of interest is 8 to 17 MeV, a region which has not been well studied previously. Almost all of the data have been obtained using pulsed polarized and unpolarized neutron beams in conjunction with the two time-of-flight (TOF) detectors located 4 and 6 m from the scattering sample.

One emphasis in the past year was to tie together our previous optical model studies for 1-p shell nuclei in a comprehensive global analysis and parametrization. We also concentrated on developing localized optical models for about ten isotopes ranging from ^{40}Ca to ^{208}Pb. Most of these later analyses, which also include a description of the analyzing power $A_y(\theta)$ data, are in the final stages. New measurements involved differential cross section $\sigma(\theta)$ and $A_y(\theta)$ for Si, S, Y, and Nb. Coupled-channel (CC) analyses of the data parallel the spherical optical model analyses. These CC calculations are performed in order to obtain nuclear structure information and to obtain a more valid model for representing neutron interaction phenomena. To provide further insight into our models, a Lane consistent method has been used in some cases in order to include (p,p) and (p,n) data from TUNL as well as the literature. Information about isospin dependent terms of the nuclear potential, the Coulomb correction terms and deformation parameters are resulting from these studies.

Our $A_y(\theta)$ data for inelastic scattering from medium weight nuclei, the first such data that have been obtained above 2 Mev, has yielded new insight into deformation of the spin-orbit potential.

The few-nucleon studies during the past year were limited to

n-d scattering. Very accurate measurements of $A_y(\theta)$ were obtained at 10 MeV to provide constraints on few-nucleon calculations and to permit the first solid evidence for differences in the $A_y(\theta)$ function for the charge symmetric systems, p-d and n-d.

Several projects for investigating elastic and inelastic scattering for angles less than 10° have been considered. Experimental tests were made to test the feasibility of accurately measuring inelastic scattering cross sections at 1.5^o to 4° for light nuclei. Results for $^{12}C(n,n')$ and $^{9}Be(n,n')$ demonstrate that an experiment is possible for neutrons in the 10 MeV range. Until now our $\sigma(\theta)$ and $A_y(\theta)$ measurements have been restricted by our physical arrangement to $\theta > 18^o$. Since discrepancies between theory and our measured $A_y(\theta)$ exist in the 18° to 40° region, we are anxious to extend our measurements to $\theta < 18^o$ for further enlightenment. We are also interested in observing the enhancement at extremely small angles of the Mott-Schwinger interaction (the interaction of the magnetic moment of a moving neutron with the static electric field of the nucleus) on the cross section and the analyzing power. For this purpose and the possibility of obtaining evidence for structure of the neutron, we have tested several arrangements for elastic scattering measurements in the $1/2^o$ to 3° interval.

A polarized target is under construction for total cross section measurements which will permit studies of the interaction of the spin of the neutron with the intrinsic spin of nuclei. Reasonable progress has been made on the beam line, neutron production target and its shielding cave, the neutron detector, as well as the cryogenic system to polarize the targets.

Lastly, a few projects on neutron source reactions have been completed and reported. The only neutron producing reactions under study now are (p,n) reactions on light nuclei for Lane model analyses in the 1-p shell.

* Present address: Los Alamos National Laboratory
** Present address: Max Planck Institut fur Kernphysik, Heidelberg
*** Permanent address: Centre d'Etudes de Bruyeres-le-Chatel, France

2. Neutron Scattering Cross Section for ^{16}O Between 9 and 15 MeV

This work has been published in Nuclear Science and Engineering 82 (1982) 393. The abstract is as follows:

"Differential cross sections are reported for elastic scattering of neutrons from ^{16}O. Source neutrons were provided by the $D(d,n)^3He$ reaction with average neutron energies of 9.21, 9.71, 10.21, 10.70, 10.95, 11.15, 11.95, 12.45, 12.94, 13.94 and 14.93 MeV. Time of flight spectra were obtained for neutrons scattered by a BeO sample at 28 angles from 25° to 160° in 5° increments. Flight paths of 4 m and 6 m were used. Spectra obtained with a separate beryllium sample were subtracted in order to remove the beryllium scattering contribution. The angular distribution data were corrected for finite source and finite sample size effects. Legendre polynomial coefficients and total elastic scattering cross sections are reported for oxygen. The data are not well reproduced by the spherical optical model because of the many resonances in the total neutron cross section. Inclusion of resonances together with an optical model background improves the fits to the angular distribution and total cross section data."

3. Optical Model Calculations for 1p-shell Nuclei

This work was reported at the Nuclear Data for Science and Technology conference at Antwerp, Belgium. The abstract of the paper follows:

"A systematic program of measurements of cross sections for neutron elastic and discrete inelastic scattering from the 1-p shell nuclei has been carried out at TUNL over the last six years. The 1-p shell nuclei comprise many elements of interest in fusion reactor design studies. Experiments have been carried out at an FN Tandem van de Graaff facility using the D(d,n) reaction as a neutron source. Time-of-flight data are presently stored in a VAX-11/780 computer interfaced to CAMAC via a micro programmed branch driver, the MBD-11. We review our current experimental methods and our results for neutron scattering from ^6Li, ^7Li, ^9Be, ^{10}B, ^{11}B, ^{12}C, ^{13}C, and ^{16}O. Data have generally been accumulated in 1-MeV steps from 7 to 15 MeV at angles from 25° to 160°. Cross sections are compared to previous work. Much of the neutron scattering data in the energy range 8 to 15 MeV is well described by the spherical optical model (SOM), particularly for nuclei in which resonance structure is not prominent. However, SOM parameters for heavier nuclei do not reproduce the data well. Parameter sets for the individual nuclei will be presented along with the results of a global SOM search over 45 neutron scattering angular distributions for all 1-p shell nuclei. The best fits are obtained for the lithium isotopes, beryllium and the boron isotopes. Volume integrals for the real and imaginary wells are compared to recent theoretical predictions. The SOM

predictions for proton elastic scattering are also compared to the available data."

4. ^{28}Si and ^{32}S Cross Section

Data have been obtained for neutron elastic and inelastic scattering to the first 2^+ state for ^{28}Si and ^{32}S at 8, 10, 12 and 14 MeV. These data were complemented with polarization data at 10 and 14 MeV. The ^{28}Si data have been processed through the multiple scattering code EFFIGY and were reported at the Nuclear Physics Division meeting at Amherst. The values for ^{32}S have not been stripped in a final form from the time-of-flight spectra.

5. Elastic and Inelastic Scattering from $^{54,56}Fe$ and $^{63,65}Cu$

These data and subsequent analyses have been submitted in two papers for publication in Nuclear Physics. The abstract of Part I follows:

ABSTRACT I

"Differential cross sections were measured at 8, 10, 12 and 14 MeV for elastic scattering of neutrons from enriched samples of ^{54}Fe, ^{56}Fe, ^{63}Cu and ^{65}Cu. Inelastic scattering to the first excited state in $^{54,56}Fe$ was also observed. For the $^{63,65}Cu$ isotopes, the inelastic cross sections for scattering to the combined group of the three (five) states were determined at 8 and 10 MeV (12 and 14 MeV). The elastic scattering data are compared to predictions of earlier global optical models. New spherical optical model representations were obtained. These data were combined with data for nickel, tin, and lead to generate a new global parametrization. Comparisons of derived volume integrals for the potentials, total cross sections, and potential radii are made to available information."

The abstract of part II follows:

ABSTRACT II

"Extended coupled channels calculations have been performed for neutron elastic and inelastic cross sections and analyzing powers for vibrational nuclei with $40<A<208$ to determine the sensitivity of these observables to the coupling to isoscalar giant resonances. The calculations concentrated on the neutron energy region between 10 and 17 MeV, and the 10 MeV results for

$^{116,120}Sn$ and ^{208}Pb and 12 MeV results for ^{40}Ca are illustrated here."

6. $^{58,60}Ni$ Cross Section

Data for $^{58,60}Ni$ isotopes were reported last year for 10, 12 and 14 MeV for elastic scattering and inelastic scattering to the first excited state. The first set of coupled channels (CC) calculations have been completed but will be redone in the near future when the input $A_y(\theta)$ data is more accurately adjusted for the influence of Mott-Schwinger scattering. (The latter process is ignored in the CC code ECIS79 (written by J. Raynal) which we employ in our calculations. To accomodate this omission, we shift our $A_y(\theta)$ data by an amount based on spherical optical model calculations made with and without the M.S. interaction.) Our preliminary studies show that the data can be fairly well represented with the CC calculations. Deformation parameters were obtained for the central and spin-orbit well and compared to values for (p,p) scattering. A spherical optical model (SOM) parametrization has been derived for each of these isotopes based on the CC parameters. It was possible to obtain a good SOM description of the data using the above CC parameters with the sole exception of adjusting the CC imaginary well depths in a systematic way.

7. Yttrium and Niobium Cross Sections

Angular distributions have been completed now at 8, 10, 12 and 14 MeV for neutron elastic scattering from Y and Nb. The TOF spectra are presently being reduced and the multiple scattering corrections are underway. Typical $\sigma(\theta)$ results are shown in Fig. A-1. The data are compared to those of Holmqvist and Wielding and show discrepancies of about 10-20% in some angular regions. It is planned to conduct SOM searches on these data as well as the $A_y(\theta)$ data we have obtained for each nucleus at 10 and 14 MeV. The Nb project was reported at the Nuclear Physics Division meeting at Amherst.

8. $^{116,120}Sn$ Cross Section

Data reported last year for $\sigma(\theta)$ at 10 and 14 MeV for ^{116}Sn and 10, 14 and 17 MeV for ^{120}Sn have now been described along with $A_y(\theta)$ data for ^{120}Sn at 10 and 14 MeV. Also included in the

SOM and CC searches were data from other laboratories, both for the (p,p) and (n,n') channels as well as for (n,n_0). A sample of the $\sigma(\Theta)$ description with the SOM is shown in Fig. A-2. The energy dependent parameters used in this SOM description were purposely highly constrained with the CC parameters.

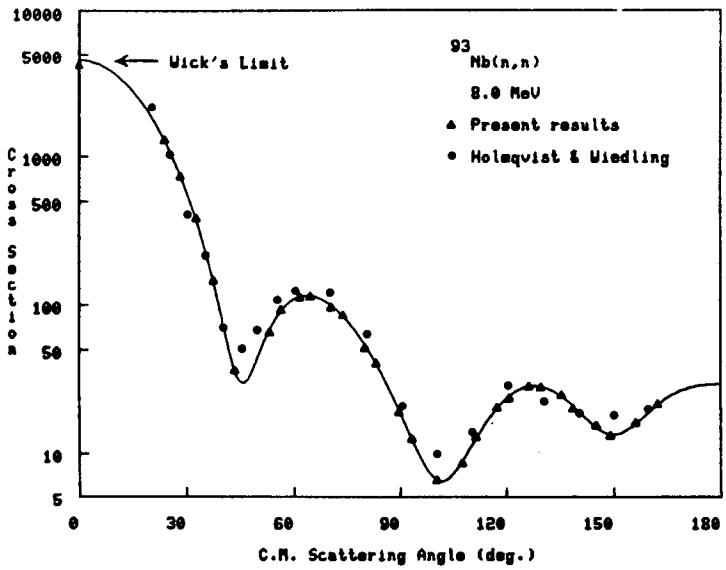

Fig. A-1. Comparison of present data to earlier results at 8 MeV.

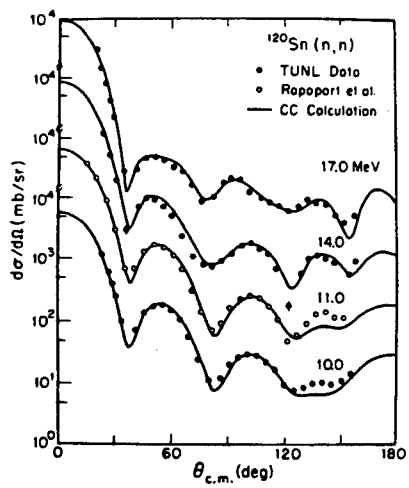

Fig. A-2. Comparison of elastic cross-section data to CC calculations.

9. Neutron Elastic and Inelastic Scattering at Very Forward Angles
(R. E. Anderson, C. R. Gould, B. Carp, K. E. Nash, R. Pedroni, H. Pfutzner, J. Templon, R. L. Walter)

During the last year we have tested the feasibility of making precision measurements of $\sigma(\Theta)$ and $A_y(\Theta)$ in neutron elastic and inelastic scattering at small scattering angles.

The motivation for this work is as follows:

(1) In neutron elastic scttering at forward angles at least one component of the electromagnetic (EM) scattering competes successfully with the nuclear scattering and may even dominate the nuclear scattering. For example, the analyzing power is almost completely determined by the Mott-Schwinger (M-S) interaction[1], the long-range interaction between the neutron magnetic moment and the EM field of the target nucleus as seen from the moving neutron frame. Near 1° the analyzing power due to M-S scattering[2] reaches its greatest possible magnitude, which is 1.0. Contributions from M-S scattering are visible at larger angles as well through interference with the nuclear contribution when that analyzing power is small, and we wish to examine how successfully such an effect can be incorporated into a description of nucleon-nucleus scattering.

(2) Additional electromagnetic scattering may arise if the neutron acquires an induced electric dipole moment due to polarization of the neutron in the intense Coulomb field near the nucleus. Although such fundamental processes within nucleons often produce only very small effects in low energy nuclear physics, they may be revealed if data of sufficient precision can be obtained.

(3) Very little neutron inelastic scattering data presently exist at far forward angles. On the other hand, it is possible[3] that large differences in the phase shifts for successive partial waves in nucleon-nucleus scattering might lead to structure in the forward angle region. We feel that this would be an interesting and informative effect if it could be observed.

Several design aspects of a collimator similar in spirit to that of Bucher et al.[4] have been tested. A highly schematic representation of such a collimator containing one observation post is shown in Fig. A-3. We wished to determine whether the face of the collimator should be made out of a heavy material (e.g., steel) or a light material (e.g., polyethylene), and whether the "wedge" shaped portion of the collimator face (shaded in Fig. A-3) should be removed in order to reduce background

events from small angle scattering in the collimator.

The results of one measurement made at a $\Theta = 0.65^{o}$ are shown in Fig. A-4. Here the scattering sample was natural lead. We determined that the polyethylene face provided a superior suppression of the background compared to steel and that the "wedge" contributed only slightly to the target out spectrum. The target out background in Fig. A-4 consists of three parts:

(i) a time-independent, constant component,

(ii) a large lump to the left of the elastic peak and

(iii) a small peak indistinguishable from the true elastic events seen with target in.

We feel that (i) and (ii) can be significantly reduced with more shielding and a detector more equally matched to the size of the collimator. By using helium bags background contribution (iii) was determined to be largely due to air scattering. We feel that this latter contribution can be greatly reduced in the final design. Based on this test run we estimate that precision measurements of $\sigma(\Theta)$ (to $\pm 3\%$) and $A_y(\Theta)$ (to ± 0.01) eventually can be made with an angular resolution of $\pm 0.01^{o}$ in the region $0.5^{o} < \Theta < 5^{o}$.

Figure A-4 also shows a spectrum for $^{12}C + n$ obtained at $\Theta = 10^{o}$ and a bombarding energy of 10 MeV using the original apparatus of Bucher et al.[4] The 2^{+} state at 4.4 MeV is clearly visible as it was also in a much shorter run taken at 1.5^{o}. The 2.4 MeV state in ^{9}Be was also observable. Based on these tests we feel that measurements of $\sigma(\Theta)$ and possibly $A_y(\Theta)$ for selected inelastic transitions in the very forward angle regions are feasible. We will proceed with these studies for (n,n') since they can be made with presently obtainable angular resolution of about 1.2^{o}, while the elastic scattering measurements described above require much finer angular resolution and more carefully designed apparatus.

---

1) J. Schwinger, Phys. Rev. 73 (1948) 407

2) W. S. Hogan and R. G. Seyler, Phys. Rev. 177 (1969) 1706

3) I. E. McCarthy, Intro. to Nuc. Theory (ch.12) 1968

4) W. Bucher et al., Nucl. Instr. and Meth. 111 (1973) 237

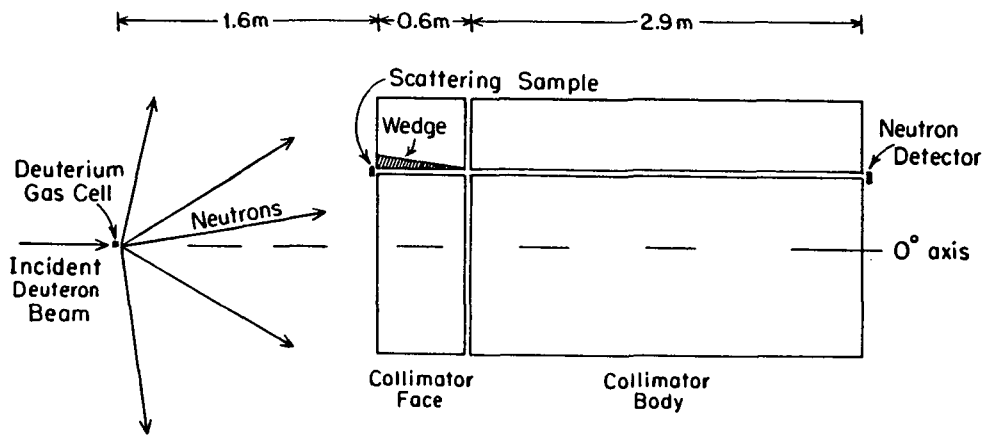

Fig. A-3. Schematic representation of the small angle collimation apparatus.

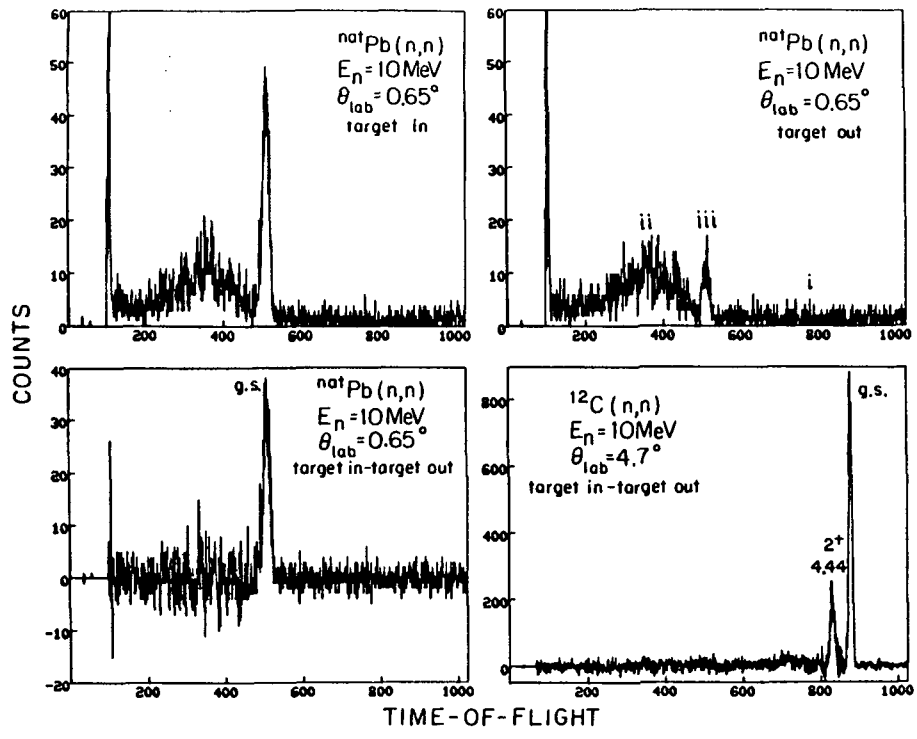

Fig. A-4. Each final spectrum is a difference spectrum obtained by subtracting data obtained with target out from that obtained with target in. Spectra of quality comparable to that shown for $^{12}C(n,n')$ at $\Theta = 4.7^{o}$ have been obtained at several other angles between 1.5^{o} and 15°.

10. The $^{1}H(^{7}Li,n)^{7}Be$ Cross Section (S. A. Wender,* C. R. Gould, J. Dave, S. M. Shafroth)

This work has been published in Nucl. Instrum. and Methods 200 (1982) 285. The abstract is as follows:

"Heavy ion bombardment of hydrogen provides a number of new possibilities for mono-energetic and quasi mono-energetic neutron beam production. Close to the threshold, the strong kinematic focussing for negative Q-value reactions gives rise to intense well-collimated beams of MeV neutrons. An experimental study of 0° neutron production in the $^{1}H(^{7}Li,n)$ reaction (Q = -1.64 MeV) has been carried out from the threshold energy, 13.15 MeV, up to 22 MeV. Measured cross sections are compared to predictions based on known $^{7}Li(p,n)$ cross sections. At 13.5 MeV the effective cross section reaches 4 b/sr, and the neutrons are confined within a cone of half angle 9°. Cross section predictions for ^{9}Be, ^{11}B and ^{13}C bombardment of hydrogen are also presented."

---

* Present address: Los Alamos National Laboratory